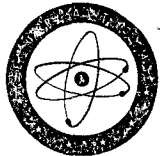


INDSWG-100

EANDC(E) 57 "U"



**IAEA
NUCLEAR DATA UNIT
MASTER COPY**

NDS LIBRARY COPY

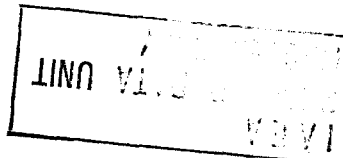
**PROGRESS REPORT
ON NUCLEAR DATA RESEARCH IN THE EURATOM COMMUNITY**

for the period 1.7.1963 to 31.12.1964

Submitted by the Joint Euratom Nuclear Data
and Reactor Physics Committee

(Secretariat : Central Bureau for Nuclear
Measurements, Euratom, Geel, Belgium)

February 1965



PROGRESS REPORT

on Nuclear Data Research

in the Euratom Community

for the period 1.7.1963 to 31.12.1964

Submitted by the Joint Euratom Nuclear Data
and Reactor Physics Committee

(Secretariat : Central Bureau for Nuclear
Measurements, Euratom, Geel, Belgium)

February 1965

EUROPEAN AMERICAN NUCLEAR DATA COMMITTEE

I N D E X
=====

	<u>Page</u>
1. INSTITUT FÜR KERNPHYSIK DER UNIVERSITÄT FRANKFURT/MAIN (Germany)	1
2. PHYSIKALISCHES STAATSINSTITUT, I. INSTITUT FÜR EXPERIMENTALPHYSIK, HAMBURG (Germany)	17
3. LABORATORIUM FÜR TECHNISCHE PHYSIK DER T.H. MÜNCHEN (Germany)	21
4. KERNFORSCHUNGSZENTRUM KARLSRUHE (Germany)	40
5. CENTRE D'ETUDE DE L'ENERGIE NUCLEAIRE, CEN-SCK, MOL (Belgium)	61
6. LABORATOIRE VAN DE GRAAFF, UNIVERSITE DE LIEGE (Belgium)	78
7. LABORATORIO DI FISICA NUCLEARE APPLICATA - CENTRO DI STUDI NUCLEARI DELLA CASACCIA DEL COMITATO NAZIONALE PER L'ENERGIA NUCLEARE, CASACCIA (Italy)	79
8. LABORATORIO DATI E CALCOLI NUCLEARI - CENTRO DI CALCOLO DI BOLOGNA DEL COMITATO NAZIONALE PER L'ENERGIA NUCLEARE, BOLOGNA (Italy)	83
9. GRUPPO DI ISPRA PER LE MISURE SEZIONE D'URTO DEL COMITATO NAZIONALE PER L'ENERGIA NUCLEARE, ISPRA (Italy)	84
10. CENTRO DI INFORMAZIONI STUDI ESPERIENZE (CISE), SEGRATE, MILANO (Italy)	85
11. ISTITUTO DI FISICA DELL'UNIVERSITA' DI CATANIA - CENTRO SICILIANO DI FISICA NUCLEARE - SEZIONE SICILIANA DELL'ISTITUTO NAZIONALE FISICA NUCLEARE, CATANIA (Italy)	87
12. LABORATORIO DELL'ACCELERATORE VAN DE GRAAFF DELLA UNIVERSITA' DI PADOVA (Italy)	91
13. SOTTOSEZIONE DI FIRENZE DELL'ISTITUTO NAZIONALE FISICA NUCLEARE - ISTITUTO DI FISICA DELL'UNI- VERSITA' DI FIRENZE (Italy)	93

Page

14.	CENTRAL BUREAU FOR NUCLEAR MEASUREMENTS, EURATOM, GEEL (Belgium)	94
15.	DEPARTEMENT DE RECHERCHE PHYSIQUE - SECTION DES MESURES NEUTRONIQUES FONDAMENTALES, CEA, SACLAY (France)	113
16.	DEPARTEMENT DE PHYSIQUE NUCLEAIRE ET DU SOLIDE - SERVICE DE PHYSIQUE NUCLEAIRE A BASSE ENERGIE - CEA, SACLAY (France)	137
17.	SERVICE DE PHYSIQUE EXPERIMENTALE DU COMMIS- SARIAT A L'ENERGIE ATOMIQUE (France)	150
18.	INSTITUT NATIONAL DES SCIENCES ET TECHNIQUES NUCLEAIRES DU C.E.A., SACLAY (France)	163
19.	SERVICE DES EXPERIENCES CRITIQUES, CEA (France)	165
20.	SERVICE DES PILES, CENTRE D'ETUDE NUCLEAIRE DE GRENOBLE (France)	172
21.	ISTITUTO DI FISICA NUCLEARE - MOSTRA D'OLTRE- MARE, NAPOLI (Italy)	173
22.	LABORATOIRE DE PHYSIQUE NUCLEAIRE, CENTRE D'ETUDE NUCLEAIRE DE GRENOBLE - C.E.A. ET UNIVERSITE DE GRENOBLE (France)	178

1. INSTITUT FUR KERNPHYSIK DER JOHANN WOLFGANG GOETHE UNIVERSITAT
FRANKFURT/MAIN (Germany)

1.1. Fast neutron cross-section measurements by activation
techniques.

(R.Bass, C.Bindhardt, K.Krüger)

The samples were irradiated with monoenergetic neutrons from the reactions $H^2(d,n)He^3$ ($E_n = 4 - 9$ MeV) and $H^3(d,n)He^4$ ($E_n = 14 - 23$ MeV). The activities were detected and identified either by γ -spectroscopy or by β -counting in 4 π geometry: in the latter case scintillation crystals ($KI(Tl)$; $CaF_2(Eu)$; $Li^6I(Eu)$) were used as samples and simultaneously as detectors. The measured cross-sections for various reactions on K- and Ca-isotopes are given in table 1.1. Figure 1.1. shows results for the reaction $Li^6(n,p)He^6$. Further the reactions $F^{19}(n,p)O^{19}$ and $F^{19}(n,\alpha)N^{16}$ were investigated in the energy range 5 - 9 MeV with an energy resolution of about 30 KeV. The excitation curves exhibit pronounced structure. the analysis has not yet been completed. Similar measurements are planned of the reactions $Na^{23}(n,p)Ne^{23}$ and $Na^{23}(n,\alpha)F^{20}$.

1.2. Investigation of fast neutron induced reactions in $NaI(Tl)$, $KI(Tl)$ and $CsI(Tl)$ by spectroscopy of prompt charged particles and coincident γ -rays.

(R.Bass, Fatma Saleh, U.Fanger)

The purpose of these experiments was both the measurement of cross-sections and the study of level schemes and γ -ray transitions of the product nuclei. As an important tool the pulse-shape discrimination technique was employed. The cross-sections measured so far are given in table 1.2. The results for K^{39} have been published in Nuclear Physics 56 (1964) 569. The results for Na^{23} are preliminary. a more comprehensive investigation is in progress. As an example of the spectroscopic information obtained, figure 1.2. shows part of the level scheme of A^{39} , which is largely based on the present measurements.

1.3. Fast-neutron-induced reactions of Ca^{40} .

(R.Bass, Fatma Saleh)

The (n,n') , (n,p) and (n,α) reactions of Ca^{40} were studied in the energy range 3.7 - 7.5 MeV with the following methods.

- a) Detection of charged particles in $\text{CaF}_2(\text{Eu})$ scintillation crystals.
- b) Spectroscopy of γ -radiation in coincidence with charged particles.
- c) Straight γ -ray measurements in ring geometry. The measured cross sections (preliminary values) are shown in figures 1.3., 1.4. and 1.5.

1.4. Inelastic scattering of neutrons from lithium.

(R.Bass)

The cross-section for inelastic scattering of neutrons to the first excited state of Li^7 (0.48 MeV) was measured by γ -ray detection in ring geometry. The data obtained so far cover the energy range 4 - 9 MeV in 100 keV steps. A preliminary analysis indicates that the cross-section falls with increasing energy from about 330 mb at 4 MeV to about 200 mb at 6 MeV and then stays approximately constant up to 9 MeV. Similar measurements are planned of inelastic scattering to the 3.56 MeV state in Li^6 .

1.5. Total neutron cross-section of Si and Al.

(E.Rössle, M.Tauber)

The total neutron cross-sections of Si and Al have been measured in the energy range $6.3 < E_n < 9.1$ MeV in 20 keV steps with an energy spread of about 22 keV in order to investigate statistical fluctuations of this cross-section. For the neutron detection the ground state transition of the reaction $\text{Si}^{28}(n,\alpha)\text{Mg}^{25}$ was used.

A special arrangement allows the determination of the total cross-section in one measurement. The error on the measurements is about 3%. The results are shown in fig. 1.6. and 1.7. The fluctuations of the cross-sections are in qualitative agreement with the theory of Ericson. From this theory the compound elastic cross-section in forward direction can be evaluated. The results are 26 and 57 mb/ster for Si and Al, respectively. The mean total cross-section of Al follows the calculation using a nonlocal optical potential, whereas for Si deviations occur which cannot be explained so far.

1.6. Neutron induced reactions in Si.

(G.Betz, E.Rössle)

Earlier measurements of these reactions have been extended to the energy range $5.2 < E_n < 7.2$ MeV. The measurements have been performed by bombarding a silicon solid state detector by neutrons of an energy spread of about 25 keV. Especially the following transitions have been analysed: $\text{Si}^{28}(n, p_{\alpha}, 1)\text{Al}^{28}$, $\text{Si}^{28}(n, \alpha_{\alpha})\text{Mg}^{25}$, $\text{Si}^{29}(n, \alpha_{\alpha})\text{Mg}^{26}$ and $\text{Si}^{29}(n, \alpha_1)\text{Mg}^{26}$. The results (fig. 1.8. to 1.11.) exhibit strong fluctuations. The errors are about 6% for the relative measurements and about 20% for the absolute scale. The fluctuations are in qualitative agreement with the theory of Ericson.

Table 1.1.: Fast neutron activation cross-sections
(Potassium and Calcium isotopes)

Reaction	neutron energy range (MeV)	σ (mb)	detected radiation.
$K^{39}(n,2n)K^{38}$	13.1 - 15.4	1.8 ± 0.9	
	19.8 - 20.5	24.3 ± 2.4	
	20.9 - 21.5	24.7 ± 2.5	
	21.9 - 22.5	24.8 ± 2.5	
	22.9 - 23.5	26.5 ± 2.7	
$K^{39}(n,2n)K^{38m}$	14.1 - 17.5	2.7 ± 1.4	
	17.1 - 18.3	5.4 ± 1.8	
	18.6 - 19.5	9.1 ± 2.0	
	19.8 - 20.5	10.6 ± 2.1	
	20.9 - 21.5	12.8 ± 2.6	
	21.9 - 22.5	12.4 ± 2.6	
$K^{41}(n,\alpha)Cl^{38}$	4.4 - 5.4	3.4 ± 1.0	β, γ
	5.5 - 6.5	7.5 ± 1.5	
	6.6 - 7.5	13.0 ± 1.3	
	7.5 - 8.4	15.7 ± 1.6	
$K^{41}(n,p)A^{41}$	3.2 - 4.4	4.2 ± 1.4	β, γ
	4.5 - 5.4	11.7 ± 2.4	
	5.5 - 6.5	16.8 ± 1.6	
	6.6 - 7.5	19.5 ± 2.0	
	7.5 - 8.4	30.0 ± 3.0	
$Ca^{42}(n,p)K^{42}$	3.0 - 4.3	3.8 ± 1.5	β
	4.4 - 5.4	13.3 ± 2.6	
	5.6 - 6.5	33.0 ± 3.3	
	6.7 - 7.5	60.0 ± 6	
	7.6 - 8.5	91.0 ± 9	
$Ca^{44}(n,\alpha)A^{41}$	6.7 - 7.5	0.3 ± 0.2	β, γ
	7.6 - 8.5	1.3 ± 0.6	
	7.8 - 8.5	1.7 ± 0.5	
	13.1 - 15.4	34.0 ± 3.5	
$Ca^{44}(n,p)K^{40}$	5.6 - 6.5	0.14 ± 0.10	β
	6.7 - 7.5	1.0 ± 0.3	
	7.6 - 8.5	3.5 ± 1.2	

Table 1.2.: Fast neutron cross-sections for charged particle production in NaJ(Tl), KJ(Tl) and CsJ(Tl) scintillators (σ in mb, E_n in MeV, $\Delta E_n \approx 200$ keV)

target	K ³⁹ (KJ(Tl))				Na ²³ (NaJ(Tl))				Cs ¹³³ + J ¹²⁷ (CsJ(Tl))			
reaction	(n, p)	(n, α)	(n, p_0)	(n, p_1)	(n, p_2)	(n, α)	(n, α_1)	(n, p)	(n, p_0)	(n, p_1)	(n, α)	(n, σ)
$E_n = 4.0$	270 ± 40	101 ± 12	128 ± 13	45 ± 7	21 ± 4	80 ± 8	18.6 ± 3.2					
4.5	280 ± 42	122 ± 15	91 ± 9	38 ± 6	22 ± 4	87 ± 9	29 ± 5					
5.0	300 ± 45	138 ± 17	64 ± 6	32 ± 5	21 ± 4	92 ± 11	40 ± 7					
5.5	320 ± 50	152 ± 18	54 ± 5	24 ± 3.5	19.3 ± 4	82 ± 12	41 ± 7					
6.0	325 ± 50	154 ± 18	38.5 ± 4	18.1 ± 2.7	18.4 ± 3.7			37 ± 6				
6.5	320 ± 50	157 ± 18	27.5 ± 3	14.3 ± 2.2	13.9 ± 2.8			33 ± 5.5				
7.0	325 ± 50	155 ± 18	20.5 ± 2	10.8 ± 1.6	12.0 ± 2.4			28 ± 5				
7.5	355 ± 50	156 ± 18	16.0 ± 1.6	9.5 ± 1.5	10.0 ± 2.0			23 ± 4				
8.0	350 ± 50	161 ± 18	14.0 ± 1.4	7.2 ± 1.2	8.4 ± 1.8			21 ± 4				
target												
reaction	(n, p)	(n, α)	(n, p_0)	(n, p_1)	(n, p_2)	(n, α)	(n, α_1)	(n, p)	(n, p_0)	(n, p_1)	(n, α)	(n, σ)
$E_n = 8.0$	47 ± 9	28.5 ± 7	17 ± 1.7	7.5 ± 1.2								
14.0					1.2 ± 1.3	0.9 ± 0.2	1.4 ± 0.15					
22.0					22 ± 5	8.5 ± 2	5.2 ± 0.8					

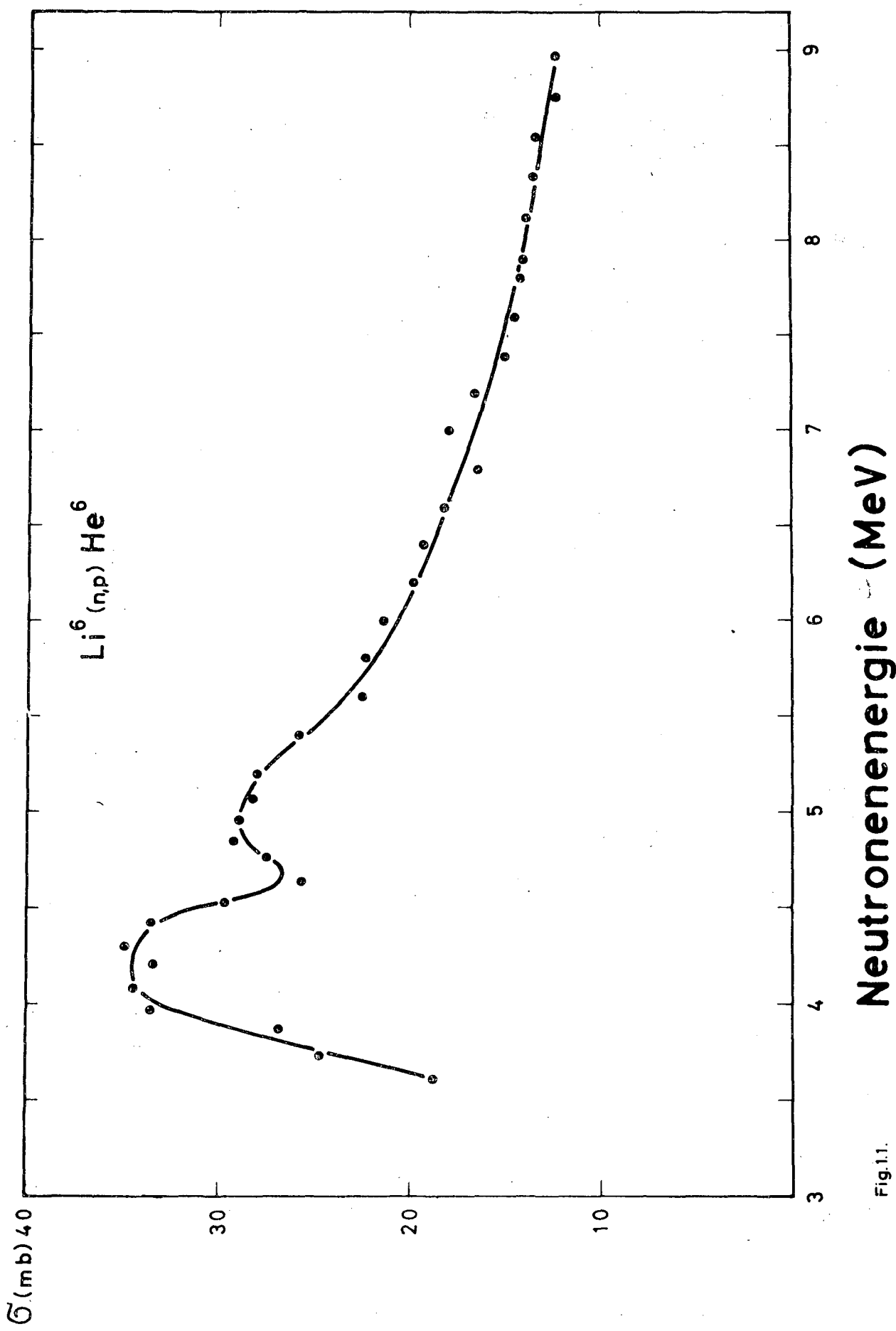


Fig.1.1.

Neutronenergie (MeV)

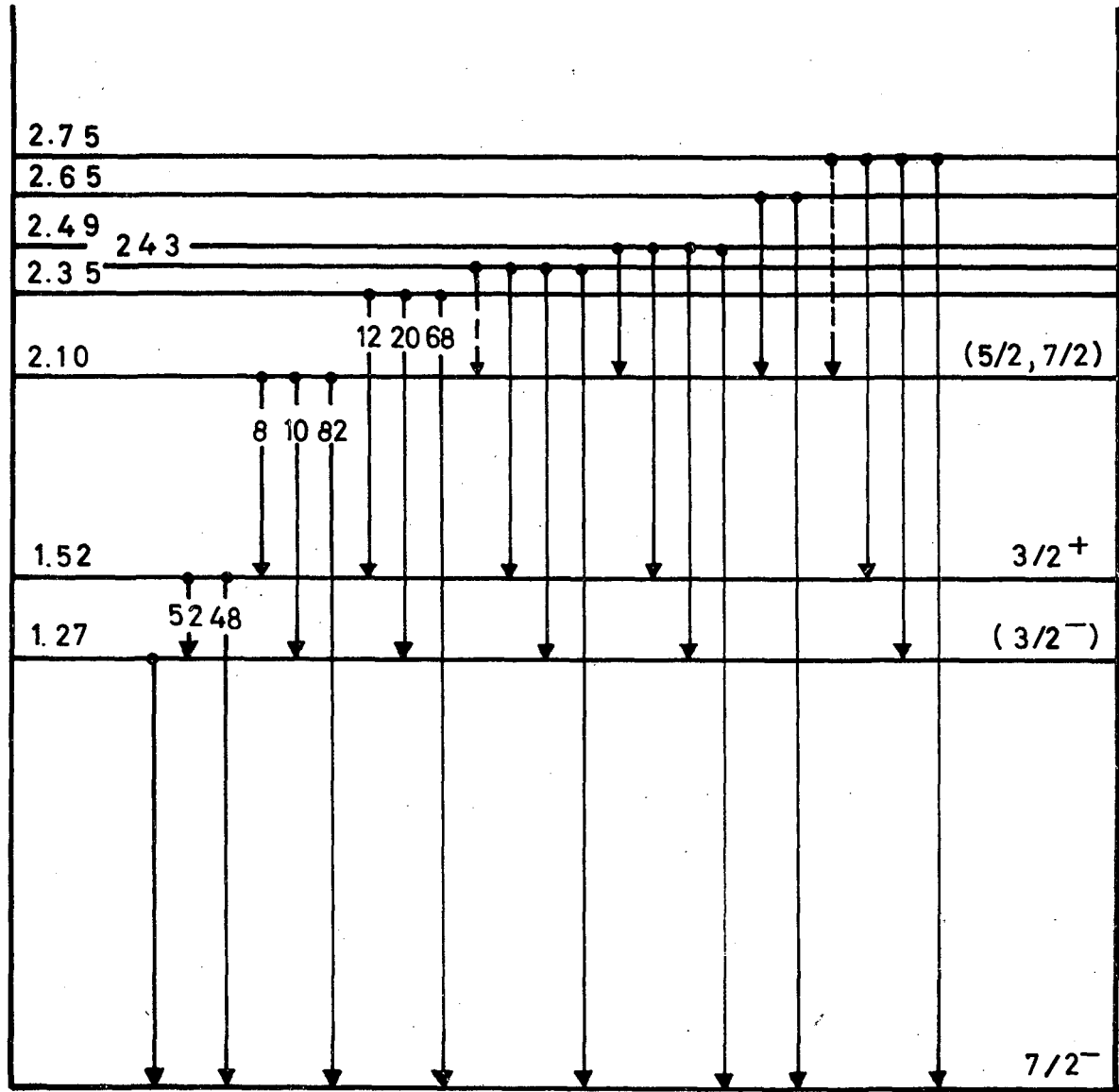


Fig. 1.2.

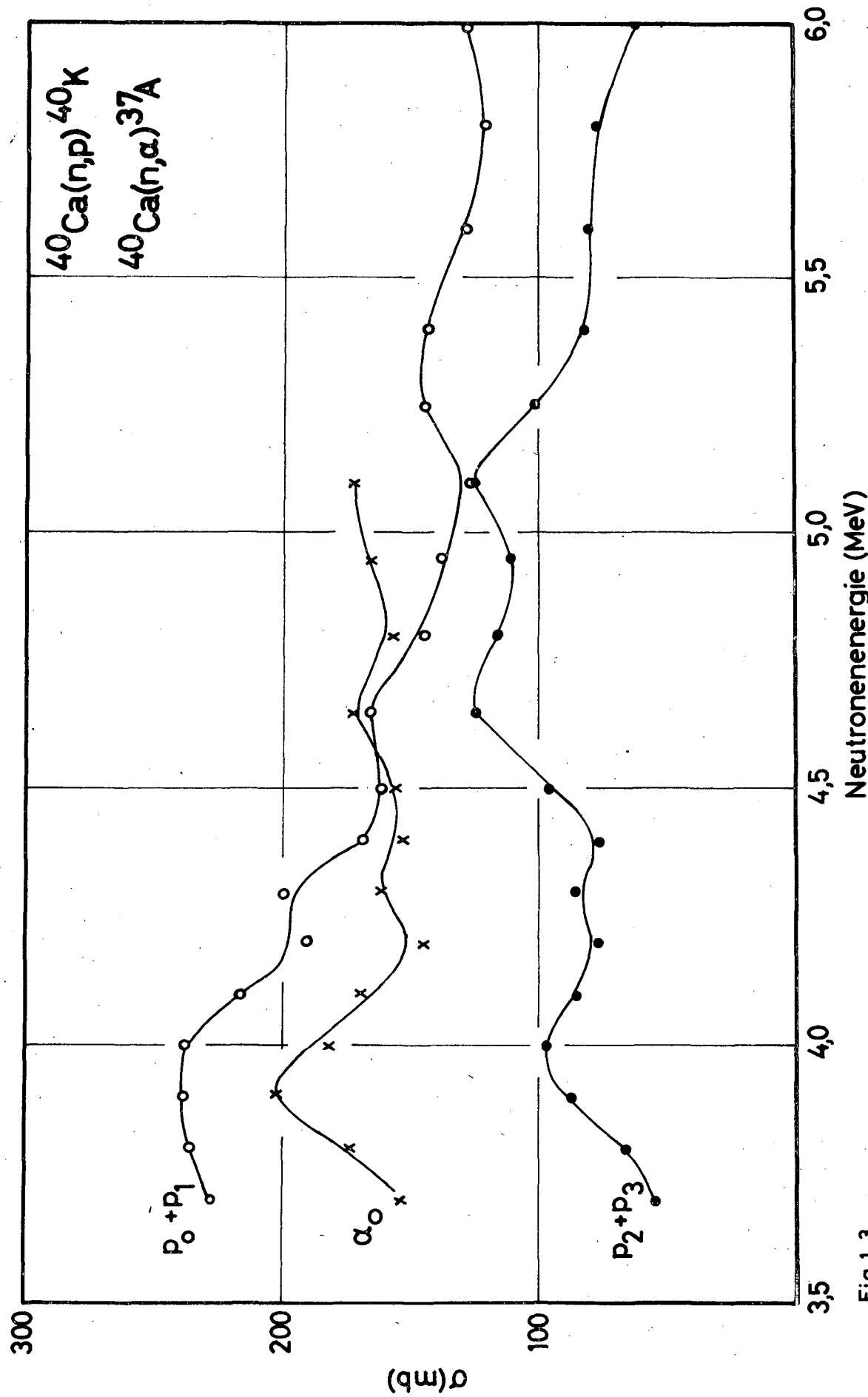


Fig. 1.3.

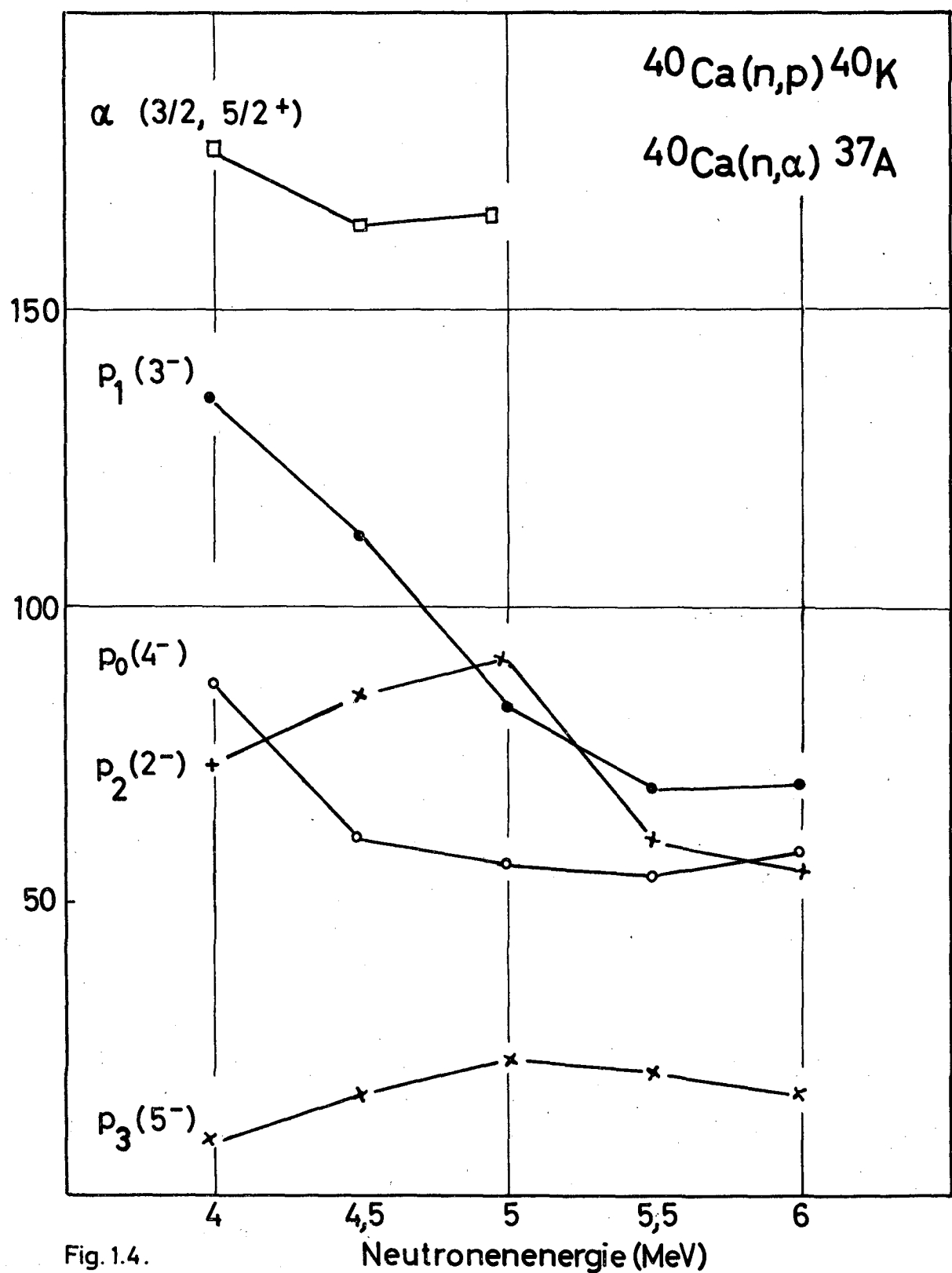


Fig. 1.4.

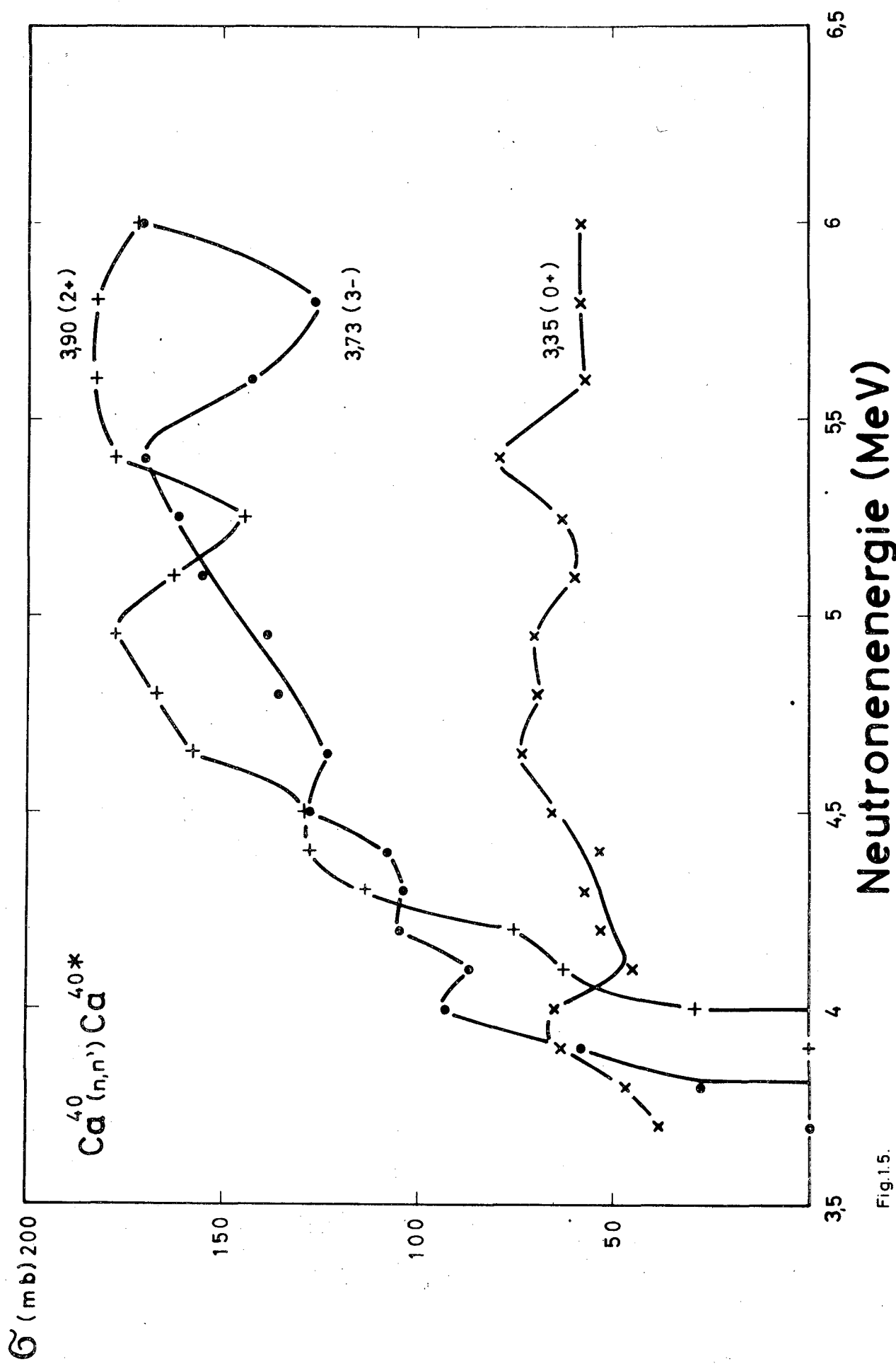


Fig.1.5.

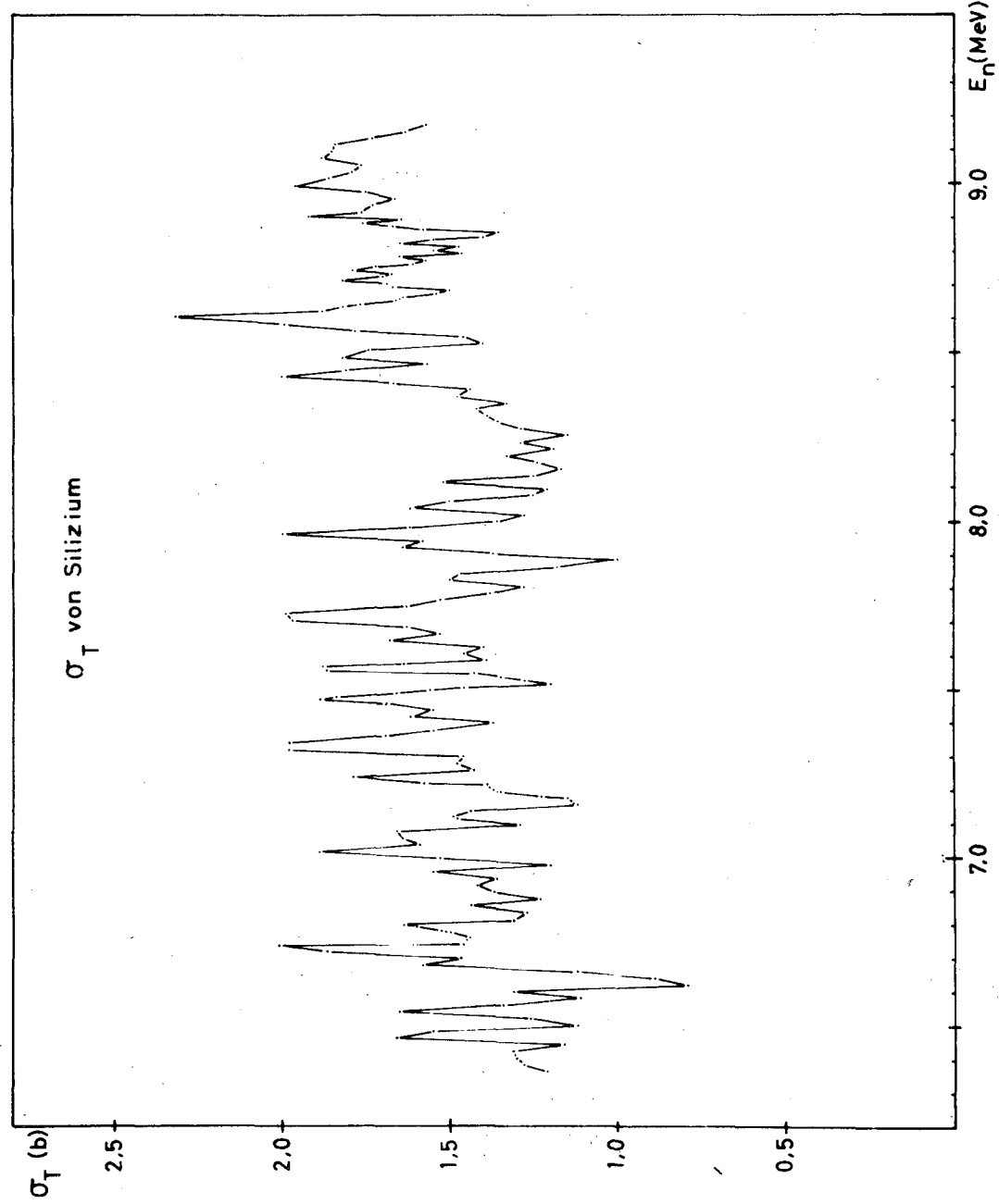


Fig. 1.6.

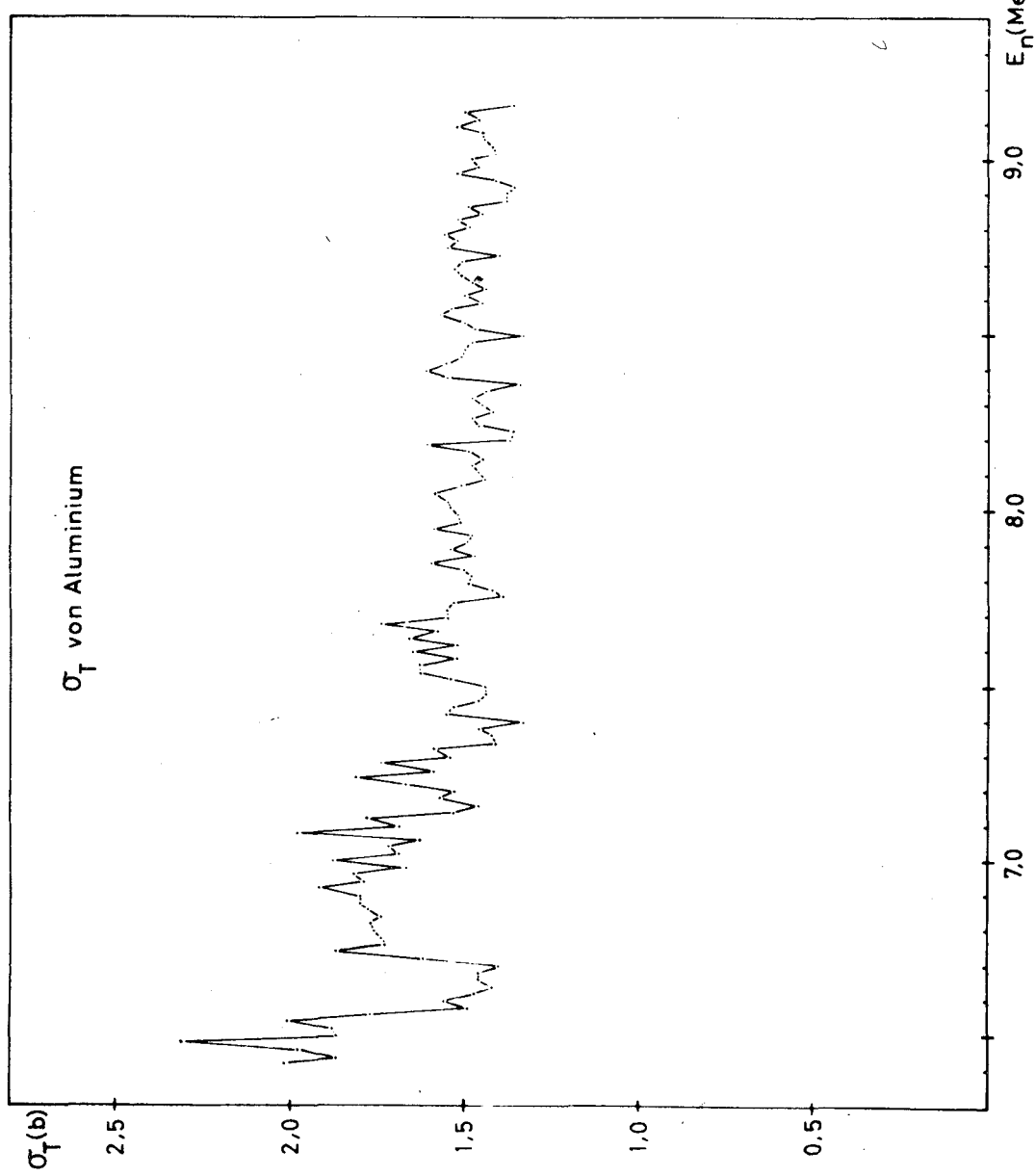


Fig. 1.7.

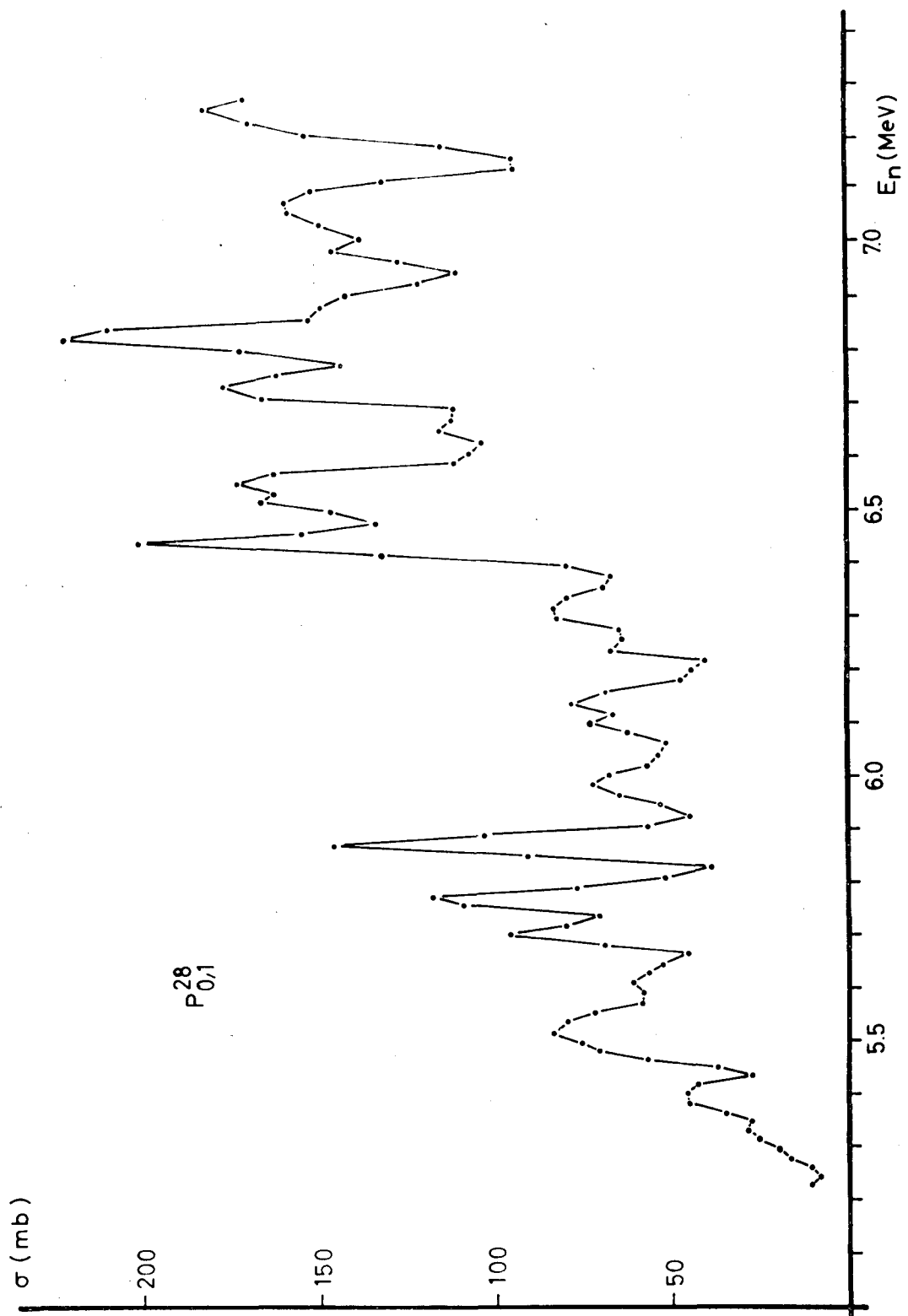


Fig.1.8.

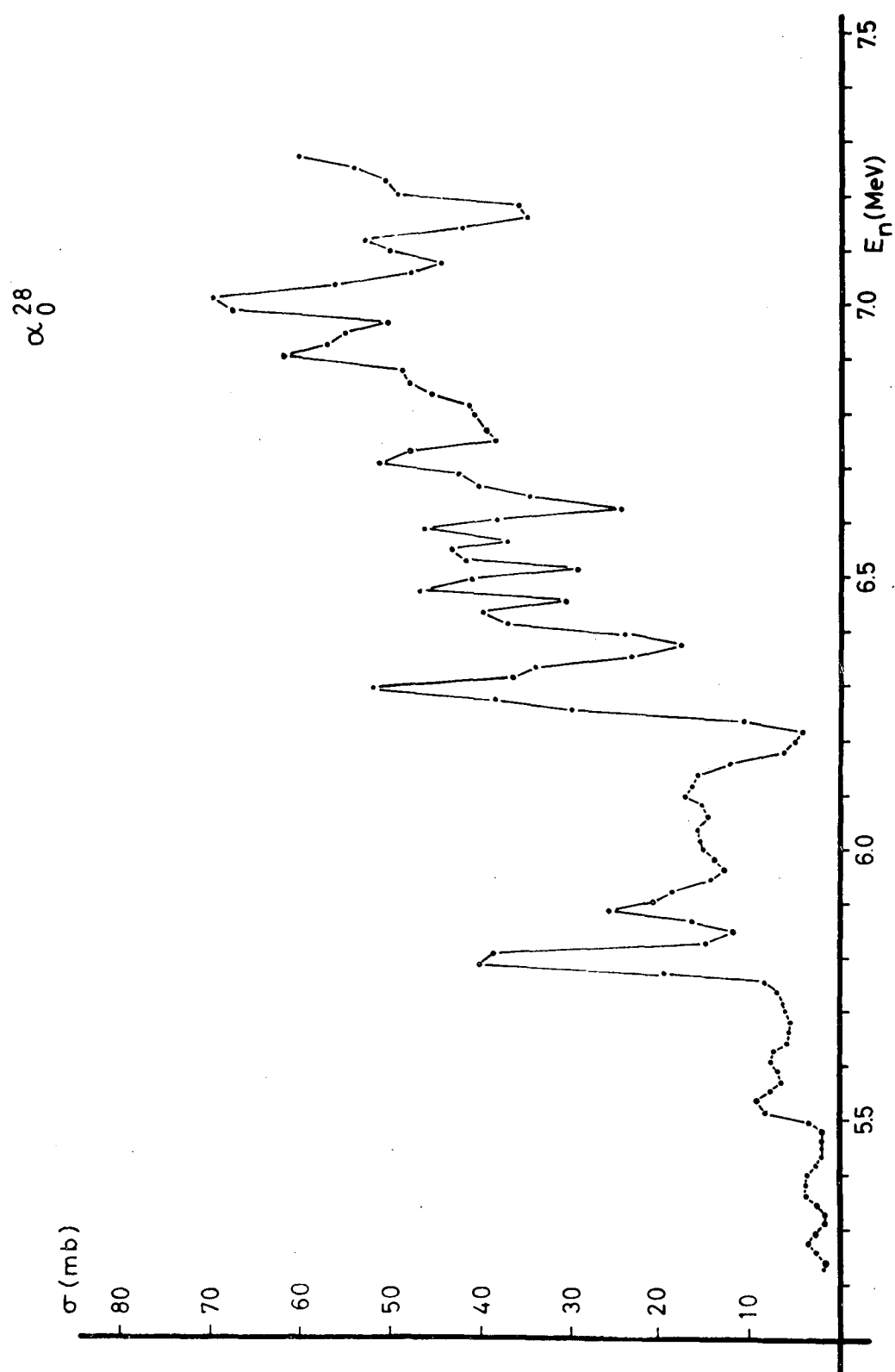


Fig. 1.9.

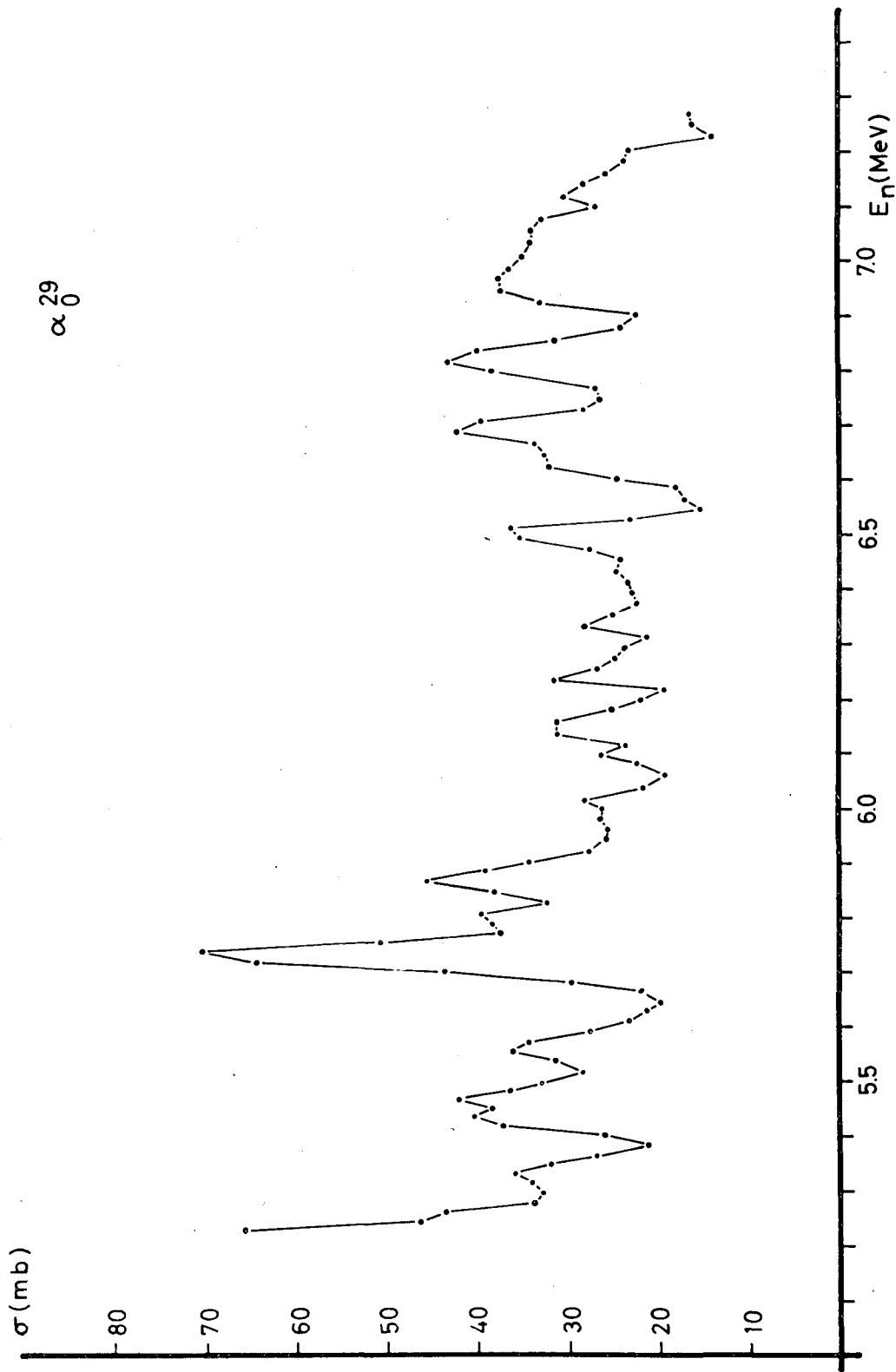


Fig. 1.10.

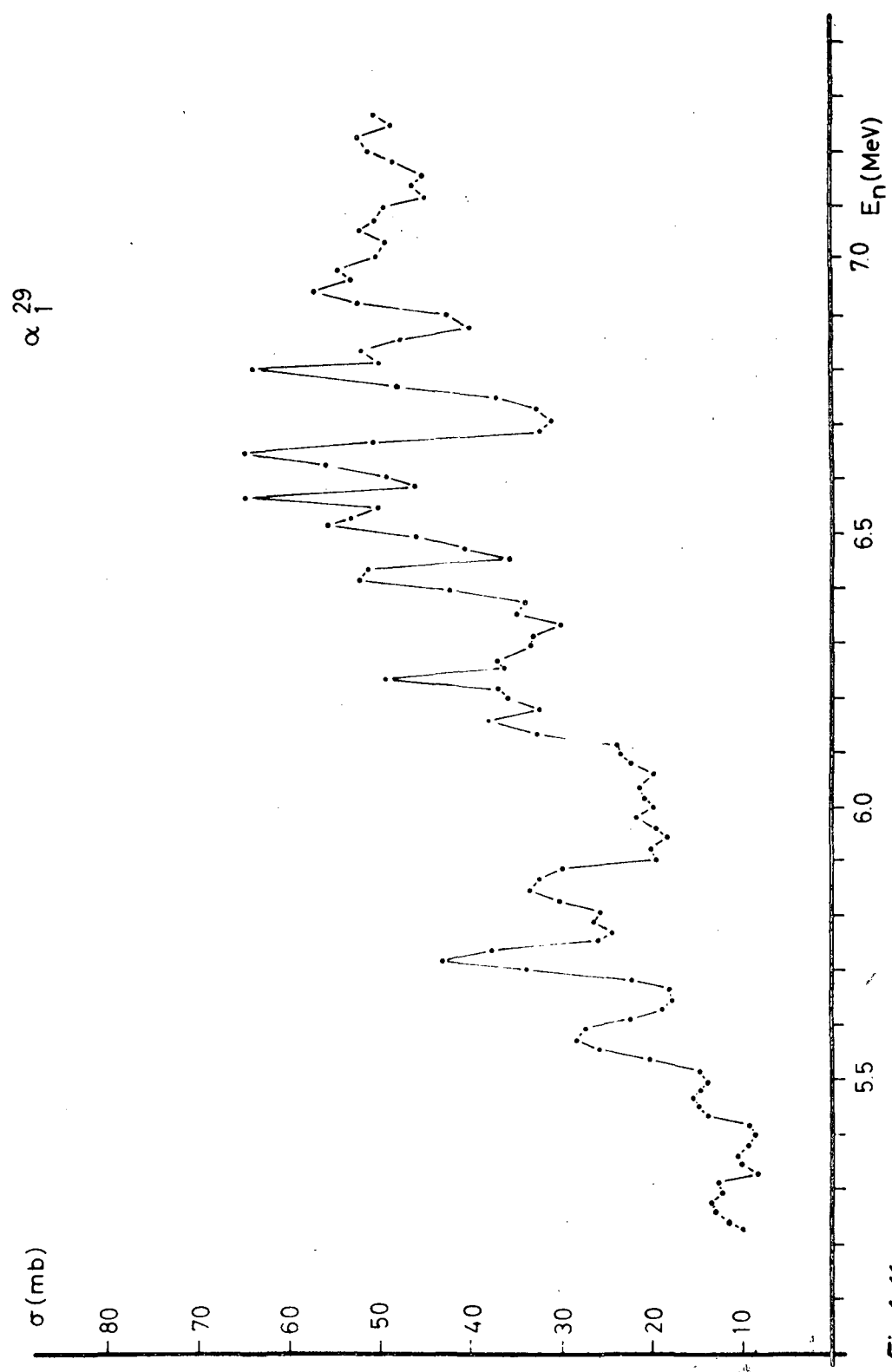


Fig.1.11.

2. PHYSIKALISCHES STAATSINSTITUT, I. INSTITUT FUR EXPERIMENTAL PHYSIK, HAMBURG (Germany)

2.1. Activation Cross-Sections of some Neutron-Induced Reactions in the Energy Range 12.5 - 19.6 MeV

(M.Bormann, F.Dreyer, E.Fretwurst and P.Schekha)

Cross-sections of neutron-induced reactions were determined for some elements at 14.1 MeV as well as in the energy range 12.5 - 19.6 MeV using the activation method. Gamma activities were measured by means of a NaI well-crystal. In some cases where the product nuclei decayed by positron emission the gamma quanta from the positron annihilation were detected with a coincidence spectrometer consisting of two NaI-crystals.

Neutrons were produced by the reaction $H^3(d,n)He^4$ in titanium-tritium targets with the 150 keV and the 3 MeV deuteron beam of a Cockroft-Walton and a Van de Graaff generator, respectively. The neutron flux was measured by recoil proton counting in a stilbene crystal using the pulse-shape discrimination method in order to separate recoil protons from gamma radiation. The results are given in table 2.1. and 2.2. The stated errors do not include uncertainties in the decay schemes.

Table 2.1. Cross-sections at 14.1 MeV

<u>Reaction</u>	<u>Cross - section (mb)</u>
$Ni^{58}(n,p)Co^{58}$	411 \pm 22
$Ni^{58}(n,2n)Ni^{57}$	22.7 \pm 1.2
$Co^{59}(n,\alpha)Mn^{56}$	27 \pm 1.5
$Co^{59}(n,2n)Co^{58}$	642 \pm 32
$Co^{59}(n,2n)Co^{58g}$	195 \pm 53
$Co^{59}(n,2n)Co^{58m}$	447 \pm 42

2.2. Energy and Angular Distributions of the Alpha Particles from
14.1 MeV Neutron Reactions in Al²⁷ and Ni⁵⁸.
(U.Seebeck, M.Bormann)

A chamber with one CsI(Tl)-scintillation counter has been constructed for the investigation of fast neutron reactions in which charged particles are emitted. For distinguishing different types of radiation the pulse-shape discrimination method was applied. In angular distribution measurements the targets are successively set up at different places around the crystal the position of which relative to the neutron source is fixed. The energy and angular distributions of the alpha particles from 14.1 MeV neutron reactions in Al²⁷ and Ni⁵⁸ have been measured. The results obtained are in agreement with the statistical theory of Weisskopf and Ewing. The alpha particles from Al²⁷ can be attributed entirely to the reaction Al²⁷(n, α)Na²⁴ for which a total cross-section of 119 ± 10 mb was measured. The total alpha particle yield from Ni⁵⁸ is the sum of the contributions from the reactions Ni⁵⁸(n, α)Fe⁵⁵, Ni⁵⁸(n,an')Fe⁵⁴ and Ni⁵⁸(n,n' α)Fe⁵⁴. The portion of alpha particles from the latter reaction is separated by means of the statistical theory analysis of the data. A cross-section of 30 ± 6 mb has been obtained for this process. For the sum of the first two reactions a cross-section of 125 ± 16 mb was determined. From energy considerations it follows that at least 90% of this cross-section can be attributed to the reaction Ni⁵⁸(n, α)Fe⁵⁵.

Table 2.2. Cross-sections in the energy range 12.5 - 19.6 MeV

Cross-sections (mb)

Neutron Energy (MeV)	$F^{19}(n,2n)_{F^{18}}$	$K^{39}(n,2n)_{K^{38}}$	$Ti^{46}(n,2n)_{Ti^{45}}$	$Ga^{69}(n,2n)_{Ga^{68}}$	$E^{19}(n,p)_{O^{19}}$	$Ti^{46}(n,p)_{Sc^{46}}$	$Ti^{48}(n,p)_{Sc^{48}}$	$Mn^{55}(n,\alpha)_{V^{52}}$
12.5+0.2	13.4+1.2	---	---	---	26.4+2.3	250+31	50.8+5.5	---
12.6+0.2	---	---	---	660+64	26.4+2.3	251+31	61.5+6.4	29.2+2.1
13.0+0.2	25.7+2.2	---	---	688+66	23.5+2.0	---	---	---
13.2+0.2	41.0+0.3	41.0+0.3	2.7+0.2	14+1	925+75	19.9+1.3	257+17	33.4+2.4
14.0+0.3	14.1+0.3	14.6+0.2	1.2+0.9	69.5+8	994+81	---	62.8+4.8	32.6+1.7
14.8+0.2	6.0+0.3	6.0+0.3	6.1+0.6	1004+96	17.3+1.5	17+30	64.0+6.7	35.4+2.6
15.0+0.3	15.2+0.3	60.2+5.2	9.6+0.8	137+17	1143+110	15.7+1.4	55.6+5.8	34.4+2.5
15.8+0.3	68.7+5.9	68.7+5.9	68.7+5.9	1204+115	1204+115	234+28	---	---
16.0+0.3	16.5+0.3	16.7+0.3	15.3+1.2	173+22	173+22	222+27	51.2+5.3	33.7+2.4
17.0+0.3	78.8+6.8	78.8+6.8	78.8+6.8	78.8+6.8	78.8+6.8	15.8+1.4	---	---
17.1+0.3	---	---	---	1169+112	1169+112	---	---	29.1+2.1
17.4+0.3	---	---	---	1286+123	1286+123	14.3+1.3	48.3+5.0	---
17.5+0.3	86.5+7.4	86.5+7.4	202+25	202+25	202+25	---	48.3+5.0	27.8+2.0
17.8+0.3	18.0+0.3	18.1+0.3	21.4+1.6	21.4+1.6	21.4+1.6	---	---	---
18.0+0.3	18.2+0.2	18.5+0.3	94.5+8.2	94.5+8.2	94.5+8.2	---	44.8+4.7	---
18.6+0.3	18.7+0.2	18.7+0.2	213+26	213+26	213+26	---	---	24.7+1.8
18.9+0.2	97.7+8.4	97.7+8.4	23.8+1.7	23.8+1.7	23.8+1.7	---	---	22.7+1.6
19.4+0.1	19.6+0.1	91.9+7.9	214+26	214+26	214+26	11.3+1.0	10.9+0.9	---
19.6+0.1	19.6+0.1	91.9+7.9	---	---	---	33.0+0.0	33.0+0.0	---

2.3. Total Neutron Cross-Section of Copper in the Energy Range

4.2 - 6.2 MeV.

(H.Genz, H.Bormann)

The total neutron cross-section of natural copper was measured in the energy range 4.2 - 6.2 MeV by means of the transmission method. Monoenergetic neutrons were obtained via the reaction $H^2(d,n)He^3$ using a gas target and the deuteron beam of a 3MeV Van de Graaff. For neutron detection a Stilbene recoil proton spectrometer was used. Its gamma-sensitivity was reduced by pulse-shape discrimination. The transmission data were corrected for neutrons elastically scattered in forward direction. The results are given in table 2.3. The neutron energy resolution is $\Delta E_n = 30$ keV. The errors of the cross-sections amount to $\Delta \sigma = \pm 3\%$.

Table 2.3. Cross-Section in the energy range
4.2. - 6.2 MeV.

E_n (MeV)	σ_j (barn)	E_n (MeV)	σ_T (barn)
4.16	3.46	5.15	3.69
4.21	3.52	5.20	3.68
4.25	3.60	5.25	3.68
4.29	3.51	5.30	3.63
4.34	3.52	5.35	3.70
4.38	3.52	5.40	3.73
4.43	3.52	5.46	3.68
4.48	3.56	5.52	3.71
4.53	3.59	5.57	3.71
4.58	3.61	5.62	3.68
4.62	3.58	5.67	3.70
4.67	3.62	5.72	3.75
4.72	3.57	5.77	3.67
4.77	3.63	5.83	3.65
4.81	3.64	5.88	3.70
4.86	3.61	5.93	3.69
4.91	3.66	5.99	3.65
4.96	3.61	6.04	3.68
5.01	3.65	6.11	3.67
5.05	3.68	6.16	3.71
5.10	3.71	6.22	3.65

3. LABORATORIUM FUR TECHNISCHE PHYSIK DER T.H. MUNCHEN (Germany)

3.1. Neutron Beam Experiments.

3.1.1. Determination of σ_{free}

(W.Triftshäuser, P.Fehsenfeld)

With a neutron energy spectrum (average neutron wave-length 0.09 Å) received with a filter-difference method the free atom neutron cross-section of various materials has been measured. The filter materials used are Boron-10, Rhodium, Cadmium, Manganese and Cobalt. The results of σ_{free} obtained with this method are 1.4083 ± 0.0011 barn for Aluminium and 9.2889 ± 0.0076 barn for Bismuth. Corrections for absorption, spin incoherent scattering, Doppler effect, atomic binding forces etc. have been made to obtain the coherent cross-section. These values are 1.5040 ± 0.0015 barn and 9.3489 ± 0.0077 barn for Aluminium and Bismuth, respectively. A schematic drawing of the apparatus used is given in Fig. 3.1. A more precise description will be published in 1965.

With the apparatus described above the scattering cross-sections of graphite and polystyrene have been determined. The values found are

	H	C
$E = 33,9 \text{ eV}$	$\sigma_{sf} = (20.578 \pm 0.013) \text{ barn}$	$\sigma_s = (4.743 \pm 0.002) \text{ barn}$
$E = 61,1 \text{ eV}$	$\sigma_s = (20.350 \pm 0.012) \text{ barn}$	$\sigma_s = (4.7264 \pm 0.0024) \text{ barn}$

These measurements have been performed to get a better information about the neutron-proton-interaction. The application will be discussed in detail in a publication next year.

3.1.2. Determination of Coherent Cross-Sections

(L.Koester, W.Nücker)

For absolute measurements of coherent scattering cross-sections a neutron refractometer ⁽¹⁾ has been installed. In this instrument neutrons hit a mirror after having passed through a 100 m flight path where they have been deflected by gravity. (See Fig. 3.2.) The accuracy of coherent scattering lengths measurements is of the order of 10^{-3} .

(1) Maier-Leibnitz H., Z. angew.Physik 14, 738 (1962).

The reactor spectrum has been measured in the region 170 to 800 m/s and by reflection on a mercury mirror the coherent scattering length has been determined as $a_{coh} = +(12.69 \pm 0.02) \cdot 10^{-13}$ cm (2).

Under investigation are measurements with molten metals and liquids.

3.1.3. Determination of Incoherent Cross-Sections

(P.Niklaus, R.Simson, W.Schmatz)

By scattering of long wave length neutrons incoherent cross-sections will be measured at the total reflecting tube. The experimental facility is described by Christ and Springer (3) and the method by Scherm and Schmatz (4) who have already measured the incoherent cross-section of Be, Al, and Bi by an other experimental facility (4).

Beryllium $\sigma_{inc} = 4 \pm 1$ mbarn

Aluminium $\sigma_{inc} = 10 \pm 1$ mbarn

Bismuth $\sigma_{inc} = 12 \pm 1$ mbarn.

With a new helium cryostat preliminary results have been obtained. The incoherent cross-section of Si is smaller than 45 mbarn, and of Pb smaller than 70 mbarn.

3.1.4. Total cross-sections of rare earth elements

(A.Knorr)

Using a mechanical velocity-selector, total cross-sections of rare earths for subthermal neutrons (45 ± 30 Å) are being determined. The measured values with estimated errors are given in table 3.1. and fig. 3.3. Metal foils of 226 mg/cm^2 (Ho) and of 406 mg/cm^2 (Tb) with a specified purity of 99% were used. The specific energy of the neutrons was found by comparison with cross-sections of Au-foils ($1/v$ extrapolation from 98.8 b for 25 meV).

(2) Koester L, Z. Physik, in press.

(3) Christ J., Springer T., Nukleonik 4, 23 (1962).

(4) Scherm R., Schmatz W., Z. Naturforschung 19a, 354 (1964)

Table 3.1. Cross-sections of Ho and Tb

E _{MeV}	error	$\bar{\lambda}$ Å	Ho		Tb	
			σ_{barn}	error	σ_{barn}	error
2.38	$\pm 1.5\%$	5.86	271.2	$\pm 1\%$	131.6	$\pm 1\%$
1.88	"	6.59	316.2	"	146.1	"
1.43	"	7.56	341.3	"	160.0	"
1.096	"	8.65	382.9	"	180.1	"
0.768	"	10.32	451.1	"	209.8	"
0.580	"	11.87	513.2	"	240.1	"
0.350	$\pm 6\%$	15.3	659.6	$\pm 4\%$	313.8	$\pm 4\%$
0.222	$\pm 6\%$	19.2	819.8	$\pm 4\%$	393.3	$\pm 4\%$

3.1.5. Determination of the diffusion constants of H_2O , phenyls, $ZrH_{1.92}$ and D_2O by neutron single-scattering experiments.

(T.Springer*, Ch. Hofmeyer, S.Kornbichler, H.D.Lemmel)

From measurements of the differential scattering cross-section $d\sigma(\theta)/d\Omega$ with a thick Li⁶I-counter for various neutron energies E and sample temperatures T_m, the average cosine of the scattering angle $\bar{\cos}\theta$, the diffusion constant D(E, T_m), and its thermal average $\langle Dv \rangle T_m$ was calculated. The latter quantity can be compared with the results of time- and space-relaxation experiments. Investigations were performed on the most important hydrogeneous moderators and on D_2O (ref. also EANDC-Report (E) 49 "L" Oct. 1963).

It was found that the scattering cross-sections $d\sigma/d\Omega$ are not very sensitive to the temperature. Therefore, the quantity $\langle Dv \rangle T_m$ can easily be evaluated within a large temperature range by means of a comparatively small number of $d\sigma/d\Omega$ -measurements. Rather strong coherence maxima have been observed in D_2O and also in the phenyl- and $ZrH_{1.92}$ -curves. Good agreement was obtained between our $\langle Dv \rangle T_m$ -data and the results of relaxation experiments both with light and heavy water. There was also good agreement with theoretical predictions for H_2O , D_2O , and reasonable agreement with calculations for $ZrH_{1.92}$.

* now at Kernforschungsanlage, Jülich.

For diphenyl, there was agreement with some of the relaxation experiments cited in literature. The consistency of the results shows that our thermal diffusion parameters $\langle D_v \rangle T_m$ as a function of T_m and the diffusion constant D as a function of E can be considered as reliable for one- or multigroup-calculations, respectively. Some results are shown in the figures 3.4. to 3.14.

A detailed description of all experiments will be published in "Nukleonik" (1965), a short review has been presented at Geneva 1964, paper 28/P/763.

3.2. Fission Physics

A survey of the work done in fission physics was given by Maier-Leibnitz at the International Conference on Nuclear Physics with Reactor Neutron (Argonne Oct. 1963) (5). Two special papers were presented at the Conference, too, (6) (7). Therefore only the summary of a newer publication will be mentioned and two experiments with the mass spectrometer.

3.2.1. Determination of the mean Primary Charge of U^{235} Fission Products.

(P. Armbruster, D. Hovestadt, H. Meister, H. J. Specht, Nucl. Phys. 54, 586-614 (1964))

Measurements of the mean primary charge for U^{235} fission products have been made using three different methods. The measured primary charge values are compared to those obtained from radiochemical results and to theoretical predictions describing asymmetric fission. A strong discrepancy with the radiochemical results has been found. The mass dependence of the mean primary charge may be understood by assuming an influence of closed nucleon shells in the late stage of the fission process.

(5) H. Maier-Leibnitz, Experiments on Fission Using Thermal Neutrons, Proceeding of the Int. Conf. on Nuclear Physics with Reactor Neutrons, edited by F. E. Throw, ANL 6797-1963 p. 424

(6) D. Hovestadt, P. Armbruster, New Method for the Detection of Shortlived Fission Products ibid. p. 455

(7) P. Armbruster, H. Specht, A. Vollmer, Investigation of Quasi-Adiabatic Atomic Collisions by Fission Products ibid. p. 464.

3.2.2. Measurement of Mass Distribution and Nuclear Charge Distribution of single Mass Chains of Fission Fragments from Thermal Fission of U²³⁵.

(E.Konecny, H.Opower)

The high resolution fission particle mass spectrometer of Mattauch-Herzog type, constructed by Ewald et al. (8) (9) was used to determine fine structure of mass distribution after emission of prompt neutrons in the low mass region of the heavy fragment group. Results show a peak at A=134 and a dip at A=137 (9), (10) suggesting that the peak is caused by a variation in the emission of prompt neutrons.

The distribution of mass separated fission fragments of A=132, 134, 136, and 137 was investigated by catching the fragments in β -sensitive emulsions in the focal plane of the spectrometer. Development of the irradiated emulsions is carried out after a time long compared with the half life of the regarded decay chain. After development of the emulsions all betatracks emerging from the end of every fission fragment track can be seen under the microscope. The possibility of correlating every single β -track to a certain fission fragment track allows the evaluation of the number n(x) of fission fragments possessing x β -tracks and thus gives not only the mean chain length but also the β -particle distribution. As the stable end product of each decay chain is known, this β -distribution is an exact image of the primary nuclear charge distribution. The most probable charges for A=132, 134, 136, and 137 are 50.0, 52.0, 52.9, and 53.2, respectively thus exhibiting the influence of neutron shell N=82 in masses 132 and 134. These data will be published (11).

(8) H.Ewald, E.Konecny, H.Opower, H.Rösler, Z. Naturforschg. 19a, 194 (1964)

(9) E.Konecny, H.Opower, H.Ewald, Z.Naturforschg. 19a, 200 (1964)

(10) H.Maier-Leibnitz in International Conference on Nuclear Physics with Reactor Neutrons, Argonne 1963, ANL-6797, p.424

(11) E.Konecny, H.Opower, H.Gunther, H.Göbel in Proceedings of the Symposium on the Physics and Chemistry of Fission, Salzburg 1965, paper SM-60/33

3.2.3. Distribution of Ionic Charge of Fission Fragments Dependent on their Kinetic Energy

(H. Opower, E. Konecny, G. Siegert)

By means of the fission particle mass spectrograph the ionic charge distribution of U-235 fission fragments as a function of their kinetic energy was investigated and compared with a theory of Knipp and Teller. Results are published in Z. Naturforschg. 20a, Jan. 1965.

3.3. Measurement of Internal Conversion Electrons Following Neutron Capture

(T.v. Egidy, E. Bieber, Th. Elze, W. Nörenberg)

With a betaspectrometer for conversion electrons following neutron capture at the FRM reactor (12, 13) some isotopes were investigated. The energy and intensity of the conversion electron lines were measured and the multipolarity of the transitions determined. The best resolution of the spectrometer is 0.07 %. Most of the measurements are made with a resolution 0.2 %.

3.3.1. Gd 156, Gd 158 (14)

The spectrum of natural Gadolinium was measured between 30 and 90 keV. The 79.51 keV line of Gd 158 is a E2 transition, the 88.97 keV line of Gd 156 is a E2 transition, too.

3.3.2. Rh 104 (15)

70 conversion lines were found in the energy region between 30 and 1500 keV. Combination of these results gave the following levels with spins and parities of Rh 104:
51.42 (2-), 97.11 (2+), 128.97 (5+), 180.85 (1,2+),
186.04 (1,2-), 197.91 (1,2+), 213.06 (1,2+), 220.81 (1,2,3+),
224.44, 266.79, 269.30, 286.13, 358.66, 359.68, 371.06,
384.95, 420.8, 426.4, 468.6, 482.2, 509.1, 524.5, 524.7,
537.7, 644.4, 830.5 (keV).

3.3.3. Tm 170 (16)

The conversion electron spectrum of Tm 170 revealed 58 lines from 30 to 800 keV. The following transition energies and multipolarities were found: 38.71 keV E2, 63.96 E2, 75.83 E2+M1, 87.54 M1, 92.65 E2+M1, 105.17 E2+M1, 114.54 E2, 130.03 E2+M1, 144.48 E1, 149.72 M1, 161.73 M1, 165.74 M1, 181.00 M1+E2, 204.45 M1+E2, 219.68 E2, 231.59 E2, 235.18 M1, 237.25 M1, 242.63 E2, 311.07 E2, 384.17 E2, 411.45 E2, 446.25 E2, 456.0 M1, 505.7 M1, 512.22 E2.

3.3.4. Ho 166 (17)

43 conversion electron lines were measured between 30 and 550 keV. Multipolarity of the following transitions were determined:

54.24 keV E2, 69.76 M1, 72.89 E2, 82.47 M1, 87.59 M1, 98.86 M1, 105.52 M1, 108.20 M1+E2, 111.32 M1, 116.83 M1, 126.23 M1+E2, 136.66 E1, 140.12 M1, 149.31 M1, 175.03 E2, 180.54 M1+E2, 181.09 E1, 197.34 E2, 199.71 E1, 221.17 E1, 232.29 E1, 233.1 E1, 239.1 E1, 290.6 E1, 304.6 E1, 333.6 E1.

3.3.5. Sm 150 (18)

Between 5 MeV and 8 MeV 20 internal conversions electron lines were found. At this energy region the conversion coefficient is only about $3 \cdot 10^{-5}$. Conversion electrons to the following transitions were measured:

5.125 MeV, 5.168, 5.232, 5.275, 5.3, 5.412, 5.485, 5.526, 5.609, 5.648, 5.721, 5.923, 5.958, 6.013, 6.532, 7.210, 7.649.

- (12) T.v.Egidy, Ann.Physik (Lpz), 7.F,9,221 (1962)
- (13) E. Bieber, T.v.Egidy, O.W.B. Schult, Z.Physik 170,465 (1962)
- (14) W. Nörenberg, Z. angew. Physik 17, 452 (1964)
- (15) E. Bieber, Dissertation T.H. München 1965, to be published 1965
- (16) T.v.Egidy, Th.Elze, E. Bieber, to be published together with O.W.B. Schult e.a. 1965
- (17) T.v.Egidy, Th. Elze, E. Bieber, to be published together with O.W.B. Schult e.a. 1965
- (18) Th. Elze, T.v.Egidy, E. Bieber, to be published Z.Physik 1965

3.4. Measurements of Activation Cross Sections

During 1963 and 1964 some measurements of activation cross sections were done, mostly on request or because of discrepancies in current literature.

3.4.1. Thermal Activation Cross Section for $A^{40}(n,\gamma)A^{41}$

(W. Köhler, Z.Naturforsch. 18a, 1339 (1963))

Natural argon (99.6 % A^{40}) was sealed in quartz-tubes and irradiated simultaneously with gold wires on a rotating disk in the water reflector of the reactor. The A^{41} - and the Au^{198} - activity was measured by a calibrated γ -counter. With $\sigma_0 = 98.8$ barn for gold the value $\sigma_0 = 0.63 \pm 0.02$ barn was determined. This result is in good agreement with absorption cross section, whereas the older activation cross section (0.53 barn) was not.

3.4.2. Epithermal Activation Resonance Integral Cross Section for $Ag^{109}(n,\gamma)Ag^{110m}$

(F. Lux, Institut für Radiochemie and W. Köhler, to be published in 1965)

For a radiochemical determination of Ag in Cd the epithermal activation integral cross section was needed. In the current literature there were only values of the epithermal absorption and of the activation integral for the ground state of Ag^{110} ($T_{1/2} = 24$ s).

By simultaneous irradiation of samples with and without Cd-covers on the above mentioned rotating disk with gold as reference material a ratio of

$$I/\sigma_0 = 14.8 \pm 0.8 \text{ was obtained}$$

$$I = \int_{0.55 \text{ eV}} \sigma'(E) \frac{dE}{E}$$

$$I_{Au^{198}} = 1549 \text{ barn.}$$

Gold and silver have nearly the same energy dependence of the cross section near the Cd cut-off energy and a large resonance at higher energies. Therefore no correction was necessary to obtain the value of I from the measured activation integrals.

With $\sigma_0 = 3.2 \pm 0.4$ barn (BNL 325) $I = 47.5 \pm 6.6$ barn was obtained. With that value the epithermal isomeric ratio is 0.041 ± 0.006 , the ratio for thermal neutrons is 0.035 ± 0.005 .

3.4.3. Averaged Cross-Sections for Fast Neutrons (W. Köhler, K. Knopf)

Measurements of the integral fast neutron flux density were often performed with titanium detectors, but the cross sections for the $Ti^{46}(n,p) Sc^{46}$ reaction are in the literature between 8 and 14mbarn. Titanium foils were irradiated together with inorganic sulfur compounds, which could be easily dissolved in water. The Sc^{46} was counted by $4\pi\beta-\gamma$ -coincidence, the P^{32} by $4\pi\beta$ -technique.

In the solution a P^{33} -activity of nearly 3% of the P^{32} activity was determined by β -absorption measurements (W. Köhler, K. Knopf, FRM-Report 1965). This is contradiction to literature, as for the (n,p) reaction of S^{33} a cross section of $\sigma_0 = 15 \pm 10$ mb is quoted in BNL 325 (for thermal neutrons). The percentage of P^{33} was the same with Cd- and without Cd-cover, and much higher than the calculated one.

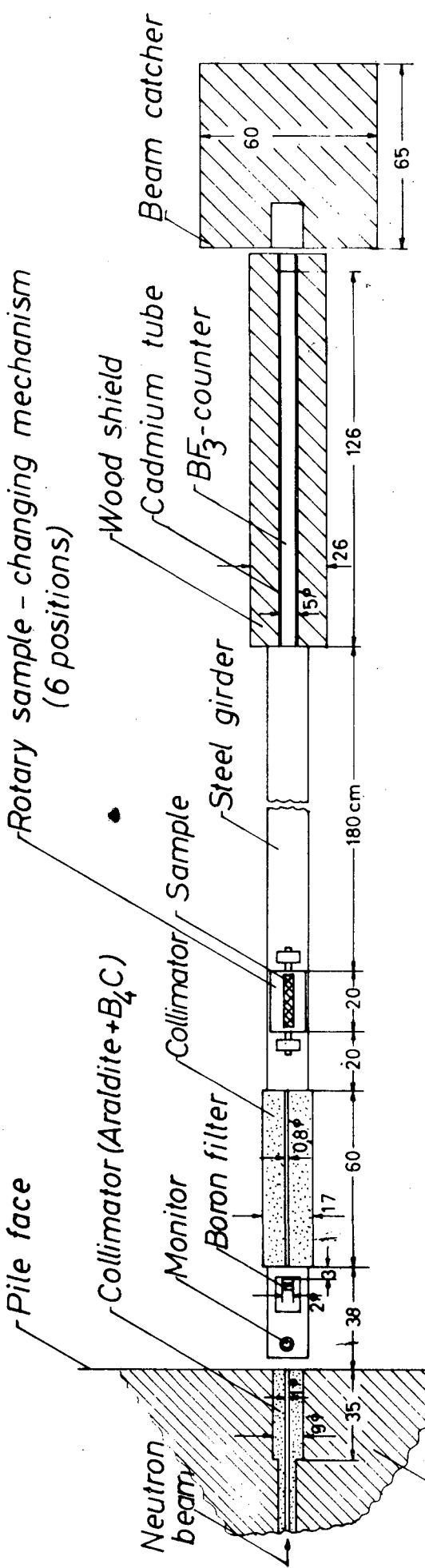
The cross sections of this reaction and the (n,p) reactions of titanium averaged over the flux density distribution $\langle\phi\rangle$, were determined relative to the $S^{32}(n,p) P^{32}$ reaction. As reference cross section for this reaction the cross section averaged over the energy distribution of fission neutrons was used ($\langle\phi\rangle = \bar{\sigma}_{fission}$). Results are given in table 3.2.

Table 3.2.: Averaged cross-sections

Reaction	$\langle \sigma \rangle$
$S^{32} (n,p) P^{32}$	66 mb (reference)
$S^{33} (n,p) P^{33}$	376 ± 20 mb
$Ti^{46} (n,p) Sc^{46}$	12.6 ± 0.4 mb
$Ti^{47} (n,p) Sc^{47}$	13.2 ± 1.0 mb
$Ti^{48} (n,p) Sc^{48}$	3.3 ± 0.2 mb.

The $\langle \sigma \rangle$ of the $Ti_{th}^{46}(n,p)$ reaction is in agreement with the cross sections found in the literature.

Activation resonance integral cross sections and averaged cross sections of (n,n') , (n,p) and (n,α) reactions of other elements are under investigation by H. Schmelz, Le Voha and G. Rau.



Schematic drawing of the apparatus for the measurement of σ_{free}

Fig. 3.1.

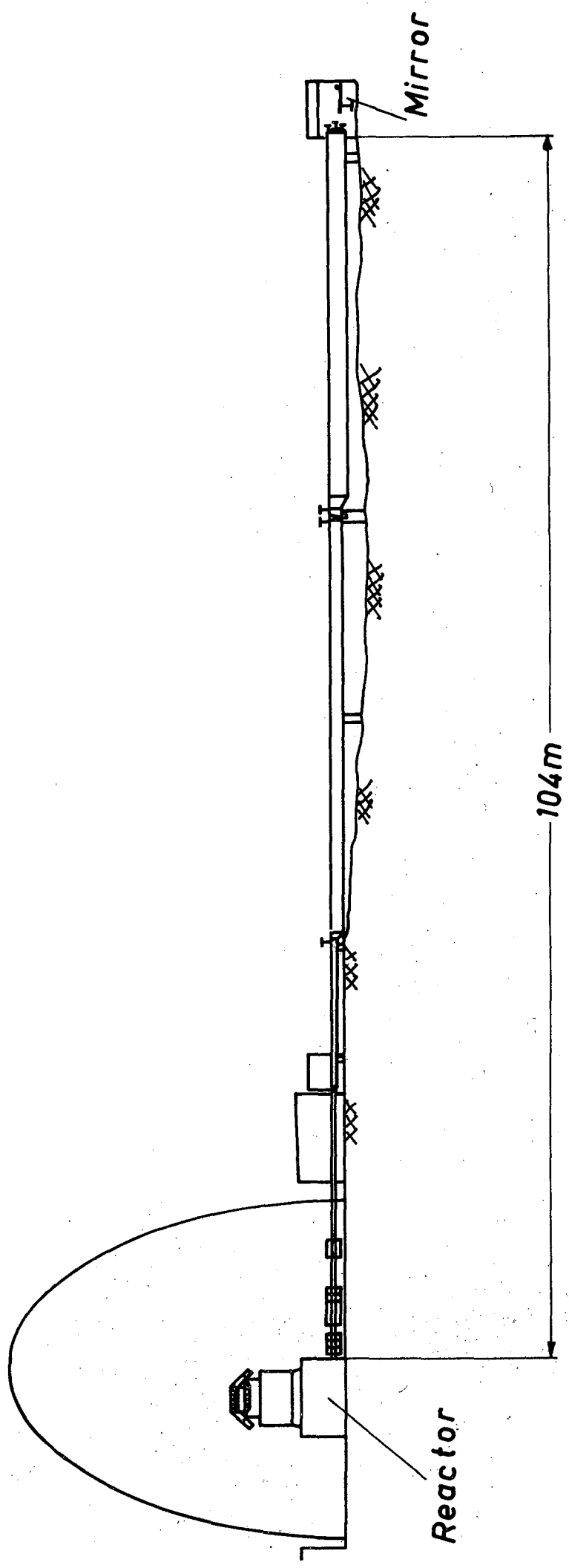


Fig.3.2.

Transmission cross section of Holmium and Terbium [metal Foils 99%]
(Nov. 1964)

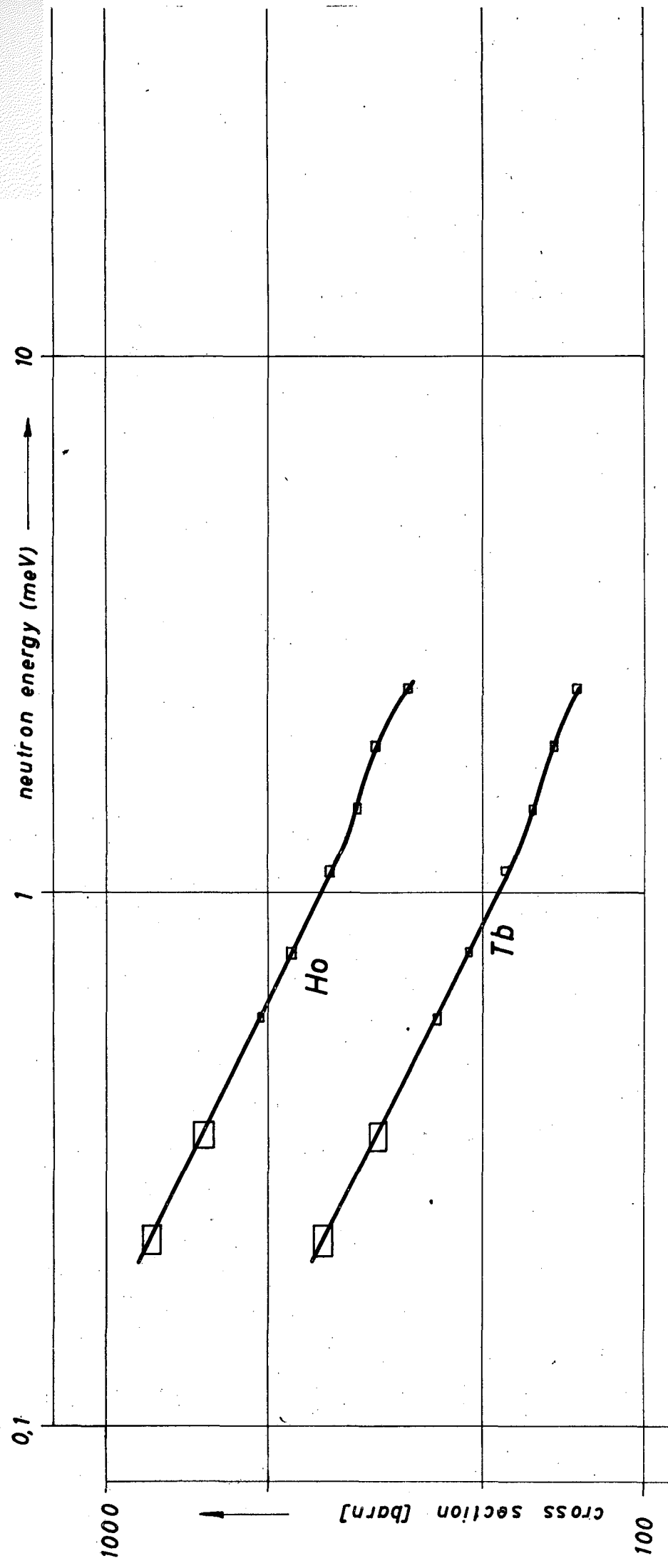


Fig. 3.3

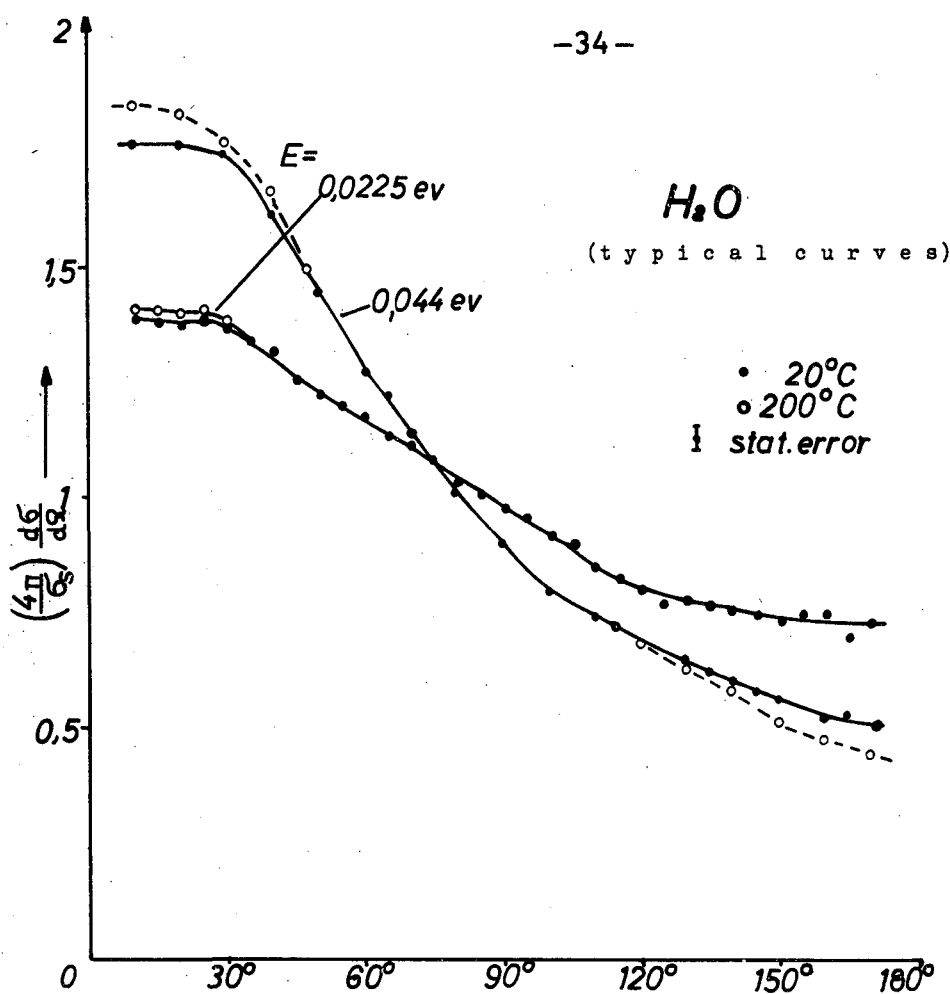


Fig. 3.4. scattering angle θ —————

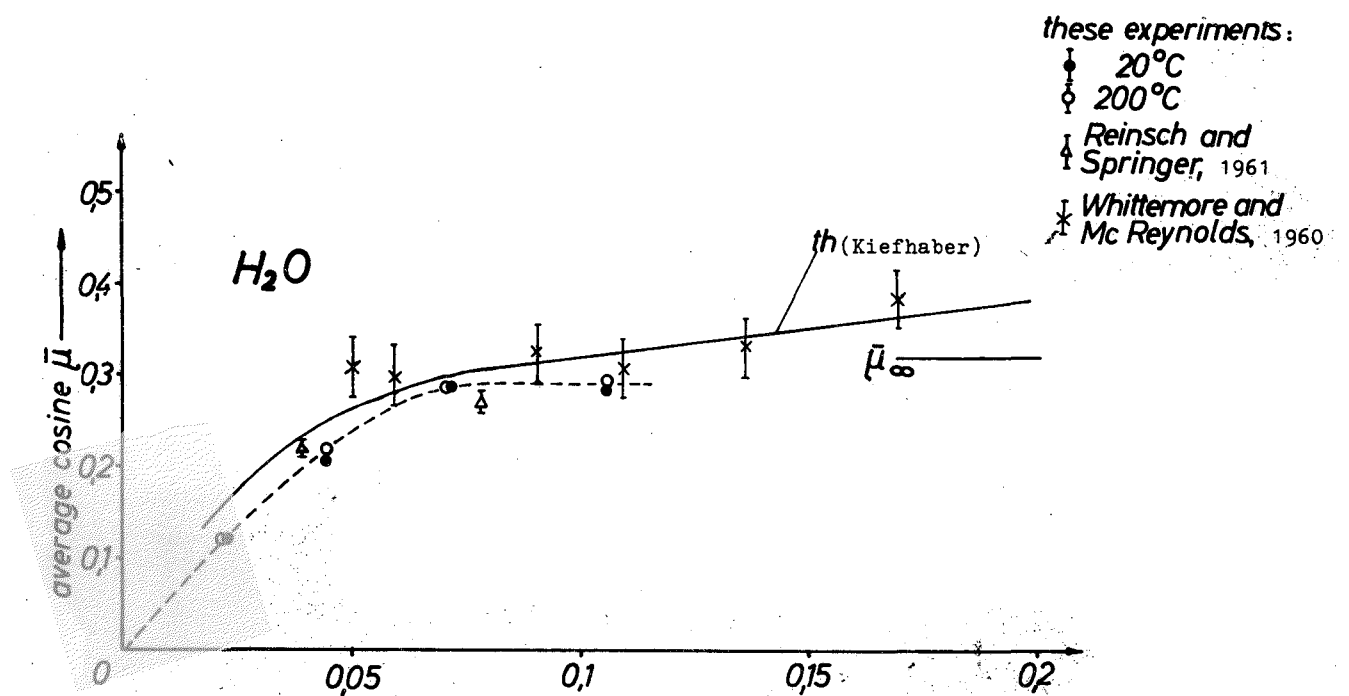


Fig. 3.5. neutron energy E (eV) —————

Kieffaber, E., Nukleonik 4, 82 (1962)

Reinsch, Ch., and Springer T., Z. f. Naturf. 16a, 112 (1961)

Whitemore, W.L., and Mc Reynolds, A.W., Symp. on Inelastic Scattering of Neutrons in Solids and Liquids, Vienna (1960), p. 511

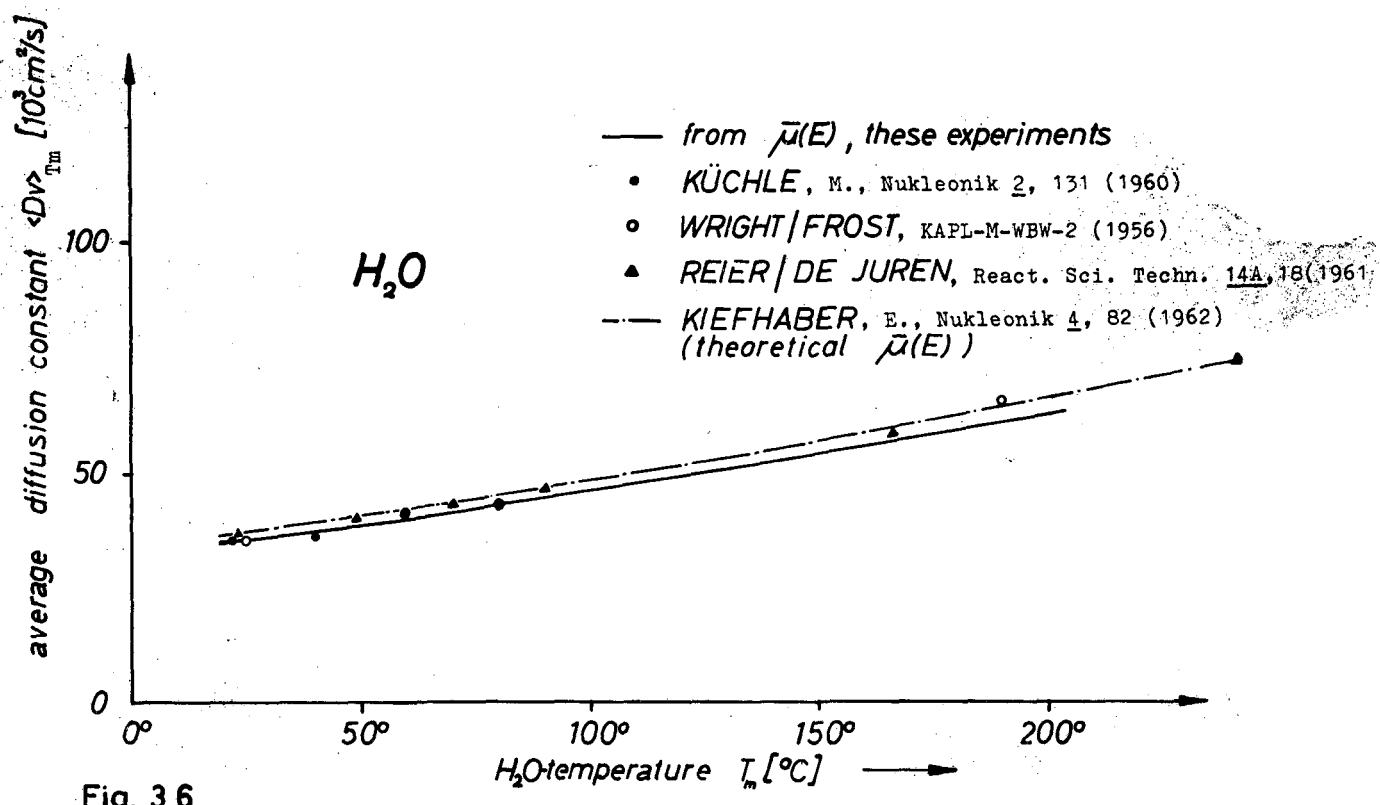


Fig. 3.6.

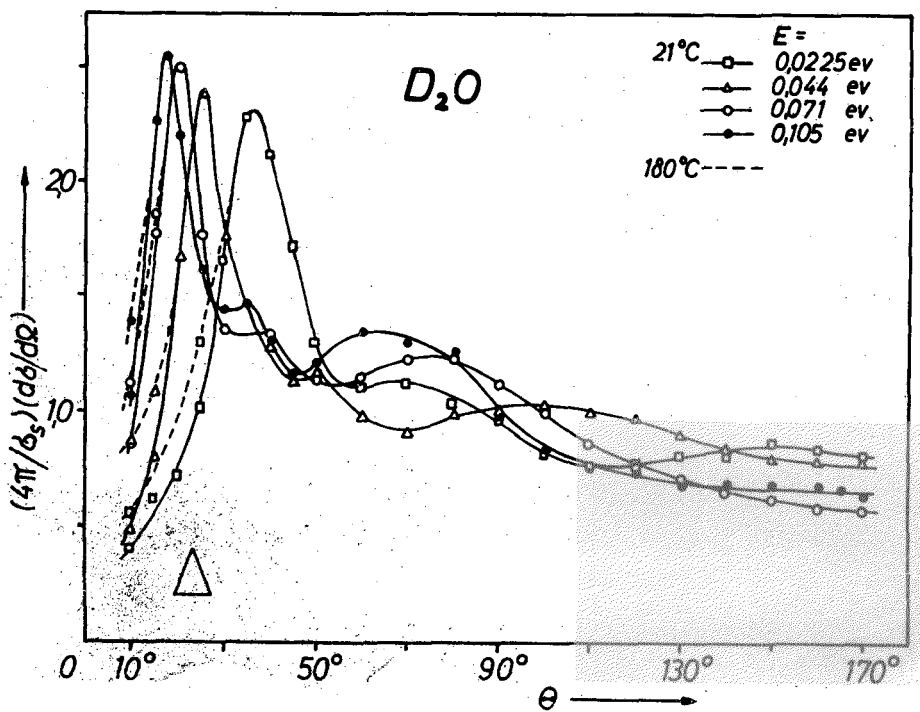


Fig. 3.7.

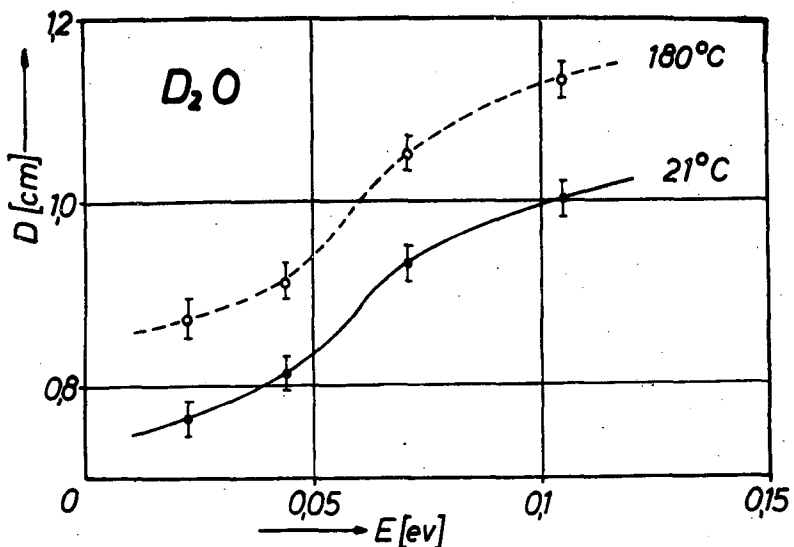


Fig. 3.8.

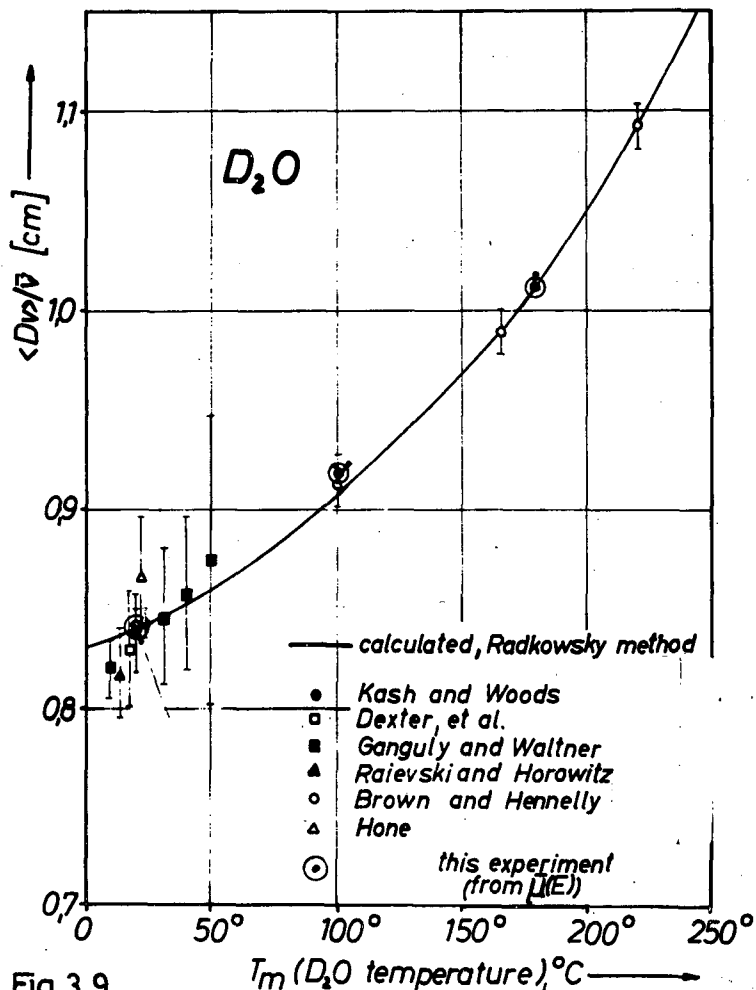


Fig. 3.9.

- Brown, H.D., and Hennelly, E.J., BNL-719, III, 879 (1962)
 Dexter, A.H. et al., ANL-4746, 14 (1951)
 Ganguly, N.K., and Waltner, A.W. Trans. Am. Nucl. Soc. 4, 282 (1961)
 Hone, D.W., J. Nucl. Eng. A (Reactor Sci.) 11, 34 (1959)
 Kash, S.W., and Woods, D.C., Phys. Rev. 90, 564 (1953)
 Radkowsky, A., ANL-4476, 93 (1950)
 Railevski, V. and Horowitz, J., Proc. Geneva Conf. 5, 42 (1955)

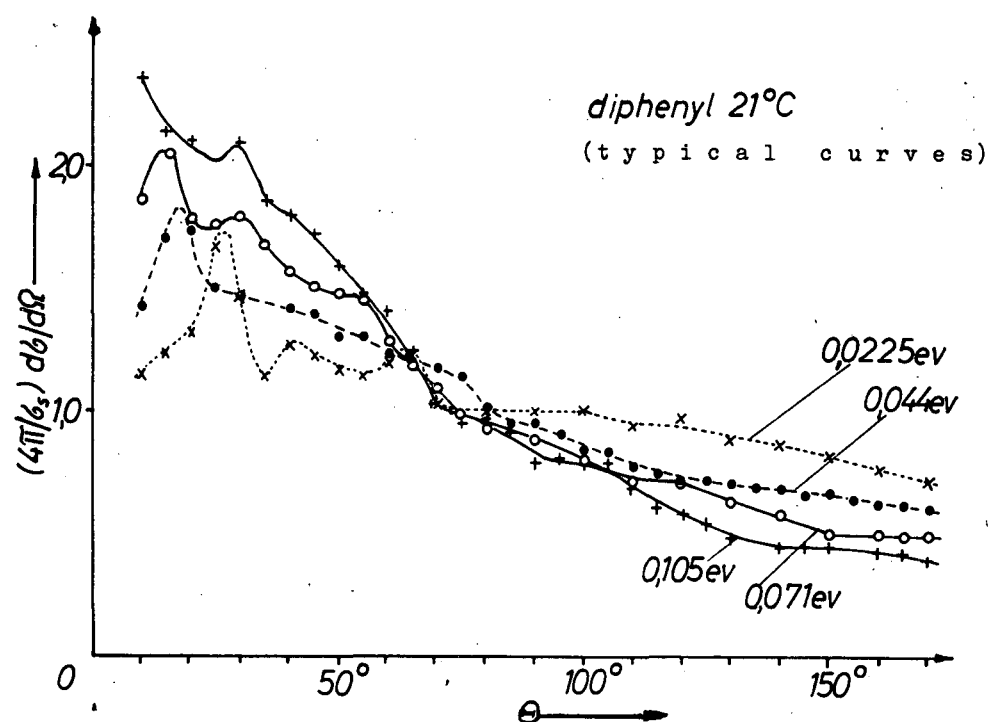


Fig. 3.10.

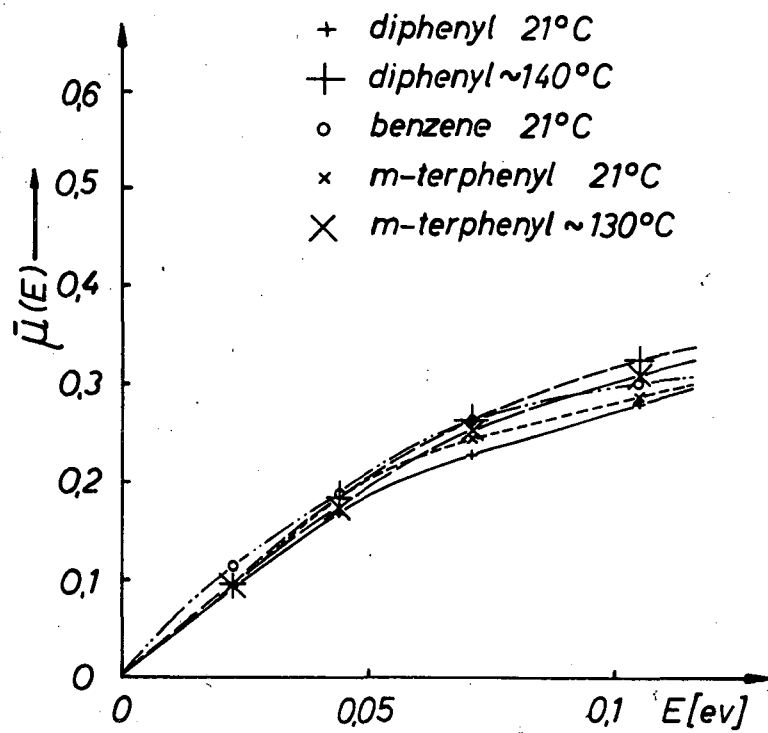


Fig. 3.11.

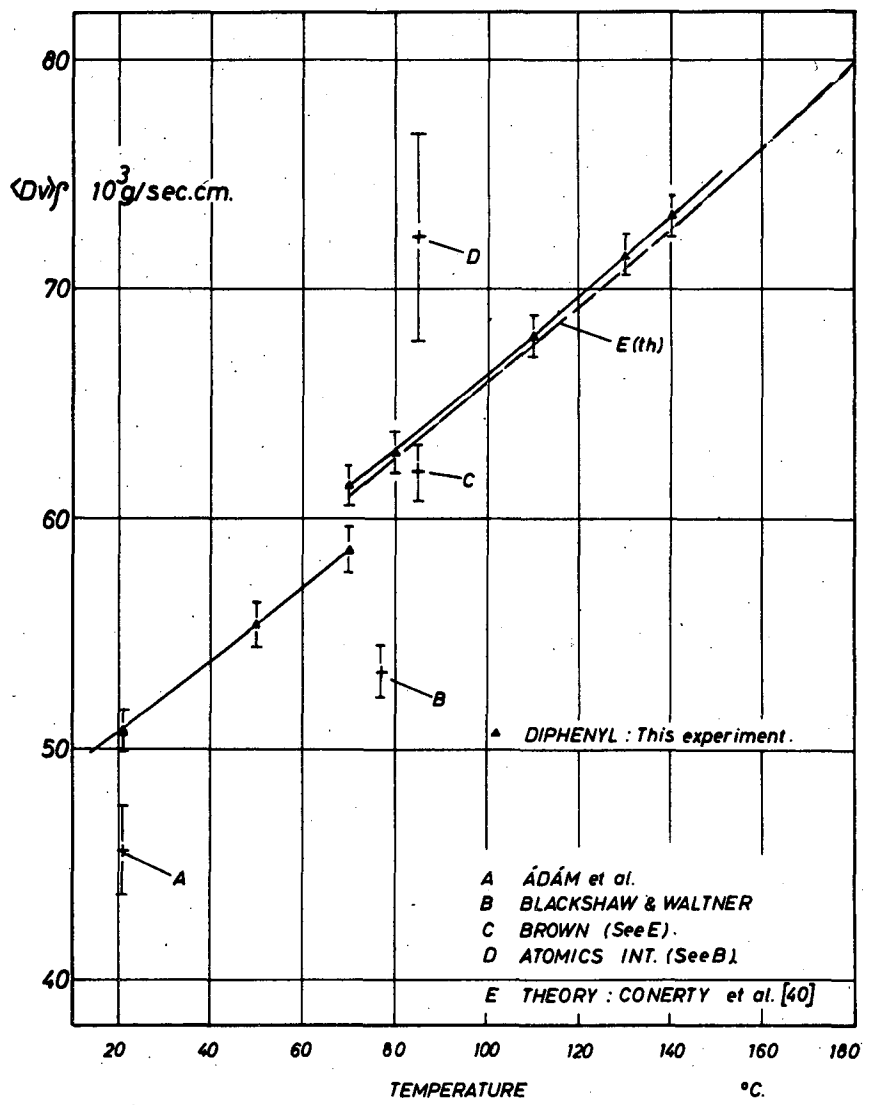


Fig. 3.12. Adám et al., Acta Phys. Hung. (1961), XIII, 25
 Blackshaw & Waltner, React. Sci. Techn. 17, 341 (1963)
 Brown, W.W., NAA-SR-MEMO-1706

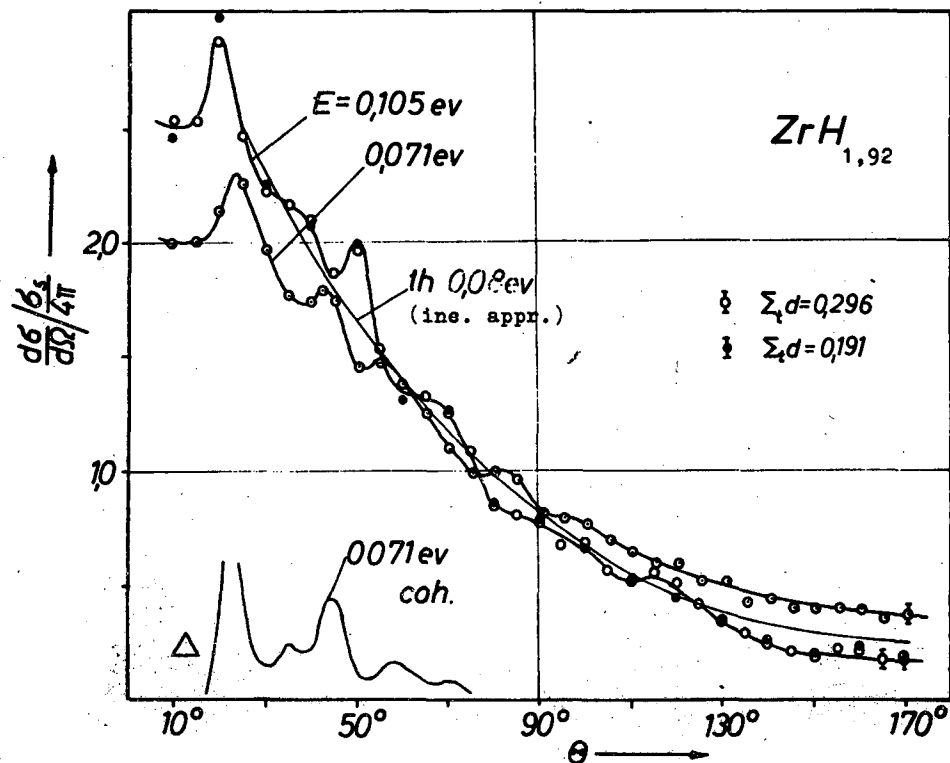
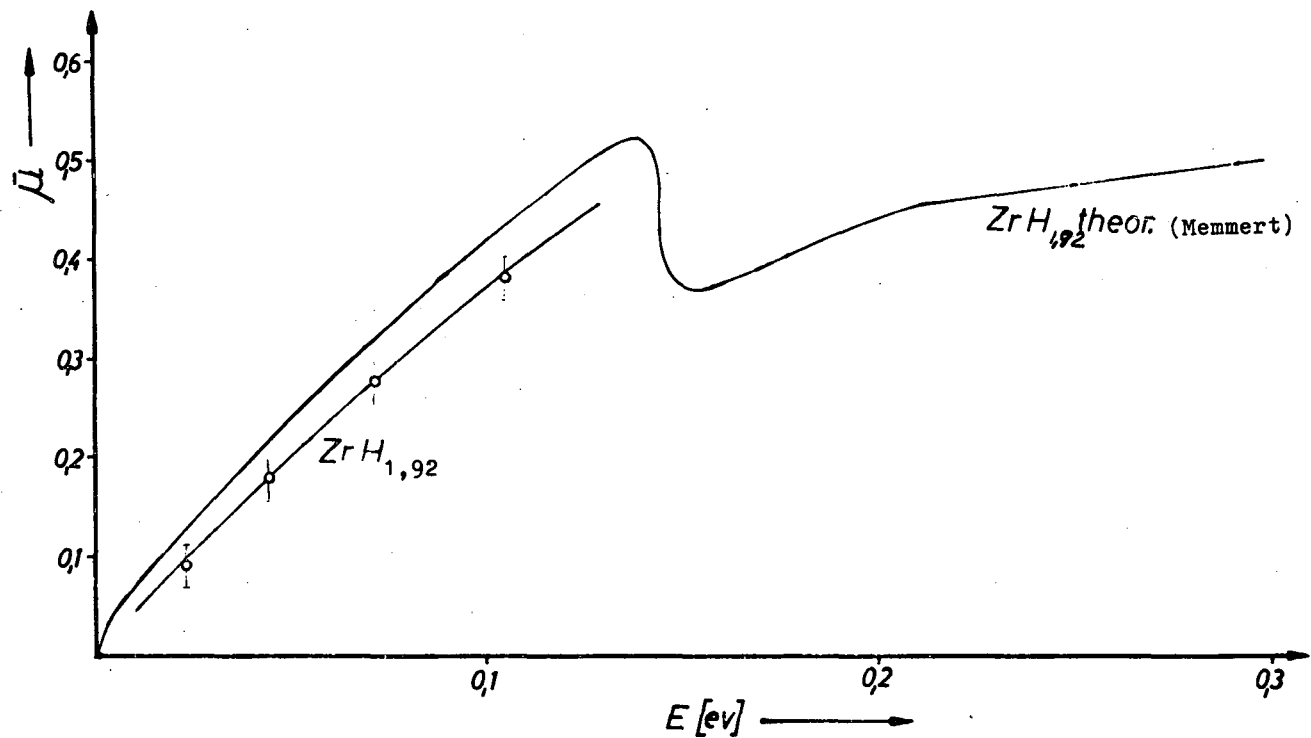


Fig. 3.13.



Memmert, G., unpublished.

Fig. 3.14.

4. KERNFORSCHUNGSZENTRUM KARLSRUHE (Germany)

4.1. Neutron cross section measurements in the keV region.

4.1.1. Measurements with a slowing-down time spectrometer
(F. Mitzel and H.S. Plendl)

A slowing-down-time spectrometer ⁽¹⁾ was used for measuring the neutron capture cross sections $\sigma_{n\gamma}$ of Ag, Mo and Fe. The spectrometer consisted of a cube of lead (side length 1.6 m) in which fast monoenergetic (14 MeV) neutrons were periodically injected for a time interval of up to 0.5 μ sec. An argon filled proportional counter of aluminium was in the block for detection of the capture γ -rays in the materials to be investigated. The substances were in the form of cylinders, in which the counter was placed.

Similarly to the time-of-flight method, energy dependent capture cross sections can be determined from the (n, γ) -reaction rates measured as a function of time. The flux measurements were carried out with a BF_3 proportional counter.

The energy resolution $\Delta E/E$ of the spectrometer depends on the average neutron energy E and is 61%, 15% and 26% at $E = 30$ keV, 10 keV and 1 eV respectively. The relation between energy and moderation time was checked with twelve resonances of Cu, Zn, Mo and Ag.

$\sigma_{n\gamma}$ -measurements of silver agree with the data of Gibbons ⁽²⁾ in the energy interval from 1 to 20 keV. The 1.2 keV resonance of iron could be confirmed with $\sigma_0 = 89$ barn eV. Investigation of Mo yielded smaller values of $\sigma_{n\gamma}$ for energies between 1 and 10 keV than those given by Block and Slaughter ⁽³⁾. A new resonance was found at 12 eV, which seems to be a p-wave resonance.

Corrections for the time dependent γ -background and the self-shielding have been performed, the latter by varying the thickness of the foils (Ag: 0.1 mm; 0.2 mm and 0.4 mm; Fe: 2.5 mm and 5 mm; Mo: 0.5 mm; 1.5 mm and 3 mm). Figures 4.1. to 4.3. show values extrapolated to zero foil thickness.

Errors are relatively high (about 30%) at neutron energies above 20 keV because of the high γ -background. In the energy range from several eV to about 20 keV the error is smaller (about 10%). At these energies, inaccuracies will mainly be caused by calibration and self-shielding.

- (1) A.A. Bergmann, A.I. Isakoff, I.D. Murin, F.L. Shapiro, I.V. Shtranikh, M.V. Kazarnovski, USSR: A Neutron Spectrometer based on Measuring the Slowing-down-Time of Neutrons in Lead, Proc. Geneva Conf. (1955) IV 135
- (2) J.H. Gibbons: General Survey on Radiative Capture Measurements by Time-of-Flight, published in "Neutron Time-of-Flight Methods", Euratom, Brussels
- (3) R.C. Block, G.B. Slaughter: Neutron Radiative Capture Measurements with the ORNL Fast-Chopper Time-of-Flight Neutron Spectrometer, ORNL-2910 (1960)

4.1.2.

3 MeV pulsed van de Graaff (G. Brudermüller, et al.)

The Karlsruhe magnetically bunched 3 MeV van de Graaff accelerator was accepted in May 1964. Preliminary time-of-flight measurements of σ_{tot} and $\sigma_{n\gamma}$ in the keV region have been made since. Especially σ_{tot} for natural iron was measured in detail. A resonance at 42 keV, as indicated in the Columbia results, could not be verified. A proton recoil scintillation detector for the nanosecond time-of-flight measurements down to neutron energies of 20 keV has been used. Moreover, some methods for the absolute determination of neutron flux in the keV region were developed and preliminary measurements have been made. There will be results in the near future from integral measurements of capture cross section by measuring the decay time of neutron fields in blocks of heavy resonance absorbers. Also the theory of these experiments was worked out.

All experiments have been greatly delayed by the very unsatisfactory operation of the accelerator. Especially for the time-of-flight measurements with wide neutron spectra satellite pulses occurring between the normal 1 ns pulses are very annoying.

The on-line data processing system, consisting of the 8K computer CAE 510 and the exchange unit CAE 592 was accepted in December 1964. It has been already used for computing directly the transmission and the total cross section from the three accumulated spectra including the conversion from time-of-flight to energy. Also the decay time of the integral measurements was directly determined from the spectra by this system.

An input circuit for this CAE system, a fully digitized time-of-flight coder for several thousand channels of 1 ns width, was delivered and will be accepted shortly.

4.2. Slow Neutron Physics

4.2.1. Measurements of the Isomeric Ratios in the Lowest Three Resonances of In 115 (E. Albold, P. von Blanckenhagen and W. Pönitz)

Indium foils were irradiated with neutrons of 0.125, 1.46, 3.9 and 9.1 eV energy at the Karlsruhe reactor FR 2 using a crystal spectrometer. Three states of In 116 were produced: In 116^g (ground state, decay: β transition to the ground state of Sn 116, $T_{1/2} = 14.08$ sec), In 116^{m1} (first isomeric state, β transitions to excited state of Sn 116, $T_{1/2} = 54.12$ min) and In 116^{m2} (second isomeric state, isomeric transition to In 116^{m1}, $T_{1/2} = 2.16$ sec).

The β -activities of foils of thickness from $1 \cdot 10^{-3}$ to $4 \cdot 10^{-2}$ cm were measured using a $4\pi\beta$ proportional gas counter. The ratios of the 14 sec to the 54 min activity were extrapolated to foil thickness zero⁽¹⁾. For $\delta = 0$ the influence of β -self-absorption is eliminated and,

therefore, the extrapolated value yields $R_g = \sigma_g / \sigma_{m1+m2}$.
The results are (2)

$$R_g(0.125 \text{ eV}) = 0.27 \pm 0.01, R_g(1.46 \text{ eV}) = 0.27 \pm 0.01,$$
$$R_g(3.9 \text{ eV}) = 0.52 \pm 0.02, R_g(9.1 \text{ eV}) = 0.27 \pm 0.01.$$

It was possible to determine the values

$$R_g(3.9 \text{ eV}) / R_g(0.125 \text{ eV}) = 1.92 \pm 0.05 \text{ and}$$
$$R_g(9.1 \text{ eV}) / R_g(0.125 \text{ eV}) = 1.00 \pm 0.02$$

with higher accuracy because these ratios are only weakly dependent on β -self-absorption.

The γ -radiation following In^{116m2} and In^{116m1} decays was measured using a NaI(Tl) crystal spectrometer. The ratio $R_{m2} = \sigma_{m2} / \sigma_{m2+m1}$ in the 1.46 eV resonance was determined from two independent methods: Firstly, from the γ -ray intensities of the transitions using the known sensitivity of the detector, and secondly, from the time-dependence of the Sn 116 γ -spectra after a short irradiation. The average value is

$$R_{m2}(1.46 \text{ eV}) = 0.51 \pm 0.05.$$

R_{m2} in the second and third resonance were related to that in the first one. The results are

$$R_{m2}(3.9 \text{ eV}) / R_{m2}(1.46 \text{ eV}) = 0.98 \pm 0.06 \text{ and}$$
$$R_{m2}(9.1 \text{ eV}) / R_{m2}(1.46 \text{ eV}) = 0.93 \pm 0.09.$$

The cross section $\sigma_{m2}(0.0253 \text{ eV}) = 81 \pm 8$ barn can be derived from $R_{m2}(1.46 \text{ eV})$ and the previously measured value $\sigma_{m1+m2}(0.0253 \text{ eV}) = 160 \pm 2$ barn (1).

The ratios R_g were compatible with the γ -ray cascade statistics theory of Huizenga and Vandenbosch (3). The comparison of R_{m2} with this theory yields the spin value 5 for the second isomeric state of In 116.

(1) K.H. Beckurts et al.: Nucl. Sci. Eng. 17, 329 (1963)

(2) E. Albold and P.v. Blanckenhagen: EANDC (E) 55 (1965)

(3) J.R. Huizenga and R. Vandenbosch: Phys. Rev. 120, 1305 (1960)

4.2.2. Neutron Scattering Measurements on Solids

(F. Carvalho, W. Gläser)

The scattering law of room temperature vanadium for a relatively large range of momentum transfer $\hbar Q$ and energy transfer $\hbar\omega$ ($0 < Q < 14 \text{ \AA}^{-1}$; $0 < \hbar\omega < 2K_B T$) was measured using the rotating crystal time-of-flight spectrometer with incident energies of 20, 40 and 80 meV. Primary energy resolution was 5% at 20 meV and time resolution about 20 $\mu\text{sec}/\text{m}$. Starting with the scattering law values and using the extrapolation technique proposed by Egelstaff values of the frequency distribution $p(\beta)$ ($\beta = \frac{\hbar\omega}{K_B T}$) have been obtained. The only assumption made for the purpose of performing the iteration of the extrapolated values is that the motions of the atoms are harmonic. But then the separation of multiphonon processes is straightforward. The derived $p(\beta)$ is shown in Fig. 4.4. An additional peak was found at $\beta = 0.4$.

4.2.3. Neutron Scattering Measurements on Hydrogenous Moderators

(G. Ehret, W. Gläser, A. Merkel)

4.2.3.1. Benzene. Double differential scattering cross sections for benzene have been measured with incident energies of 25, 32 and 59 meV ($T = 20^\circ\text{C}$). The range of α and β values covered was: $0 < \alpha < 12$, $0 < \beta < 3$. The generalized frequency distribution $p(\beta)$ derived by the extrapolation technique and with the help of programs LEAP and ADDELT is shown in Fig. 4.5. The broad peak of the distribution near $\beta=2$ may be attributed to the lowest normal vibration of the benzene ring. The broad peak centred at about $\beta = 0.48$ is very probably caused by torsional vibrations of the benzene molecule in the field of its neighbours.

4.2.3.2. Water Vapour. To get a reasonable amount of scattering from a small volume of H_2O vapour a temperature of 241°C and a pressure of 25 atmospheres were chosen (12 mg/m^3). Runs with incident energies of 18 and 32 meV were made and the

evaluated energy and momentum transfer ranges were $0 < \beta < 5$ and $0 < \alpha < 5$. The derived scattering law values $S(\alpha, \beta)$ were compared with Krieger-Nelkin theory using an effective mass 1.9 for the H_2O molecule. The theory agrees with experiment only for great momentum transfer values. A good description of the experimental results was obtained also by approximating the H_2O molecule as a symmetric top. A set of experimental $S(\alpha, \beta)$ points is shown in Fig. 4.6.

- 4.2.3.3. Zirconium Hydride. Runs with incident energies of 0.018, 0.032 and 0.064 meV have been made. Although the high energy peak contributes the most important part to inelastic scattering, the main aim of this work was to determine the contribution of the low energy acoustical modes. The high energy line has been carefully studied by Mc Reynolds et al.⁽¹⁾ with higher accuracy than this work yields using 4. Å neutrons. Therefore, we used the peak half width of these authors in our data evaluation. As is expected from theory, the low energy modes take only a few percent of the frequency distribution. We obtained the best fit with the S/α values using the distribution $p(\beta)$ shown in Fig. 4.7.

(1) Mc Reynolds, A.W., et al.: GA-471 (1958)

4.3. Nuclear Spectroscopy

4.3.1. Excited States of Heavy Nuclei (F. Horsch and W. Michaelis)

For studying excited states of heavy nuclei, a versatile alpha-gamma coincidence arrangement was set up. The circuitry permits alpha fine-structure investigations with high resolution and alpha-gamma coincidence measurements. Using these methods along with $\gamma-\gamma$ -coincidence measurements, a study of the Pu 239 α -decay revealed the existence of at least 17 α -groups and 24 γ -transitions which could be accounted for by the following levels in ⁽¹⁾ U 235:

ground state,	$7/2^-$	$7/2$	$/743/$;	0.080 keV,	$1/2^+$	$1/2$	$/631/$;
13 keV,	$3/2^+$	$1/2$	$/631/$;	46 "	$9/2^-$	$7/2$	$/743/$;
53 " ,	$5/2^+$	$1/2$	$/631/$;	83 "	$7/2^+$	$1/2$	$/631/$;
104 " ,	$11/2^-$	$7/2$	$/743/$;	130 "	$5/2^+$	$5/2$	$/633/$;
152 " ,	$9/2^+$	$1/2$	$/631/$;	172 "	$13/2^-$	$7/2$	$/743/$;
172 " ,	$7/2^+$	$5/2$	$/633/$;	200 "	$11/2^+$	$1/2$	$/631/$;
229 " ,	$9/2^+$	$5/2$	$/633/$;	297 "	$13/2^+$	$1/2$	$/631/$;
(297 " ,	$11/2^+$	$5/2$	$/633/$);	333 "	$5/2^+$	$5/2$	$/622/$;
368 " ,	$7/2^+$	$5/2$	$/622/$;	394 "	$(13/2^+$	$5/2$	$/633/$);
424 " ,	$9/2^+$	$5/2$	$/622/$;	470 "	$(11/2^+$	$5/2$	$/622/$);
526 " ,	$(13/2^+ 5/2 /622/)$;								

A study of the radiation from Am 241 revealed 21 α -groups and at least 33 γ -transitions. Analysis of the results suggests the following levels in ⁽²⁾ Np 237:

ground state,	$5/2^+$	$5/2$	$/642/$;	33 keV,	$7/2^+$	$7/2$	$/642/$;
60 keV,	$5/2^-$	$5/2$	$/523/$;	77 "	$9/2^+$	$5/2$	$/642/$;
103 " ,	$7/2^-$	$5/2$	$/523/$;	159 "	$9/2^-$	$5/2$	$/523/$;
225 " ,	$11/2^-$	$5/2$	$/523/$;	270 "	$3/2^-$	$1/2$	$/530/$;
306 " ,	$13/2^-$	$5/2$	$/523/$;	332 "	$1/2^+$	$1/2$	$/400/$;
359 " ,	$3/2^+$	$3/2$	$/651/$;	370 "	$5/2^+$	$1/2$	$/400/$;
370 " ,	$3/2^+$	$1/2$	$/400/$;	393 "	$15/2^-$	$5/2$	$/523/$;
440 " ,	$(3/2^- 3/2 /521/)$;				460 "	$9/2^+$	$1/2$	$/400/$;
460 " ,	$7/2^+$	$1/2$	$/400/$;	487 "	$(5/2^-$	$3/2$	$/521/$);
550 " ,	$(7/2^- 3/2 /521/)$;				722 "	$5/2^-$	$5/2$	β -vibr.	
753 " ,	$7/2^-$	$5/2$						$5/2$	$/523/$;

At present sources for an investigation of the Pu 242 α -decay are prepared.

(1) F. Horsch, to be published in Z. Physik

(2) W. Michaelis, to be published in Z. Physik

4.3.2.

Status of (n, γ) -Experiments at the FR 2

(W. Michaelis, G. Markus, H. Schmidt, C. Weitkamp)

At the FR 2 three facilities have been installed for the study of γ -rays from the capture of thermal neutrons: a 5-crystal-pair spectrometer which is capable of working in coincidence with a large single crystal spectrometer, a sum coincidence and $\gamma-\gamma$ -coincidence arrangement using three single crystal detectors, and an apparatus for the investigation of the angular correlation of $\gamma-\gamma$ -cascades. The pair spectrometer is placed at a tangential channel which provides a very good cadmium ratio. The energy resolution is 3.2% at 7.6 MeV and the counting efficiency was found to be 10^{-4} (count per 7.6 MeV γ -quantum emitted by the source). In the two other experiments neutrons from core channels are monochromized by diffraction from lead crystals. At present, the (n, γ) -reactions on the following target nuclei are investigated: Ge 73, Sr 87, Dy 164, and Yb 168. The subject of these experiments is the investigation of multiple phonon states in Ge 74 and Sr 88 and the examination of the Nilsson theory and the superfluid model for the deformed nuclei Dy 165 and Yb 169.

4.4.

Some New Developments in Instrumentation

4.4.1.

On-line Computer Facility at the FR 2 Reactor

(G. Krüger, G. Dimmler)

A data processing system, called MIDAS⁽¹⁾ (Multiple Intput Data Acquisition System), was designed for the acquisition, control and processing of the data from neutron physics experiments. All these experiments are of the multi-channel - multiparameter type. Up to 8 independent multichannel experiments may be connected to MIDAS and all of them can be processed simultaneously. During the reported period, both the "hardware" part - consisting of commercial equipment and home-made units - and the package of on-line programs were designed and checked. The hardware system involves (fig. 4.8):

- five data communication lines with remote control and buffer stations at the location of the experimental setup. For each experiment, a maximum of 20 bits (10^6 channels) is available.
- Remote program selector boards for manual control of the computer by number codes.
- A specially designed two-CRT-display system working either in the computer or switch-controlled modes⁽²⁾. Using his own display system, each experimenter can examine the stored results in the memory in 'live' display without interrupting the data acquisition which is going on.
- A multiplexer unit involving a 4 x 24 bit buffer store.
- A small computer Control Data 160-A with 8^K core storage (6.4 μ sec cycle time) and two independent input/output channels. Further peripheral equipment includes: paper tape puncher, paper tape reader, and a typewriter.
- Two magnetic tape units CD-603.
- A real-time clock.

Much effort was spent in writing a program package to govern the function of the whole system. All routines responsible for the entire data flow, independent of the individual experiments, and for automatic and manual control are permanently stored in the computer. This executive program is expanded by a series of experiment-oriented data reduction routines. The easily exchangeable reduction routines permit flexible adaption to change experimental conditions.

The whole system is in full operation. Starting from a basic system in June, 1963⁽³⁾ and going up to the complex MIDAS installation, the computer has run 10 000 hours in routine operation with excellent reliability.

(1) Krüger, G. and G. Dimmeler: Proc. EANDC Conf. on Automatic Acquisition and Reduction of Nuclear Data, Karlsruhe, July 13-16, 1964

- (2) Dimmler, G. and G. Krüger: Proc. EANDC Conf. on Automatic Acquisition and Reduction of Nuclear Data, Karlsruhe, July 13-16, 1964
- (3) Krüger, G. and G. Dimmler: Proc. Int. Symp. on Nuclear Electronics, Paris, Nov. 15-27, 1963, p.533

4.

4.2.

The Rotating Crystal Spectrometer Facility

(H. Ripfai, W. Gläser)

In the period covered by this report, the rotating-crystal time-of-flight spectrometer at the FR 2 has been improved in several ways.

4.

4.2.1.

Simultaneous use of 4 monochromatic neutron beams

With a rotating crystal several monoenergetic beams at different reflecting angles, i.e. with different neutron energies, can be used simultaneously. Besides the arrangement for scattering law measurements in isotropic materials, which has been described previously, three additional secondary spectrometers have been installed. Fig. 4.9. is a scheme of our present experimental arrangement.

1. Arrangement for measuring small momentum transfers. For studying small energy and momentum transfers, an experiment using a monochromatic beam in the energy range from 5 to 10 meV was set up. The length of the flight path is 3.5 metres. A total of 60 detector positions between 1° and 30° are available. At each position up to three counter tubes 1' diameter and 8' length can be mounted. An energy resolution of about 2% at 5 meV will be attained.

2. Dispersion law spectrometer. Today mainly the triple-axis spectrometer in the "constant Q" or other special modes is used for measuring phonon frequencies in coherent scattering single crystals. The time-of-flight technique offers great potentialities also in this direction. In the present setup 6 He^3 counters (4 atmospheres) diameter 1', active length 4'

were placed side by side at a distance of 2 m from the scatterer. The experimental procedure is the "scattering surface" method.

3. Diffractometer using time-of-flight. In a provisional setup, we have tried to use the time-of-flight method for structure research. This means using a pulsed monochromatic beam from the crystal chopper and determining scattering angles by time-of-flight. A wide range of angles of interest can be covered in one run. A scheme of the arrangement is given in Fig. 4.10.

4.

4.2.2. Methods for filtering the monochromatic beams

For energies below 10 meV, the total reflection of neutrons at polished metal surfaces was used, installing a pair of Soller collimators ($10'$ collimation) inclined with an angle greater than twice the geometrical collimation. A transmission of about 50% and an improvement of the peak-to-background ratio in the monochromatic beam of a factor 10 has been reached with mechanically polished surfaces. For higher energies, a rotating collimator with 288 straight slits, 10 cm in height and 0.3 cm in mean width with slit walls of 0.03 cm thick stainless steel was built (speed of rotation 3600-7000 rpm.).

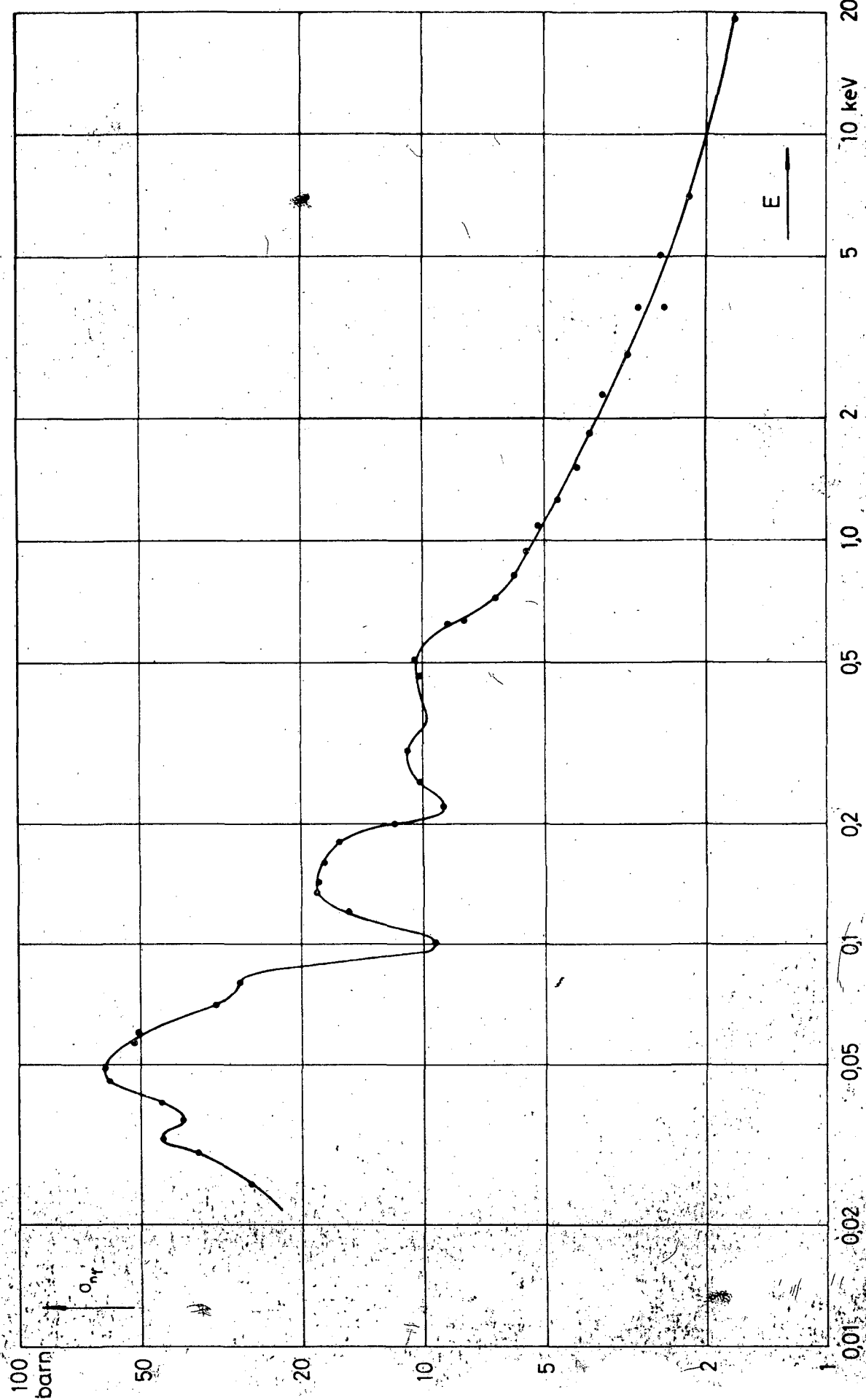


Fig. 41 Capture Cross Sections of Silver

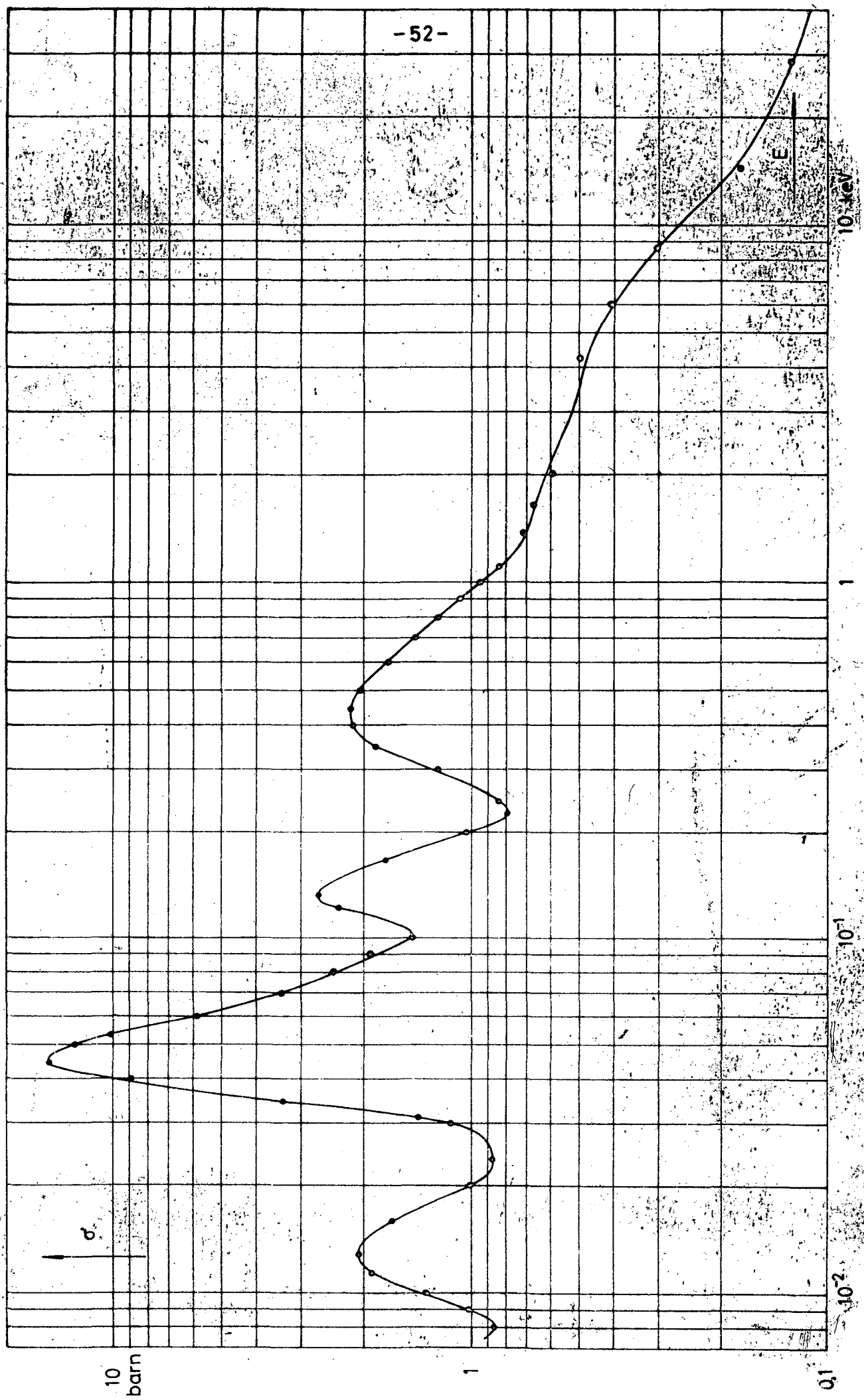


Fig. 4.2a Capture Cross Sections of Molybdenum

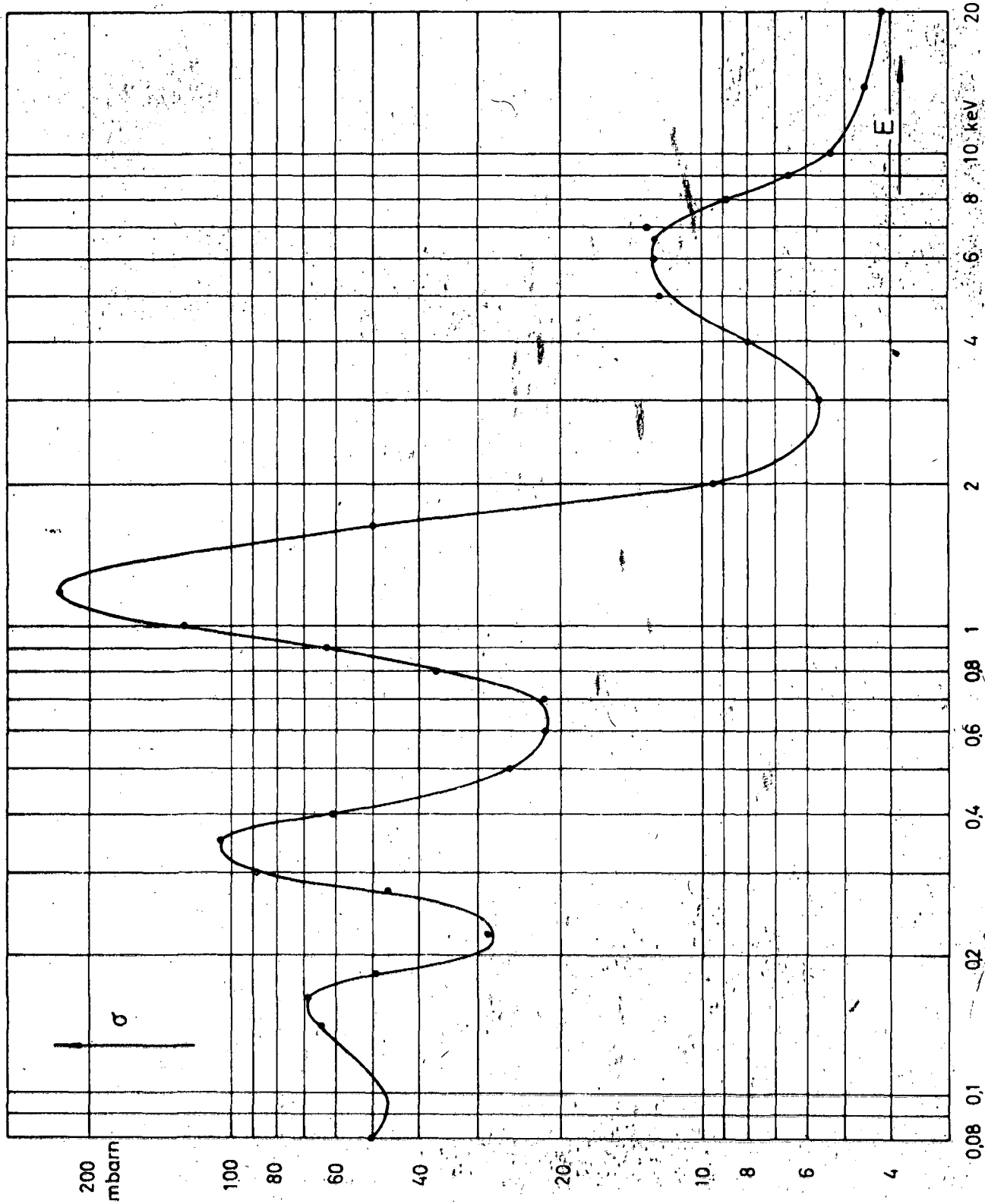


Fig. 4.3. Capture Cross Sections of Iron

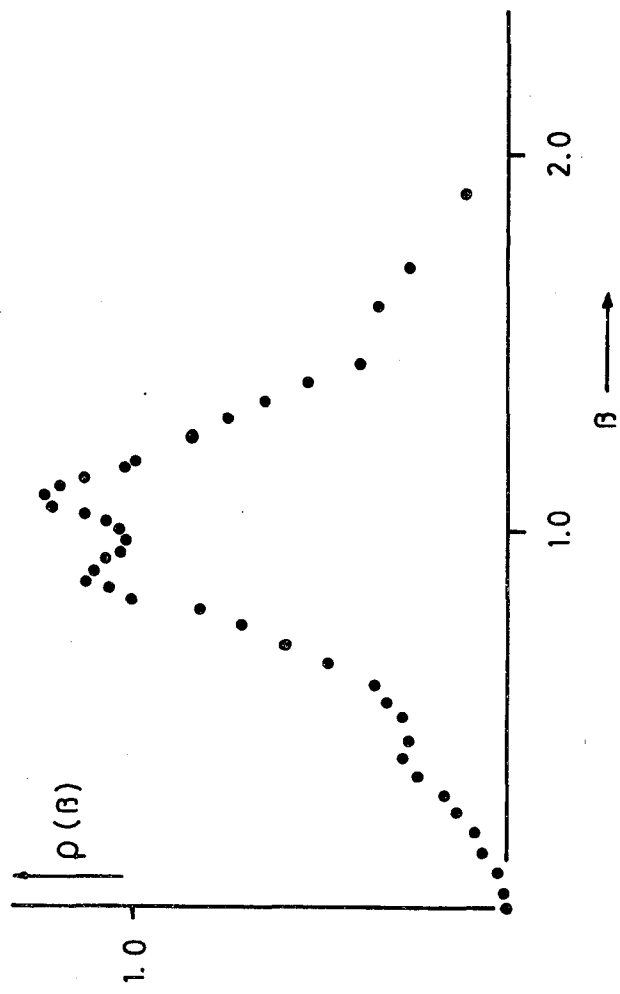


FIG. 4.4.
FREQUENCY DISTRIBUTION $\rho(\beta)$ FOR VANADIUM

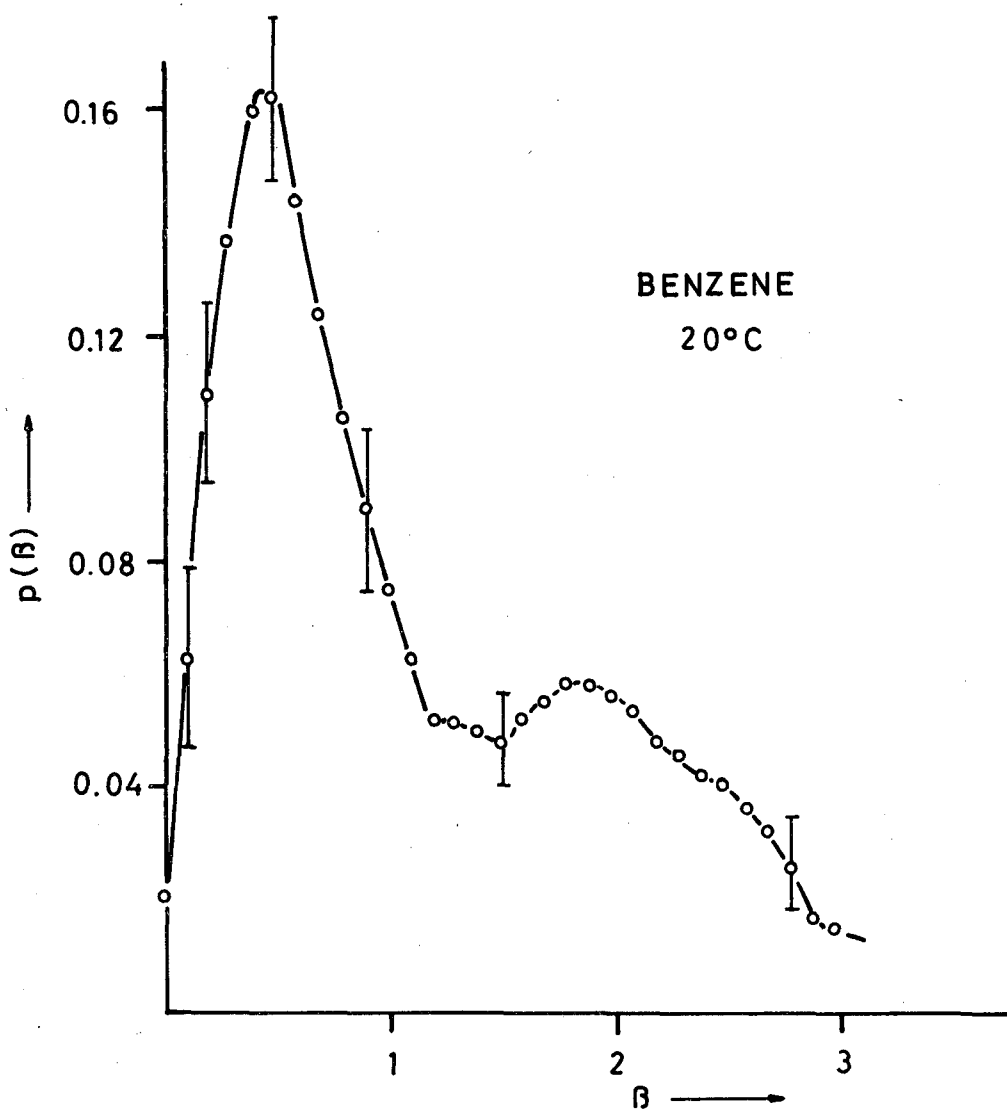


Fig. 4.5.

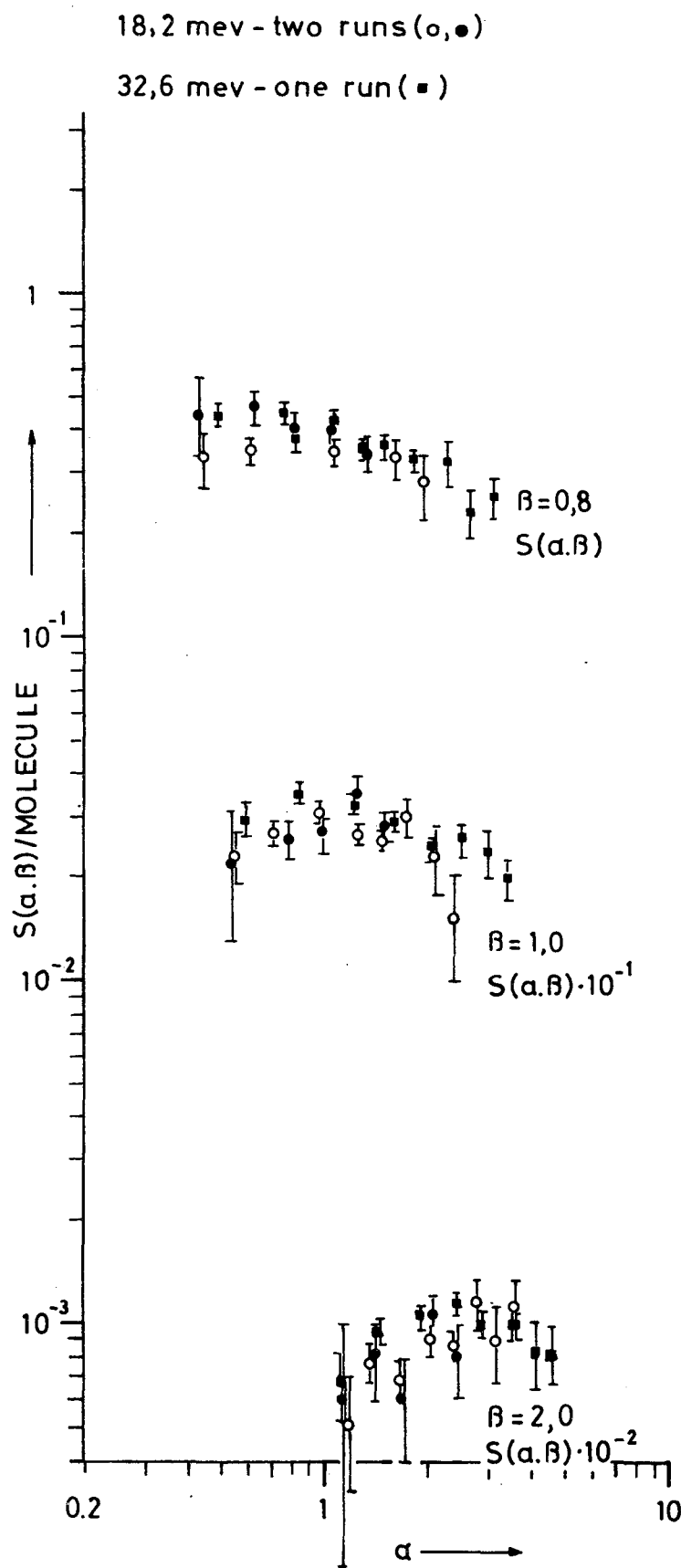
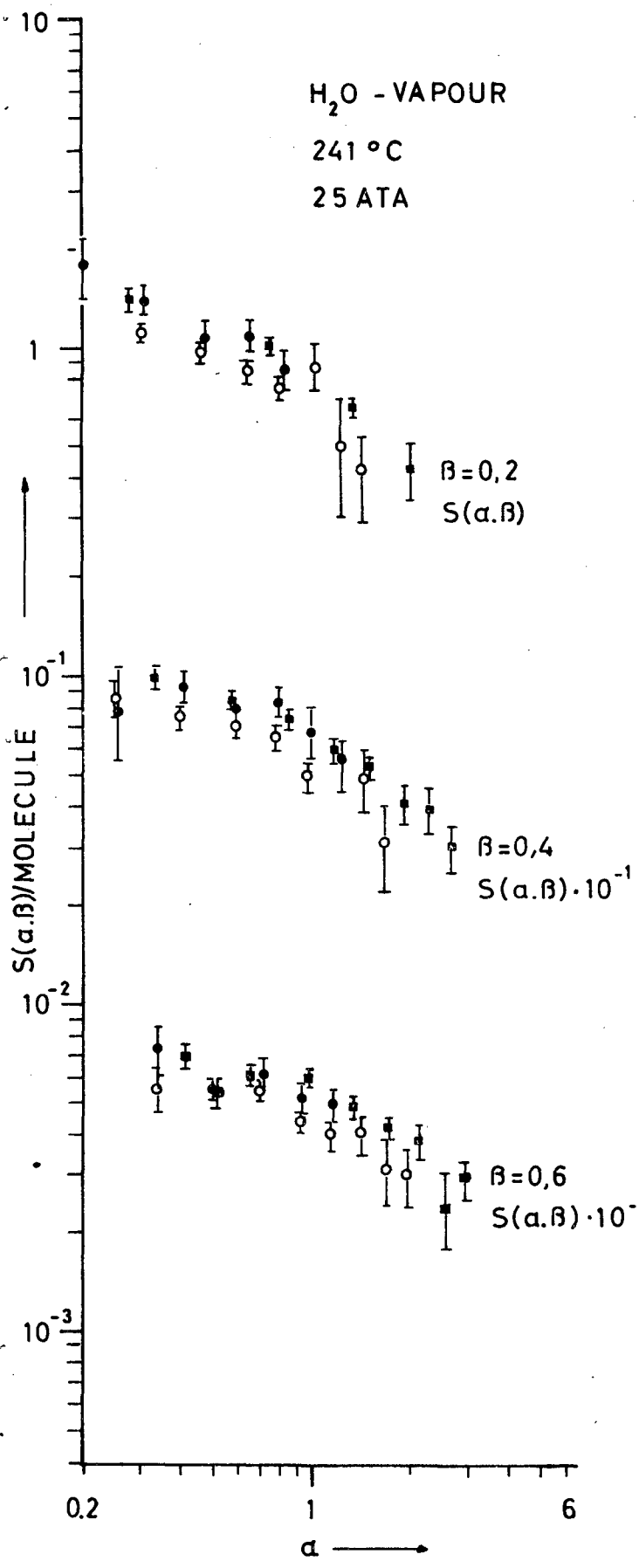


Fig. 4.6.

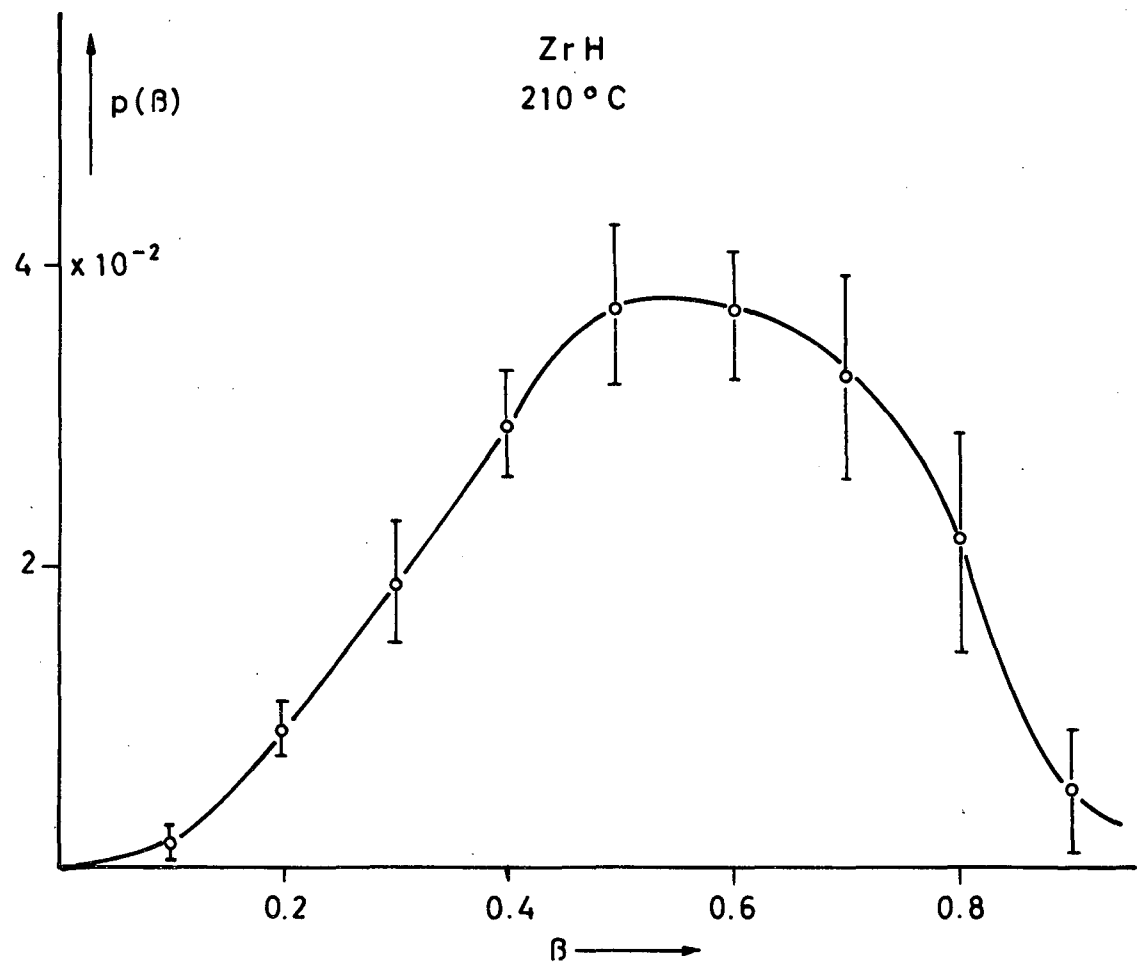


Fig. 4.7.

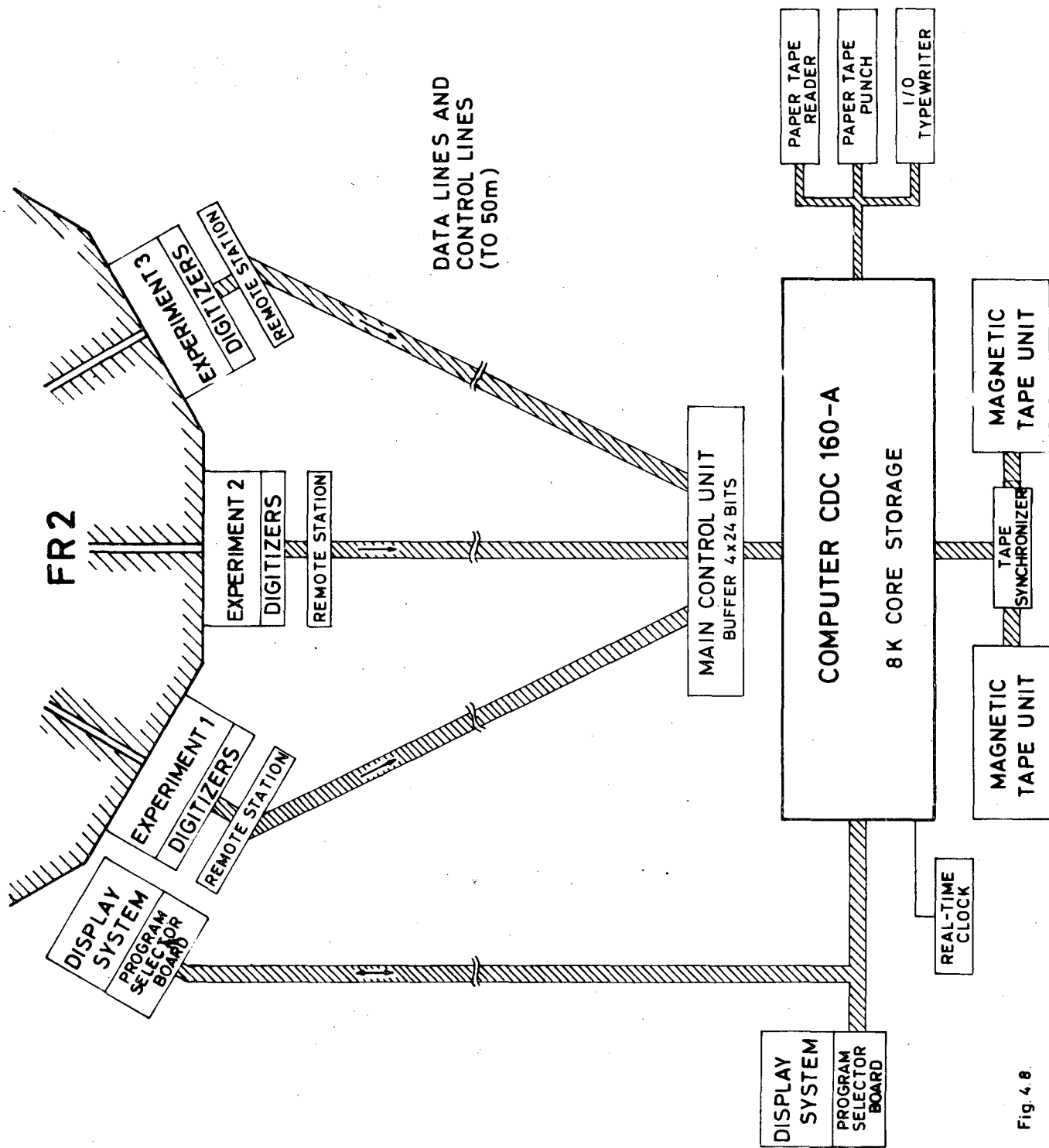


Fig. 4.8

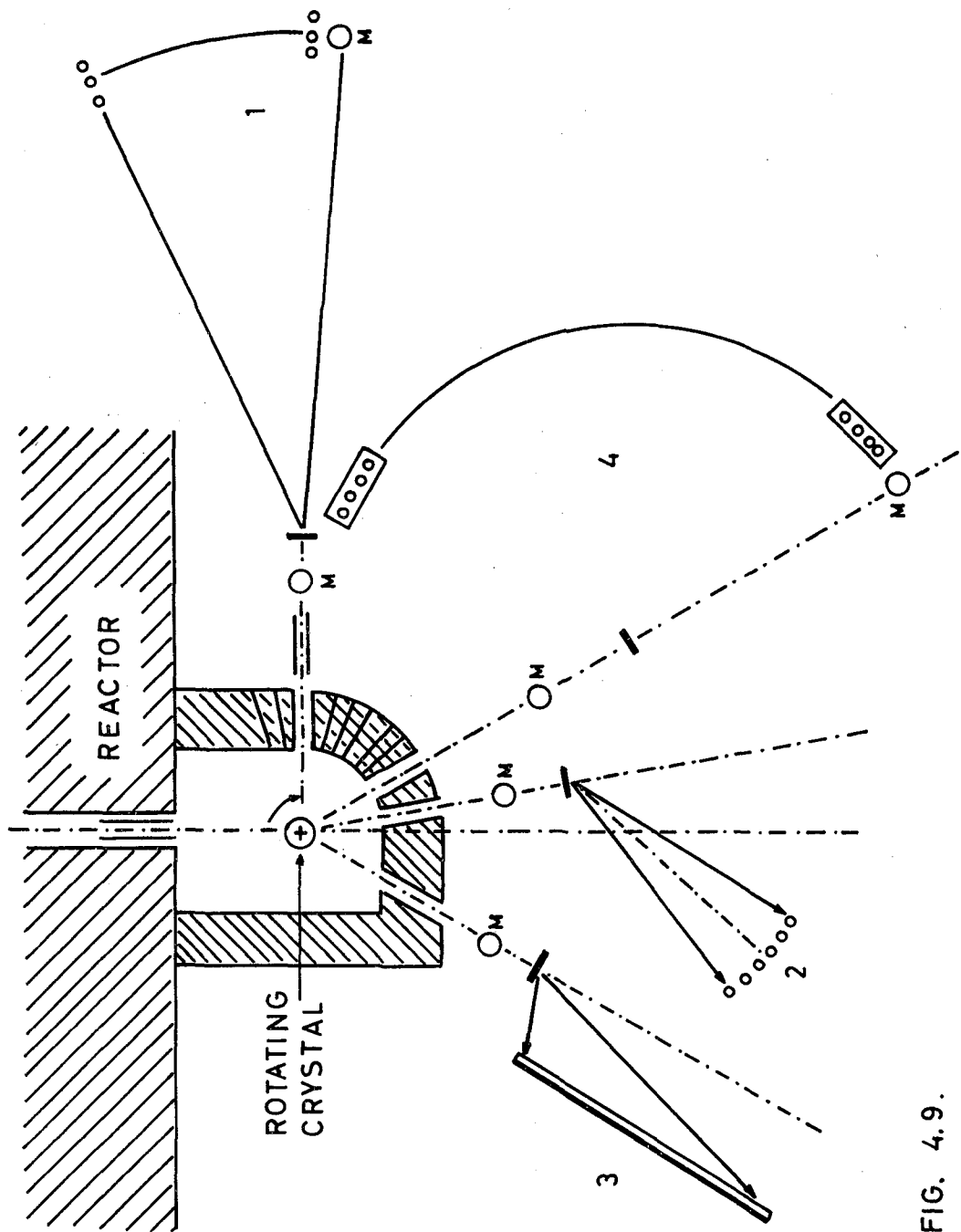


FIG. 4.9.

- 1 = LOW MOMENTUM TRANSFER SPECTROMETER
2 = DISPERSION LAW SPECTROMETER 3 = DIFFRACTOMETER
4 = SCATTERING LAW SPECTROMETER
- M = MONITOR, ○ = DETECTOR, ┃ = SAMPLE

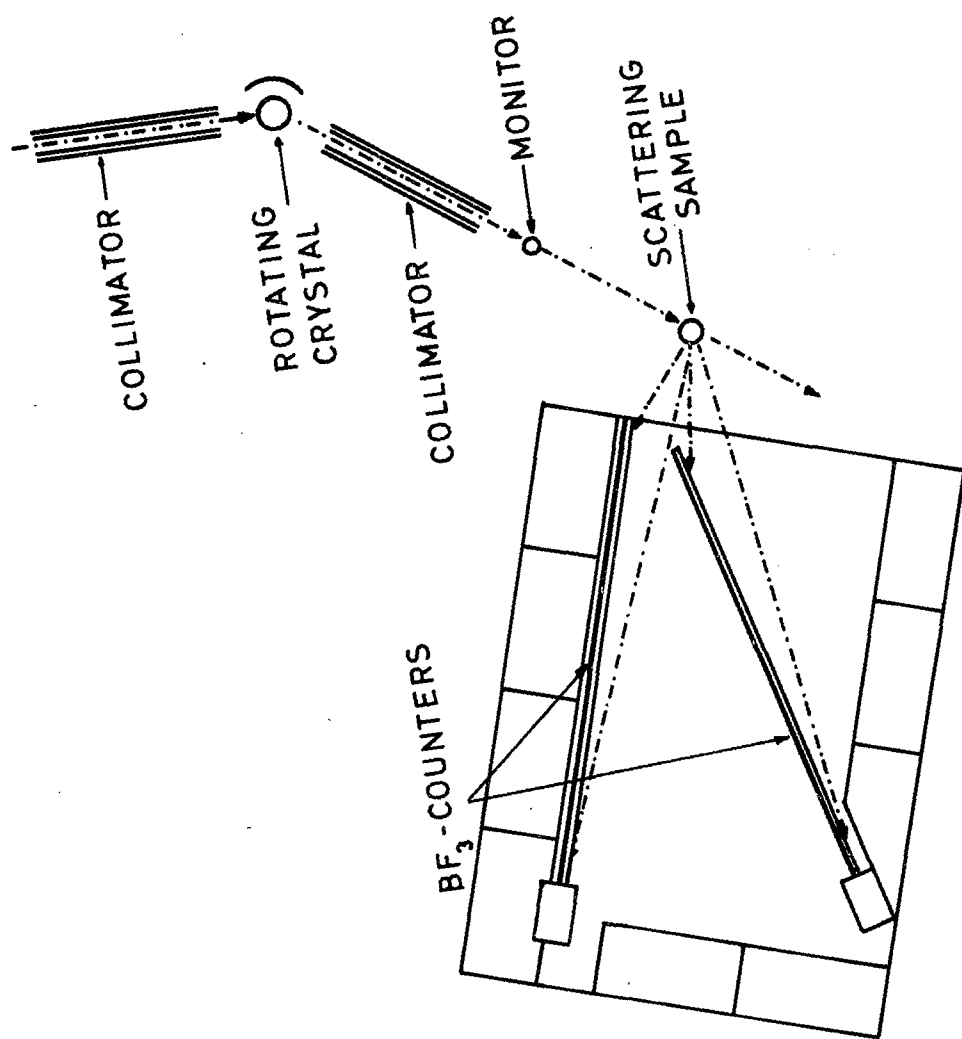


Fig. 4.10.

5. CENTRE D'ETUDE DE L'ENERGIE NUCLEAIRE (CEN - SCK), MOL
(Belgium)

5.1. Slow Neutron Resonances
(F.Poortmans, H.Ceulemans)

5.1.1. Apparatus

The BR2 crystal spectrometer has been in routine operation since June 1964. As compared with the BR1 spectrometer, the neutron flux is approximately 150 times higher and the background in the scattering counters 10 times higher, but this can certainly be reduced further.

The spectrometer is working automatically with the aid of a punched-tape electronic program-unit. The angle of the crystal table is read by counting the lines of a Moiré pattern, produced by two circular gratings, one fixed and the other moving with the crystal table. The system has a precision of better than 10 seconds of arc. The 1 : 2 coupling system between crystal table and spectrometer arm is similar to the Dumond bent quartz-crystal spectrometer at Argonne (Hamermesh, Rev.Sc.Instr. 28, 233 (1957)).

5.1.2. Measurements

5.1.2.1. Sm149 (n,α)Nd146

The Sm149(n,α)Nd146 reaction has been studied for incident neutron energies between 0.004 eV and 0.1 eV. Previous experiments (E.Cheifetz e.a., Phys. Lett. 1, 289 (1962). R.D. Macfarlane, I.Almadovar, Phys. Rev. 127, 1665 (1962) on this reaction with thermal neutrons have shown two alpha transitions starting from the Sm150 capturing state (with spin and parity either 3^- or 4^-) and going to the 0^+ ground state and to the 2^+ (460 keV) first excited state of Nd146. We have measured the α -spectra of this reaction with the following incident neutron beams.

- (1) A BR2-beam filtered by 30 cm of polycrystalline Be and 15 cm of a Bi single crystal, with a mean neutron energy of 0.004 eV.
- (2) A beam of monochromatic neutrons with an energy of 0.097 eV from the BR2 single crystal spectrometer. The in-pile collimator has a divergence of 6 minutes of arc and the monochromator was Cu(111).

(3) A thermal neutron beam extracted from the BR1 thermal column. The target (diameter: 2 cm. thickness: approximately 300 μg per cm^2) consisted of 97.5 per cent enriched Sm149. The α -spectra were obtained with a gold-surface barrier detector made from 3000 Ω cm n-type silicon and operated at a reverse bias of 6 V. Fig. 5.1. shows the α -spectrum in the case of the most difficult of the three experiments, namely with monochromatic neutrons of 0.097 eV. The cross-section for this reaction is only of the order of 200 mb, so that our measurements were done with a rather thick sample and with a large detector (diameter = 3 cm). The counting rates per channel at the 8.75 MeV peak were approximately:

at 0.097 eV 6 c/hour,
at 0.004 eV 50c/hour,
with BR1 thermal beam 30 c/hour.

These experiments have yielded the following results:

(1) The α -spectrum changes considerably in the small neutron energy range explored. So, the study of capture α -spectra can yield information similar to those deduced from the study of capture gamma-ray spectra at resonance energies.

(2) The relative intensity of the α -transition to the 0^+ ground state of Nd146 is about 7 times higher in the experiment with cold neutrons than in the experiment with 0.097 eV neutrons. A($4^- \rightarrow 0^+$) α -transition being forbidden, this means that the negative energy resonance has certainly spin 3^- and that the resonance at 0.097 eV has probably a spin 4^- , which confirms the results obtained by B.N.Brockhouse (Can. J.Phys. 31, 432 (1953) and by Marshak e.a. (Phys.Rev. 128, 1287 (1962)).

(3) In the experiment with thermal neutrons, which has a good statistical accuracy, an α -transition to one or both of the excited levels at 1.06 MeV (probably 4^+) and 1.21 MeV (spin unknown) of Nd146 has been seen. The relative intensity of this α -transition is of the order of a few percent as predicted by R.D.Marcfarlane (Loc.cit.)

5.1.2.2. Spin measurements by resonance scattering

Using the BR2 crystal spectrometer, we have measured first these resonances for which we had already obtained some results with the BR1 crystal spectrometer but who were in disagreement with other published values. Secondly, we have chosen some resonances for which thin samples are not available. In these cases we have measured σ_s/σ_t in the wings, i.e. for energies $E_0 + \Delta E$ and $E_0 - \Delta E$ (E_0 = resonance energy), so that taking the mean value of these results, the interference term in σ_s cancels out and T_n/T can be obtained. E is chosen so that the transmission of the sample is high enough and the correction for absorption of the scattered neutrons can be calculated with enough precision. Table 5.1. gives the results we have obtained.

Table 5.1.

<u>Isotope</u>	<u>Resonance Energy</u>	<u>J</u>
Sm147	3.4 eV	3
Sm149	0.87 eV	4
Ir191	0.654eV	under analysis
	5.36 eV	2
Ir193	1.303eV	2
Re185	2.156eV	3

Additional measurements have also been performed on the 0.097 eV resonance of Sm149 with vanadium as a standard scatterer. The 18.3 eV resonance of Sm147 has also been measured and the analysis is underway.

For the 3.4 eV resonance in Sm147, ($J = 3$) is in agreement with capture gamma-ray experiments of Carpenter (ANL 6589), but this result was not expected from the Sm147(n, α)N α 144 experiments (Cheifetz E, Loc. cit.)

For the 0.87 eV resonance in Sm149, we had reported (F. Poortmans, H. Ceulemans, Int. Conf. on Nucl. Phys. with Reactor Neutrons, ANL 6797, 363) a preliminary value $J = 3$ for this resonance, in disagreement with other authors (H. Marshak, loc. cit.). We have now measured with a much better statistical accuracy the contribution from σ_p and from neighbouring resonances to the scattering counting rate between 0.5 eV and 2.5 eV.

Fig. 5.2. shows the scattering counting rate, corrected for the variations of beam intensity and of detector efficiency in this energy interval. The monochromator was Be (1011) for which third order reflection is forbidden. The peaks at 0.5 eV and at 2 eV are due to the 8 eV resonance of Sm152 which has a Γ_n of 130 meV.

The experiment yielded for the statistical weight factor g the value ($g = 0.61 \pm 0.5$). The two possible values being $g = 0.56$ ($J = 4$) and $g = 0.44$ ($J = 3$) we can conclude that $J = 4$ for this resonance.

The measurements with Ir and Re have been performed with thick targets. For each resonance, the value of σ_s/σ_t has been determined for several energies on both sides of the resonance. The results given in table 5.1. agree with the preliminary results reported previously (F. Poortmans, H. Ceulemans, loc. cit.: H. Ceulemans, F. Poortmans, M. Nève de Mévergnies, Bull. Am. Phys. Soc. 8, n° 1, 70 (1963) and the Re results of Stolovy (BAPS, 9, 461 (1964)).

5.2. Fission Physics

5.2.1. Kinetic energy-balance for spontaneous fission of Pu240 and fission of (Pu239 + nth).

(A.J. Deruytter, M. Nève de Mévergnies).

A paper on this topic was presented at : "Congrès Internationale de Physique Nucléaire", Paris 2 - 8 juillet 1964, and will appear in the Proceedings of this conference (Session 4e, paper C 191).

Abstract: "The sum of the kinetic energies of both fission fragments was compared for the spontaneous fission of Pu240 and for the thermal neutron induced fission of Pu239 with a back-to-back arrangement of solid state detectors".

"Within the accuracy of our results, it seems that in spite of the 6.4 MeV difference in excitation energy between both fissioning systems, the total kinetic energies are equal within 3 percent".

These preliminary results have been further improved thanks to the higher statistical accuracy of the Pu240-data, and better fitting procedures.

The measured spectra are shown in Fig. 5.3. The full line is the best fit to the total kinetic energy data for $(\text{Pu}^{239} + n_{\text{th}})$, whereas the dashed one is the best fit to the Pu^{240} spontaneous fission results. If we take the maximum values with errors deduced from this fitting procedure we find a difference in the positions of the maxima $\Delta E = (2.2 \pm 0.3) \text{ MeV}$. Without doubt the shift is in the correct direction, yielding a higher total kinetic energy for neutron induced fission.

An inspection of the data of Hopkins and Diven (J.D.Hopkins and B.C.Diven, Nucl. Phys. 48, 433 (1963)) on the average number of neutrons emitted in the spontaneous fission of Pu^{240} ($\bar{\nu}_o$) and in the thermal neutron induced fission of Pu^{239} ($\bar{\nu}_t$) yields a value of $(\bar{\nu}_t - \bar{\nu}_o) = 0.642$ neutrons per fission.

On the other hand from the difference in excitation energy between both fissioning systems the difference in neutron emission is expected to be $B_n \frac{d\bar{\nu}}{dE} = 0.832$. B_n is the binding energy of the neutron and $d\bar{\nu}/dE_n$ is the slope of the well-known linear dependence of $\bar{\nu}(E_n)$ at higher neutron energies, known to be 0.13 MeV^{-1} .

This difference of 0.190 neutrons between the experimental result and the expected value of $(\bar{\nu}_t - \bar{\nu}_o)$, when all supplementary excitation energy of the compound nucleus would be converted into excitation energy of the fragments, can be most logically explained by an increase of the total kinetic energy of the fragments for the thermal neutron induced fission of Pu^{239} , equal to 0.190. $(\frac{d\bar{\nu}}{dE}) \approx 1.5 \text{ MeV}$. Within the experimental errors this figure is in agreement with the result of our direct measurement of ΔE_K .

Following J.A.Wheeler (J.A.Wheeler, Fast Neutron Physics, Vol. 2, editors J.L.Fowler and J.B.Marion, Interscience New-York, 1963, p. 2051) the neutron binding energy is about 1.6 MeV above the first fission threshold of Pu^{239} (Stokes, Boyer, Northrop, Phys. Rev. 115, 1227, 1959). Consequently our direct result and the indirect deduction from the neutron emission values agree with the assumption that the supplementary excitation energy above the threshold is converted into kinetic energy of the fragments.

So this assumption should be given some attention, although jumping to conclusions needs a certain degree of caution in view of the small effects involved. This agreement might be accidental, as it is based on the tacit assumption that the distribution of the fragment masses and charges in the region of E_n under study does not change. Although it is hoped that both fissioning systems pass through the 0^+ channel (the only channel open according to Wheeler) there are some indications that the total kinetic energy distributions are not exactly alike (see fig. 5.3.).

The Pu240 total kinetic energy distribution is wider and shows some asymmetry not present for ($Pu239 + n_{th}$). In connection with this we plan to measure for both fissioning systems the distribution of the energy differences ($E_L - E_H$) which is strongly dependent on the mass distribution, so as to see whether there is a change in the mass distribution or not and to what extent this change can account for the difference in the average total kinetic energy \bar{E}_k .

5.2.2. Ternary fission and possible (n,α) -reactions in U233 and U235. (A.J.Deruytter, M. Nève de Mevergnies)

A paper on this topic was presented at: "Congrès International de Physique Nucléaire" Paris 2 - 8 juillet 1964, and will appear in the Proceedings of this Conference (Session 4e, paper C 192).

Abstract: the ratio of binary-to-ternary fission for U233 was measured for thermal neutrons and epi-Cd neutrons with a surface-barrier detector and found to be independent of neutron energy and equal to 445 ± 13 . The energy distribution of the ternary particles has its maximum at (14.8 ± 0.5) MeV and a width of (8.7 ± 0.3) MeV. At 9 to 10 MeV there is an indication for another group of particles, that may be interpreted as α -particles from an (n,α) -reaction. A precise measurement of the B/T-fission ratio for U235 did not show any change of this ratio in the neutron energy-range from 0.005 eV to 0.2 eV. Two groups of particles are found in the low energy-portion of the spectrum of ternary particles, which may be interpreted as respectively tritons and α -particles from an (n,α) -reaction.

Supplementary work has been performed since, especially on the measurement of the ratio of binary-to-ternary fission for U235.

- (a) The slow-chopper data obtained at BR1 were completed.
- (b) Two precise measurements were made of the B/T-ratio, the one for a beam from the thermal column at BR1, and the other a measurement with a cold neutron beam at BR2, with the following not normalised results:

thermal beam $R(B/T) = 643 \pm 7$, cold neutron beam $R(B/T) = 613 \pm 9$ which shows a difference outside statistics.

- (c) Similar measurements are in progress at two energies (0.2 eV and 0.07 eV) with the BR2 crystal spectrometer.

This more complete information will be presented at the Salzburg IAEA Conference, 22 - 26 March 1965. In this progress report we only present fig. 5.4. that summarizes:

- (1) the variation of $\sigma_f \sqrt{E}$ as a function of E (BNL 325, D.J. Hughes and R.B. Schwartz, 1958).
- (2) the ratio of symmetric to asymmetric fission, measured for some nuclei in the peak- and valley region of the mass-distribution (H.W. Burgus, AEC-Report, IDO 16797, 1962).
- (3) the relative yield of fission with high total kinetic to total fissions (L.G. Miller and M.S. Moore, BAPS II 9, 4, 1964).
- (4) our results for the (B/T)-ratio as a function of neutron energy.

The open circles are the slow chopper data, the full circles are the data from the BR1-thermal column beam and the BR2 cold neutron beam.

The B/T ratio exhibits a small and smooth variation, which seems to be correlated with other fission parameters as measured in the same neutron energy range.

5.2.3. Pulse-height defect of surface-barrier detectors for fission fragments.

(A.J.Deruytter)

Additional work on U233 was completed and an account of this work will be submitted for publication in Nucl. Instr. and Methods. Similar results were obtained with U233 as with U235 for the values of the PH-defects of the average light and heavy fragment.

5.2.4. Search for delayed neutron precursors of antimony and arsenic
(P. del Marmol and M. Nève de Meergnies)

The apparatus shown in fig. 5.5. has been mounted at the BR2 reactor to separate and detect short lived fission products of As and Sb that could be delayed neutron precursors. The part surrounded by dotted lines is enclosed in an aluminium box facing the T-7 channel so the neutron beam after opening of a fast shutter can irradiate the quartz cell B. The box is surrounded by a suitable shielding.

The fast separation used is based on the formation of AsH_3 and SbH_3 by reaction of a H_2SO_4 solution containing U235, fission products, As and Sb carriers on heated zinc (A.E. Greendale and D.L. Love: Anal. Chem. 35, 632, 1963).

D is an extensible rubber balloon and H a glass flask both containing nitrogen. flasks E and F, the latter containing drierite, can stop any splash from the solution.

The operations proceed as follows:

The solution to be irradiated is introduced in A: all electromagnetic valves being closed but V_2 and V_4 : stopcocks R_1 , R_2 R_4 and R_5 are open, R_3 is closed. The whole apparatus is evacuated by means of the vacuum pump P. then R_2 is closed.

V_2 is closed, V_1 open, and the solution fills the irradiation cell B. All further operations proceed automatically by means of preset timers. The shutter is opened and B is irradiated in a flux of about $1.6 \times 10^9 \text{ n/cm}^2 \times \text{sec}$. At the end of the irradiation, the shutter is closed, V_2 is opened and the solution falls in C on zinc preheated at 100°C . AsH_3 and SbH_3 are sucked by the vacuum of flask G through E and F and are partially decomposed and stopped after passing through quartz furnace F_1 and F_2 which can be heated at preset temperatures, from room temperature to 1000°C . Heating variations induce variation in stopping power for AsH_3 and SbH_3 , the latter being stopped at lower temperatures.

EANDC(E)
57"U"
February 1965

- 69 -

F₂ is surrounded by six He³ neutron counters protected from the furnace by a water cooled copper tube.

After the gas burst, V₃ is open, V₄ closed and V₅ opened for a short time to wash eventual residual gases in from the system. This step is immediately followed by counting the neutron activity on a multiscaler.

Results showed a 2-second acticity which could not be attributed to known delayed neutron emitters. Work is in progress, by varying the temperatures of the furnace and by using As and Sb tracers, to track which of these two elements is responsible for this 2-second neutron activity.

5.3. Reactor Physics

(F.Motte)

5.3.1. Measurements of mean fission spectrum cross-sections for threshold reactions.

(A.Fabry, J.P.Deworm)

Use has been made of a natural uranium converter box located in the reflector of BR1 reactor to measure a lot of mean fission spectrum cross-sections for threshold reactions of direct interest in relation with fast neutron dosimetry.

The different possible perturbations of the spectrum shape have been investigated either experimentally or theoretically and found to be negligible, at the exception of inelastic scattering in uranium-238, whose influence was difficult to be ascertained.

Recently an enriched uranium plate converter has become available. ⁽¹⁾ It has been proved that the spectrum of that converter is very pure, even for measurements with reactions such as U²³⁵(n,f) and Pu²³⁹(n,f), for example ⁽²⁾.

A detailed and accurate comparison of the two converters has been done, showing that the fast neutron spectrum in the natural uranium converter is also pure between 2.5 and 14 MeV, a slight deviation occurring only between 1 and 2.5 MeV and supposed to be due to inelastic scattering. The comparison has not yet been extended to lower energies.

Corrections to measured mean fission spectrum cross-sections resulting of this deviation amounted to a maximum of 6% for the reactions with lowest threshold.

The fast flux in natural uranium converter was monitored with cobalt for pile power variations between different runs. The absolute calibration of the converter has been realized by means of the following reactions, using the quoted mean fission spectrum cross-sections.

$$S^{32}(n,p)P^{32} \quad \bar{\sigma} = (6.5 \pm 3) \text{ mb} \quad (1)$$

$$Fe^{56}(n,p)Mn^{56} \quad \bar{\sigma} = (1.04 \pm 0.05) \text{ mb} \quad (3)$$

$$Al^{27}(n,\alpha)Na^{24} \quad \bar{\sigma} = (0.61 \pm 0.03) \text{ mb} \quad (4)$$

From these measurements a mean value of the fission flux in converter has been defined for a unit activity of the monitor. The accuracy of such a calibration is better than $\pm 5\%$, the individual error on the basic cross-sections.

This can be seen from the upper part of table 5.2. when comparing the measured cross-sections for the basic reactions with their quoted values.

The lower part of the table 5.2. reports some other results of that work.

The NaI(Tl) 3"x3" crystal used for these measurements was calibrated with standard sources of Ce¹⁴¹, Hg²⁰³, Cr⁵¹, Au¹⁹⁸, Na²², Cs¹³⁷, Nb⁹⁵, Mn⁵⁴, Sc⁴⁶, Rb⁸⁶ and Co⁶⁰ supplied by the CEN absolute measurement group (Mr. Jacquemin) or by the BCMN (Mr. Vaninbrekha). Maximum deviation of points from least squares fit curve amounted to 2.5%, mean deviation to 1%. A comparison with BCMN⁽⁵⁾ for measurements on Co⁵⁸ has shown an agreement of 2.5%.

Measurements have also been done or are in progress for the reactions Rh¹⁰³(n,n')Rh^{103m}, Nb⁹³(n,n')Nb^{93m}, Ti⁴⁷(n,p)Sc⁴⁷, U²³⁸(n,f), Pb³¹(n,p)Si³¹, Al²⁷(n,p)Mg²⁷, Zn⁶⁴(n,p)Cr⁶⁴, Ti⁴⁸(n,p)Sc⁴⁸, Cu⁶³(n, α)Co⁶⁰, Mo⁹²(n,p)Nb⁹² and Mo⁹⁵(n,p)Nb⁹⁵.

In the course of that work, a source of manganese-54 was followed for decay during more than one year and a half life of (302 ± 6) d. has been determined. in close agreement with the recent result of reference⁽⁶⁾.

EANDC(5)

- 71 -

57" "

Dec. 1965

Table 5.2.

Reaction	Half life of reaction product	$\bar{\sigma}$ (mb)	Method for determi- nation of absolute activity
$S^{32}(n,p)P^{32}$	14.2 d (5)	67 ± 4	$4 \pi \beta$ (1)
$Fe^{56}(n,p)Mn^{56}$	2.58 hr (5)	1.02 ± 0.05	$4 \pi \beta-\gamma$
$Al^{27}(n,\alpha)Na^{24}$	15.0 hr (5)	0.61 ± 0.035	$4 \pi \beta-\gamma$
		0.64 ± 0.040	calibrated crystal
$Mg^{24}(n,p)Na^{24}$	15.0 hr (5)	1.29 ± 0.014	relatively to $Al^{27}(n,\alpha)$
$Ni^{58}(n,p)Co^{58g}$	71.3 d (5)	65.3 ± 3.5	-
$Ni^{58}(n,p)Co^{58m}$	9.0 hr (5)	29.7 ± 1.6	-
$Ni^{58}(n,p)Co^{58}$	71.3 d (5)	95 ± 5	calibrated crystal
$Ti^{46}(n,p)Sc^{46}$	84.0 d (5)	10.0 ± 0.05	calibrated crystal
$Fe^{54}(n,p)Mn^{54}$	303 d (6)	68.5 ± 3.8	$4 \pi \beta-\gamma$ calibrated crystal
$Mn^{55}(n,2n)Mn^{54}$	303 d (6)	0.207 ± 0.011	$4 \pi K-\gamma$ relatively to $Fe^{54}(n,p)$
$Nb^{93}(n,2n)Nb^{92}$	10.15d (5)	0.403 ± 0.022	calibrated crystal
$In^{115}(n,n')In^{115m}$	4.5 hr (7)	174 ± 9	calibrated crystal

5.3.2. Measurement of the 2200 m/sec cross-section for the $Fe^{58}(n,\gamma)$
 Fe^{50} reaction.

(A.Fabry, J.P. Deworm)

As a part of the work carried out about the use of natural iron for fast neutron flux integration (9), a new determination of the 2200 m/sec activation cross-section of iron-58 has been done.

The measurements were realized in the purely maxwellian (10) neutron spectrum of BR1 thermal column, relatively to the well-known 2200 m/sec activation cross-section of gold-197: (98.8 ± 0.3) b.

The thermal flux perturbation has been taken into account experimentally.

Absolute activities have been deduced from $4\pi\beta-\gamma$ and $4\pi\beta$ measurements for gold, from $4\pi\beta-\gamma$ for iron.

They agree very well with additional determinations by means of calibrated crystal, the deviations between the different methods being lower than $\pm 1\%$ in all cases.

Taking a half life of (45.0 ± 0.5) d for iron-59 and assuming a content of 0.33% of iron-58 in natural iron, one obtains

$$\sigma_0(\text{Fe}^{58}(n,\gamma)) = (1.23 \pm 0.035) \text{ b},$$

if the energy differential cross-section is supposed to follow an $1/V$ law. This is to be compared with a literature value of $(1.01 \pm 0.10) \text{ b}$ ⁽¹¹⁾.

References.

1. DEPUYDT, NEVE DE MEVERGNIES - Reactor Sci.Techn. 16, 447 (1962)
2. FABRY - Use of a convertor for the standardisation of fast neutron dosimetry in the energy range above 10 keV.
To be presented to the Euratom Dosimetry Working Group.
3. BUTLER, SANTRY - Can.J.Phys. 42, 1030 (1964).
4. BUTLER, SANTRY - Can.J.Phys. 41, 371 (1963).
5. WAY and co-workers - Nuclear Data Sheets. Nat.Ac.Sci.-Nat. Res. Council. Washington D.C.
6. MARTIN, CLARE - TRG report 700 (c)(1964)
7. MISRA, MERRITT - AECL 2044, p31 (1964).
8. VANINBROUKX - Eur 524.n (1964).
9. FABRY, DEWORM - Progress in the use of iron as a neutron flux integrator. Euratom Dosimetry Working Group (30 October 1964)
10. DERUYTTER - React. Sci. Techn. 15, 165 (1961).
11. HUGHES et.al. BNL-325 suppl. 1, second edition (Jan. 1960).

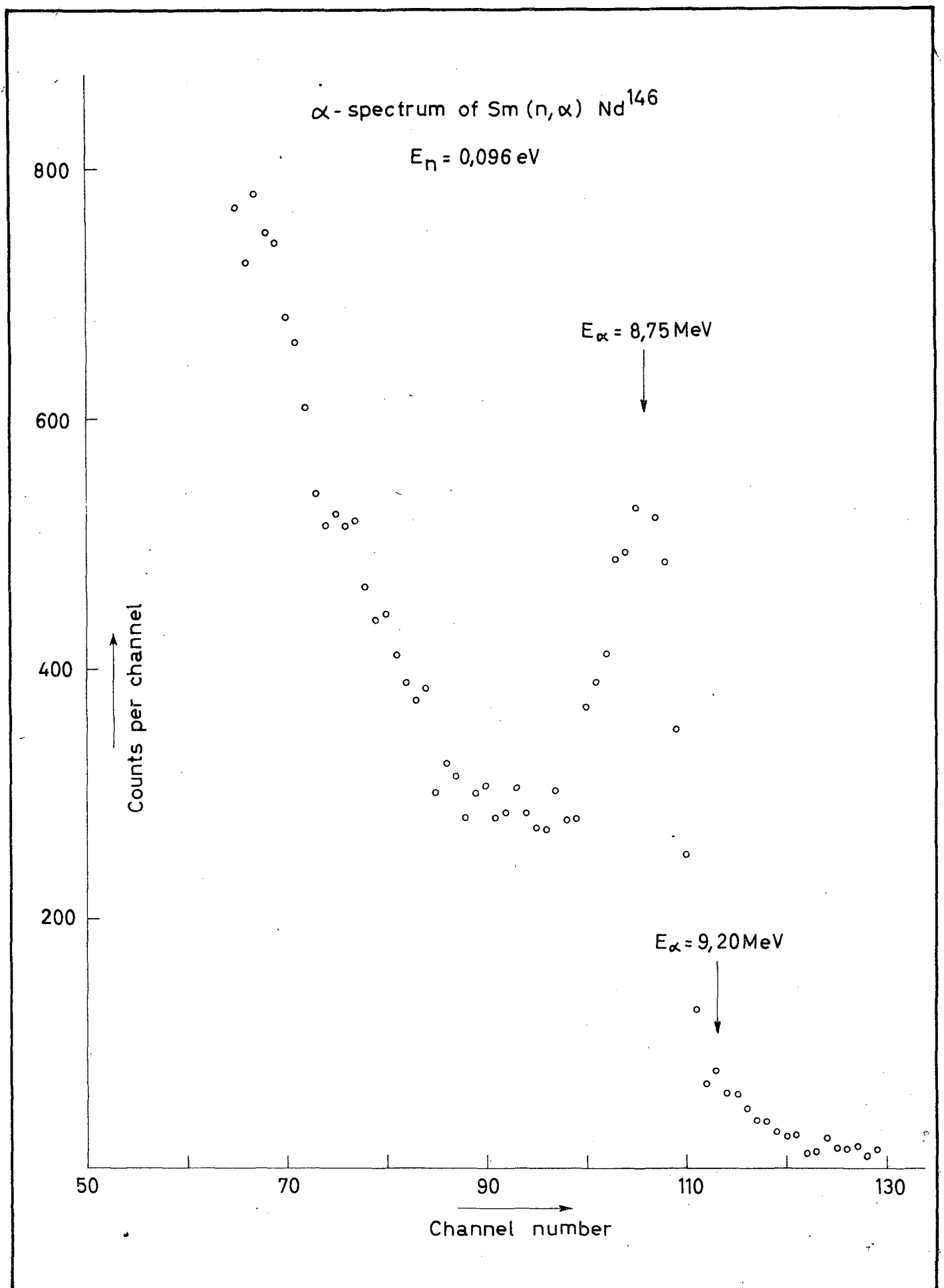


Fig. 5.1.

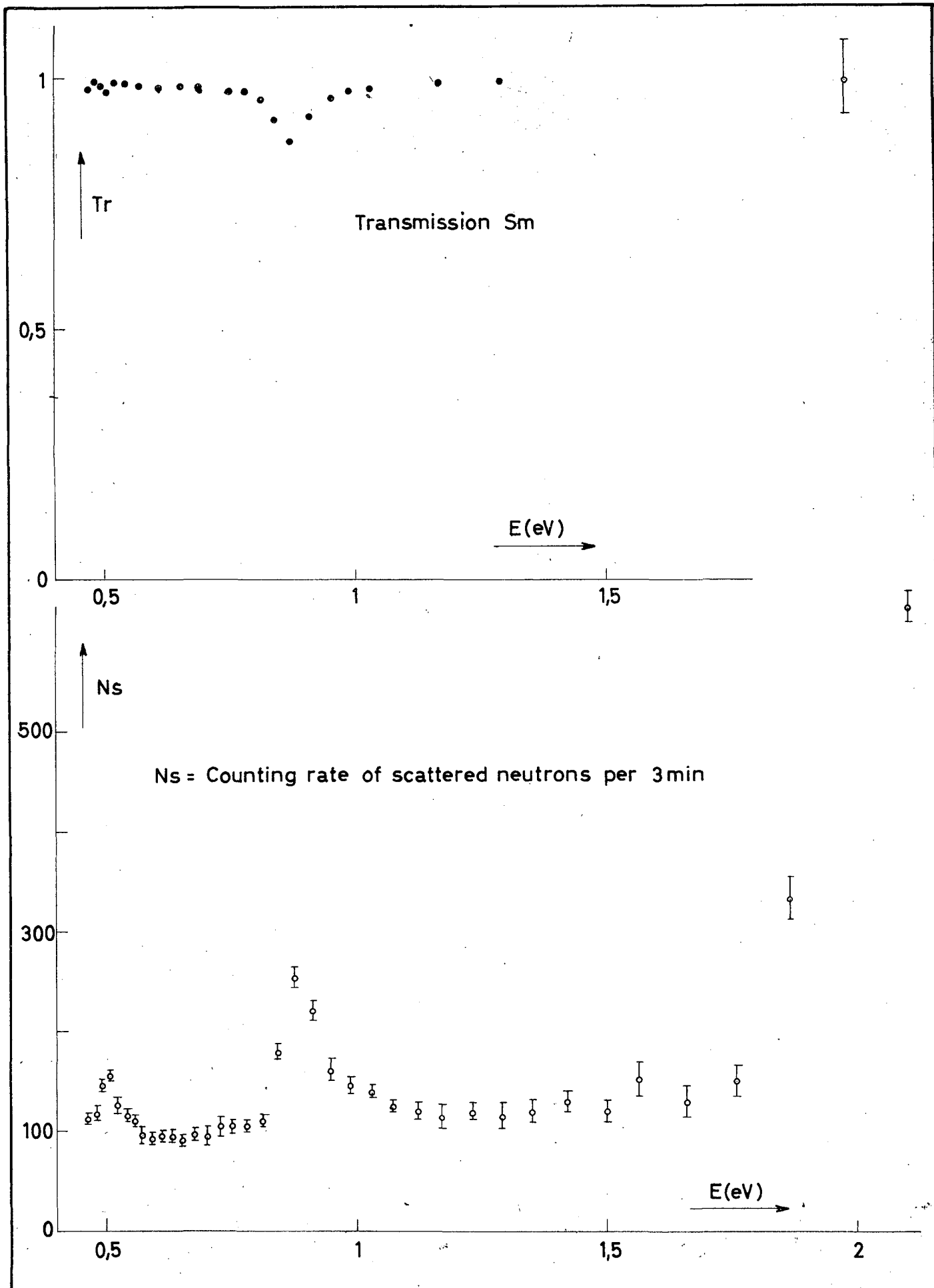


Fig. 5.2.

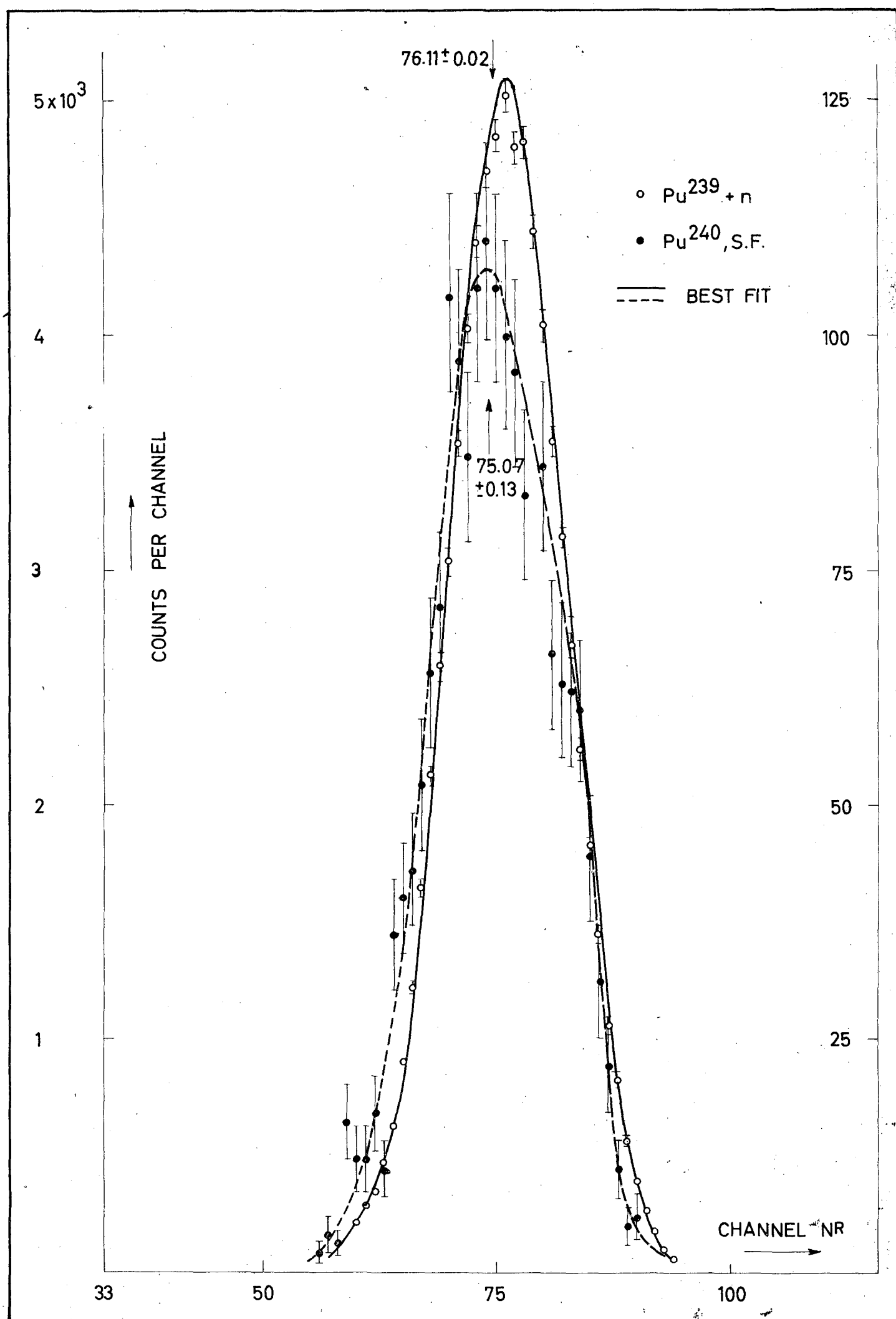


Fig. 5.3.

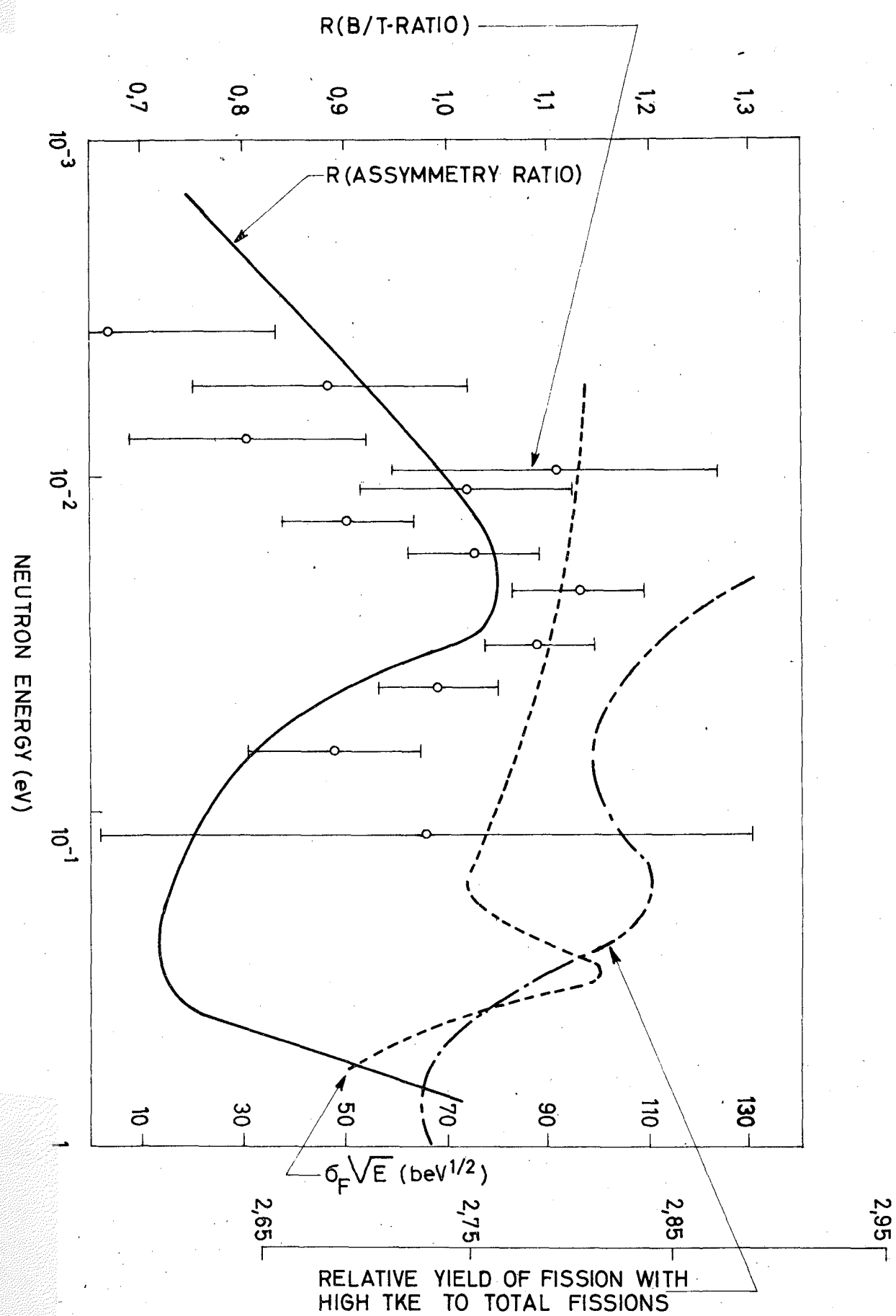


Fig. 5.4.

Projet PN8 - T7-BR2

PN 2297
20-4-64

Circuit d'irradiation

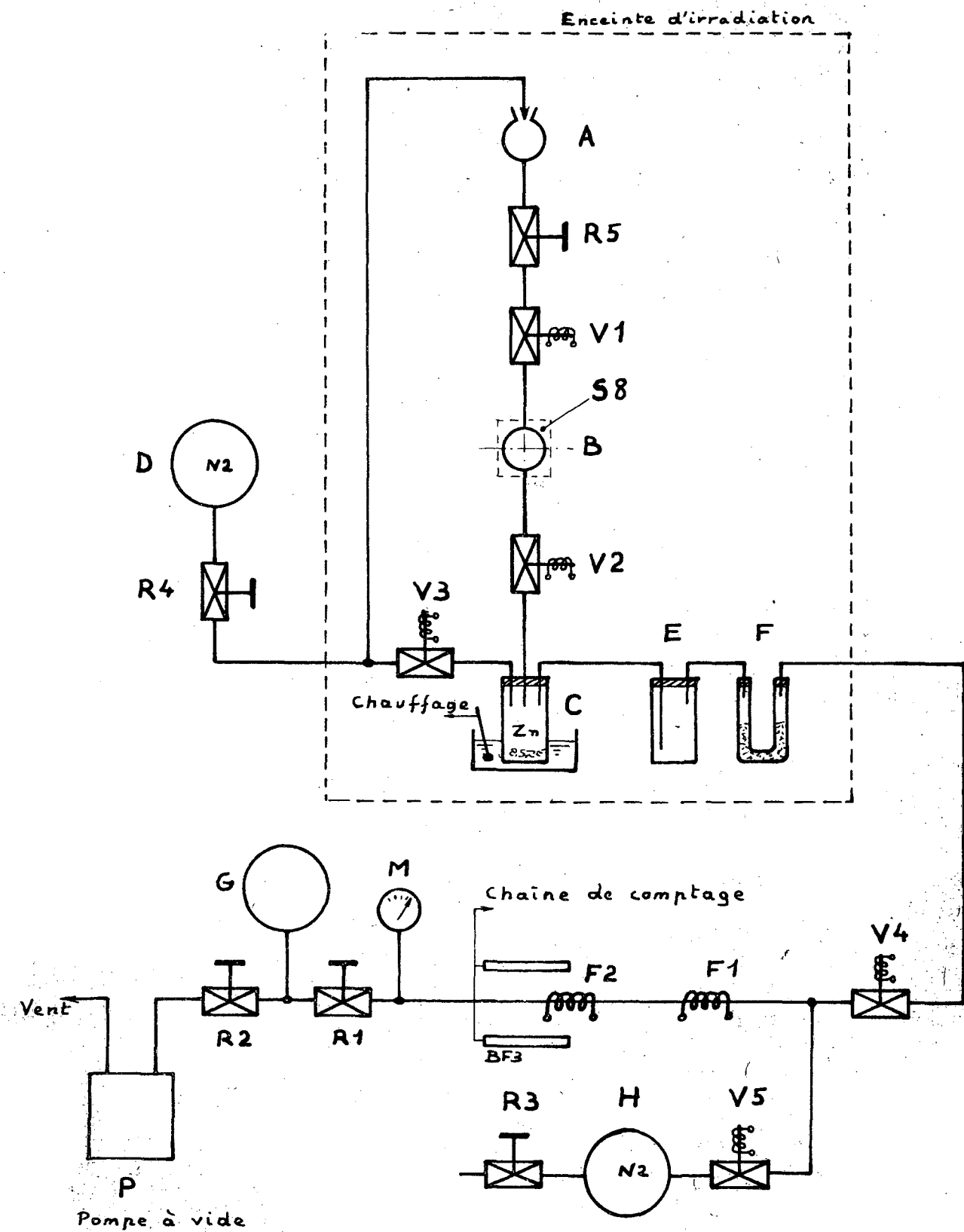


Fig. 5.5.

6.

LABORATOIRE VAN DE GRAAFF, UNIVERSITE DE LIEGE (Belgium)

Measurements of the angular distribution of $^6\text{Li}(n,t)^4\text{He}$ tritons have been continued. This work is done under Euratom-University of Liège contract nr. 008/7/62 RAPB (see former publications on this subject).

In 1964 angular distribution measurements have been finished for the following neutron energies:

$$E_n = (90 \pm 20) \text{ keV} \text{ (paper in press),}$$

$$E_n = (250 \pm 20) \text{ keV and } E_n = (390 \pm 20) \text{ keV.}$$

In 1965 investigations will be continued for $E_n < 250$ keV (in collaboration with CEN Cadarache) and $E_n \geq 500$ keV.

The techniques used are solid state detectors for $E_n \geq 250$ keV and nuclear emulsions for $E_n < 250$ keV.

7. LABORATORIO DI FISICA NUCLEARE APPLICATA - CENTRO DI STUDI
NUCLEARI DELLA CASACCIA DEL COMITATO NAZIONALE PER L'ENERGIA
NUCLEARE - CASACCIA (Italy)

7.1. Neutron Physics

7.1.1. Accelerator experiments

By means of pulsed neutron source (Van de Graaff 400 keV) we are determining the cross-section for inelastic reactions $n + n'$ on the following nuclei: Al²⁷, Si²⁸, Mg²⁴, S³². The energy selection of the neutron groups inelastically diffused, which permits to determine the single levels cross-section, is obtained by means of a solid state spectrometer with converters of Li⁶F (90 μ gr/cm² and 150 μ gr/cm²).

From the sum of the energies of the Li⁶(n, α)T reaction products and taking into account the Q of 4.78 MeV, we determine the neutron energy with a line width at half height of 130 keV, with the best efficiency of the converter.

The diffusing geometry is spherical, with the spectrometer in the center; the thickness is 2/3 of the neutron mean free path in order to minimize the multiple diffusion.

In these conditions, with only one cycle of measurements, with and without diffusor, one obtains the experimental data on the inelastic cross-section, on the transmission and on the elastic cross-section. The energy range of the source neutrons is between 2.5 and 3.4 MeV.

The cycles of measurements with Si and Mg diffusors have been completed. We are now performing experiments on C¹², (elastic transmission and diffusion) and measurements without diffusors are also in progress.

In the meantime we are performing a cycle of measurements on the differential cross-section of the Li⁶(n, α)T reaction in the same energy range in order to determine theoretically the response of the diffusor-spectrometer assembly.

7.1.2. Reactor experiments - Slow chopper

By means of the slow neutron chopper described in a previous paper total neutron cross-section of benzene and diphenyl at room temperature have been measured in the energy range between 0.1 and 0.001 eV.

Our experimental data for benzene agree reasonably with the Krieger-Nelkin curve at $\lambda < 4 \text{ \AA}$, while at $\lambda > 4 \text{ \AA}$ the points stay higher.

As far as the curve calculated by Boffi et al. is concerned, we notice a better agreement for the curve which takes into account beside the vibrational modes, also the translational and rotational ones. We point out that the curves calculated either according to the Boffi et al. or to the Krieger-Nelkin theory, both consider rotational modes only from a classical point of view. It would be also interesting to compare the experimental points with the Boffi curve beyond 4 \AA , since at this point the influence of rotations on the total cross-section becomes bigger. From what we can see from the behaviour of the curve at $\lambda < 4 \text{ \AA}$, it seems that agreement also for $\lambda > 4 \text{ \AA}$ would be better with the curve which takes into account all the degrees of freedom. The experimental data on diphenyl show a deviation from the Krieger-Nelkin curve which increases with the neutron wavelength.

We have really a good agreement of the neutron results for diphenyl with the curve calculated for benzene in the energy range which is most sensible to vibrations. We point out that our experimental results are in agreement with infrared measurements, which indicate that the vibrational spectra of benzene and diphenyl differ in the fine structure only.

Further measurements are now in progress on solid benzene at low temperature and liquid diphenyl at high temperature, as on liquid and solid dowlterm A, for a more accurate study of the internal degrees of freedom of the molecules and the solid-liquid transition.

7.2. Nuclear Physics

7.2.1. Resonant scattering and absorption of γ -lines.

The study of high excitation nuclear levels is performed by means of monochromatic γ -rays produced in (n, γ) reactions inside the reactor. In the inner part of a tube tangential to the core of RC-1 Reactor ($7 \cdot 10^{11} \text{ n/cm}^2 \text{ sec}$) we put a sample of an element which, following neutron capture, emits a certain number of γ -lines. A borated paraffin absorber placed above the sample stops the scattering neutrons.

At the end of the tube we thus have a well collimated photon beam with a line spectrum.

The beam hits a target made of the element we want to study, and γ -rays scattered at a laboratory angle of 135° are detected by 5"x5" or 4"x6" NaI(Tl) scintillators which feed a multichannel analyser.

The idea underlying this experiment is the following. as in medium-heavy nuclei the level density in the 5-10 MeV interval is high and the mean-life of these levels is comparatively short, there is a substantial probability (of the order of some percent) that a γ -line emitted by the source, is resonantly scattered by the target element.

In the present time we have applied this technique to six source scatterer pairs. By the measurement of scattering and absorption cross-sections at different temperatures we have found total and partial radiative widths of high energy levels in Bi²⁰⁹, Pb²⁰⁸, Cd¹¹⁴, Ni⁶², Cu⁶³.

Further, we have studied an experimental technique employing a mechanical rotor which allows to shift the energy of the γ -lines on the energy of the resonant levels.

7.2.2. Nuclear Spectroscopy

We have carried out an experiment on the decay of the isomeric level of the odd-odd nucleous Ta¹⁶². By means of a magnetic spectrometer characterized by a high resolution (about 1%) we have measured conversion coefficients and α_K/α_L , α_K/α_M ratios of γ -lines in the range 100-500 keV. The obtained level scheme is in agreement with the theoretical previsions of the Nilsson model, if neutron-proton residual forces of the usual kind are introduced.

Further we have carried out some $\alpha - \gamma$ angular correlation experiments in Rn²¹⁹ \rightarrow Po²¹⁵, Ra²²³ \rightarrow Po²¹⁹, Th²²⁷ \rightarrow Ra²²³.

7.2.3. Theoretical work

In order to complete the information obtained from the experimental work in nuclear spectroscopy, we have developped a program of theoretical calculations.

In the present time are in progress some programs on the following arguments: a) the role of the residual forces in odd-odd nuclei, both spherical and deformed; b) the self consistent nuclear fields in the framework of linearization technique.

8. LABORATORIO DATI E CALCOLI NUCLEARI - CENTRO DI CALCOLO DI BOLOGNA DEL COMITATO NAZIONALE PER L'ENERGIA NUCLEARE - BOLOGNA (Italy)

8.1. Theoretical Activities

During this period, theoretical activities have been mainly devoted to the development of computer programmes for optical model as well as statistical model calculations.

As regards the optical model calculations, a particular effort has been made in order to take into account the effects due to nuclear deformations. On these bases, an analysis of U-238 angular distributions has been carried out. Work is in progress in order to evaluate deformation effects for non zero spin nuclei.

The statistical model has been extensively used for the analysis of capture cross sections of heavy mass nuclei. ($70 \leq A \leq 170$) in the energy range ~ 1 KeV - 10 MeV.

8.2. Experimental Activities

The experimental work is at its very beginning. The main effort was centered on testing the electronic equipment built for elastic and inelastic cross section measurements in the MeV region. Preliminary measurements of Na elastic scattering angular distributions, using as neutron source the 5 MeV pulsed V.d.G. of Padua University are under way.

9. GRUPPO DI ISPRA PER LE MISURE SEZIONI D'URTO DEL COMITATO NAZIONALE PER L'ENERGIA NUCLEARE, ISPRA (Italy)

9.1. Study of Slow Neutron Resonances in Palladium
(C. Coceva, F. Corvi, P. Giacobbe, M. Stefanon)

Transmission measurements on samples of natural palladium of different thicknesses have been completed.

Isotopic identification of several resonances has been made by means of the study of low energy gamma ray capture spectra. Also the spin of several levels of Pd^{105} has been assigned on the basis of a measurement of the ratio of double coincidences over singles for capture events. A shape analysis of the first few resonances has been completed; other resonances are under analysis.

A report on this work has been given at the Catania meeting of the Italian Physical Society.

10. CENTRO DI INFORMAZIONI STUDI ESPERIENZE (CISE)
- SEGRATE (MILANO) (Italy)

10.1. On the Angular Correlation Analysis in Compound Nucleus Reactions.

The theory of the angular correlations in compound nucleus reactions has been extended to large energy intervals, when slow variations with the energy of the penetrabilities and of the number of competing channels are taken into account. A slightly modified definition of the correlation function is given, which allows the deviation of explicit formulae, suitable for comparison with the experimental data. Formulae for the average differential cross-section are also obtained.

10.2. U^{235} Fission Mechanism.

The U^{235} fission mechanism has been analyzed with a statistical model as far as 20.4 MeV excitation energy of compound nucleus U^{236} .

The following computation has been performed:

total kinetic energy and mass distribution of the final fragments at different excitation energies of U^{236} , number of neutrons emitted by the single fragments and scission widths of U^{236} compound nucleus for excitation energies from zero (spontaneous scission) to 12.4 MeV corresponding to $U^{235}(n,f)$ reduced by 6 MeV neutrons.

10.3. Nuclear Reactions at Low Energy.

In the field of low energy nuclear reactions, the reactions $Al^{27}(d,\alpha)$ and $Al^{27}(d,p)$ have been studied, both theoretically and experimentally, for several emission angles and for incident deuteron energies. In particular, the measurement of the cross section for proton emission at an angle of 7° with respect to the incident beam has been performed up to a deuteron energy of 2.9 MeV.

There have been obtained excitation functions at each angle for the various proton and alpha groups corresponding to the different final states of the residual nuclei. In the

whole, there have been performed measurements for 11 different angles from 7° to 171° , in the laboratory system, with overall good deuteron energy resolution (10-20 MeV).

All of these excitation functions are characterized by evident fluctuations with energy, the average widths of which are interpreted, after Ericson theory, as characteristic features of the compound nucleus which is the same for both (d, p) and (d, α) reactions, while the relative average amplitude, of these fluctuations, depends on the particular selected reaction channel and on the emission angle. It was obtained a particularly good agreement between the theoretical and experimental value of the average width \bar{f} of the compound nucleus Si^{29} at an excitation energy of about 20 MeV ($\bar{f} = 30-45$ KeV).

The theoretical value has been calculated with the statistical model and the experimental one has been obtained from the correlation width for the fluctuations themselves.

As concerns the dependence of the relative fluctuation amplitude on the angle and channel reaction, the experimental result has been compared with the theoretical predictions on the basis of the "black nucleus model".

The average behaviour of the excitation functions for the Al^{27} (d, p) reaction reveals the presence of direct effect. In particular, the transition to the ground state of Al^{28} shows a dominant direct effect, as can easily be seen from the very rapid increase with the energy of the experimental excitation function at 7° .

Angular distributions for the transition to the ground state of Al^{28} have been calculated for various incident deuteron energies, on the basis of D.W.B.A. theory. Therefore, it has been possible to compare the average theoretical behaviour at 7° , which is assumed to be equal to the sum of direct effect and evaporation contribution, with the average behaviour of the experimental excitation function, the fluctuations of which are attributed to interference effects between the mechanisms of direct and evaporative interactions. This work, as briefly discussed, is still on way of refinement and will be published as soon as completed.

II. ISTITUTO DI FISICA DELL'UNIVERSITA' DI CATANIA - CENTRO
SICILIANO DI FISICA NUCLEARE - SEZIONE SICILIANA DELL'ISTIUTO
NAZIONALE FISICA NUCLEARE, Catania (Italy)

II.1. Nuclear Fission

The fission cross section and the angular distribution of fragments of fission induced in U^{238} by monoenergetic neutrons between 1.8 and 5 MeV have been studied.

The cross section shows around 3.3 MeV a minimum more evident than that found by other authors. The fragment anisotropy in the angular distribution varies between 1.47 ± 0.03 at $E_n = 1.71$ MeV and 1.17 ± 0.03 at $E_n = 5.19$ MeV (1).

The angular distribution of fragments of fission induced by neutrons in Th^{232} is in progress. The angular distributions are peaked forward; preliminary results show that at neutron energy of 1.89, 2.20 and 2.66 MeV the anisotropy is 1.39 ± 0.04 , 1.47 ± 0.05 and 1.44 ± 0.02 respectively (2).

II.2. Fast Neutron Spectrometer

A proton recoil fast neutron spectrometer for energies in the range between 10 and 17 MeV has been realized with two solid state detectors and a cylindrical polyethylene converter. The measured resolution was 7.3% at $E_n = 16.5$ MeV. (3).

II.3. Nuclear Photoeffect

The energy spectra of the photoneutrons from Al irradiated with bremsstrahlung have been studied at $E_{\gamma max}$ of 24 and 30 MeV. Resonances at $E_{\gamma} = 18$, 19.4, 21.2 and 26.5 MeV have been found (4).

II.4. (d,n) Reaction

The neutron spectra from the $Li^7(d,n)Be^8$ reaction have been studied with a fast neutron proton recoil spectrometer. The experimental results have been discussed assuming a Lorentz distribution for the neutrons that leave the Be^8 in various states (5).

11.5. Angular distributions and energy spectra

These have been studied in $\text{Ca}^{40}(n,\alpha)\text{A}^{37}$ and $\text{Zn}^{64}(n,\alpha)\text{Ni}^{61}$ reactions. The results seem to indicate the existence of intermediate reaction mechanism which involves excitation of doorway states giving strong interference patterns in angular distribution. Some results have been presented at the "Congrès international de physique nucléaire" 1964 Paris (6) and at the "50th Meeting of S.I.F." 1964 Catania (7).

11.6. Theoretical Research.

Work has been carried out on the physics of nuclear reactions with special emphasis on:

11.6.1. (n,p) and (p,n) reactions on nuclei of mass number between 12 and 40.

Cross sections, energy spectra and polarization effects are studied in the distorted wave Born approximation with a finite range effective n-p interaction including exchange effects (8,9,10). Recently, it has been investigated the effect of spin and isotopic spin dependence of the n-p interaction (10, 11, 12, 13).

11.6.2. Theory of nuclear photoeffect.

The photodisintegration of the deuteron near the threshold. In the framework of the phenomenological theory, the electric and magnetic dipole transition amplitudes are evaluated including tensor forces and tensor coupling in the final states of the n-p system (14).

References

- (1) Fission of U^{238} with neutrons from 2 to 5 MeV. V. Emma, S. Lo Nigro, C. Milone and R. Ricamo. To be published in "Nuclear Physics 1965".
- (2) Distribuzione angolare dei frammenti di fissione del Torio. S. Lo Nigro and C. Milone. Report to the 50th SIF Meeting, Catania 1964.
- (3) A proton recoil fast neutron spectrometer with solid state detectors. A.S. Figuera and C. Milone. Nucl. Instr. and Meth. 27, 339, 1964.
- (4) Energy spectra of photoneutrons from Al and neutron emission processes. C. Milone. Nucl. Phys. 47, 607, 1963.
- (5) Energy spectra of the neutrons from the $Li^7(d,n)$ reaction. C. Milone and R. Potenza. Congr. Intern. Physique Nucléaire, Paris 1964.
- (6) Angular distributions of (n,α) reactions on Ca^{40} and Zn^{64} for E_n between 4 and 5 MeV. G. Calvi, A.S. Figuera and R. Potenza. Congrès Intern. Physique Nucléaire, Paris 1964.
- (7) Reazioni (n,α) per $4 \text{ MeV} \leq E_n \leq 5 \text{ MeV}$. G. Calvi, S. Cavallaro, A.S. Figuera and R. Potenza. 50th S.I.F. Meeting, Catania 1964.
- (8) Analysis of direct (n,p) reactions. A. Agodi, R. Giordano and G. Schiffner. Nucl. Phys. 46, 545, 1963.
- (9) Numerical Methods for DWBA Calculations on (n,p) Reactions. A. Agodi, R. Giordano, G. Schiffner, M. Giannini. Nuovo Cimento, 30, 644, 1963.

- (10) Finite range and exchange effects in the reaction $^{28}\text{Si}(\text{n},\text{p})^{28}\text{Al}$.
A. Agodi, G. Schiffner.
Nucl. Phys. 50, 337, 1964.
- (11) Finite range D.W. calculations between 5 and 20 MeV.
Congrès Intern. de Physique Nucl., Paris, 1964.
A. Agodi and G. Schiffner.
- (12) Distorted waves Born approximation in the theory of direct reactions.
A. Agodi.
Invited paper to the 50th Italian Physical Society Meeting,
Catania 1964.
- (13) Direct (n,p) and (p,n) reactions on light nuclei.
A. Agodi, R. Parisi, G. Schiffner.
Report to the 50th SIF Meeting, Catania 1964.
- (14) The photodisintegration of the deuteron near the threshold.
S. Cantone, R. Giordano, D. Gutkowski.
Report to the 50th SIF Meeting, Catania 1964.

12. LABORATORIO DELL'ACCELERATORE VAN DE GRAAFF DELLA UNIVERSITA'
DI PADOVA - PADOVA (Italy)

12.1. The $^6\text{Li}(p, ^3\text{He})^4\text{He}$ reaction in the energy range $3 \div 5.6$ MeV.
(U. Fasoli, D. Toniolo and G. Zago)

The $^6\text{Li}(p, ^3\text{He})^4\text{He}$ reaction has been studied between $3 \div 5.6$ MeV proton bombarding energy. The angular distributions obtained in energy steps of 200 KeV have been fitted by an expansion of Legendre polynomials. The coefficients of Legendre polynomials and the total cross section were extracted.

The presence of odd terms in the expansion implies interference between nearby lying levels, but effect of direct reaction is not excluded. Absence of structure in the total cross section at about 10 MeV excitation energy of ^7Be indicates that α -particle width is small.

12.2. The elastic scattering of protons by ^6Li in the energy range $1.3 \div 5.6$ MeV. (U. Fasoli, E.A. Silverstein, D. Toniolo and G. Zago)

Excitation curves at various angles and angular distributions were analysed by Legendre polynomial expansion. A broad maximum in the excitation curves was observed at 4.6 proton bombarding energy corresponding to a level of the nuclide Be at about 10 MeV excitation energy. Qualitative interpretation of the data suggests $4P_{3/2}$ configuration for this level with $J^\pi = \frac{3}{2}^-$.

12.3. Elastic and inelastic scattering of protons by ^7Li in the energy interval $3.0 \div 5.5$ MeV. (U. Fasoli, D. Toniolo and G. Zago)

Excitation curves at various angles and angular distributions were measured for the reactions $^7\text{Li}(p,p)^7\text{Li}$ and $^7\text{Li}(p,p')^7\text{Li}^*$. Best fit of this angular distribution was performed with Legendre polynomial expansion up to the 4th order. The excitation curves of the reaction $^7\text{Li}(p,p)^7\text{Li}$ show a large peak at 4.2 MeV proton bombarding energy, whose experimental width

is about 1.2 MeV. It was attributed to a new level of the ${}^7\text{Be}$ nuclide. The most favourable assignment for the J^π value of this level is 1^+ or 3^+ . A broad peak is observed in the ${}^7\text{Li}(\text{p}, \text{p}') {}^7\text{Li}^*$ excitation curves at about 3 MeV bombarding energy. The data suggest a value $J^\pi = 1^+$ for this level.

13. SOTTOSEZIONE DI FIRENZE DELL'ISTITUTO NAZIONALE FISICA NUCLEARE -
ISTITUTO DI FISICA DELL'UNIVERSITA' DI FIRENZE - FIRENZE (Italy)

In the period from 1.7.63 to 1.7.64, the Florence group has completed the study of the reactions $\text{Si}^{28}(\gamma, p)$ and $\text{Si}^{28}(\gamma, \alpha)$ around $E_\gamma = 17.64$ MeV and of the reaction $\text{Ne}^{20}(n, \alpha)\text{O}^{17}$, at $E_n = 14$ MeV. The results on the silicon photodisintegration have been presented at the Paris Conference (2-8 July 1964 contribution C 284) and are in the press in "Nuclear Physics". The preliminary evidence for the existence of wide fluctuations of the Ericson's type has been confirmed the presence of a direct contribution (up to say 50%) is, however, not excluded; on the contrary, it may appear necessary to account for some discrepancy between the relative experimental value of σ (averaged over a 116 keV energy interval) for different transitions and the theoretical one, evaluated on the basis of transmission coefficients (this effect is established, however, with only 5% confidence limit, due to residual fluctuations). The average cross section (in the same 116 keV energy interval) for the (γ, α) reaction (ground and 1st excited state) comes out still about 10 times smaller, with respect to the (γ, p) reaction, due to account having been taken of the pertinent transmission coefficients. This is probably an example of the Gell-Mann Telegdi isospin selection rule for (γ, α) reactions. The results on $\text{Ne}^{20}(n, \alpha)\text{O}^{17}$ reaction at $E_n = 14$ MeV have been completely evaluated and are in the press in Nuclear Physics. Energy and angular distributions have been obtained with good statistics, the most peculiar characteristics being a backward preference in the angular distribution of α -particles in the c.m. system, which seems to indicate the presence of a heavy particle stripping mechanism.

14. CENTRAL BUREAU FOR NUCLEAR MEASUREMENTS

DURATOM, Geel (Belgium)

14.1. 3 MeV Van de Graaff

14.1.1. Activation cross-section measurements
(H. Liskien, A. Paulsen)

A series activation cross-sections of threshold reactions listed on EANDC request lists has been measured. Monoenergetic neutrons were produced with energies varying between 12.6 and 19.6 MeV by using the $T(d,n)^4\text{He}$ reaction at 1 and 3 MeV deuteron energy.

The angular distribution of the neutrons from this reaction was remeasured at the same deuteron energies ⁽¹⁾. Absolute values of neutron intensities were obtained by means of a proton telescope counter.

The induced activities were determined absolutely by comparison with calibrated γ -sources. The average neutron energy spread is of the order of ± 250 keV, the accuracy of the obtained cross-sections falls between $\pm 6\%$ and $\pm 7\%$.

14.1.1.1. Cross-sections determined with the single γ -counter technique.

The following reactions have been studied at 28 different energies in the energy range between 12.6 and 19.6 MeV (2, 3):



14.1.1.2. Cross-sections determined with the $\gamma-\gamma$ coincidence technique

Energy range: from 12.6 to 16.6 MeV

Number of different energies: resp. 11, 16 and 17
Studied reactions ⁽⁴⁾:



14.1.1.3. Cross-section determined with a single γ -coincidence technique

In the case of the reaction $Mn^{55}(n, 2n)Mn^{54}$ which was studied at 23 different energies in the interval 12.6 to 19.6 MeV the coincidence between a signal from a Compton scattered γ in one crystal and the photopeak of the residual γ quantum in another crystal was utilised.

14.

14.1.4. Compilation

Supplementary sheets for the compilation on neutron induced threshold reactions (EUR 119.e) have been issued.

14.

14.1.5. Publications

- (1) Paulsen, A., and H. Liskien:

Angular distribution for the $T(dn)$, 4He reaction at 1 and 3 MeV deuteron energy,
Nuclear Physics 56, 394 (1964)

- (2) Liskien, H., and A. Paulsen:

Cross-section measurements of some threshold reactions between 12.6 and 19.6 MeV neutron energy, J. Nuclear Energy, in press.

- (3) Paulsen, A., and H. Liskien:

Anregungsfunktionen der Reaktionen $^{58}Ni(n, 2n)^{57}Ni$,
 $^{65}Co(n, 2n)^{64}Cu$ and $^{64}Zn(n, 2n)^{63}Zn$ im Energiebereich von 12.6 bis 19.6 MeV,
Nukleonik, in press.

- (4) Paulsen, A., and H. Liskien:

Cross-sections for the reactions $^{63}Cu(n, \alpha)^{60}Co$,
 $^{60}Ni(n, p)^{60}Co$, $^{46}Ti(n, p)^{46}Sc$ and $^{23}Na(n, 2n)^{22}Na$,
Nuclear Physics, in press.

14.

14.2. Determination of total cross-sections in the energy range between 2 and 30 keV.

(K.H. Böckhoff, G. Cardinael, A. De Keyser, H. Martin,
E. Migneco)

Fast time-of-flight techniques are applied to 1 nsec bursts of neutrons produced by the $^7Li(p, n)$ reaction near threshold.

The detector is a 2.5 mm resp. 5 mm thin slab of sintered ^{10}B viewed by NaI crystals.

The complete experimental equipment includes among other items:

a reduction system for the accelerator burst repetition rate which scales this rate in binary steps down to 1/8 of the first installed fixed rate of 1 Mc;

an automatic sample changer;

automatic storage of "sample in" and "sample out" spectra in two different magnetic core memories before final storage on magnetic tape;

electronic devices for fast timing with slow pulses.

The first measurements have been devoted to background determinations and to the application of a method which allows the determination of proton energies slightly above the threshold of the $^7\text{Li}(\text{p},\text{n})$ reaction by measuring the flight times of the slow and fast neutron group and of the target gammas.

First cross-section measurements will concern ^{238}U .

14.

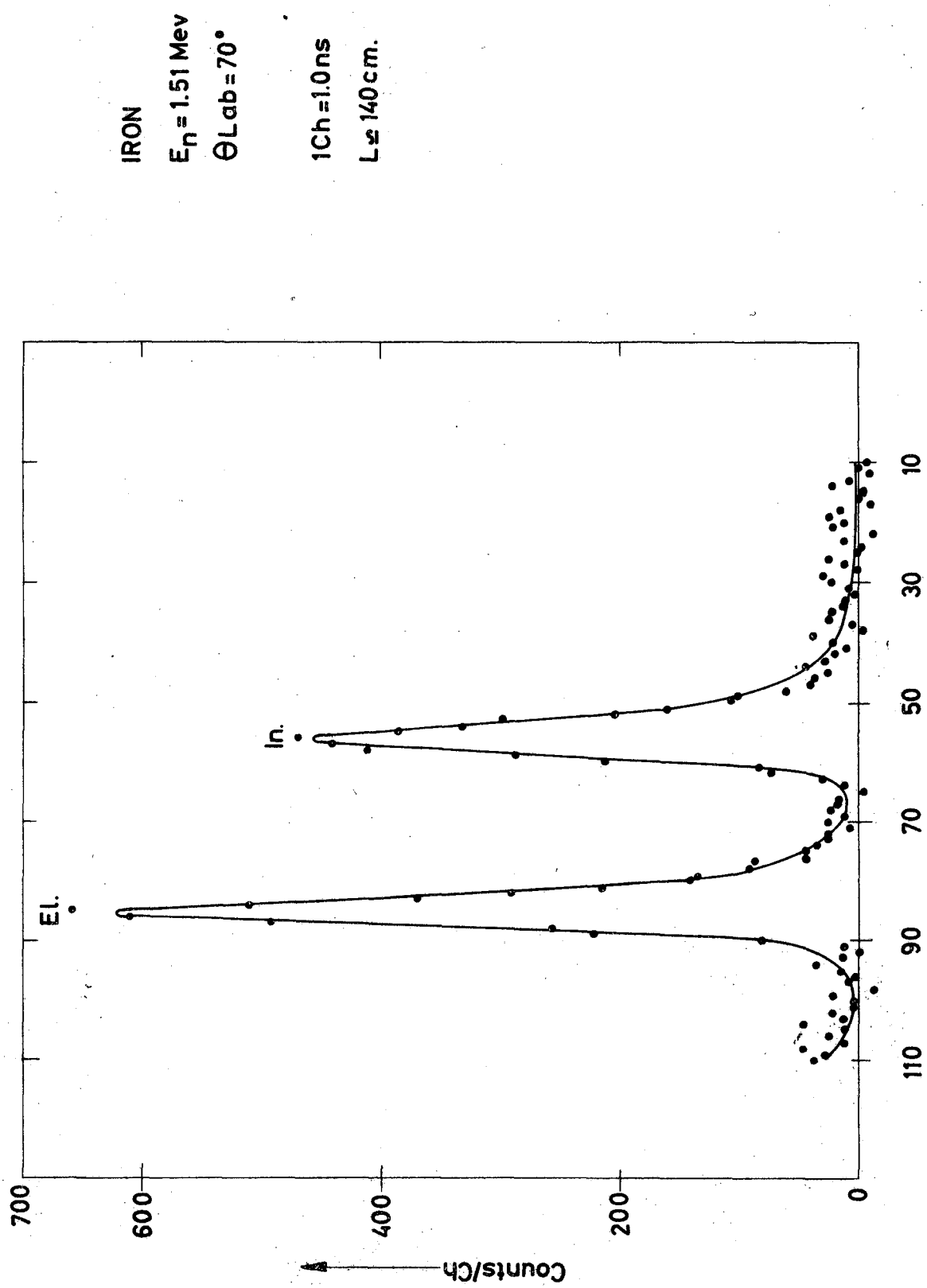
~~14.~~ 1.3. Scattering cross-sections

~~14.~~ 1.3.1. Measurements on natural iron.

(A. Jacquot, C. Rousseau)

The Cranberg technique for the measurement of fast neutron time-of-flight spectra has been employed to measure the differential scattering cross-sections of iron in the energy range between 0.45 MeV and 2.3 MeV in steps of 250 keV and at 8 angles between 20° and 143° . Absolute values of cross-sections have been obtained by referring to the well known scattering cross-section of hydrogen.

The preliminary report has been written but has to be completed by the corrections for multiple scattering and beam attenuation. The adaptation of the programme Maggie (Aldermaston) to the IBM 7090 computer of CETIS (Ispra) is in progress. Uncorrected results for the already integrated elastic and inelastic scattering cross-sections as well as



Fast neutron elastic and inelastic scattering

Fig.14.1.

an example of the differential data are given in table 14.1 and fig. 14.1.

Table 14.1.:

E_n MeV	σ_{el} barns	σ_{in} barns
2.28	2.39 \pm 0.12	0.95 \pm 0.06
2.03	2.34 \pm 0.12	1.01 \pm 0.06
1.77	2.14 \pm 0.11	0.75 \pm 0.05
1.51	2.08 \pm 0.11	0.87 \pm 0.05
1.26	2.15 \pm 0.12	0.57 \pm 0.04
1.00	2.03 \pm 0.10	-
0.73	3.13 \pm 0.16	-
0.45	3.47 \pm 0.17	-

14.1.3.2. Measurements on Silicon
(M. Coppola, C. Rousseau)

The equipment developed for the scattering measurements on iron has been improved, mainly with respect to time resolution. Measurements on silicon will start soon.

14.1.3.3. Further scattering experiments

Further isotopes to be investigated are ^6Li , ^7Li and ^{239}Pu .

14.2. 60 MeV Linear Accelerator

14.2.1. Accelerator and neutron targets
(C. Allard, J.M. Salomé)

For measurements mainly with neutrons in the resonance region the CBNM has been provided with a 60 MeV electron linear accelerator and associated neutron time-of-flight installations. In the period under report the Linac building has been constructed and the accelerator with all the necessary equipment has been mounted. The tests of the machine carried out until now, let expect that the specifications guaranteed (Table 14.2.) will be reached in February, 1965.

Table 14.2.: Principle Characteristics and Expected Performances of the Linac

	Operation	Energy at $I \sim 0$ (MeV)	Energy band for I_{max} (MeV)	Maximum peak intensity (A)	Beam power (kW)	Neutrons per sec	Neutrons per sec in the burst
0.01 μ s 1000 pps	Guarantee	57	$55 \pm 4\%$	3	1.6	$5 \cdot 10^{12}$	$\sim 5 \cdot 10^{17}$
	Maximum at full power	100	$96 \pm 4\%$	5	4.6	$1.5 \cdot 10^{13}$	$1.5 \cdot 10^{18}$
0.1 μ s 880 pps	Guarantee	57	$49.5 \pm 1.6\%$	1	3.7	$\sim 10^{13}$	$1.1 \cdot 10^{17}$
	Maximum at full power	100	$85.5 \pm 1.3\%$	1.8	11.2	$3.7 \cdot 10^{13}$	$4.2 \cdot 10^{17}$
1 μ s 380 pps	Guarantee	57	$41.5 \pm 5\%$	0.2	3.2	$\sim 10^{13}$	$2.6 \cdot 10^{16}$
	Maximum at full power	100	$52 \pm 5\%$	0.6	12	$3.8 \cdot 10^{13}$	$1 \cdot 10^{17}$
2 μ s 250 pps	Guarantee	57	$41.5 \pm 5\%$	0.2	4.2	$\sim 10^{13}$	$2 \cdot 10^{16}$
	Maximum at full power	97	49	0.6	15	$6 \cdot 10^{13}$	$1 \cdot 10^{17}$

The Linac is provided with a deviation system allowing horizontal or vertical shooting of the electron beam onto the remote-handled targets. At first a target will be used, the active part of which is of mercury with variable thickness. A natural uranium target is under preparation. A Saclay type target for about 2 kW target power is at our disposal at Saclay. A target for 10 to 15 kW will be realized after studying the first results obtained by the above-mentioned prototypes.

14.

2.2. Neutron flight paths

(K.H. Böckhoff, K. Gubernator)

Eight neutron flight paths with lengths of 200, 400 (under + 90° with respect to the accelerator axis), 200, 30, 30, 100, 140 (under - 90°), 100 meters, respectively, and 16 detector stations are under construction. The flight tubes (diameter 50 cm) are made of aluminium, and will be evacuated to about 1 torr. The distances between the centre of the target and check points in the detector stations are being measured with an accuracy better than 10^{-4} . Between the detectors and the electronic equipment comprising five 4096 channel analyzers in the Linac building, 7/8-inch "Flexwell" UHF cables are used.

14.

2.3. Fission cross-section measurements

(K.H. Böckhoff, E. Migneco, J. Theobald)

Remeasurements on ^{235}U and ^{239}Pu in the resonance region are in preparation using both fragment and neutron detection. Several methods for fission fragment detection have been tried:

A 0.2 mm thick ^7Li -glass scintillator has been covered with a ^{235}U layer and irradiated with thermal reactor neutrons. The pulse heights of scintillations attributed to fission fragments were lower than those due to the alphas from the natural decay. Similar results have been obtained with several glasses (produced by a specialized laboratory) into which uranium and cerium were incorporated.

The use of very thin plastic foils coated with fissile layers gave better results. Here the fission fragment pulses were

clearly resolved from the alpha pulses. This method is being further developed using coincidence techniques.

Further detectors under development are a liquid scintillation chamber for neutron detection and a spark counter for fragment detection in the presence of high alpha backgrounds.

14.2.4. Total cross-section measurements of ^{235}U , ^{240}Pu and Ca
(K.H.Böckhoff, G.Cardinael, A.De Keyser, H.Martin)

A detector consisting of a ^{10}B slab viewed by 8 NaJ crystals is being constructed involving photomultiplier pulsing and automatic gain stabilization. All heavy equipment like neutron collimators, γ -shields, a four position sample changer etc. are under construction.

14.2.5. Neutron flux standard for the energy range 1 to 100 keV
(K.H.Böckhoff, M.G.Cao)

A feasibility study of a method was made to measure the anisotropy near threshold of the $^7\text{Li}(\text{p},\text{n})$ reaction in the centre-of-mass system. The idea was to use a hydrogenous scatterer of such special shape that neutrons scattered from a $^7\text{Li}(\text{p},\text{n})$ point source to a point detector have the same energy, independently of the energy distribution of the neutrons impinging on the scatterer. The time-of-flight spectra of scattered neutrons reaching the detector spot should give information about the degree of anisotropy of the reaction.

The results of the study were discouraging and the method was abandoned.

The $(\text{n}\alpha,\gamma)$ reaction rates from a thick ^{10}B slab detector are being calculated with a Monte Carlo Method. The "blacker" this detector is, the less uncertainties in our knowledge of the ^{10}B $(\text{n}\alpha,\gamma)$ cross-section will influence the accuracy of the calculated reaction rates.

The calculations will be extended to hydrogenous compounds of boron.

As an auxiliary measurement the energy dependence of the ratio $\sigma_{n,\alpha}/\sigma_{n,\gamma}$ for ^{10}B is planned to be measured in the energy range between 1 and 100 keV using ^{10}B loaded glasses.

14.2.6. Surface barrier detectors

(H. Meyer)

For future applications in neutron experiments the speed of response for ionising particles of 15 produced surface barrier detectors was measured with ^{241}Am -alphas. Pulse rise times between 1.3 ns and 1.7 ns were obtained for the different detectors (material, 2000 ohm . cm; sensitive surface, 0.5 cm^2 , 1 cm^2 and 2.8 cm^2 ; thickness-fully depleted about 0.3 mm).

An amplifier (transistorized) with a risetime smaller than 1 ns, and a current gain greater than 20, was developed for that purpose. Detectors from silicon of lower resistivity (500 ohm . cm) and with a sensitive surface up to 7 cm^2 are in preparation.

14.3. Data Handling and Evaluation.

14.3.1. Data handling equipment.

14.3.1.1. Teleprocessing system.

(H. Horstmann ⁽¹⁾, A. De Keyser ⁽²⁾)

A preliminary teleprocessing system for transmission of punched card data to the IBM 1401 computer in Brussels has been put into operation on October 15. Since then the information of about 21000 cards have been transmitted in both directions. The retransmission rate due to incorrectly transmitted cards was 2%.

The data handling installation has been further completed by a Calcomp Model 506 digital incremental plotter. The data transfer capacity will be considerably increased by a negative tape terminal teleprocessing link between Geel and Isyra via Brussels (to be installed begin 1965).

14.

3.1.2. Nanosecond time coder

(H. Meyer ⁽³⁾, H. Vereist, P. Klopf)

Time coders to be used for high precision long range neutron flight time analysis are in development. A completed and improved version of a coder developed in 1963 ⁽⁴⁾, has been realized now.

The equipment shall be used at the Van de Graaff generator working with lower burst rates and at the linear accelerator having improved burst widths. The main characteristics of the coder are:

one nanosecond smallest channel width,
380 μ sec maximum analysis range,
accuracy about $\pm 10^{-5} \pm 0.5$ nsec.

The coder will be used first for comparative studies in connection with Van de Graaff experiments. An improved and extended (more than one measurement per analysis cycle) final version of the time coder shall be built next.

14.

3.1.3. Buffer stores

(B. Idzerda, W. Stüber)

Buffer stores for a maximum word length of 20 bits were developed and realized (5, 6). A unit with tunnel diodes as memory elements has three words and a resolution of about 0,05 μ sec for the connection to the second final version of the nanosecond time coder. Final units with a word capacity of ten words and magnetic cores as memory elements have a resolution of about 1 μ sec.

Studies on the influence of buffer store parameters on possible spectrum distortions for long range time-of-flight experiments have been done (5).

14.

3.1.4. Magnetic tape handling equipment

(B. Idzerda, W. Stüber)

Stepping techniques were developed to allow high information densities on tape also for low data rates by stepwise propagation of tape during recording. A cheap commercially available tape deck system for one inch tape and 24 tracks was chosen

for the developments.

The most important features of the equipment are, word densities greater than 300 words/inch (word length up to 20 bits) for data rates from 20000 words/sec down to zero and playback speeds up to 120 inches/sec (7, 8).

14.

3.1.5. Storage display equipment

(B. Idzerda, W. Stüber)

For the qualitative storage and integration as well as for the visualization of nuclear data with great word length, the characteristics and possibilities of display storage tubes, produced from different manufacturers (mainly for radar applications) were studied. The preliminary investigations have shown, that high quality tubes, in connection with suitable electronic equipment being under development, will probably allow a resolution of 0.1%, i.e. a maximum of 10^6 different words can be stored for integration and display.

Data, stored on magnetic tape, shall be visualized also directly with the display equipment.

14.

3.1.6. Automatic data reduction

(H. Meyer⁽³⁾, W. Stüber)

A study was made to use standard memories as associative devices for automatic data reduction in multiparameter experiments. The necessary electronic equipment was planned in some detail⁽⁹⁾.

14.

3.2. Applied mathematics

(M.G. Cao, H. Horstmann, H. Schmid)

Tabulation of kinematic parameters of some important neutron producing reactions used at the Van de Graaff accelerator (H. Horstmann, H. Liskien).

Tabulation of intensity distributions with angle and energy of the $^{7}\text{Li}(\text{p},\text{n})$ reaction.

(M.G. Cao, E. Migneco)

Modification of several extensive O.R.N.L. computer programs for use at CETIS (Ispra):

Shape analysis of neutron resonances,
Area analysis of neutron resonances,
A general least squares fit program.
(H. Horstmann)

Calculations of cross-sections for two-particle emission according to the statistical theory. The results were used for the interpretation of activation cross-section measurement data.

(H. Horstmann, H. Schmid).

Multiple scattering and beam attenuation corrections for fast neutron scattering cross-section results. In cooperation with CETIS the Monte Carlo program Maggie (Aldermaston) is being modified for use on the IBM 7090 computer in Ispra.
(H. Horstmann).

Calcomp plotter programming. A subroutine package of Calcomp has been adapted to our plotter model. A new program is being written in order to be able to use the plotter subroutines of CETIS.

(H. Schmid).

Calculation of a pulse shape discrimination electronic circuit. A figure of merit for the optimization of special pulse shape discrimination circuits is being calculated.
(M.G. Cao, E. Migneco, J. Theobald).

14.3.3. Publications

- (1) HORSTMANN, H.: Data handling installation for the linear accelerator of the C.B.N.M., Proceedings of the EANDC Conf. on Automatic Acquisition and Reduction of Nuclear Data, Karlsruhe, July 1964, p. 413.
- (2) DE KEYSER, A.: Neutron time-of-flight multichannel analysers for the linear accelerator of the C.B.N.M., Proceedings of the EANDC Conf. on Automatic Acquisition and Reduction of Nuclear Data, Karlsruhe, July 1964, p. 79.
- (3) MEYER, H.: Studies for a data handling instrumentation system in the C.B.N.M., EUR 2101.e (1964).
- (4) KLOFF, P., H. MEYER, W. STÜBER, H. VERELST: A nanosecond time coder with great analysis range for time-of-flight experiments, EUR 491.e (1964).
- (5) STÜBER, W.: Studies and development of buffer storage systems for nuclear experiments, EUR 2160.e (1964).
- (6) STÜBER, W.: Some theoretical and practical results of buffer storage systems developments, Proceedings of the EANDC Conf. on Automatic Acquisition and Reduction of Nuclear Data, Karlsruhe, July 1964, p. 362.
- (7) IDZERDA, A.B.: Studies of magnetic tape instrumentation for on-line recording and off-line analysis of data from multi-parameter nuclear experiments, EUR 2119.e (1964).
- (8) IDZERDA, A.B.: A magnetic tape data collection system with an instrumentation tape deck and high possible storage density for information rates from almost zero to greater than 20000 events per second, Proceedings of the EANDC Conf on Automatic Acquisition and Reduction of Nuclear Data, Karlsruhe, July 1964, p. 104.
- (9) MEYER, H., STÜBER, W.: Use of standard memory systems as associative memories for integrating storage of multiparameter data by automatic data reduction, Proceedings of the EANDC Conf. on Automatic Acquisition and Reduction of Nuclear Data, Karlsruhe, July 1964, p. 357.

14.4. Isotopic Standards of Stable and Fissile Isotopes.

14.4.1. Boron

(G.H. Debus, P. De Bièvre)

The determination of the mass discrimination has been continued for boron. The present results point to a small dependence of mass discrimination as function of the sample isotopic composition. Calibration solutions with nominal ^{10}B content of 10 - 20 - 50 - 80 - 90 % were carefully prepared and measured. The measurements are fully completed on two mass spectrometers (MS-5 and OEC 21-702). Preliminary investigations have been started on a third one (Nuclide Tandem) in order to determine the nature of the observed bias.

14.4.2. Uranium

(G.H. Debus, P. De Bièvre)

In 1964 most of the NBS U Isotope Standard, ranging from 0.5% to 93% ^{235}U content, have been measured and no significant deviations observed from the certified values up to now.

These measurements were performed on our instruments as a preliminary test for the establishment of depleted uranium standards.

The necessary starting materials for the preparation of these depleted uranium standards have been decided upon. The complete a priori precision calculation and optimization of preparation and measuring procedures is nearing its end.

14.4.3. Plutonium

(G.H. Debus, P. De Bièvre)

Material with a nominal content of 1 - 3 - 10 - 30% ^{240}Pu is available. The Chemistry Department has been asked to study and prepare a program to eliminate ^{241}Am prior to measurements.

A mathematical treatment of optimalizing conditions to determine overall mass discrimination is ready and is being plotted.

The laboratory cooperated in an international measurement program (8 laboratories participated) initiated by NBS, in order to determine a preliminary value for a Pu Isotope Standard.

14.

~~14.4.~~ 4.4. Lithium

(G.H. Debus, P. De Bièvre)

Preliminary calculations have been started in order to establish a Lithium Isotope Standard. Measurements on a mass spectrometer yielded the well known variations of isotope ratios during one measurement.

14.

~~14.5.~~ 4.5. Deuterium

(G.H. Debus, T. Babeliowski)

An international cooperation is being organized in order to coordinate the experience resulting from D/H measured ratios, obtained by infrared techniques, nuclear magnetic resonance, density measurements and mass spectrometry; determine the most accurate method for the determination of the isotopic composition of heavy water samples; measure physical constants of very enriched heavy water; evaluate methods of storing, handling and shipping of heavy water samples; prepare a heavy water standard.

A questionnaire was sent to 10 laboratories with possible interest in the subject. All of them replied. Eight institutes are willing to participate actively in the program. As a first step quantities of the same batch of heavy water will be sent to these institutes. Later on these containers will be sent to a second laboratory as a check.

14.

~~14.6.~~ 4.6. Publications

DE BIEVRE, P.J., and G.H. DEBUS: Precision mass spectrometric isotope dilution analysis, Nucl. Instr. Methods, in press.

DE BIEVRE, P.J., and G.H. DEBUS: Optimal conditions for mass spectrometric quantitative determination by isotope dilution, EUR report in press.

14.5. Sample preparation and assay

(G.H. Debus, J. Van Audenhove, K.F. Lauer, V. Verdingh, H. Moret, H.L. Eschbach)

A facility for the preparation of well defined samples for nuclear measurements was installed at the C.B.N.M. This facility offers services to the European Research laboratories, and more general to all research institutes performing experiments supported by EANDC.

The program is not fixed but continuously adapted to the applications received. However, some restrictions are made since no facilities are available for γ -emitting material, which cannot be handled in standard glove-boxes.

The new building, designed for activities with α -material provides three hundred square meter floor space (for laboratories, i.e. not including corridors, offices, store rooms, etc.), which is sufficient to group all equipment designed for preparation and definition of samples of α -material.

The personnel assigned to sample preparation consists at present of one metallurgist, 13 technicians, but a much larger number of people is concerned with the preparation and definition of samples since substantial help is obtained from the groups metrology and chemistry, and from the workshop.

Due to the special task: the preparation and assay of samples according to specifications required, development and applied research are continuously adapted to new problems. However, standard techniques are now available for a large variety of samples asked for, and more than 2250 samples were prepared, assayed, packed and delivered. About 900 samples are in different stages of preparation.

Publications:

J. VAN AUDENHOVE, Vacuum evaporation of metals by high frequency levitation heating, Rev. Scient. Instr. (scheduled issue: February, 1965).

J. VAN AUDENHOVE, Teorie en toepassingen van het elektronen-bombardement, Het ingenieursblad 33 (1964).

V. VERDINGH and K.F. LAUER, Equipment for electrospraying, letter to the editor to be published in Nucl. Instr. Methods.

H.L. ESCHBACH, Herstellung von gleichmässigen Aufdampfschichten auf Platten und Zylindern. Vakuumtechn. 13, 141 (1964), EUR 1654 d

V. VERDINGH and K.F. LAUER, The preparation of sodium cylinders and sodium spheres, EUR report, in press.

V. VERDINGH and K.F. LAUER, Preparation of samples by high-tension electrophoresis, EUR report in preparation.

14.

~~14.~~ 6. Radioisotopes

14.

~~14.~~ 6.1. Radioisotope standard sources

(W. Bambynek, G. Bortels, E. De Roost, A. Spernol, W. Van der Eijk, R. Vaninbroukx)

Standards of the following radionuclides have been prepared for absolute calibrations during different neutron measurements: Na^{22} , Na^{24} , Sc^{46} , Mn^{54} , Mn^{56} , Co^{58} , Co^{60} and Am^{241} . The precision was always $\pm 0.1\%$, the accuracy between ± 0.3 and 0.5% , except in the case of Co^{58} , where the accuracy was only $\pm 1\%$ ⁽¹⁾. This high accuracy has been reached by using always several different methods for every standardization. Some of the methods used have been improved considerably. This pertains especially to the liquid scintillation method⁽²⁾, the low geometry method for alpha counting⁽³⁾ and the gas counting method⁽⁴⁾. Also the coincidence method has been thoroughly re-investigated.⁽⁵⁾ (its 0.1% limit of accuracy has been proved) and the foil absorption correction for 4π -counting has been determined with high precision⁽⁶⁾.

14.

~~14.~~ 6.2. Determination of physical constants concerning radionuclides.

(W. Bambynek, E. De Roost, A. Spernol, W. van der Eijk, R. Vaninbroukx).

Measurements of the ratio of the thermal neutron cross-sections of Co^{59} and Au^{197} in a Maxwellian spectrum under wellknown conditions have been finished and are under calculation. The results will also yield a very precise correction for flux perturbations in Co-detectors⁷⁾. Precision measurements of the EC/ β^+ -ratio in the decay of Na^{22} , V^{48} and Mn^{52} have been finished, too, and are under calculation. Some work has been done on the branching in the Kr^{85} decay, the absolute number of conversion electrons in the Am^{241} decay and the half life of Tl^{204} (by microcalorimetry).

14

6.3. Publications.

- (1) R. VANINBROUKX and G. GROSSE, "Standardization of Co⁵⁸", EUR 524 n, 1964.
- (2) R. VANINBROUKX and A. SPERNOL, "High precision liquid scintillation counting", IJARI, in press.
- (3) A. SPERNOL and O. LERCH, "0.2% accurate alpha counting with plastic detectors", Nucl. Instr. Meth., in press.
- (4) A. SPERNOL and B. DENECKE, "Precision counting of tritium", IJARI 15, 139, 195 and 241, 1964.
- (5) A. SPERNOL, E. DE ROOST and O. LERCH, "High precision 4 $\pi\beta-\gamma$ coincidence counting", EUR 477e, 1964.
- (6) W. VAN DER EIJK, "Foil absorption correction in high precision 4 π -counting", EUR-report in press.
- (7) A. SPERNOL, R. VANINBROUKX and G. GROSSE, "Thermal flux perturbation by Cobalt detectors", "Neutron Dosimetry" I, 547, 1963 (IAEA Vienna).

DEPARTEMENT DE RECHERCHE PHYSIQUE - SECTION DES MESURES
NEUTRONIQUES FONDAMENTALES, CEA, Saclay (France)

15.

1. Groupe des Neutrons Thermiques (H. Nifenecker)

15.

1.1. Etude des rayonnements γ émis après la capture des neutrons thermiques.

15.

1.1.1. Détermination des niveaux par la méthode de Hoogenboom.

L'installation expérimentale⁽¹⁾ mise en place auprès de la pile EL.3 de Saclay a été achevée. Le bruit de fond au-dessus de 100 KeV a été ramené à une valeur inférieure à 500 coups/seconde pour un cristal I Na (Tl) de 5" x 4" et en l'absence de cible sur le trajet du faisceau ($\phi \sim 10^6 n/cm^2/s$). Ce bruit de fond est dû en grande partie à l'activation de l'Argon atmosphérique.

On a mis à profit l'existence de ce pic de l'Argon pour stabiliser électroniquement le gain des deux chaînes d'analyse γ . La stabilité obtenue est de l'ordre de 0,2 % pendant huit jours.

On a pu ainsi étudier les cascades $\gamma-\gamma$ issus du niveau de capture et aboutissant à l'état fondamental des noyaux suivants, formés lors de la capture neutronique: Hg²⁰⁰, Fe⁵⁷, Mn⁵⁶, Co⁶⁰⁽²⁾. Nous avons pu non seulement confirmer l'existence de cascades déjà étudiées, essentiellement par des spectromètres magnétiques, mais encore mettre en évidence de nouvelles cascades (fig. 15.1.1. à 15.1.4.).

Afin d'améliorer l'appareillage nous prévoyons l'installation pour l'étude des rayons γ de haute énergie ($E_\gamma > 3$ MeV) d'un ensemble I Na à cristal central et anneau anti-compton. L'essai d'un tel ensemble s'est en effet avéré satisfaisant pour l'étude des cascades $\gamma-\gamma$ de Hg²⁰⁰ aboutissant au premier niveau excité⁽³⁾.

15.

1.1.2. Mesures de corrélations angulaires.

Des mesures de corrélations angulaires ont été tentées sur les gamma de capture du Co⁵⁹. Des défauts dans la géométrie ont empêché d'en tirer parti. Un nouveau montage a été

réalisé et, s'il donne satisfaction, devrait permettre de recommencer ces mesures tout prochainement.

15.

1.2.

15.

1.2.1.

Etudes sur la fission.

Etude de la distribution des masses des fragments avant émission neutronique.

La méthode de mesure des masses, fondée sur l'égalité des quantités de mouvement au moment de scission, consiste à mesurer simultanément les énergies des 2 fragments associés, au moyen de détecteurs à jonction au Si.

Les mesures effectuées ont permis essentiellement de vérifier l'existence de structures fines sur la distribution des masses et d'en faire une étude systématique en fonction de l'énergie cinétique totale des 2 fragments⁽⁴⁾.

15.

1.2.2.

Etude de la distribution des masses des fragments après émission neutronique.

La Méthode consiste à mesurer simultanément pour chaque fragment son énergie et sa vitesse, donc d'en déduire directement sa masse. La mesure de l'énergie est faite par un détecteur à barrière de surface Au-Si, la mesure de vitesse est faite par la méthode du "temps de vol": les détecteurs "start" et "stop" sont constitués par des photomultiplicateurs sans fenêtre dont la photocathode a été remplacée par un film métallique de quelques dizaines de $\mu\text{g/cm}^2$. La résolution en temps est de l'ordre de 1 ns. L'appareillage est complètement réalisé et l'expérience sur l' U^{235} est actuellement en cours; des mesures sur l' U^{233} et le Pu^{239} sont également prévues.

15.

1.2.3.

Détermination du spin des résonances de l' U^{235} dans un domaine allant des énergies thermiques à quelques dizaines d'eV.

Le principe de l'expérience est de déterminer le spin des résonances à partir des propriétés de la distribution de probabilité $P(E_1, E_2)(E_1 \text{ et } E_2 \text{ étant les énergies cinétiques des 2 fragments associés})$ en fonction de l'énergie du neutron incident.

Un appareillage a été développé comportant l'analyse tridimensionnelle de chaque fission détectée (E_1 , E_2 et E_n), le stockage des informations sur bande perforée et dépouillement sur calculateur IBM 7094. Les énergies E_1 et E_2 sont mesurées à l'aide d'une double chambre à grilles, un convertisseur temps-amplitude permet de déterminer l'énergie E_n du neutron incident.

Une expérience préliminaire sur l'accélérateur linéaire de SACLAY nous a permis :

- d'une part, de vérifier le fonctionnement correct de la chambre à grille et de son électronique associée dans les conditions suivantes : base de vol : 10 mètres, bouffées de 1 μ sec à la fréquence de 500c/sec,
- d'autre part, d'évaluer à 100 heures la durée de l'expérience pour obtenir au moins 10.000 coups dans une dizaine de résonances pour une cible d' U^{235} de 20 cm^2 de surface et de 100 $\mu g/cm^2$ d'épaisseur.

15.

1.1.1.3.

"Dépouillement des mesures sur la section efficace de fission de U^{233} "

Une analyse par la méthode des moindres carrés de la section efficace de fission de U^{233} entre 1, 7 et 35 eV a été faite. Cette analyse n'utilise que des formules de Breit et Wigner à un niveau. Si l'on ajoute aux niveaux apparents un nombre limité de niveaux cachés, la section efficace observée correspond remarquablement bien à une somme de courbes à un niveau et il est inutile de faire appel à un formalisme à plusieurs niveaux.⁽⁵⁾

Par ailleurs l'analyse de la distribution des espacements par une méthode de maximum de vraisemblance semble indiquer que la perte d'un certain nombre de niveaux ne suffit pas à expliquer les anomalies constatées. On envisage l'hypothèse que la loi d'espacement de Wigner ne serait pas valable pour les corps où Γ/D n'est pas petit devant 1. Cette hypothèse trouverait une justification dans le cas de la théorie de la matrice R.

15.1.4. Appareillage

15.1.4.1. Mise en oeuvre d'un ensemble multiparamétrique.

Afin d'augmenter les possibilités de l'installation d'étude de rayons γ de capture, nous avons réalisé un ensemble multiparamétrique. Cet ensemble comporte une unité d'écriture sur bande magnétique et une unité de lecture. Chaque évènement peut être caractérisé par un ensemble de quatre nombres binaires compris entre 0 et 512 au maximum (par exemple dans le cas de coincidences triples par les trois énergies mesurées par les trois photomultiplicateurs et par une mesure de temps séparant les impulsions provenant de deux des détecteurs).

A l'unité de lecture est associé un ensemble de conditionnement comportant essentiellement un conditionneur multiple (sélecteur à une bande digital) et un additionneur binaire permettant éventuellement d'étudier des spectres de somme.

Des mesures préliminaires ont été faites avec cet ensemble sur les rayonnements γ de capture du Fer, du Manganèse et du Mercure dans l'intention d'étudier les possibilités de mesurer les temps de vie de certains niveaux excités de ces noyaux.

15.1.4.2. Électronique rapide.

Deux ensembles de conversion temps-amplitude ont été mis au point.

Le premier est utilisé pour les mesures de temps de vie citées plus haut ; il comporte :

- deux mises en forme à diode tunnel permettant de détecter l'arrivée des tout premiers électrons sur l'anode (~ 20 mV) et donc d'obtenir une définition excellente du temps.
- un convertisseur temps-amplitude ayant une résolution intrinsèque de 10^{-11} s. pour une gamme d'analyse de 0 à 50 ns.⁽⁶⁾

L'ensemble donne une résolution en temps de 3 ns pour une cascade 7 MeV - 83 KeV du Manganèse détectée par cristaux NaI (Tl) à température ordinaire.

Le deuxième ensemble est utilisé pour des mesures de temps de vol de fragments de fission. Une résolution de $4 \cdot 10^{-10}$ s. a été obtenue avec des scintillateurs plastiques et pour des impulsions d'amplitude variant dans un rapport 20.

15.1.4.3. Amélioration de la réponse aux rayons γ des cristaux Na I (Tl).

La méthode employée consiste essentiellement à n'observer que les événements ayant donné lieu à une scintillation dans la partie centrale du cristal⁽⁷⁾.

15.1.4.4. Etude de l'émission d'électrons secondaires par les fragments de fission ⁽⁸⁾.

Les résultats expérimentaux s'inscrivent correctement dans le cadre d'une théorie de l'émission secondaire due à Sternglass. Toutefois, il est apparu que les formules habituelles permettant de calculer la perte d'énergie spécifique des fragments de fission en début de parcours laissaient à désirer. Enfin, les avantages des détecteurs mettant en oeuvre l'émission secondaire ont été mis en lumière dans le cas où l'on veut étudier la fission de corps ayant une forte radioactivité α .

15.2. Groupe des Neutrons Intermédiaires. (P. Ribon)

15.2.1. Méthodes et techniques expérimentales.

15.2.1.1. Transmission.

Le détecteur a été modifié afin d'étendre la gamme de mesures vers les plus hautes énergies (300 ou 400 keV); pour cela, les photomultiplicateurs 54 AVP ont été remplacés par des photomultiplicateurs rapides XP 1040, ce qui permet :

- d'améliorer la résolution ; le temps est défini à mieux de 5 ns, valeur compatible avec des largeurs de bouffée de neutron et de sélecteur de 10 ns.
- d'avoir un fonctionnement correct du détecteur pour des temps de vol de 8 ou 10 μ s, ces photomultiplacteurs rapides étant plus faciles à "bloquer" pour éviter la perturbation due à la bouffée γ .

Un nouveau cryostat - ne permettant de refroidir les échantillons qu'à la température de l'azote liquide, mais monté sur un chariot à déplacement automatique - a été étudié et est en cours d'achèvement.

15.2.1.2. Fission.

Un nouveau scintillateur gazeux est en cours de réalisation pour la mesure de la section efficace de fission du Np 237 à basse énergie. Compte tenu de la faible valeur de cette section efficace, le détecteur est conçu pour utiliser jusqu'à 6 g. de Np 237.

Un compteur à étincelles pour la détection des fissions est en essais; il fonctionne de façon satisfaisante avec des α . Il sera utilisé pour la mesure de la section efficace de fission des éléments à très grande activité α (Am 241 et Pu 241 notamment).

15.2.1.3. Diffusion.

Une première expérience vient d'être réalisée avec un ensemble de 25 compteurs BF₃. Les conditions de fonctionnement de cet ensemble ont pu être améliorées au cours des derniers mois, mais le "jitter" en temps est de l'ordre de 0,5 μ s.

Afin d'améliorer la sécurité de fonctionnement, le "jitter" et l'efficacité, nous étudions un nouveau type de détecteur - verre au lithium avec discrimination de forme.

15.2.1.4.. Etude de la diffusion résonnante des rayons γ .

Un premier essai vient d'être effectué, et a montré la nécessité d'améliorer la protection contre les neutrons diffusés.

15.2.1.5. Méthodes de dépouillement.

Le programme d'analyse de forme par moindres carrés de mesures de transmission a été légèrement amélioré (gain de temps de calcul, nombre total de résonances porté de 20 à 32).

Un nouveau programme d'analyse de forme a été écrit pour la fission, et a été appliqué au cas du Pu 239.

L'écriture d'un programme d'analyse multi-niveaux (formalisme de Vogt) a été terminée en Juillet 1964 ; il est en cours d'essais.

- 15.2.1.6. Un calculateur CAE 510 qui travaillera "en ligne" doit être livré à la fin de Février 1965. Les préparatifs nécessaires à la conduite automatique de l'expérience (programmes et liaisons aux sélecteurs) sont en cours de mise au point. L'utilisation secondaire du calculateur pour le traitement des données est également en cours d'élaboration, spécialement du point de vue de la compatibilité avec les gros calculateurs IBM pour effectuer des échanges de données et de résultats quel que soit leur support (bandes magnétiques et cartes).

15.2.2. Résultats expérimentaux.

15.2.2.1. Uranium-235.

Les mesures de σ_t sur l'U 235 sont pratiquement terminées et toutes dépouillées. Elles ont fait l'objet d'une thèse et de diverses publications^{(9) (10)}.

Les données numériques, jusqu'à 600 eV, ont été transmises au "Centre de compilation" de Saclay. Nous donnons la section efficace de l'échantillon étudié (composition isotopique : U 235 - 93,36 %, U 238 - 5,01 %, U 234 - 1,05 %; U 236 - 0,58 %) et la section efficace de l'uranium 235 seul, après correction des sections efficaces potentielles des isotopes 234, 236 et 238, ainsi que des résonances de ces isotopes identifiées.

La figure 15.2.1. représente, à titre d'exemple, la section efficace totale de U 235 de 50 à 82 eV.

Les paramètres des résonances, déterminés par analyse de forme d'après les mesures de σ_t et de σ_f , ont été obtenus jusqu'à 150 eV.

a) Il apparaît que 20 % des résonances n'ont pas été détectées, ce qui semble plus dû à la structure résonnante de l'uranium 235 qu'à un effet de résolution (le niveaux non détectés correspondent à de petits espacements ou

de faibles σ_{f}) (fig. 15.2.2.).

b) A partir de paramètres des résonances de 0 à 50 eV, on peut déduire :

$$S_0 = (0,915 \pm 0,05)10^{-4}$$

$$D = (0,53 \pm 0,03)$$

En tenant compte des résonances de 50 à 150 eV, on trouve :

$$S_0 = 0,958 \cdot 10^{-4}$$

c) Les largeurs de capture radiative fluctuent fortement de résonance en résonance, et correspondent à une distribution de Porter et Thomas à 32 degrés de liberté ; (fig. 15.2.3.) les largeurs de fission suivent une loi à 4 degrés de liberté (fig. 15.2.4.).

d) Il existe une corrélation entre les largeurs de fission et de capture, et il est possible de mettre en évidence deux valeurs moyennes pour ces largeurs qui peuvent correspondre aux deux états de spin.

e) Enfin, il semble qu'il y ait des corrélations entre des niveaux espacés d'une trentaine d'eV.

f) A haute énergie (1 keV à 20 keV), un désaccord avec les mesures faites par Harwell n'a pu encore être résolu.

15.2.2.2. Fission ternaire de U 235

Le dépouillement des mesures de section efficace de fission ternaire de U 235 est terminé.⁽¹¹⁾. Le rapport de la probabilité de tripartition à celle de fission a été déterminé pour 22 résonances entre 1 et 40 eV. L'application du critère de Birge^(x) montre que :

a) Si seuls les α de plus de 10,9 MeV sont détectés, une valeur unique de cette probabilité est possible. Il en est de même pour un seuil de 14,3 MeV (fig. 15.2.5.).

(x) Treatment of Experimental Data, A. Worthing et, J. Geffner, J. Wiley Edit. N.Y. 1950.

b) Si les α de plus de 7,3 MeV sont détectés, une valeur unique n'est pas admissible. (Fig. 15.2.6.)

Il semble qu'il y aurait deux composantes dans le spectre des rayons α de tripartition :

- une de basse énergie, non proportionnelle à la fission binaire,
- une de haute énergie, proportionnelle à la fission binaire.

Cela est à rapprocher des résultats de Solov'eva (Akad. Naud USSR 1955)

15.

~~15.~~ 2.2.2. Thorium-232.

L'analyse de forme des résonances du Th 232 jusqu'à 3 keV sera terminée au début de Février. Environ 290 résonances ont été identifiées dont 180 seraient des résonances "s" et 110 des résonances "p", d'après la distribution des Γ_n^0 de la figure 15.2.7. ⁽¹²⁾. Pour les ondes s, les valeurs de Γ_γ ne semblent pas tout à fait compatibles avec une valeur unique moyenne de 22.3 ± 1 meV.

15.

~~15.~~ 2.2.3. Rhodium-103.

Nous avons repris des mesures de section efficace totale en-dessous de 800 eV avec un échantillon très épais (41 g/cm^2) et une bonne résolution (3 ns/m). Nous avons identifié 65 résonances jusqu'à 760 eV contre 46 précédemment ⁽¹³⁾.

L'analyse des résultats par moindres carrés permet de déterminer le spin de certaines résonances. En effet, le programme tient compte des interférences entre résonances, ce qui permet d'identifier des couples de résonances de même spin.

Les résultats seront prochainement publiés.

15.

~~15.~~ 2.2.4. Plutonium-239 ⁽¹⁴⁾

La section efficace de fission a été mesurée en Mai et Juin 1964. Le détecteur était un scintillateur gazeux au Xénon (pression 200 g/cm^2) contenant 0,31 g de Plutonium 239.

Plusieurs mesures ont été effectuées : deux d'entre elles sont résumées dans le tableau ci-dessous (fig. 15.2.8.).

	Mesure à basse énergie (0,16 à 100 eV).	Mesure à haute énergie (11 eV à 5 keV) ^(x)
Accélérateur		500 impulsions de 100 ns/s
Sélecteur à temps de vol à largeur de canal variable	Réglée entre 50 et 1600ns	Réglée entre 50 et 400ns
Longueur de vol	10,80 m	19 m base de vol perpendiculaire au ralentisseur
Durée d'accumulation	34 h.	140 h.
Résolution expérimentale	1,2 μ s/m à 0,16 eV 46 ns/m à 100 eV	35ns/m à 12 eV, 11ns/m à 100 eV, 6 ns/m à 5keV

(x) Une mesure de 50 h. a été faite dans les mêmes conditions sauf une largeur d'impulsion accélérateur de 20 ns : la résolution à 5 keV est alors 3 ns/m.

L'analyse de forme des résonances est en cours ; une expérience vient d'être reprise afin de vérifier la normalisation.

Nos résultats sont en bon accord avec les mesures faites par Bollinger et al. jusqu'à 50 eV (Genève 1958), nous identifions néanmoins 3 résonances nouvelles à 9,59 - 11,48 et 49,6 eV.

Par ailleurs, la mesure de la section efficace totale du Pu sera commencée en Mars 1965.

15.

15.2.5. Diffusion.

Une première mesure a été effectuée sur l'Argent pour tester l'appareillage et les méthodes de dépouillement sur un cas déjà étudié par d'autres laboratoires (Harwell). Les dépouilllements sont en cours.

~~15.~~ 15.

Groupe des Neutrons Rapides (J.L. Leroy).

~~15.~~ 3.1.

Implantation du Laboratoire à Cadarache.

Le Van de Graaff de 5 MeV de Saclay a été consacré dès la mi-1963 à des mesures de données neutroniques. Malheureusement, la petiteur de la salle des cibles, limitait sévèrement les possibilités dans ce domaine. Il a donc été décidé de construire un nouveau laboratoire, spécialement conçu pour obtenir un faible bruit de fond. Au printemps 1964, le bâtiment était terminé, et l'accélérateur était remis en fonctionnement en août 1964, après un arrêt de sept mois, au cours duquel il a été démonté, remonté et partiellement rénové.

Une source pulsée donnant des bouffées de 0,5 mA avec une durée de 5 à 20 ns, à la fréquence de 3,5 MHz, est en cours de montage.

Un dispositif de regroupement magnétique, permettant de comprimer ces bouffées jusqu'à 1,5 ns, est en cours de réalisation (15).

Dans la nouvelle installation, le bruit de fond en neutrons lents est environ 20 fois plus faible que dans l'ancienne.

~~15.~~ 15.

Mesure de la section efficace de capture du sodium entre 10 et 140 KeV (16)

La section efficace de capture neutronique du Sodium a été mesurée par rapport à la section efficace de la réaction $\text{Li}^6(n,\alpha)\text{T}$. Cette mesure consiste en une série d'activations d'un échantillon dans un faisceau de neutrons monoénergétiques fournis par le Van de Graaff de 5 MeV, à partir de la réaction $\text{Li}^7(p,n)\text{Be}^7$.

L'activité de l'échantillon de Sodium était mesurée au moyen d'un scintillateur d'iodure de Sodium dont l'efficacité a été déterminée dans une expérience complémentaire, par comparaison avec un compteur β en géométrie 4π . On a tenu compte des diffusions multiples se produisant dans l'échantillon au cours d'irradiations, en calculant une correction par une méthode de Monte Carlo (17)(18).

Le flux de neutrons était mesuré au moyen d'un scintillateur de verre chargé au Li⁶. Le nombre des atomes de cet élément contenus dans l'appareil a été calculé à partir d'une mesure d'absorption totale des neutrons thermiques faite dans la pile ZOE par la méthode d'oscillation de phase. L'erreur totale sur ce nombre d'atomes est de 2,2 %.

Pour obtenir des valeurs absolues et la section efficace du Sodium à partir de notre mesure, nous avons utilisé les valeurs mesurées récemment par SCHWARZ et coll.^(x). Les résultats se trouvent dans le tableau 15.3.1. et sont représentés par la courbe 15.3.2. On a également représenté les résultats obtenus par d'autres chercheurs.

La courbe indique nettement la présence d'une résonance à 33 keV, en plus de celle à 55 keV déjà identifiée par les mesures de la section efficace totale.

15.

3.3.

Etude théorique de la distribution angulaire de la réaction Li⁶ (n, a) T entre 10 et 600 keV (19)

Le but de cette étude était de voir si l'ensemble des résultats expérimentaux publiés sur ces distributions angulaires était cohérent et si l'on pouvait en déduire la distribution angulaire à une énergie quelconque de ce domaine.

Pour faire la représentation de ces résultats, on a utilisé la théorie de la matrice dérivée.

Dans ce domaine d'énergie, la réaction peut être considérée comme étant due à un niveau $5/2^-$, du noyau composé Li⁷, donnant lieu à la résonance de 255 keV. Il faut en outre introduire une contribution en $\frac{1}{\sqrt{V}}$ due à des résonances éloignées. Les distributions angulaires faites à des énergies inférieures à celle de la résonance sont fortement anisotropes, ce qui implique une interférence entre le niveau donnant lieu à la

(x) SCHWARZ FOA4 Rapp. A4393 411 (Sept. 64)

résonance et certains des niveaux donnant la contribution en $\frac{1}{\sqrt{V}}$: il s'agirait alors de niveaux $3/2^+$. Néanmoins pour rendre compte numériquement de cette anisotropie on doit supposer qu'il existe un mélange d'états $1/2^+$ $3/2^+$ dans la proportion de 3/4 à 1/4 respectivement. En prenant les paramètres de résonance équivalents à ceux déterminés par SCHWARZ et col. et en utilisant le mélange statistique dont il vient d'être question, on obtient des courbes représentées par les fig. 15.3.3. à 15.3.5. On voit que les points expérimentaux correspondant aux distributions angulaires (fig. 15.3.5.) représentent une certaine incohérence qui limite les possibilités d'interpolation entre mesures différentes ; il semble donc nécessaire de faire des mesures supplémentaires.

15.3.4. Mesure absolue des flux de neutrons.

Il a été proposé d'utiliser dans ce but la particule associée He^3 produite dans la réaction $T(p, n) \text{He}^3$ (20). On a continué à développer cette méthode. Le problème de la contamination des particules He^3 détectées par des tritons diffusés élastiquement a été résolu en ajoutant un 2ème détecteur solide capable de détecter les protons associés à un triton se dirigeant vers le compteur principal.

La seule difficulté restant à résoudre pour rendre cette méthode tout à fait pratique, est la fabrication de cibles tritiées sur support mince ayant une durée de vie suffisante. Des progrès ^(x) ont été réalisés dans ce sens et il est permis d'espérer une solution prochaine.

(x) La fabrication des cibles est faite en collaboration par le BCMN de GEEL (Belgique) et le C.E.N. de SACLAY.

Liste des Publications

- 1) P. CARLOS, H. NIFENECKER, R. SAMAMA, J. FAGOT - J. de Phys. - Phys. Appliquée 25, 203 A (1964)
- 2) P. CARLOS, H. NIFENECKER, J. FAGOT, J. MATUSZEK - J. de Phys. 25, 957 (1964).
- 3) P. CARLOS, H. NIFENECKER, J. FAGOT, J. MATUSZEK - J. de Phys., à paraître.
- 4) M. CHAHRTACHE, Thèse (Déc. 1963).
- 5) H. NIFENECKER, J. de Phys. 25, 877, (1964).
- 6) M. RIBRAG, H. NIFENECKER, C. SIGNARBIEUX - Note C.E.A. - N 467 (1964)
- 7) M. DE ABREU, H. NIFENECKER, Nucl. Inst. and Methods, à paraître
- 8) A. AUDIAS - Thèse C.N.A.M. (1965)
- 9) A. MICHAUDON - Thèse (1964) et Rapport C.E.A. 2552.
- 10) A. MICHAUDON, H. DERRIEN, M. SANCHE, P. RIBON - Nucl. Phys. à paraître.
- 11) A. MICHAUDON, A. LOTTIN, D. PAYA, J. TROCHON - Nucl. Phys. à paraître.
- 12) P. RIBON, H. DERRIEN, A. MICHAUDON, M. SANCHE - Congrès Int. de Phys. nucl. (Paris - Juillet 1964).
- 13) P. RIBON, A. MICHAUDON - J. de Phys. 24 987 (1964)
- 14) C.R. Ac. des Sc. 259 3498 (1964)
- 15) D. HEBERT, J. TOCQUER - Rapp. DRP/SMNF/Ca 64/06 (1964).
- 16) C. LE RIGOLEUR, H. BEIL, J. LEROY, Rapp. DRP/SMNF/Ca 64/01 (1964)
- 17) J. BLUET, Rapp. DRP/SMNF/Ca 64/02 (1964)
- 18) J. BLUET, Rapp. DRP/SMNF/Ca 64/03 (1964)
- 19) J. BLUET, Rapp. DRP/SMNF/Ca 64/04 (1964)
- 20) J. LEROY, H. BEIL, Rapport EANDC-33 U, 150 (1963).

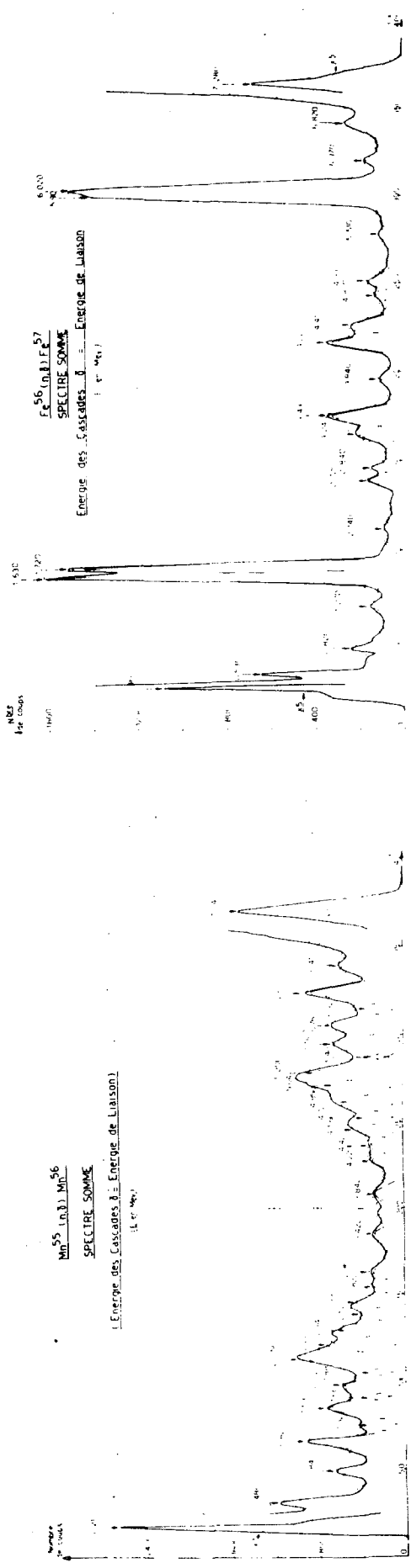


Fig. 15.1.1.

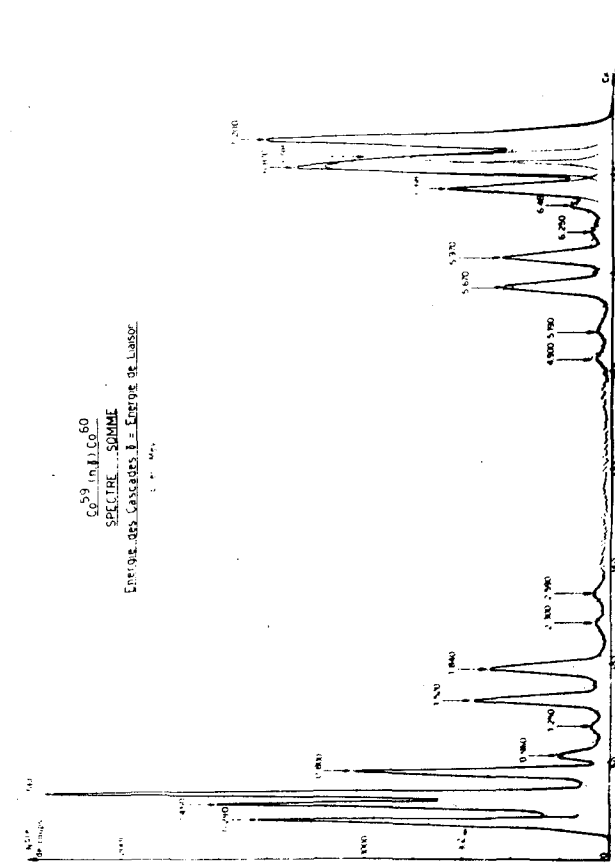


Fig. 15.1.3.

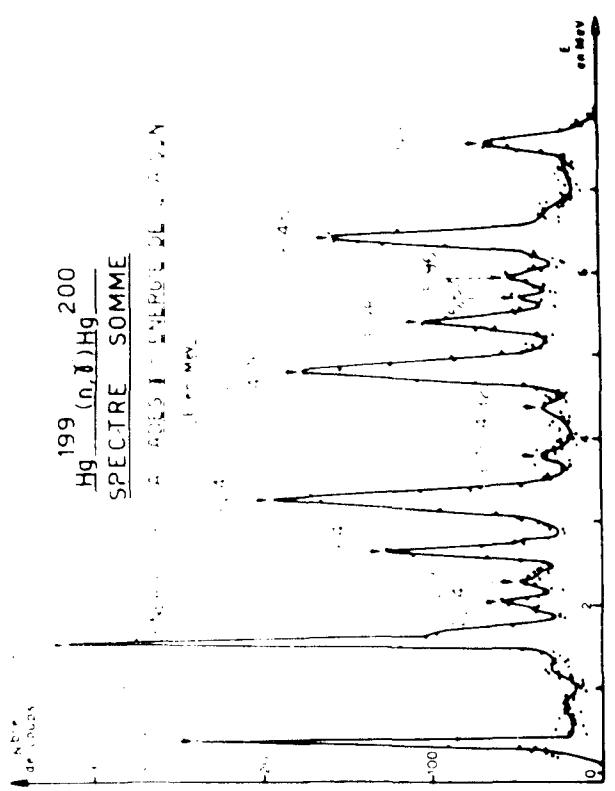


Fig. 15.1.2.

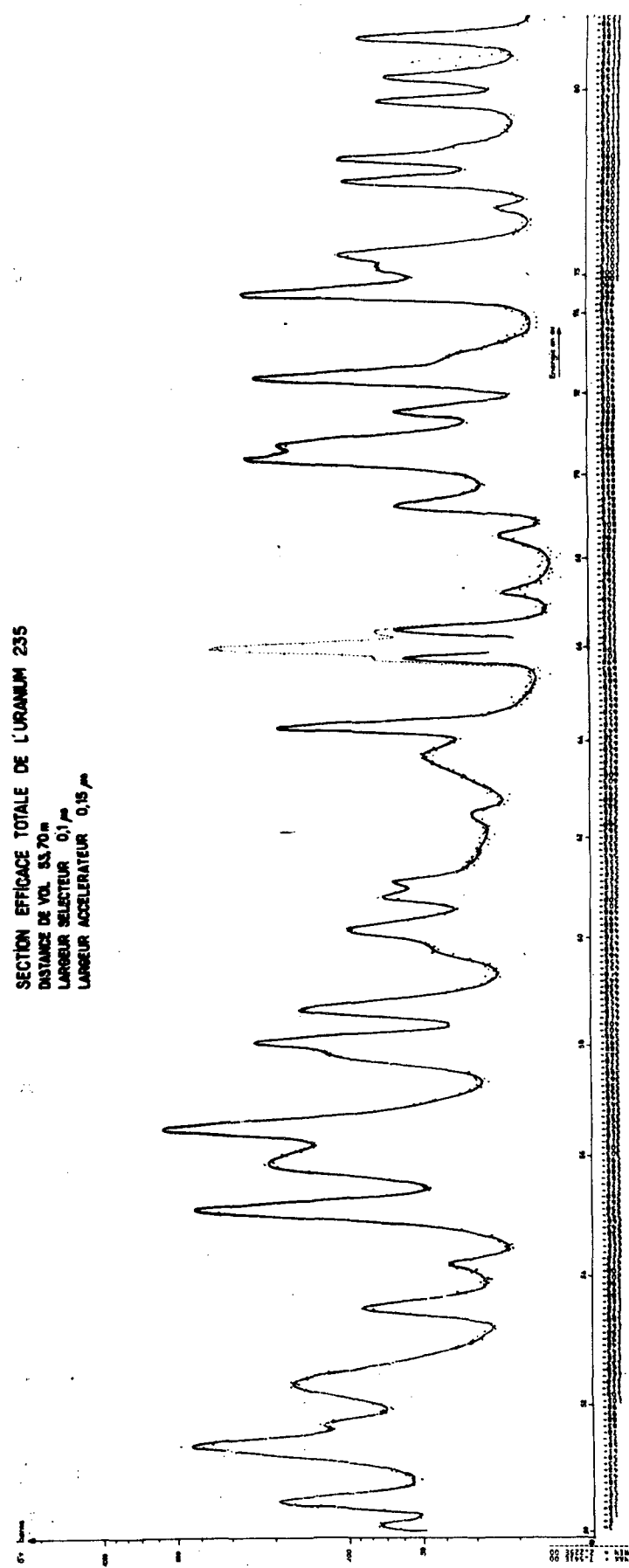


Fig. 15.21.

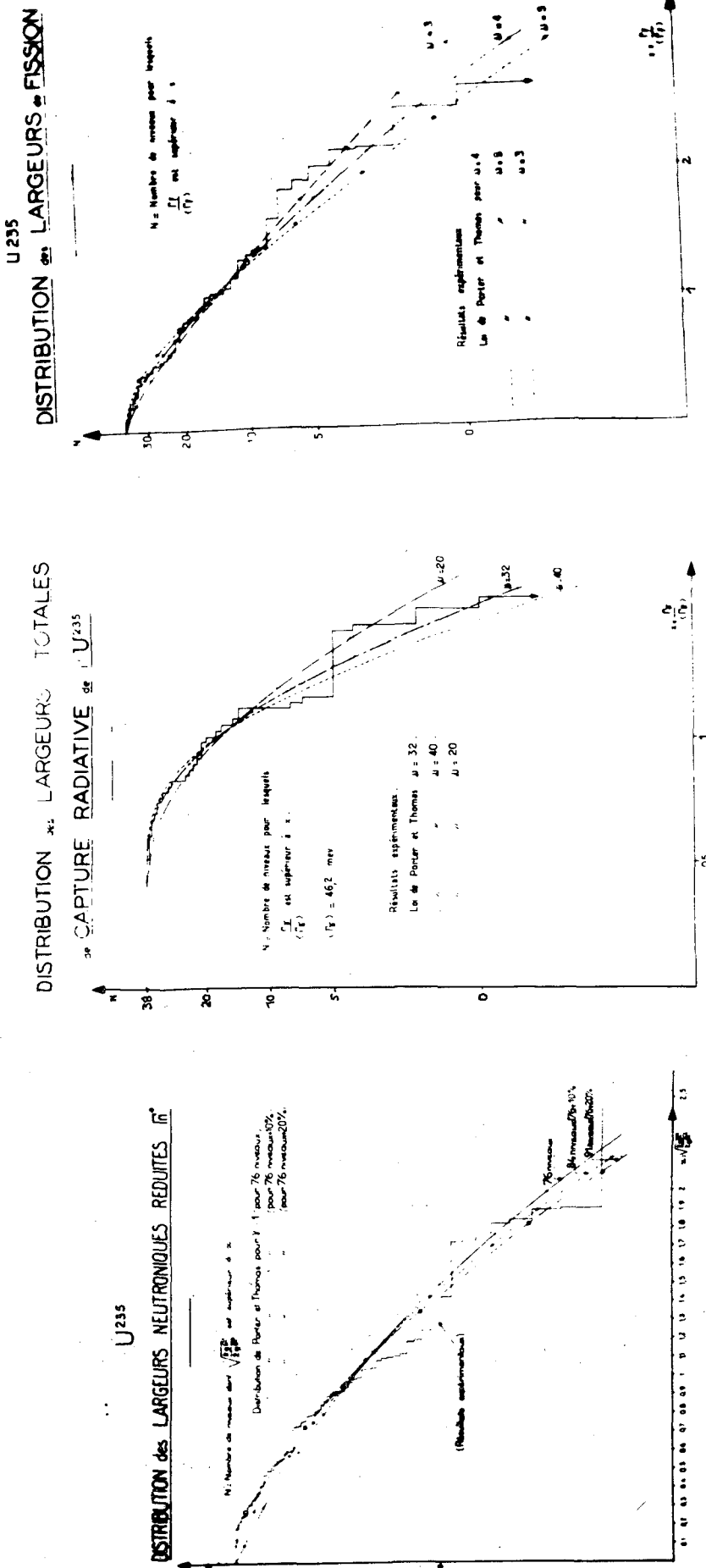


Fig. 15.2.2.

Fig. 15.2.3.

Fig. 15.2.4.

$R_f^\alpha = \frac{\text{Fission ternaire}}{\text{Fission binaire}}$
(Unités arbitraires)

TRIPARTITION DE L'U²³⁵

Chambre n° 4 (épaisseur d'aluminium 6.10⁻² mm)

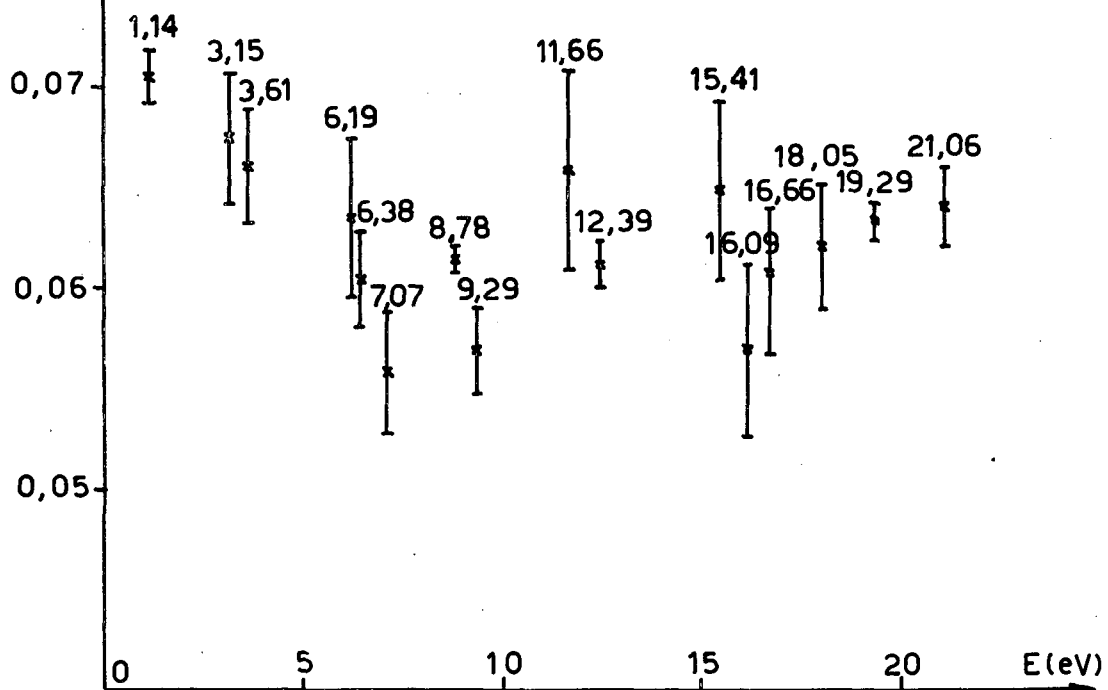


Fig. 15.2.5.

TRIPARTITION DE L'U²³⁵

$R_f^\alpha = \frac{\text{Fission ternaire}}{\text{Fission binaire}}$
(Unités arbitraires)

Chambre n° 2 (épaisseur d'aluminium 3.10⁻² mm)

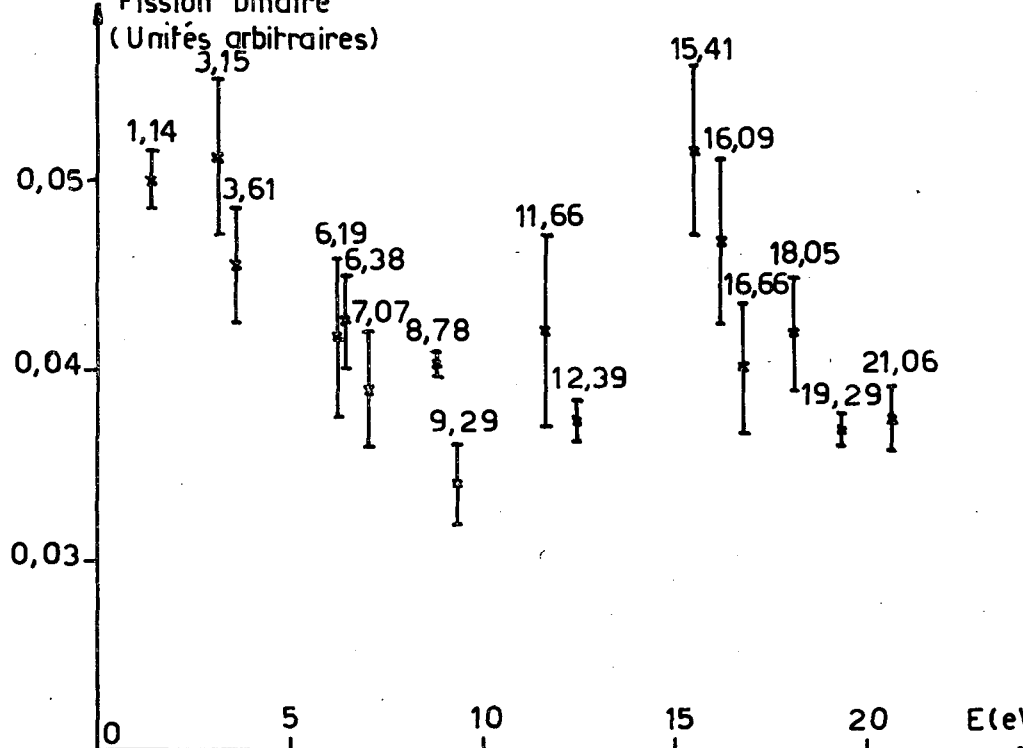


Fig. 15.2.6.

Th. 232

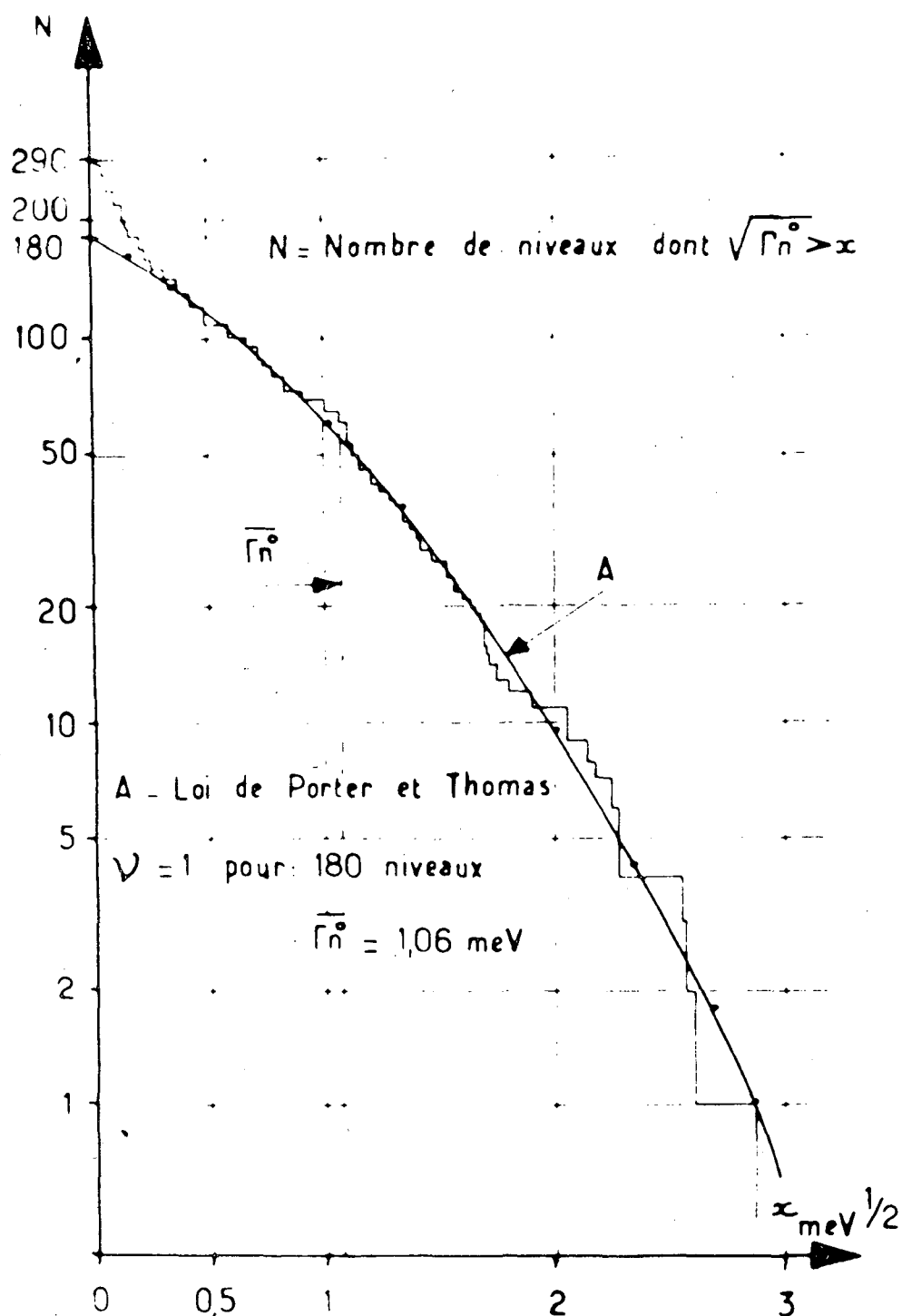


Fig.15.2.7.

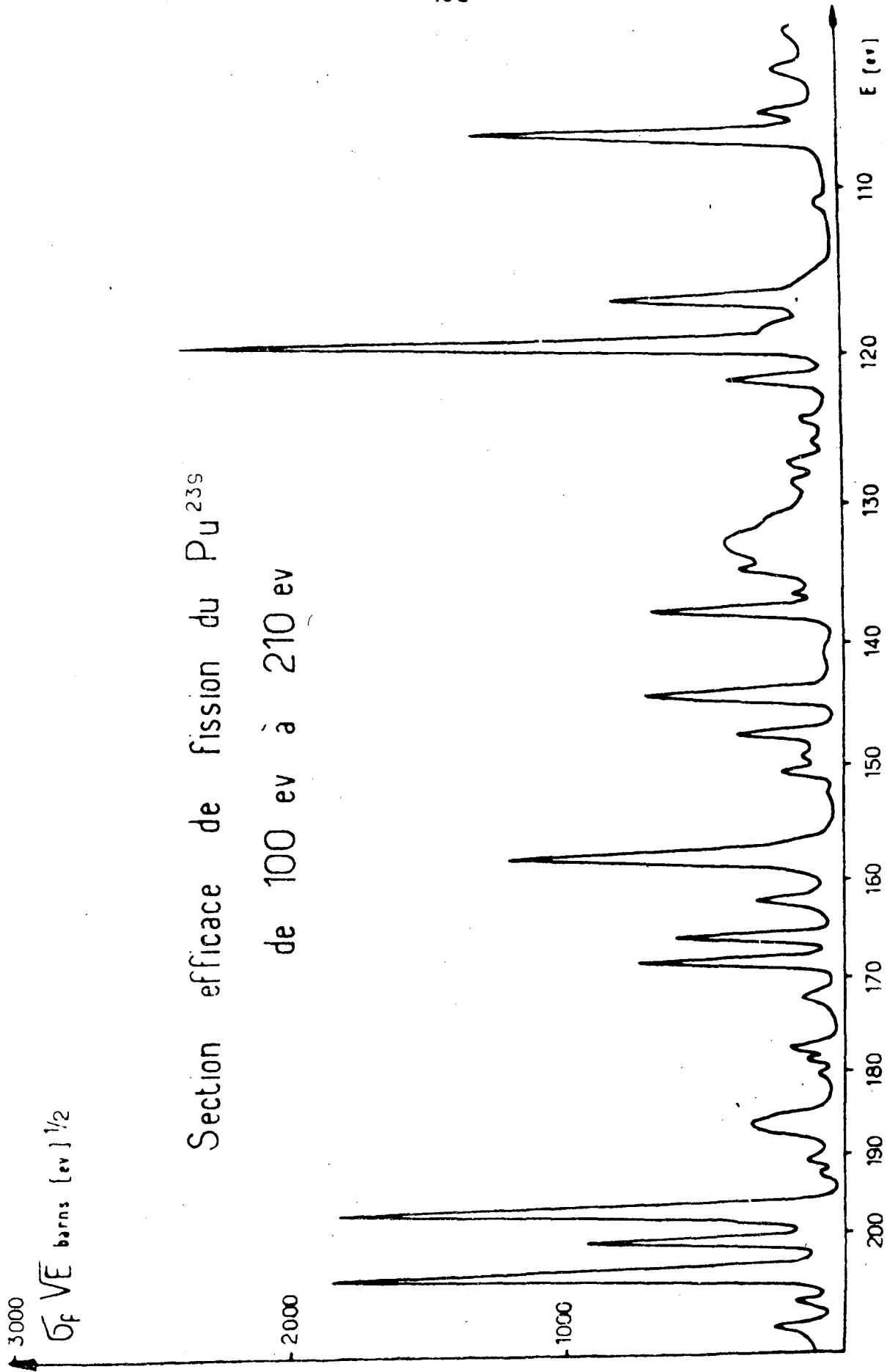


Fig. 15.2.8.

TABLEAU 15.3.1

Energie moyenne en keV	Plage d'énergie	$\frac{\text{Na}}{\text{Li}} \times 10^3$	Na (mb)
8.55	10.9 6.4	$0.95 \pm 6.8\%$	1.56
18.9	22.2 16.8	$0.75 \pm 7.1\%$	0.84
26.6	30.4 22.9	$0.62 \pm 7.4\%$	0.59
39.5	36.3 43.3	$2.05 \pm 3.25\%$	1.67
40	43.8 36.2	$1.81 \pm 7.4\%$	1.46
47.5	43.9 52.1	$1.13 \pm 3.25\%$	0.86
48.75	53 45	$1.34 \pm 7.6\%$	0.98
55	48.9 60.8	$3.65 \pm 3.25\%$	2.63
57.35	62.7 53	$1.82 \pm 7.7\%$	1.30
66.55	72.3 61.3	$0.60 \pm 7.6\%$	0.41
76.5	72.2 81.9	$0.405 \pm 3.25\%$	0.27
81	87 75	$0.37 \pm 7.5\%$	0.24
96	103 90	$0.32 \pm 7.2\%$	0.21

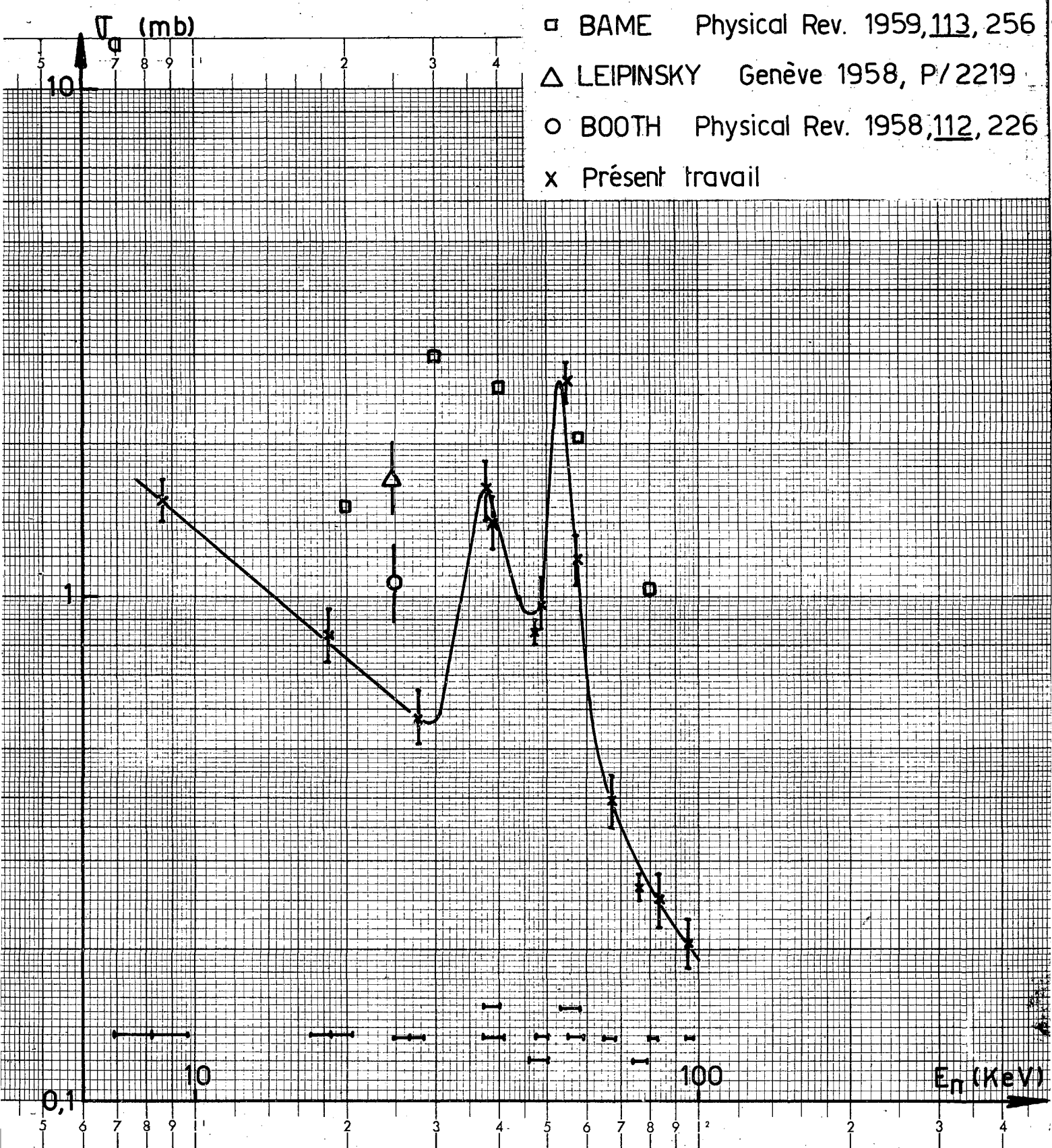
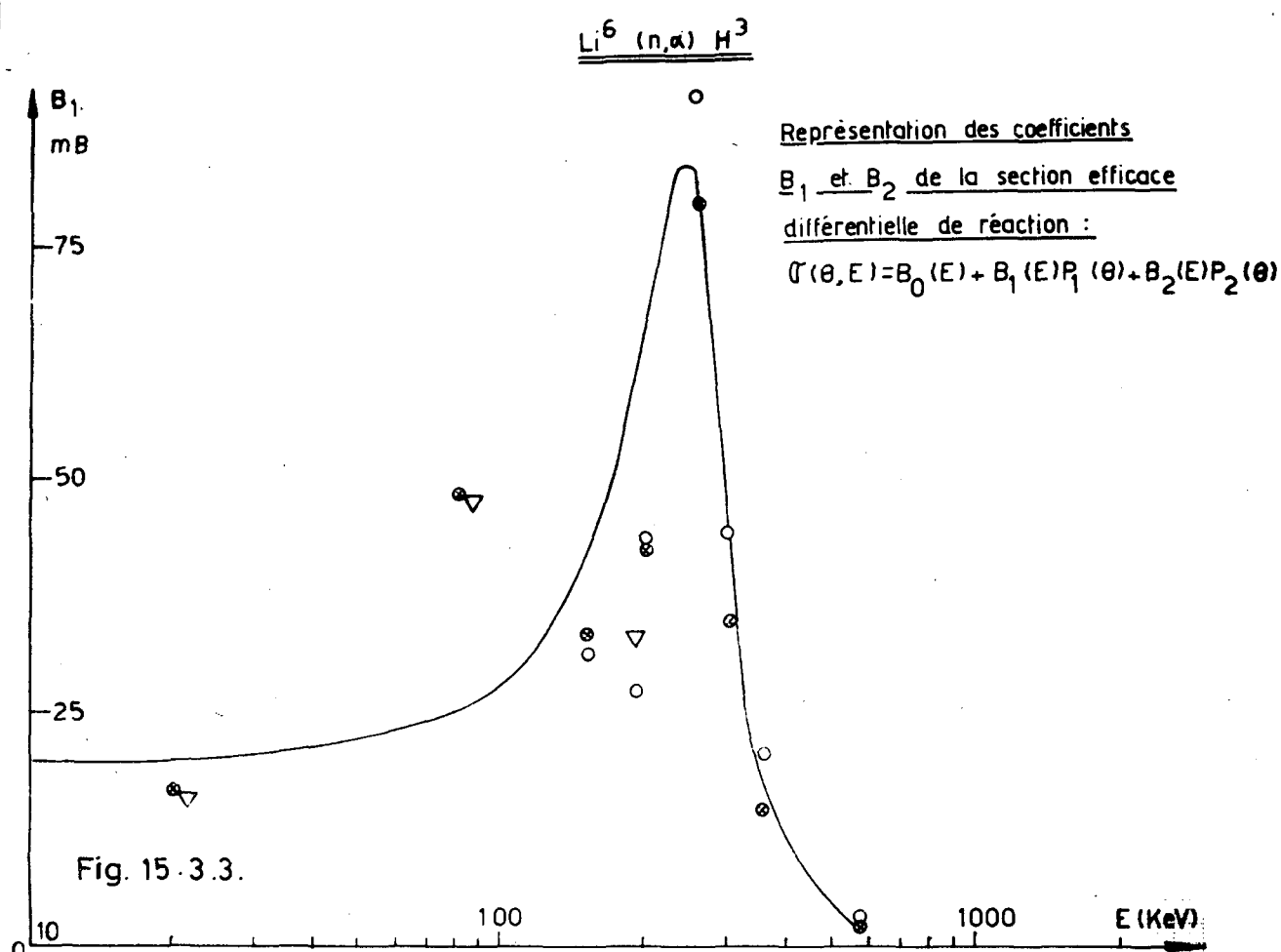


Fig. 15.3.2.

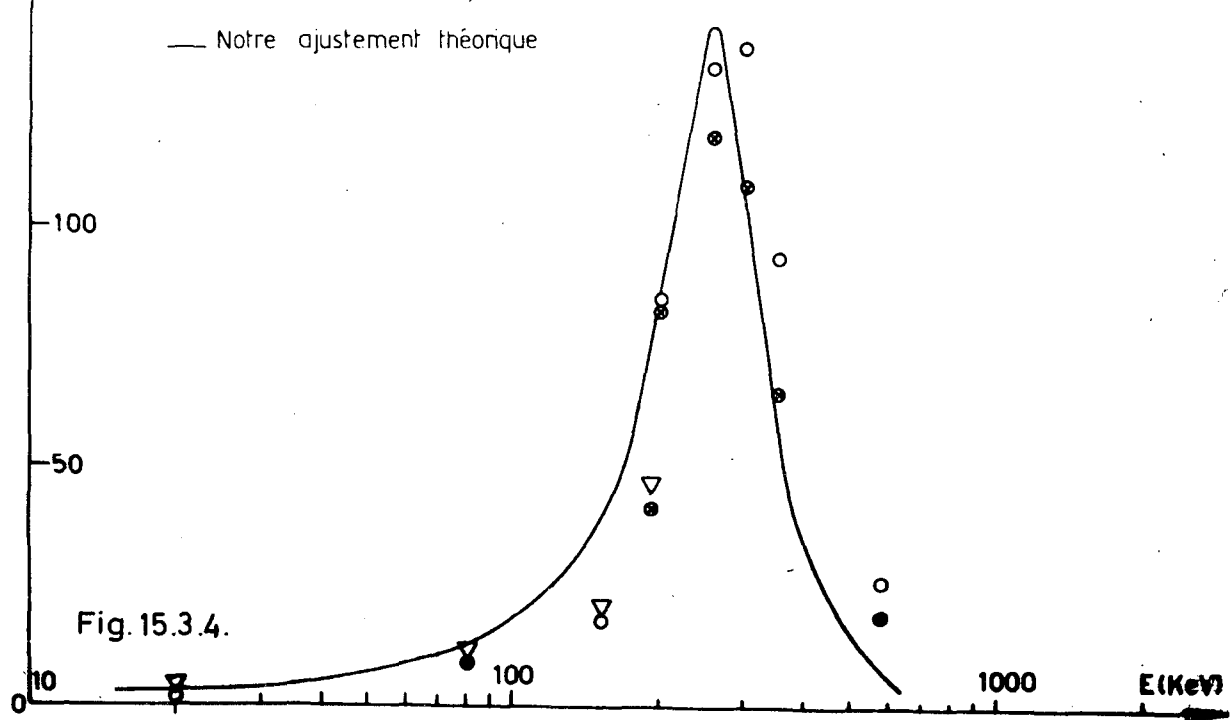


▽ BEETS Journal de Phys 1963, 24, 803

○ BAME Physical Rev. 1959, 113, 256

⊗ Valeurs expérimentales précédentes renormalisées sur les mesures de Γ_T de SCHWARZ 1964, A 4393 / 411

— Notre ajustement théorique



0,150 MeV

σ mb

200

0

0

0

0

0

0

0

0

0

0

0

0

0

0

0

0

0

0

0

0

0

0

0

0,200 MeV

σ mb

300

0

0

0

0

0

0

0

0

0

0

0

0

0

0

0

0

0

0

0

0,258 MeV

σ mb

400

0

0

0

0

0

0

0

0

0

0

0

0

0

0

0

0,300 MeV

σ mb

300

0

0

0

0

0

0

0

0

0

0

0

0,350 MeV

σ mb

150

0

0

0

0

0

0

0

0

0,565 MeV

σ mb

60

0

0

0

0

0

Cos θ CM

-1

0

1

20 KeV

80 KeV

190 KeV

$\text{Li}^6(n, \alpha) \text{H}^3$

Distributions angulaires

○ Points expérimentaux renormalisés

○ Rèf: Bame rapport Wash 1958, 1013
Darlington P.R. 1953, 90, 1049
Beets J. de Phys. 1963, 24, 803

— Courbes théoriques

Fig. 15.3.5.

16. DEPARTEMENT DE PHYSIQUE NUCLEAIRE ET DU SOLIDE -
SERVICE DE PHYSIQUE NUCLEAIRE A BASSE ENERGIE -
CEA - Saclay (France)

Les expériences de temps de vol décrites dans le précédent rapport ont été poursuivies à l'accélérateur linéaire de Saclay par S. de BARROS, G.BIANCHI, P.CHEVILLON, C.CORGE, V.D.HUYNH, J.JULIEN, G.LE POITTEVIN, J.MORGENSTERN, F.NETTER, C.SAMOUR. Les mesures de transmission, de capture totale et de spectres de rayonnement gamma dans les résonances ont été effectuées simultanément sur trois bases de temps de vol et ont permis une étude systématique du spin J des résonances considérées.

16.1. Progrès dans l'appareillage et le traitement des données.

16.1.1. Mesures de transmission

Elles ont été poursuivies sur une base de 103 mètres. En combinant une largeur d'impulsion fournie par l'accélérateur de 20 nanosecondes et une largeur de canal de détection de 10 nanosecondes, la résolution effective obtenue, tenant compte de tous les effets, est de 0,3 nanoseconde par mètre. Un nouveau poste de détection vient d'être installé à 200 mètres, ce qui permettra, grâce à des améliorations apportées au détecteur, de travailler avec une résolution de 0,1 nanoseconde par mètre.

Les programmes d'analyse sur l'ordinateur IBM 7094 de Saclay ont été perfectionnés et permettent d'explorer la région d'énergie de neutrons de 1 à 100 keV en incluant les effets d'interférences entre résonances et en traitant, par une méthode des formes, une cinquantaine de résonances à la fois, tenant compte des effets Doppler et de résolution (problème SPNBE 109). Un autre programme mettant en œuvre une formule utilisant le formalisme de la "matrice R" est en cours d'achèvement.

16.1.2. Mesures de la largeur totale de radiation.

Ces mesures sont effectuées à la fois à partir des résultats d'expériences de transmission à haute résolution et à l'aide du détecteur Ar à scintillation liquide.

Grâce aux méthodes soignées utilisées pour l'analyse, la précision atteinte pour ces mesures est bonne. F_γ est en général connu avec une erreur inférieure à 8%.

16.1.3. Mesures de transitions radiatives partielles.

Le spectromètre à cristal entouré par un cristal annulaire déjà décrit a été utilisé systématiquement avec l'analyseur multi-dimensionnel à 16 voies. Des progrès dans l'analyse sur calculateur électronique ont permis de décomposer avec précision les spectres complexes obtenus dans les résonances (problème SPNBE 102). La mise en fonctionnement du calculateur CAE 510 directement associé aux appareillages expérimentaux utilisés par notre service (cf. description donnée à la conférence de Karlsruhe en juillet 1964) a donné lieu à l'élaboration de divers programmes d'exploitation et d'analyse.

Un nouveau poste de détection à une base de parcours de 50 mètres a été installé pour accroître la résolution en temps de vol dans ce type d'expériences.

16.2. Résultats récents.

Ils sont rassemblés dans divers articles à paraître dans "Nuclear Physics" au cours de l'année 1965.

16.2.1. Variation de la fonction densité (strength function) avec le spin des résonances pour les noyaux cibles de spin $I = 3/2$.

En combinant les expériences de transmission et les expériences de capture radiative pour procéder aux attributions de spin, l'étude a porté sur As (de 0 à 4000eV), Ga et Br (de 0 à 2000eV), Ba et Au (de 0 à 1000eV). La table 16.1. donne les paramètres des résonances pour As, la table 16.2. pour les isotopes de Ga, les tables 16.3. et 16.4. pour les isotopes de Br (des lettres identiques dans la première colonne signifient que les résonances correspondantes appartiennent à des isotopes différents, ce qui est prouvé par la présence ou

l'absence d'un effet d'interférence entre résonances). La table 16.5. donne les valeurs de $g\Gamma_n^0$ pour les résonances de Br pour lesquelles les épaisseurs d'échantillons employées et la résolution utilisée n'ont pas permis d'attribuer le spin avec certitude ce sont en général des résonances faibles sauf celle à 788 eV pour laquelle la proximité d'une résonance du bismuth (dont un écran servait à la détermination permanente de la loi de bruit de fond) a perturbé la mesure avec un échantillon épais (la valeur pour $g\Gamma_n^0$ a été déterminée avec un échantillon mince et d'autres écrans de bruit de fond).

La table 16.6. donne les paramètres de résonances de l'or. Dans ce cas, comme dans les précédents, on constate que la valeur de spin $J = 2$ correspond systématiquement à la plus forte valeur de la fonction densité. La table 16.7. compare ces résultats avec ceux, étudiés précédemment, de Se (premier cas où nous avons mis en évidence l'effet de dépendance du spin) et de Pt (cas où la fonction densité ne varie pas sensiblement avec le spin).

Les résultats concernant Ba sont en cours de dépouillement.

16.2.2. Mesures de transmission à haute résolution entre 1 et 100 keV.

Les noyaux étudiés sont V, Mn et Co. Le dépouillement n'est pas achevé sauf pour une partie des résultats concernant Co, portés dans la table 16.8. et qui ne permettent pas de conclure à un effet de dépendance de la fonction densité avec le spin des résonances.

16.2.3. Etude des résonances "s" et "p" pour le niobium et les noyaux de masse voisine de 90.

Les paramètres des résonances ont été déterminés pour Nb entre 30 et 4000 eV. L'identification des résonances dues aux neutrons "p" a été faite à basse énergie grâce à l'étude des spectres de rayonnements gamma de capture et au-dessus de quelques centaines d'électron-volt à partir de mesures de transmission d'échantillons très épais.

La table 16.9. rassemble les résultats de cette étude qui a permis pour la première fois de déterminer la valeur de la fonction densité S_1 pour les ondes "p" à partir des paramètres des résonances prises individuellement:

$$S_1 = (5 \pm 1) \cdot 10^{-4}.$$

On constate que la valeur de la fonction densité pour les ondes "s"

$$S_0 = (0,35 \pm 0,06) \cdot 10^{-4}$$

est très basse, ce qui est caractéristique du voisinage de la masse $A \sim 100$.

La table 16.10. rassemble les résultats concernant la largeur totale de radiation pour les résonances de Nb, confirmant l'effet déjà annoncé que cette largeur est très différente pour les neutrons "p"

$$\Gamma_\gamma (l = 1) = 230 \pm 50 \text{ meV}, \text{ de la valeur pour les neutrons "s"}$$

$$\Gamma_\gamma (l = 0) = 140 \pm 30 \text{ meV}.$$

L'étude du spectre de rayonnement gamma de capture révèle d'ailleurs de sérieuses différences entre les résonances "s" et "p".

Les expériences sur les isotopes de Zr contribueront à préciser le comportement des fonctions S_0 et S_1 dans cette région de masse.

16.2.4. Corrélations entre niveaux.

Des études de corrélation entre espacements des niveaux de résonances et aussi entre les espacements et les largeurs sont effectuées pour les noyaux comportant un nombre suffisant de résonances analysées. Les résultats figurent dans les articles en cours de parution. La table 16.11. concerne le cas du Nb.

16.2.5. Etude systématique des largeurs totales de radiation.

Elle porte sur les résonances "s" de très nombreux noyaux entre les nombres de masse $A = 50$ et $A = 201$: ^{56}Fe , ^{63}Cu , ^{65}Cu , ^{69}Zn , ^{69}Ga , ^{75}As , ^{77}Se , ^{79}Br , ^{81}Br , ^{91}Zr , ^{93}Nb , ^{139}La , ^{96}Zr , ^{141}Pr , ^{143}Nd , ^{145}Nd , ^{169}Tm , ^{183}W , ^{195}Pt , ^{197}Au , ^{199}Hg , ^{201}Hg , .

Des valeurs assez grandes de Γ_γ sont trouvées pour Fe, ^{63}Cu , As, Ga, Br. Au contraire, vers $A = 145$, Γ_γ est voisin de 0,1 eV et reste faible dans la région des noyaux déformés. La valeur de Γ_γ croît à nouveau au voisinage de la couche saturée de 126 neutrons, par exemple, pour ^{201}Hg .

On constate que, pour les résonances où le spectre gamma de désexcitation comporte des transitions électriques dipolaires E_1 à l'état fondamental et aux premiers états excités, on trouve parfois des variations de Γ_γ en fonction du spin de la résonance (cas de Se, Pt, Hg).

Par ailleurs, dans le cas de ^{199}Hg et ^{201}Hg et pour une valeur de spin donnée, des mesures précises montrent que Γ_γ varie de résonance à résonance.

16.2.6. Etude des transitions radiatives partielles.

Les résultats récents concernent W, Pt, Au, Hg et ^{238}U . Des corrélations entre les transitions radiatives partielles sont examinées dans les résonances de $^{183}\text{W} + n$.

Pour $^{195}\text{Pt} + n$, on a obtenu la distribution des largeurs partielles correspondant à la somme des trois transitions les plus énergiques pour 13 résonances de spin $J = 1$ (figure 16.1.) et la distribution globale des 39 largeurs partielles correspondant à chacune de ces trois transitions pour les 13 résonances ce qui donne une valeur de l'ordre de deux pour le nombre V de degrés de liberté (figure 16.2.).

Une recherche particulière a été effectuée dans le cas de $^{197}\text{Au} + n$ où la transition vers 6 MeV apparaît avec une largeur partielle importante dans de nombreuses résonances pour déceler une éventuelle contribution de la capture radiative directe. L'étude détaillée de cette transition dans la première résonance de l'or à 4,9 eV a permis (figure 16.3.) de donner une limite supérieure de 6 millibarns pour la section efficace de capture potentielle à 4,9 eV.

Table 16.1. ARSENIC.

E_0 eV	$g\Gamma_n$ meV	J	Γ_n meV	Γ meV	Γ_γ meV	$g\Gamma_n^o$ meV	Γ_n^o meV
3993 ± 40	1200 ± 120	1	3200 ± 320	3500 ± 400	300	19 ± 2	51 ± 5
2819 ± 25	1340 ± 120	1	3560 ± 330	3850 ± 400	290	25,2 ± 2	67 ± 6
2507 ± 25	610 ± 60	1	1620 ± 160	1900 ± 200	280	12 ± 1	32 ± 3
2046 ± 20	190 ± 30	1	500 ± 80	700 ± 150	200	4,3 ± 0,5	11,5 ± 2
1804 ± 20	335 ± 30	1	890 ± 80	1200 ± 150	310	7,8 ± 0,8	21 ± 2
1351 ± 12	260 ± 25	1	690 ± 70	950 ± 100	260 ± 120	7 ± 0,7	19 ± 2
1296 ± 10	1120 ± 100	1	2980 ± 270	3250 ± 300	270	31 ± 3	85 ± 7
1108 ± 10	73 ± 6	1	195 ± 17	520 ± 50	325 ± 50	2,2 ± 0,2	6 ± 0,5
894 ± 7	75 ± 7	1	200 ± 20	540 ± 60	340 ± 60	2,5 ± 0,3	6,7 ± 0,7
734 ± 6	430 ± 50	1	1150 ± 130	1500 ± 180	350 ± 200	16 ± 2	42,1 ± 5
663 ± 6	168 ± 13	1	450 ± 35	680 ± 70	230 ± 80	6,1 ± 0,5	17,5 ± 1,5
327 ± 2	198 ± 15	1	514 ± 40	860 ± 80	346 ± 90	10,7 ± 0,9	28,5 ± 2
3927 ± 40	3120 ± 270	2	5000 ± 450	5300 ± 500	300	50 ± 5	80 ± 8
3846 ± 40	1750 ± 150	2	2860 ± 260	3100 ± 300	250	29 ± 3	46 ± 4
3706 ± 35	2700 ± 280	2	4320 ± 450	4550 ± 500	230	44 ± 5	71 ± 8
3498 ± 35	3360 ± 335	2	5400 ± 500	5700 ± 600	300	57 ± 6	91 ± 9
3453 ± 35	2250 ± 220	2	3570 ± 350	3900 ± 400	330	38 ± 4	61 ± 6
3158 ± 30	1450 ± 150	2	2320 ± 230	2600 ± 250	280	26 ± 2	41,5 ± 4
2729 ± 25	2440 ± 230	2	4300 ± 400	3900 ± 400	400	47 ± 4	75 ± 7
2612 ± 25	1470 ± 140	2	2350 ± 220	2650 ± 250	300	29 ± 3	46 ± 4
1901 ± 20	1790 ± 130	2	2860 ± 210	3100 ± 250	240	41 ± 3	66 ± 5
1680 ± 15	2210 ± 200	2	3540 ± 320	3850 ± 350	270	54 ± 5	86 ± 8
1440 ± 15	840 ± 70	2	1350 ± 110	1600 ± 170	250	122 ± 2	35,6 ± 3,5
928 ± 7	370 ± 40	2	310 ± 60	1200 ± 100	290 ± 120	19,2 ± 1,4	30 ± 2
738 ± 6	1120 ± 100	2	1600 ± 170	2100 ± 250	300	41,3 ± 3,5	66 ± 6
533 ± 4	1710 ± 100	2	2700 ± 160	3100 ± 200	270	74 ± 4,5	117 ± 7
319 ± 2	311 ± 25	2	500 ± 40	820 ± 80	320 ± 80	17,5 ± 1,5	28 ± 2

$$S_o(J=2) = 0,5 \cdot 10^{-4} \pm 0,6 \cdot 10^{-4}$$

$$S_o(J=1) = 1 \cdot 10^{-4} \pm 0,3 \cdot 10^{-4}$$

Table 16.2. GALLIUM.

Isotopes	E_0 eV	$g\Gamma_n$ meV	J	Γ_n meV	Γ meV	Γ_γ meV	$g\Gamma_n^o$ meV	Γ_n^o meV
71	287,5 ± 1	4100 ± 300	2	6560 ± 450	6800 ± 600	340	241 ± 20	384 ± 30
69	334 ± 1	167 ± 11	2	171 ± 18	380 ± 40	210 ± 40	5,8 ± 0,6	9,3 ± 1
71	376,5 ± 1	1360 ± 120	1	3630 ± 330	4000 ± 400	370	70 ± 6	187 ± 16
69	692 ± 4	720 ± 70	2	1150 ± 80	1500 ± 200	350	27 ± 2,7	43 ± 4
71	706 ± 5	280 ± 28	2	450 ± 45	800 ± 100	350 ± 110	10,5 ± 1	17 ± 1,5
69	1529 ± 15	1500 ± 200	2	2400 ± 350	2800 ± 400	400	38,5	61,6
69	1586 ± 15	1360 ± 200	2	2180 ± 300	2500 ± 400	320	34	54,4
69	1640 ± 15	1880 ± 230	2	3000 ± 400	3300 ± 500	300	46,5	74,4
69	1872 ± 20	1700 ± 220	2	2820 ± 400	3000 ± 600	180	39	62,4
69	2463 ± 30	4550 ± 600	2	7280 ± 1000	7500 ± 1200	220	91	146

$$S_o(J=2) = 1,8 ± 0,9 \cdot 10^{-4}$$

$$S_o(J=1) < 0,4 \cdot 10^{-4}$$

Table 16.3. -BROME-

Isotope	E_o (eV)	$g\Gamma_h$ (meV)	J	Γ_h (meV)	Γ (meV)	Γ_h^o (meV)	$g\Gamma_h^o$ (meV)	Γ_h^o (meV)
81	135.45	158 ± 14	1	420 ± 40	730 ± 70	310	13.6 ± 1.3	36 ± 3.5
	604.2	200 ± 16	1	535 ± 40	835 ± 60	300	8.1 ± 0.7	21.7 ± 2
	749.2	177 ± 20	(1)	472 ± 50	780 ± 100	310	6.5 ± 0.8	17.3 ± 2
	930	195 ± 20	(1)	517 ± 50	820 ± 90	300	6.4 ± 0.6	17.1 ± 1.7
f	1146.3	655 ± 50	1	1750 ± 130	2100 ± 200	350	19.3 ± 1.5	51.5 ± 4
f	1208.9	1670 ± 130	1	4500 ± 350	4800 ± 380	300	48.1 ± 4	130 ± 10
	1453.9	500 ± 60	(1)	1330 ± 150	1600 ± 200	270	13 ± 1.5	35 ± 4

Table 16.4.

Isotope	E_o (eV)	$g\Gamma_h$ (meV)	J	Γ_h (meV)	Γ (meV)	Γ_h^o (meV)	$g\Gamma_h^o$ (meV)	Γ_h^o (meV)
81	101.05	97 ± 8	2	155 ± 12	440 ± 40	285	9.7 ± 0.8	15.5 ± 1.2
79	238.8	379 ± 30	2	606 ± 50	900 ± 70	295	24.5 ± 2	39.2 ± 3
79	318.5	372 ± 30	2	595 ± 50	880 ± 70	285	20.9 ± 1.6	33.4 ± 2.5
	564.6	327 ± 25	2	525 ± 40	840 ± 80	315	13.7 ± 1	22 ± 1.8
	578.6	241 ± 20	2	385 ± 30	680 ± 60	295	10 ± 0.8	16 ± 1.4
	645.8	226 ± 20	2	362 ± 35	660 ± 60	300	8.9 ± 0.8	14.2 ± 1.5
	668.6	975 ± 80	2	1560 ± 120	1900 ± 150	340	37.6 ± 3	60.2 ± 5
	1101.2	511 ± 40	2	820 ± 70	1100 ± 120	280	15.4 ± 1.2	24.6 ± 2
a	1200.4	1465 ± 110	2	2340 ± 220	2650 ± 220	310	42.3 ± 3.4	67.6 ± 5.2
b	1275.1	2013 ± 160	2	3220 ± 250	3550 ± 300	330	56.4 ± 4.5	90 ± 7
c	1468.5	327 ± 50	(2)	530 ± 80	830 ± 130	300	8.5 ± 1.4	13.5 ± 2
c	1530.8	1529 ± 120	2	2450 ± 200	2800 ± 280	350	39.1 ± 3	62.6 ± 5
d	1547	2250 ± 180	2	3600 ± 300	3950 ± 400	350	57.3 ± 4.5	91.6 ± 7.3
c	1589	713 ± 60	2	1140 ± 90	1500 ± 150	360	17.9 ± 1.4	28.6 ± 2.3
e	1828	1630 ± 180	2	2560 ± 300	2900 ± 300	340	38.2 ± 1.4	61.1 ± 6
e	1873.1	1870 ± 150	2	3000 ± 250	3200 ± 300	200	43.2 ± 3.5	69.6 ± 6

Table 16.5. -BROME-

Isotope	E_o (eV)	$g\Gamma_h$ (meV)	Γ_h^o (meV)	E_o (eV)	$g\Gamma_h$ (meV)	Γ_h^o (meV)
	35.78	25.7 ± 2	4.3 ± 3			
	53.75	11.8 ± 1.4	1.6 ± 0.18			
	189.5	32 ± 4	2.3 ± 0.3			
	294	40 ± 5	2.3 ± 0.3			
	394.6	70 ± 10	3.5 ± 0.5			
	468	30 ± 5	1.4 ± 0.3			
	483.5	35 ± 5	1.6 ± 0.2			
	637.5	49.3 ± 5	1.95 ± 0.2			
	788.1	380 ± 50	13 ± 1.5			
	849.5	26 ± 4	0.9 ± 0.2			
	892.5	25 ± 4	0.83 ± 0.16			
	993.4	25 ± 5	0.8 ± 0.2			
	1042.7	30 ± 6	1.1 ± 0.2			
	1110.6	16 ± 4	0.5 ± 0.15			
	1227	30 ± 7	0.85 ± 0.2			
	1311	31 ± 6	0.82 ± 0.17			
	1378.6	36 ± 7	1 ± 0.2			
	1570.7	96 ± 20	2.5 ± 0.5			
	1706.4	65 ± 20	1.6 ± 0.3			
	1719.9	320 ± 50	7.7 ± 1.5			
	1770.5	265 ± 35	6.3 ± 1			
	1883	120 ± 40	2.8 ± 0.8			
	1895.7	47 ± 10	1.1 ± 0.2			
	1967.8	210 ± 30	4.7 ± 0.7			

Table 16.6.: OR

E_0	δ	$\gamma \Gamma_n$ (meV)	Γ_n (meV)	Γ meV	Γ_x meV	$g\Gamma_n^0$ meV	Γ^0 meV
ev							
4.906	2	9.76	15.6	140	124	4.41	7.05
46.5		0.055					
58.03	(1)	1.65 ± 0.07					
60.25	2	40.6 ± 1	65 ± 1.5	210 ± 10	145 ± 12	5.25 ± 0.10	8.4 ± 0.2
78.43	(1)	6.1 ± 0.3	16 ± 0.8	155 ± 10	139 ± 10	0.69 ± 0.02	4.84 ± 0.1
107.	(2)	5.06 ± 0.3	8 ± 0.5	130 ± 10	127 ± 10	0.43 ± 0.01	0.77 ± 0.04
122.2		0.4				0.03	
144.2	(1)	3.35 ± 0.15	9 ± 0.5	127 ± 10	118 ± 13	0.2 ± 0.01	0.75 ± 0.04
151.2	2	13.8 ± 0.5	22 ± 0.9	141 ± 10	119 ± 10	1.13 ± 0.01	1.8 ± 0.07
162.9	1	18.7 ± 0.9	50 ± 2	165 ± 12	155 ± 12	1.67 ± 0.07	3.92 ± 0.2
164.9	(2)	5.8 ± 0.3	9.3 ± 0.5	115 ± 15	106 ± 15	0.49 ± 0.02	0.72 ± 0.05
189.9	1	18 ± 0.6	48 ± 1.6	174 ± 12	166 ± 12	1.31 ± 0.04	3.5 ± 0.1
208.9							
240.3	2	44.6 ± 2.5	72 ± 3.6	175 ± 12	103 ± 12	2.91 ± 0.15	4.65 ± 0.2
255.4							
261.9	1	51 ± 2	136 ± 5	260 ± 16	124 ± 17	3.15 ± 0.13	8.4 ± 0.3
273.6	1	2.6 ± 0.1					
293.1	2	226 ± 10	362 ± 16	470 ± 25	108 ± 30	13.20 ± 0.6	21.1 ± 1
329	2	28.6 ± 1.4	46 ± 2.3	180 ± 15	134 ± 13	1.57 ± 0.08	2.51 ± 0.13
330.3	1	123.4 ± 1.2	62.4 ± 4.8	200 ± 17	138 ± 17	1.26 ± 0.06	3.4 ± 0.17
355.1	2	124.5 ± 1.2	39.2 ± 2	180 ± 20	140 ± 20	1.30 ± 0.06	2.08 ± 0.09
370.7	2	52.5 ± 4	83.5 ± 7	205 ± 20	122 ± 21	2.71 ± 0.2	4.33 ± 0.35
375.1	1	5.2 ± 0.5					
381.5	2	38.2 ± 4	61 ± 6	140 ± 14	130 ± 18	0.27 ± 0.03	
400.3	1			180 ± 20	119 ± 21	1.96 ± 0.2	3.13 ± 0.3
401.5	1						
440.2	1	1108 ± 8	285 ± 22	420 ± 35	135 ± 40	5.1 ± 0.36	13.6 ± 1
450.9	2	40.3 ± 3	64.5 ± 4.5	190 ± 20	126 ± 20	1.90 ± 0.13	3.04 ± 0.2
477.3	2	1206 ± 14	329 ± 22	480 ± 40	150 ± 45	9.30 ± 0.6	15 ± 1
489.7	1	22.5 ± 2	60 ± 6	190 ± 20	130 ± 21	1.02 ± 0.01	2.67 ± 0.03
493.8	2	17.1 ± 1.5	24 ± 2	160 ± 17	136 ± 17	0.77 ± 0.06	1.23 ± 0.1
534	2	21.7 ± 1.5	35 ± 2.5	160 ± 15	125 ± 15	0.94 ± 0.07	1.50 ± 0.1
540.5	1	22.2 ± 1.8	59 ± 5	180 ± 20	120 ± 20	0.95 ± 0.08	2.53 ± 0.23
561.4	1	1.8 ± 0.2				0.08 ± 0.01	
579	2	1231 ± 13	370 ± 22	520 ± 40	150 ± 45	9.63 ± 0.6	15.4 ± 1
580.8	1	55.3 ± 3.5	145 ± 9	260 ± 25	115 ± 27	2.29 ± 0.16	6.11 ± 0.5
586.7	1	13 ± 1.3				0.54 ± 0.05	
602.8	2	1140 ± 7	224 ± 11	335 ± 30	160 ± 30	5.72 ± 0.3	9.15 ± 0.5
617.2	2	149 ± 3	78 ± 7	240 ± 25	160 ± 25	1.96 ± 0.15	3.14 ± 0.2
624.6	1	13.5 ± 1.5				0.74 ± 0.06	
628.2	2	14 ± 1.2				0.55 ± 0.04	
639.7	2	1300 ± 15	460 ± 24	630 ± 40	150 ± 45	11.9 ± 0.6	19 ± 0.9
658.7	1	2.4 ± 0.4				0.09 ± 0.002	
665.9	1	5 ± 3.7				0.19 ± 0.02	
695.7	1	1250 ± 20	665 ± 50	830 ± 80	165 ± 90	9.45 ± 1.5	25.2 ± 2
699	2	1460 ± 30	736 ± 50	880 ± 80	144 ± 90	17.4 ± 2	27.8 ± 3
715.6	2	1.72 ± 6	115 ± 9	260 ± 35	145 ± 35	2.7 ± 0.2	4.3 ± 0.35
738.4	1	5 ± 0.7				0.13 ± 0.02	
759.9	1	1160 ± 11	426 ± 30	580 ± 50	154 ± 60	5.78 ± 0.4	15.4 ± 1.2
773.8	1	1178 ± 13	474 ± 35	600 ± 50	126 ± 60	6.37 ± 0.5	17 ± 1.3
784.3	2	75 ± 6	120 ± 10	270 ± 30	150 ± 30	2.7 ± 0.35	4.3 ± 0.35
796	2	1111 ± 9	177 ± 14	325 ± 30	150 ± 30	3.94 ± 0.30	6.3 ± 0.50
813.3	1	0.3 ± 1				0.29 ± 0.03	
819.3	2	1144 ± 11	290 ± 18	380 ± 40	150 ± 45	5.06 ± 0.4	8.1 ± 0.6
823	2	1333 ± 20	533 ± 40	700 ± 55	165 ± 65	11.6 ± 0.8	18.5 ± 1.3
864.2	1	12.4 ± 1.2				0.42 ± 0.04	
873.3	1	20.5 ± 1.7				0.69 ± 0.6	
932.4	2	257 ± 17	612 ± 30	560 ± 45	150 ± 55	8.44 ± 0.6	13.5 ± 0.8
936.1	1	4 ± 1					
961.2	1	41 ± 3	110 ± 9	260 ± 35	150 ± 35	1.32 ± 0.1	3.52 ± 0.3
964.2	2	207 ± 13	329 ± 20	480 ± 50	150 ± 45	6.63 ± 0.5	10.6 ± 0.75
968.3	2	75.6 ± 7	121 ± 12	290 ± 60	170 ± 60	2.44 ± 0.3	3.9 ± 0.4
975.4	2	310 ± 20	500 ± 35	650 ± 60	150 ± 65	9.94 ± 0.6	15.9 ± 1

Table 16.7.

Table 16.8.

LISTE DES RÉSONANCES

	Nombre total de résonances observées	Domaine d'énergie de neutrinos	Nombre de résonances pour lesquelles le spin a été déterminé	Spin	Nombre de résonances ayant ce spin	Fonction densité S_0 évol.	Rapport expérimental	Probabilité
69 Co	12	200 - 2500 ev	7	$J = 2$	7	$1.8 \pm 0.9 \cdot 10^{-4}$		
75 As	55	40 - 4000 ev	27	$J = 1$	0	$< 0.4 \cdot 10^{-4}$		
77 Se	10	900 - 15000 ev	9	$J = 2$	15	$2.5 \pm 0.6 \cdot 10^{-4}$	2.5	1%
79,81 Br	82	30 - 20000 ev	23	$J = 1$	12	$1 \pm 0.3 \cdot 10^{-4}$		
195 Pt	19	10 - 310 ev	19	$J = 0$	6	$2.3 \pm 1.3 \cdot 10^{-4}$		
197 Au	64	50 - 1000 ev	43	$J = 1$	13	$1.9 \pm 0.7 \cdot 10^{-4}$		
				$J = 2$	28	$2.5 \pm 0.5 \cdot 10^{-4}$	2	1%
				$J = 1$	15	$12 \pm 0.3 \cdot 10^{-4}$		

• Pour chaque isotope

La probabilité donnée dans le tableau est celle de trouver un rapport égal ou supérieur au rapport expérimental en supposant S_0 indépendant de J .

Table 16.10.

Table 16.11.

93 Nb + n

$I = 0$		$I = 1$	
E (ev)	Γ_g (meV)	E (ev)	Γ_g (meV)
105,8	170 ± 40	35,9	250 ± 50
119	136 ± 20	42,2	220 ± 50
193	135 ± 30	94,3	150 ± 50
335,4	163 ± 30	184,3	250 ± 50
378,3	167 ± 40	244	262 ± 50
4460,3	162 ± 35	319	220 ± 50
935,4	140 ± 90	392	200 ± 30
1149,2	145 ± 65	500,9	225 ± 50
1393,3	171 ± 60		

93 Nb + n

93 Nb + n

Coefficient de corrélation r (population finie)				Population infinie			
1er intervalle	2ème	3ème	4ème	Moyenne	Confiance 95 %	Moyenne	Confiance 95 %
$g_{\text{fr}}^n = 0$ 29 résonances $\Delta E = 2300 \text{ ev}$	-0,31	-0,00001	0,33	-0,006	-0,02 < $r < 0,31$	-0,014	-0,02 < $r < 0,22$
Spacements quel que soit I 110 résonances $\Delta E = 4100 \text{ ev}$	+0,02	-0,035	-0,037	-0,045	-0,05 < $r < 0,0$	-0,01	-0,02 < $r < 0,1$
Spacements $I=0$ 29 résonances $\Delta E = 2300 \text{ ev}$	-0,13	-0,29	-0,01	-0,14	-0,22 < $r < 0,22$		
Spacements $I=1$ 36 résonances $\Delta E = 2300 \text{ ev}$	+0,16	-0,26	-0,37	-0,16	-0,50 < $r < 0,2$		
Spacements g_{fr}^n 29 résonances $\Delta E = 2300 \text{ ev}$	+0,90	+0,22	+0,57	+0,96	+0,20 < $r < 0,76$		

Table 16.9.

93
Nb + 0

E (eV)	g Γ_n (MeV)	Γ (MeV)	I	J	E (eV)	g Γ_n (MeV)	Γ (MeV)	I	J
35,9	0,054 ± 0,005	250 ± 50	1		1982,2	4,7 ± 1	250 ± 60	1	
42,2	0,044 ± 0,005	200 ± 50	1		1992,4	14,8 ± 3	130 ± 30	0	(4)
94,3	0,180 ± 0,02	150 ± 35	1		2023,7	378 ± 60	840 ± 130	0	5
105,8	0,225 ± 0,005	170 ± 40	0		2070,2	33 ± 6	300 ± 40	1	
119	2 ± 0,2	140 ± 20	0		2076,1	95 ± 14	324 ± 50	0	(5)
184,3	0,1 ± 0,02	250 ± 50	1		2118,8	27 ± 5	300 ± 50	1	
193	15,3 ± 1,5	175 ± 30	0		2149,4	40 ± 6	330 ± 60	1	
244	1,2 ± 0,1	262 ± 50	1		2156,7	156 ± 25	410 ± 60	0	5
319	1 ± 0,1	220 ± 40	1		2186,4	11 ± 2	270 ± 60	1	
335,4	8,33 ± 1	180 ± 30	0		2231,8	91 ± 13	230 ± 50	0	
363	0,18 ± 0,02	135 ± 30	(1)		2310**				
364,9	0,33 ± 0,03	150 ± 30	(0)		2335**				
378,3	53,5 ± 5	287 ± 40	0	(4)	2341**				
392,6	1,25 ± 0,12	200 ± 30	1		2360**				
460,3	3,9 ± 0,4	170 ± 35	0		2392**				
500,9	2,65 ± 0,26	230 ± 50	1		2421	1250 ± 360	2400 ± 700	0	
599,2	0,61 ± 0,1	145 ± 40	(0)		2455	13,2 ± 5			(1)
604,1	1,72 ± 0,17	160 ± 40	0		2462	62,5 ± 20			1
617,5	0,72 ± 0,1	150 ± 40			2507	16,5 ± 5			(1)
641,1	2,74 ± 0,3	150 ± 40	0		2543	30 ± 15			
672,3	4,42 ± 0,4	220 ± 40	1		2574	20 ± 10			
678,3	1,1 ± 0,1	135 ± 30	1		2637	1197 ± 300	2950 ± 900	0	
721,5	8 ± 0,8	250 ± 50	1		2661	26 ± 12			1
741,6	95,6 ± 9,6	355 ± 50	0	(5)	2684	38 ± 16			(0)
757,7	1,33 ± 0,15	250 ± 50	1		2708	27 ± 12			(0)
912,8	1,96 ± 0,2	200 ± 60	0	4	2831	14 ± 7			
935,4	189,5 ± 20	564 ± 90	0	4	2854	12 ± 6			
953,4	6,38 ± 0,64	262 ± 80	1		2884	5 ± 3			
1009,6	243 ± 36	870 ± 170	0		2923	141 ± 40	370 ± 100	0	
1016,8	13,3 ± 1,9	280 ± 70	1		2948	231 ± 60	510 ± 150	0	
1108,4	5,4 ± 0,8	250 ± 50	(1)		2983	11 ± 6			
1127,9	8,8 ± 1,4	250 ± 50	1		3143	20 ± 10			
1149,2	90,5 ± 12	310 ± 60	0	5	3222	15 ± 7			
1175,7	151,5 ± 21	560 ± 100	0	4	3252	13 ± 7			
1194,9	19,1 ± 3	210 ± 50	0		3270	38 ± 19			
1229,8	20,3 ± 3	195 ± 50	0		3278	1,9 ± 9			
1243,7	7,2 ± 1	264 ± 50	1		3352	143 ± 40			0
1283,7	6 ± 1	245 ± 50	1		3371	38 ± 16			
1351,3	16,8 ± 3,2	285 ± 50	1		3391	400 ± 100	900 ± 300	0	
1355,3	6,5 ± 1,3	260 ± 50	1		3406	10 ± 8			
1393,3	89,5 ± 13	370 ± 60	0	4	3420	10 ± 8			
1452,5	443 ± 60	1176 ± 180	0	4	3520	500 ± 150	970 ± 300	0	
1467,9	21,3 ± 3	288 ± 60	1		3584	50 ± 20			(1)
1530	7,7 ± 1,4	280 ± 60	1		3605	130 ± 40			(1)
1541,3	15 ± 3	280 ± 60	1		3666	130 ± 40			
1557	8,3 ± 1,2	266 ± 60	1		3759	358 ± 120	750 ± 220	0	
1576,9	84 ± 12	730 ± 100	0		3836	135 ± 40			(1)
1617	16,7 ± 3,3	270 ± 60	1		3918	172 ± 50			(1)
1654,6	29 ± 4,5	220 ± 50	0		3939	136 ± 40			
1678,5	2,3 ± 0,4	225 ± 50	1		3973	454 ± 110	900 ± 300	0	
1714	15,8 ± 3	170 ± 40	1		3985	50 ± 15			
1768,5	15,6 ± 3	180 ± 40	1		4019	46 ± 15			
1812,7	54,9 ± 8	195 ± 30	0	(5)	4033	87 ± 27			
1834,1	354 ± 50	1026 ± 150	0	(4)	4066	766 ± 210	1750 ± 500	0	
1946	2,7 ± 0,6	257 ± 60	1						

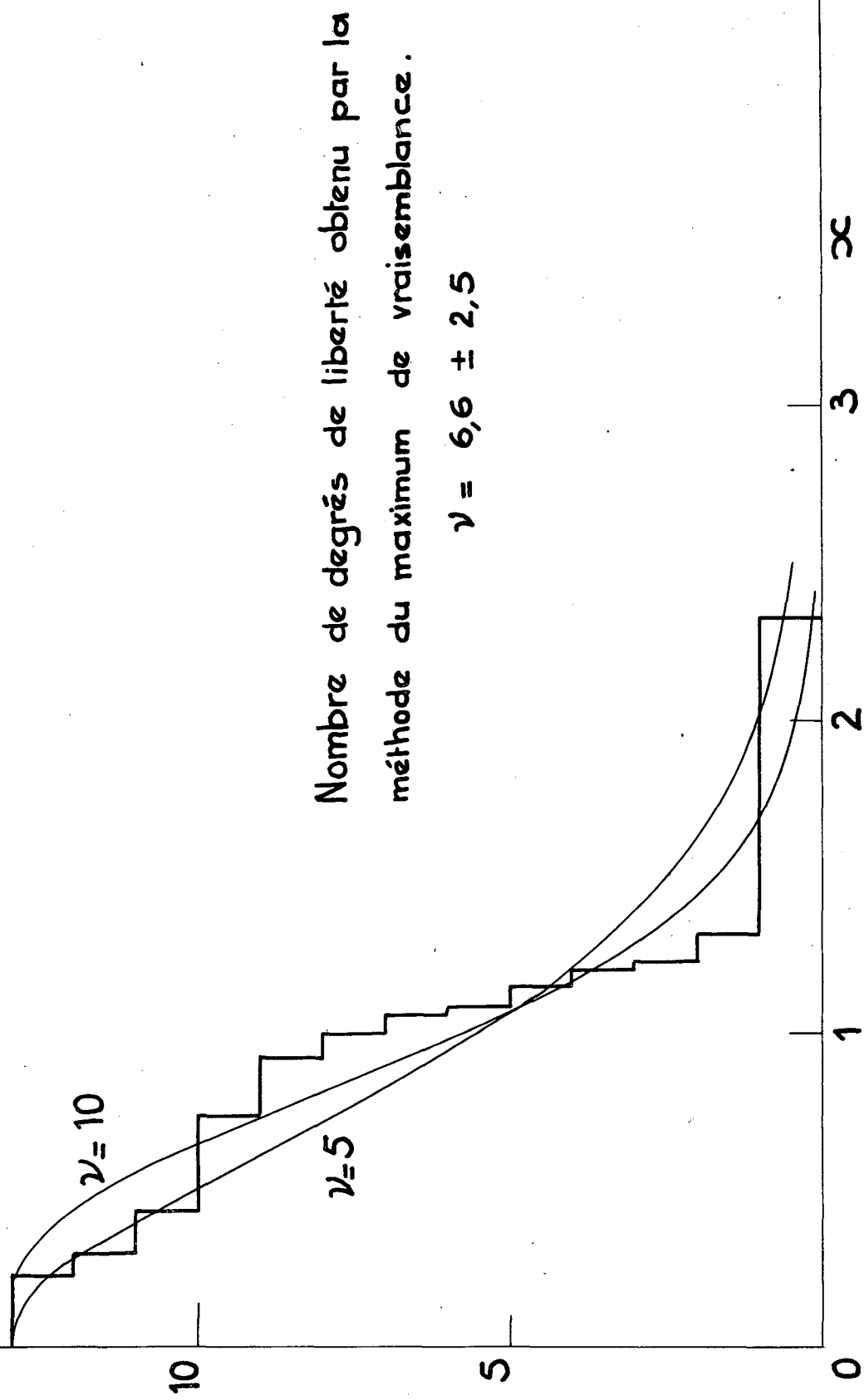
* Probablement un doublet

** Une résonance noire de l'écran de bruit de fond ne permet pas l'analyse de ces résonances

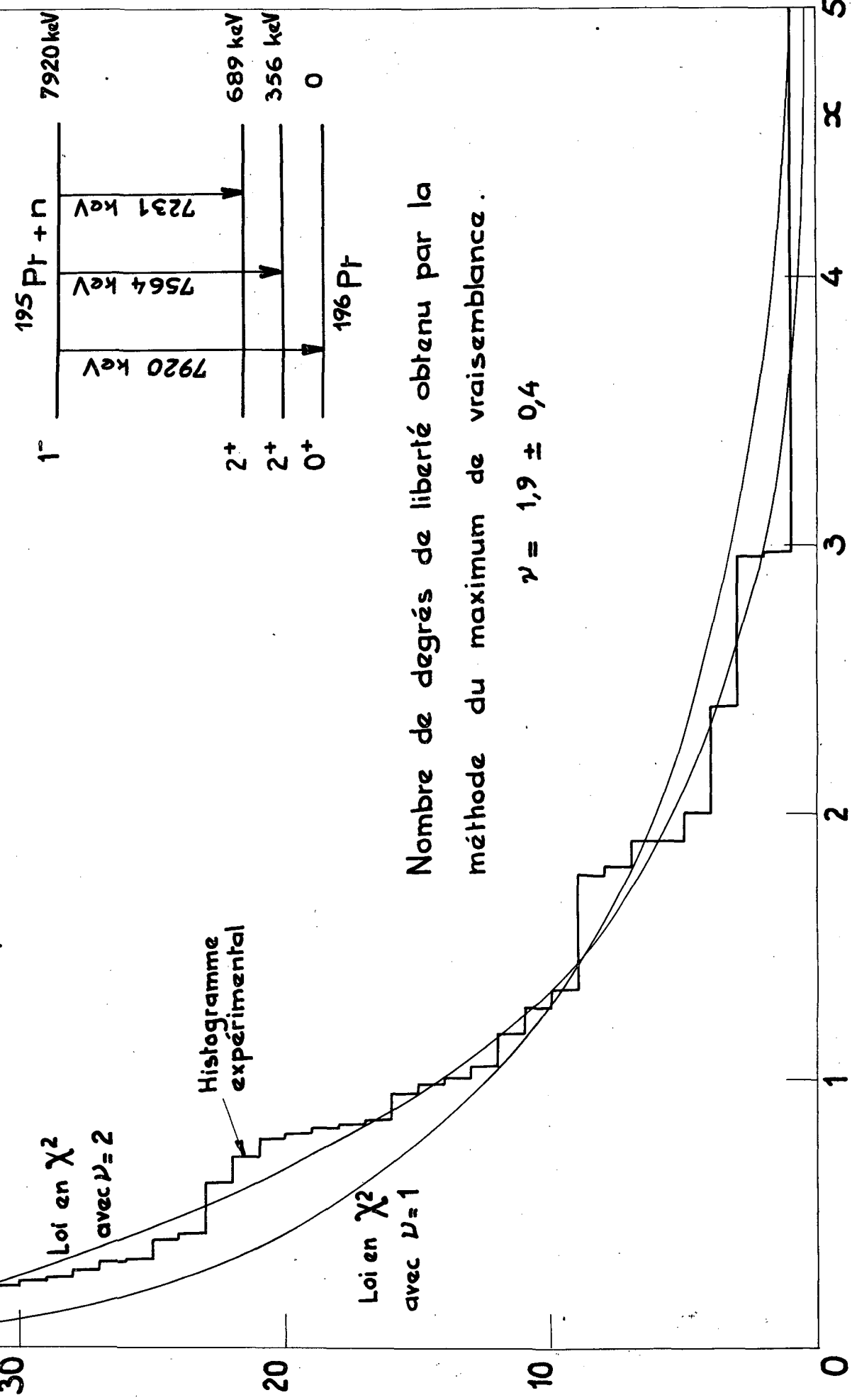
Nombre N de niveaux du ^{196}Pr dont la largeur radiative partielle, correspondant à la somme des 3 transitions

$$\left\{ \begin{array}{l} 1^- \rightarrow 0^+ \\ 1^- \rightarrow 2^+ \\ 1^- \rightarrow 2^+ \end{array} \right.$$

est telle que $\frac{\Gamma_{\gamma_i}}{\langle \Gamma_{\gamma_i} \rangle} > x$.



Nombre N de niveaux de largeur radiative partielle $\langle \gamma_i \rangle$
telle que $\frac{\langle \gamma_i \rangle}{\langle \gamma_i \rangle} > x$, pour l'échantillon de 39 largeurs
constitué par 13 résonances du ^{196}Pr .



Nombre de degrés de liberté obtenu par la
méthode du maximum de vraisemblance.

$$\nu = 1,9 \pm 0,4$$

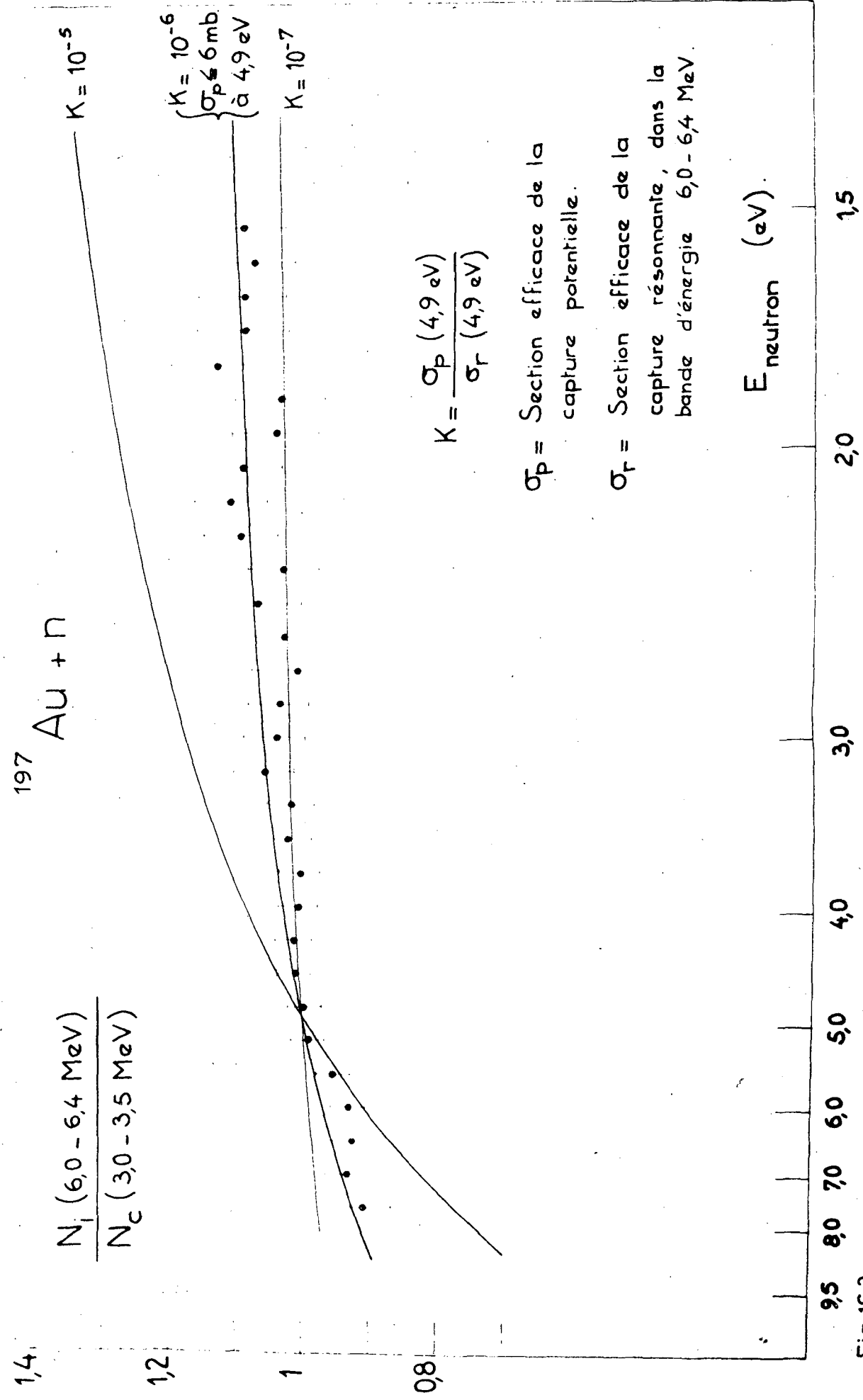


Fig. 16.3.

17. SERVICE DE PHYSIQUE EXPERIMENTALE DU COMMISSARIAT A L'ENERGIE ATOMIQUE (France)

17.1. Measures de sections efficaces neutroniques totales entre 400 keV et 1200 keV
(J.Cabe, M.Iaurat, P.Yvon).

Ce travail fait suite à une série de mesures de section efficaces totales sur quelques corps tels que le Carbone, Silicium, Phosphore, Chrome, Manganèse et Nickel dont les résultats ont déjà été diffusés en Octobre 1963 (EANDC-E-49 L). Ces mesures ont été poursuivies avec une définition en énergie du faisceau meilleure.

Les neutrons sont obtenus par la réaction $T(p,n)^3He$ en bombardant par des protons accélérés par un Van de Graaff de 2 MeV une cible de Tritium adsorbé dans du Titane. Les neutrons sont détectés par un cristal de Stilbène 1 x 1,5 pouces couplé à un photomultiplicateur 56 AVP. Nous utilisons deux voies lentes, à savoir une discrimination de forme neutron gamma et une voie linéaire provenant de la treizième dynode qui sont envoyées dans un sélecteur de coïncidences lentes du type Dynatron.

L'imprécision sur l'énergie des neutrons due à l'étalonnage est inférieure à 5 keV. La dispersion moyenne en énergie est de 3 keV. L'erreur moyenne sur σ_T est de 3%.

17.1.1. Fluor (fig. 17.1.1.)

La mesure a été faite pour des neutrons de 450 keV à 1150 keV.

17.1.2. Aluminium (Fig. 17.1.2.)

La mesure a été faite pour des neutrons de 600 keV à 1200 keV.
(Référence (1) de la figure. Phys. Rev. 72 439 (1947)).

17.1.3. Vanadium (fig. 17.1.3.)

La mesure a été faite entre 400 keV et 1200 keV.
(Référence (1) de la figure. Phys. Rev. 79 28 (1950)).

17.1.4. Fer (fig. 17.1.4.)

La mesure a été faite entre 350 keV et 1200 keV.
(Référence (1) de la figure. Phys. Rev. 73 659 (1948)).

17.1.5. Cobalt (fig. 17.1.5.)

La mesure a été faite de 450 keV à 1200 keV.

Référence (1) de la figure. Phys. Rev. 84 902 (1951).

Référence (2) de la figure. Phys. Rev. 89 1271 (1953)

17.1.6. Gallium (fig. 17.1.6.)

La variation de la section efficace totale du Gallium a été étudiée pour des neutrons de 350 keV à 1200 keV.

Référence (1) de la figure. Phys. Rev. 89 1271 (1953).

17.1.7. Plomb (fig. 17.1.7.)

Nous avons mesuré la section efficace neutronique du plomb naturel (52% ^{208}Pb , 23% ^{207}Pb , 24% ^{206}Pb et 1% ^{204}Pb) entre 600 keV et 1200 keV.

Référence (1) de la figure. Phys. Rev. 76 1146 (1949)

Référence (2) de la figure. NP 1948 (1950).

17.2. Mesures de sections efficaces neutroniques totales entre 3,6 MeV et 5,3 MeV.

(J.Cabe, M.Laurat, P.Yvon)

Nous avons mesuré des sections efficaces totales entre 3,6 et 5,3 MeV sans nous efforcer d'obtenir une très haute résolution mais plutôt des résultats moyens susceptibles d'être utilisés sur un programme de calcul relatif au modèle optique. La dispersion moyenne en énergie est de l'ordre de 30 keV, les points sont espacés de 60 keV en 60 keV. Les neutrons sont obtenus par la réaction $\text{D}(\text{d},\text{n})^3\text{He}$ en bombardant par des deutérons accélérés par un Van de Graaff de 2 MeV une cible de Deutérium adsorbé dans du Titane. La méthode et l'appareillage sont semblables à ceux utilisés pour la mesure des sections efficaces neutroniques entre 400 keV et 1200 keV. L'imprécision sur la mesure absolue de l'énergie des neutrons est de l'ordre de 15 keV. L'erreur moyenne sur σ_T ne dépasse pas 3%.

Le contrôle est effectué à l'aide d'un compteur Mac-Kibben d'une part et d'autre part de la détection du proton dans la réaction $\text{D}(\text{d},\text{p})\text{T}$. Le calcul des sections efficaces a été fait en utilisant les deux moniteurs.

17.2.1. Aluminium (Fig. 17.2.1.)

La mesure a été faite pour des neutrons de 3,690 MeV à 5,240 MeV.

Référence (1) de la figure. Private Communication (1952)

R.L.Henkel

Référence (2) de la figure. Phys. Rev. 110, 446 (1958)

17.2.2. Gallium (Fig. 17.2.2.)

La mesure sur le Gallium a été faite pour des neutrons de 3,640 MeV à 5,240 MeV.

17.3. Mesure de la section efficace ($n,2n$) pour Cu⁶³ et Zn⁶⁴ de 16,6 MeV à 18,1 MeV.

(J.Cabe, M.Iaurat, P.Yvon)

Cette mesure est en cours, par une méthode d'activation, pour des neutrons d'une résolution en énergie de 30 keV, en effectuant des mesures de 25 keV en 25 keV.

17.4. Mesures neutroniques à 14 MeV.

(D.Didier, G.Mouilhayrat, F.Perrault, F.Thouvenin)

17.4.1. Mesure des Sections Elastiques Différentielles.

La diffusion élastique des neutrons de 13,9 MeV a été étudiée par la méthode du temps de vol avec la particule associée, sur les éléments suivants. Pu, U, Ag, Ni.

Les résultats bruts sont représentés sur les figures 17.4.1. à 17.4.4.

Ces résultats seront corrigés pour tenir compte des diffusions multiples, de la géométrie, de l'expérience et de la variation du rendement du détecteur avec l'énergie.

17.4.2. Spectres des neutrons nonélastiques.

Le spectre des neutrons produits en bombardant des échantillons d'Uranium et de Plutonium par des neutrons de 13,9 MeV a été étudié par la méthode du temps de vol avec la particule associée.

Les neutrons ont été détectés à l'aide d'un scintillateur NE 213 de 4" de diamètre et 2" de long couplé à un photomultiplicateur XP 1040.

Ce détecteur était muni d'un circuit de différentiation de forme pour impulsions neutrons et gamma. il était placé à 1,20 m de l'échantillon (1 cm d'épaisseur - 5 cm de diamètre).

Le courbe de rendement du détecteur a été déterminée en observant la diffusion neutron-proton à l'aide de deux détecteurs à scintillation. Le seuil de détection se situe aux environs de 1,5 MeV.

Les spectres de temps de vol obtenus sont représentés sur les figures 17.4.5. et 17.4.6.

L'interprétation des résultats, à partir des données continues, sur la diffusion élastique, les neutrons d'évaporation et les neutrons de fission, est en cours d'achèvement.

17.5. Mesure du nombre de neutrons émis par fission
(J.Labbe, F.Ouvry, M.Soleilhac)

La mise en point de cette expérience a été faite en étudiant les neutrons émis lors de la fission spontanée du Californium 252.

Le matériau fissile est placé au centre d'un scintillateur liquide sphérique chargé du Gadolinium. Les premiers résultats nous donnent une efficacité de 85% pour la détection des neutrons de fission. L'électronique associée nous permet d'enregistrer sous forme digitale le nombre de neutrons émis par fission et d'obtenir directement la courbe de probabilité $P(n)$ d'émission de n neutrons par fission (n pouvant varier de 0 à 19).

Nous envisageons la mesure du nombre moyen de neutrons émis et de $P(n)$ lors de la fission provoquée de différents éléments fissiles en fonction de l'énergie des neutrons incidents.

17.6. Détermination de la section efficace absolue de production d'alpha par la réaction $\text{Li}^6(\text{d},\alpha)\text{He}^4$.

(G.Bruno, J.Decharge, A.Perrin, G.Surget, C.Thibault)

Nous avons fait une mesure absolue de la section différentielle de la réaction $\text{Li}^6(\text{d},\alpha)\text{He}^4$ pour une énergie de deutérons de 1 MeV (Lab) à 136° (Lab). Le détecteur utilisé était une jonction RCA de type C4 75 02 diaphragmée par un rubis qui définit un angle solide de $1,38 \pm 0,02 \cdot 10^{-3}$ st.

Le faisceau de deutérons est collecté dans un cylindre de Faraday relié à un intégrateur de courant dont la précision est de 1%. Deux sortes de cibles ont été utilisées. $\text{F}^{\text{II}}\text{Li}^6$ d'épaisseur $45,2 \pm 0,9 \mu\text{g/cm}^2$ - Li^6 métallique de $28,0 \pm 0,5 \mu\text{g/cm}^2$ déposées sur des feuilles d'aluminium de $0,5 \mu\text{m}$. Ces deux types de cibles donnent des résultats identiques.

Dans ces conditions nous avons trouvé pour la section efficace différentielle de production d'alphas :

$$\sigma(2\alpha)_{140^\circ(\text{CM})} = 5,3 \pm 0,3 \text{ mb/st (1 MeV Labo).}$$

Les fonctions d'excitation aux angles 81° , 105° et 136° (Lab) de la réaction $\text{Li}^6(d,\alpha)$ ont été tracées pour des énergies de deutérons variant de 0,550 à 1,750 MeV de 50 en 50 keV en utilisant le même dispositif. Les courbes présentent la résonance bien connue autour de 700 keV suivie d'une décroissance régulière (fig. 17.6.1.).

Enfin, les distributions angulaires des α ont été tracées de 10 en 10 degrés de 160° (Lab) à 20° (Lab) pour les énergies de deutérons comprises entre 1,0 et 1,5 MeV. Elles correspondent à une distribution de la forme $\sigma(\theta) = (90^\circ)(1 + A_2(E)\cos^2\theta + A_4(E)\cos^4\theta)$. Les valeurs de $A_4(E)$ sont négligeables, celles de $A_2(E)$ sont données en fonction de l'énergie incidente. Elles concordent avec les valeurs données dans les travaux antérieurs.

L'intégration de la section différentielle sur ces distributions angulaires reliées entre elles par les fonctions d'excitation ci-dessus, conduit à la section efficace totale de production de deux alphas. Elle décroît régulièrement (fig. 17.6.1.) de

$$59,8 \pm 3,6 \text{ mb à } 1,05 \text{ MeV} \quad \text{à} \\ 41,3 \pm 2,5 \text{ mb à } 1,55 \text{ MeV.}$$

Nous donnons aussi pour les mêmes énergies et angles :
-- les fonctions d'excitation des protons p_0 et p_1 des réactions $\text{Li}(d,p_0)\text{Li}^7$ et $(d,p_1)\text{Li}^7$ * 478 keV (fig. 17.6.2.) ainsi que les rapports $\frac{P_0}{\alpha}$, $\frac{P_1}{\alpha}$ et $\frac{P_0}{P_1}$.

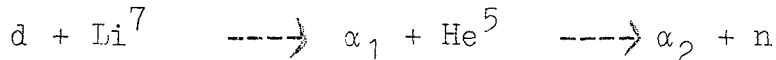
On observe une augmentation régulière du nombre des protons p_0 et p_1 avec l'énergie présentant cependant un maximum très large pour les p_0 autour de 1 MeV, et une décroissance régulière du rapport $\frac{p_0}{p_1}$ (fig. 17.6.3.).

- les distributions angulaires des deux groupes de protons p_0 (fig. 17.6.4.) et p_1 (fig. 17.6.5.) qui présentent toutes deux un pic autour de 30° caractéristique du striping du deutéron avec un moment orbital de capture du neutron $l_n = 1$. Les sections efficaces différentielles sont données en valeur absolue par comparaison à la réaction (d, α) .

17.7. Distribution angulaire des α de désintégration du niveau fondamental de He^5 .

(H.Bruno, J.Decharge, A.Perrin, G.Surget)

L'étude des corrélations angulaires α_1, α_2 entre particules α provenant de la réaction.



permet de remonter à la distribution angulaire des α_2 de désintégration du niveau fondamental de He^5 .

Nous trouvons que la probabilité d'émission $\sigma(\theta)$ d'une particule α dans une direction faisant l'angle θ (C.M.) avec la vitesse initiale de He^5 peut se mettre sous la forme:

$$\sigma(\theta) = \sigma(0) (1 + A \sin^2 \theta) \text{ avec } A = 3 \pm 1.$$

Les détecteurs utilisés étaient des jonctions diffusées au Silicium. Les deutérons étaient accélérés par un Van de Graaff 2 MeV HVEC. L'énergie utilisée dans ces mesures était de 1 MeV.

17.8. Etude de la réaction $d-Be$ à 150 KeV

(J.Ferchereau, J.Lac\`{e}kar, J.P.Crettez)

Les distributions angulaires des tritons, protons et α obtenues par réaction $d + Be^9$, correspondant aux niveaux fondamentaux du Be^8 , Be^{10} , Li^7 et 1er excité du Li^7 , ont été réalisées à $E_d = 150$ keV.

La détection a été effectuée par semi-conducteurs.

Les courbes obtenues font apparaître une forte remontée vers l'arrière et de nettes oscillations.

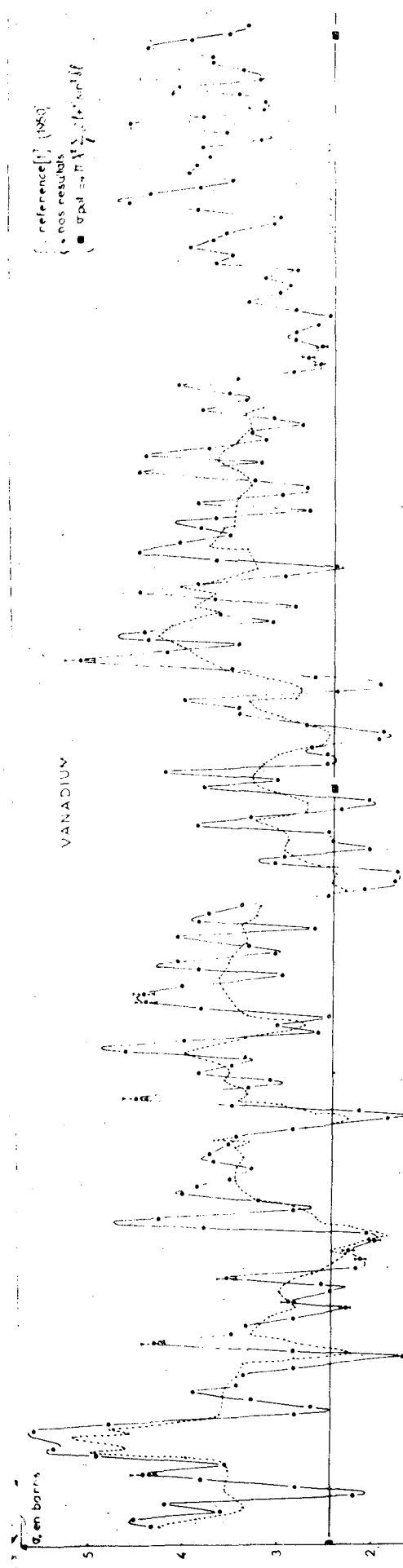


Fig.17.1.3.

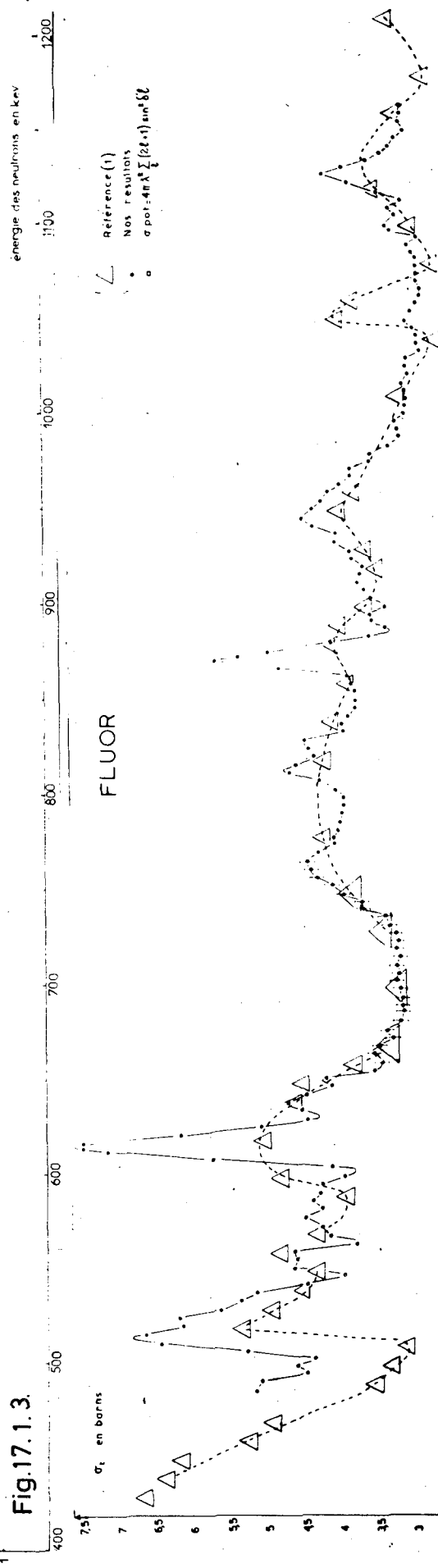


Fig.17.1.3.

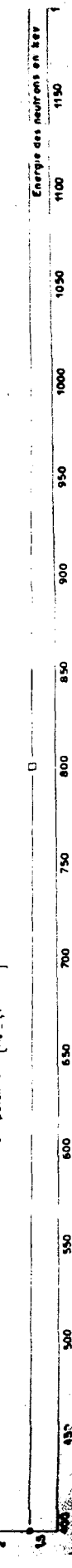
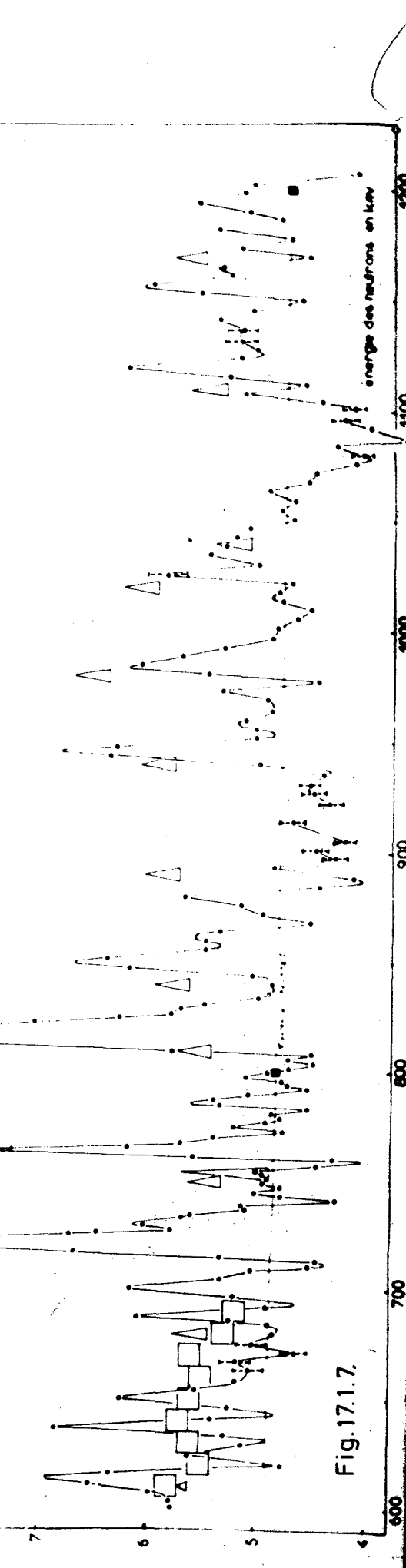
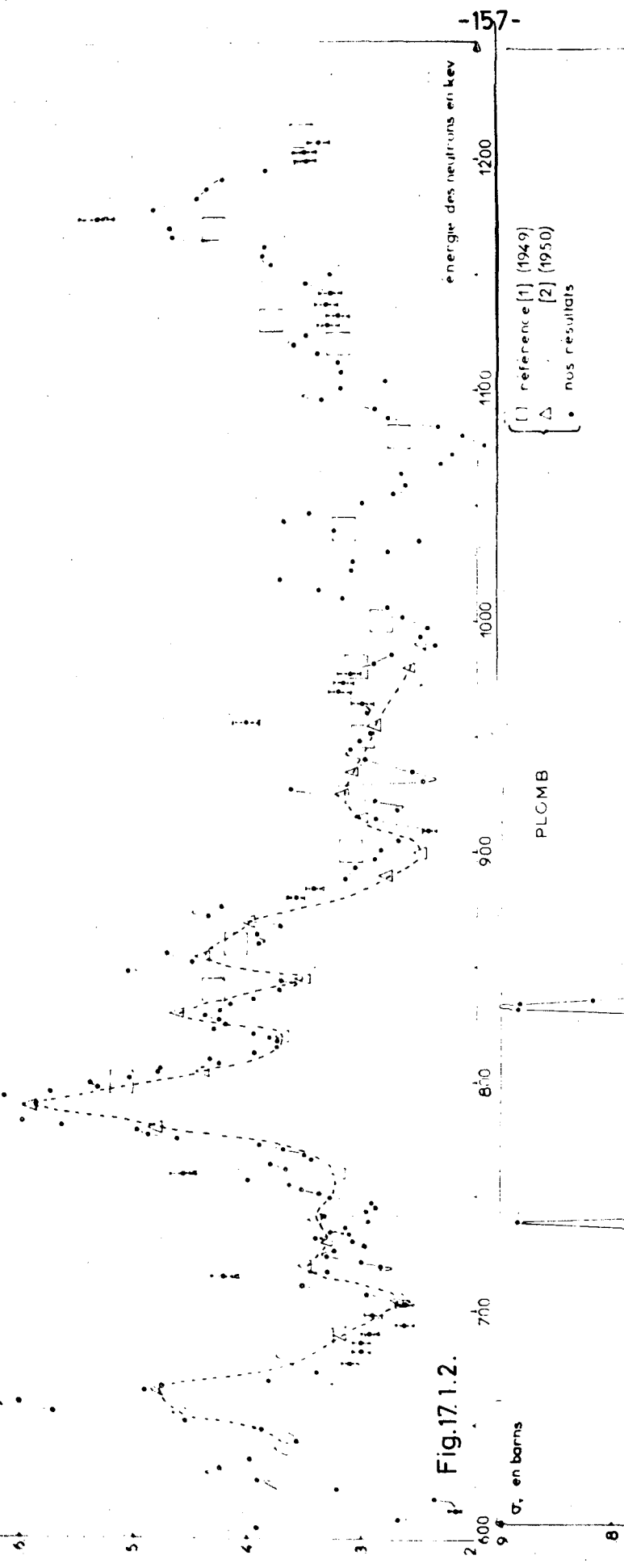


Fig.17.1.1.

ALUMINIUM

▲ référence [1] (1949)
 △ [2] (1950)
 ● nos résultats

σ_t en barns



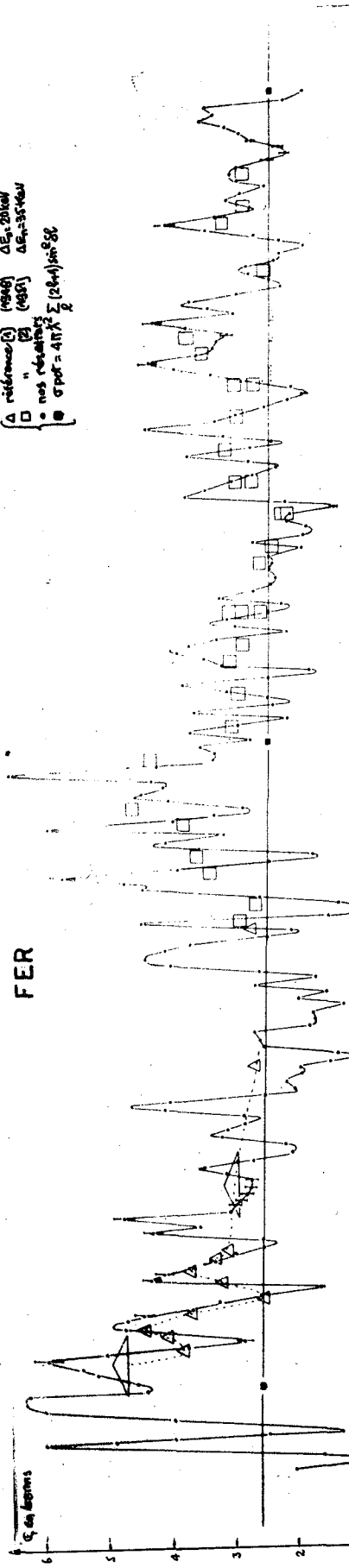


Fig. 17.1.4.

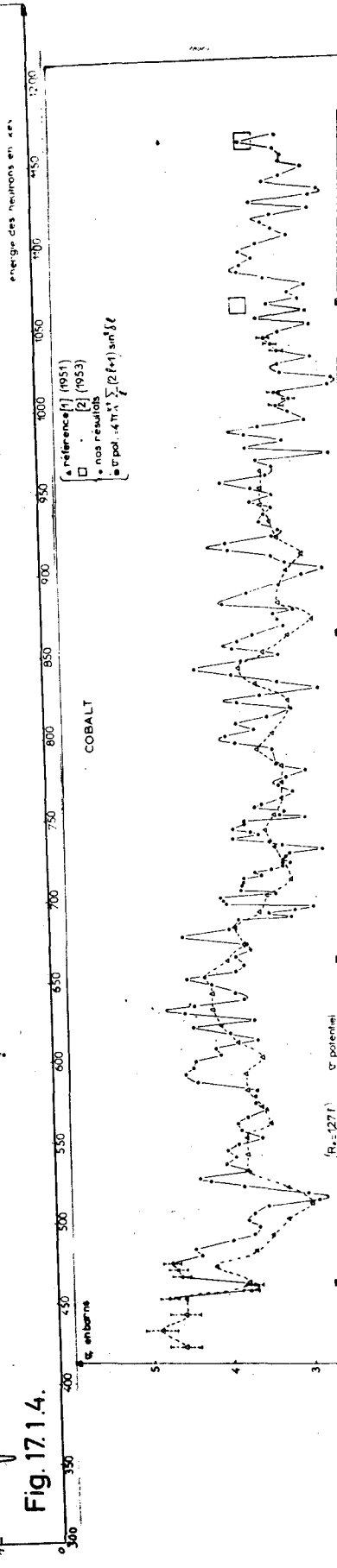


Fig. 17.1.5.

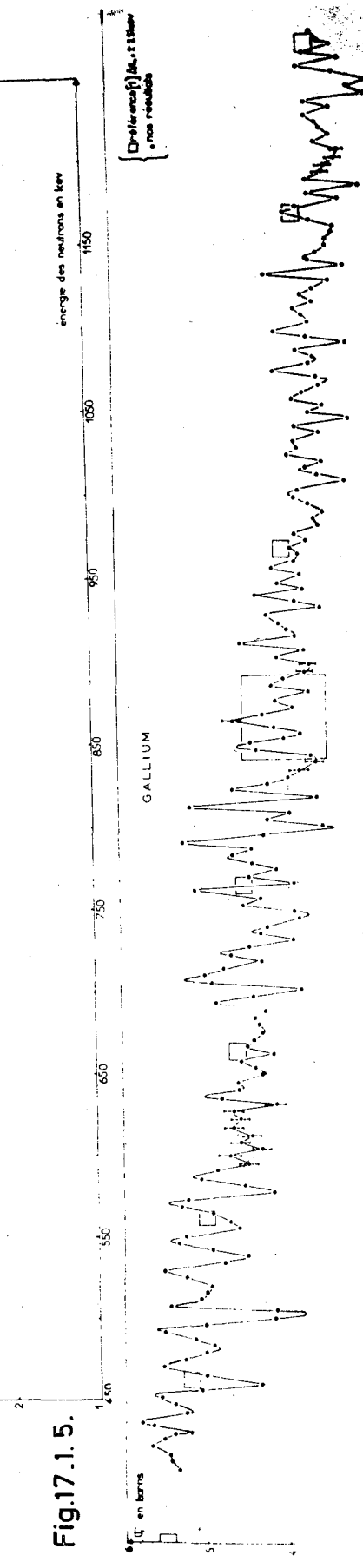


Fig. 17.1.6.

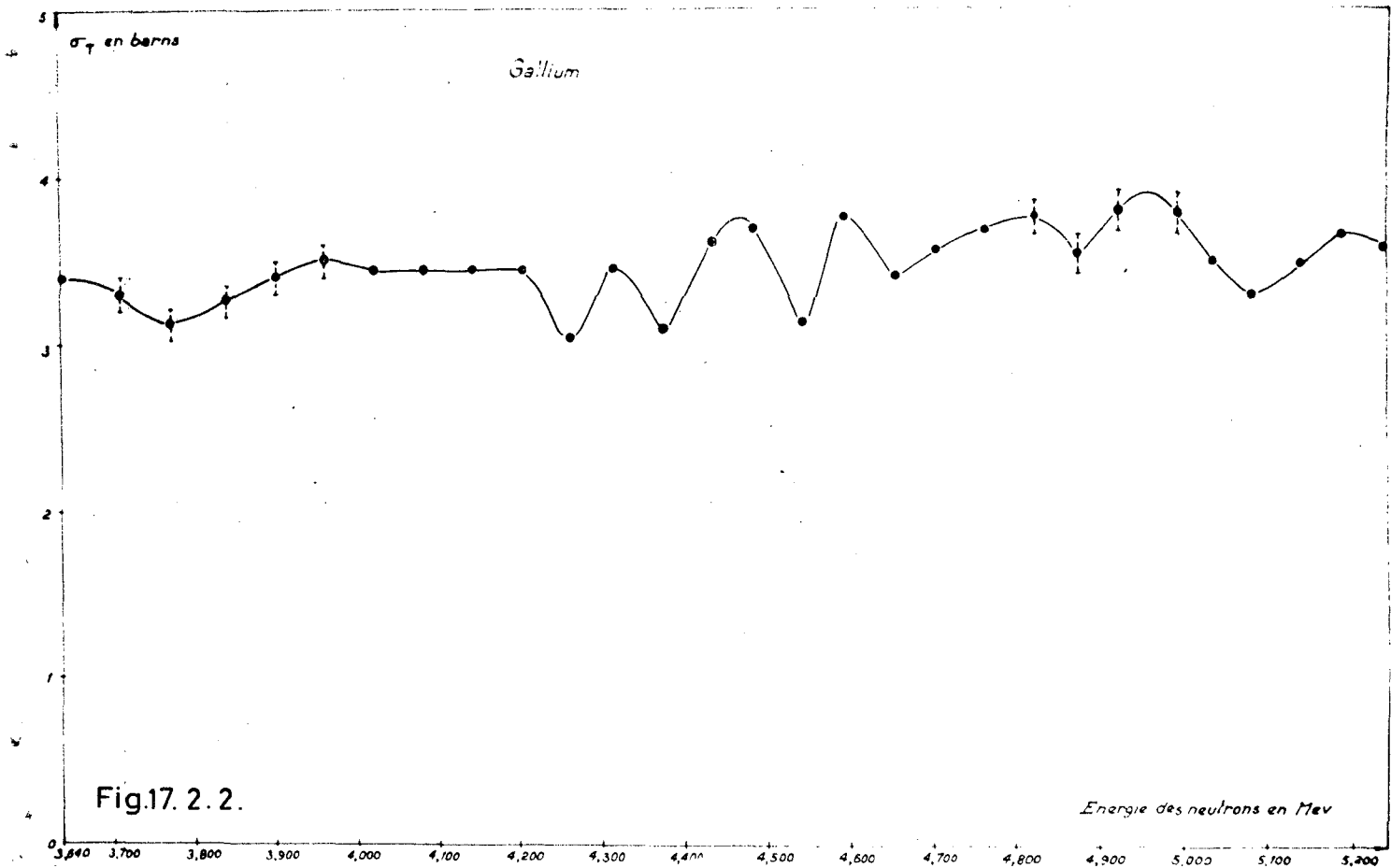


Fig.17.2.2.

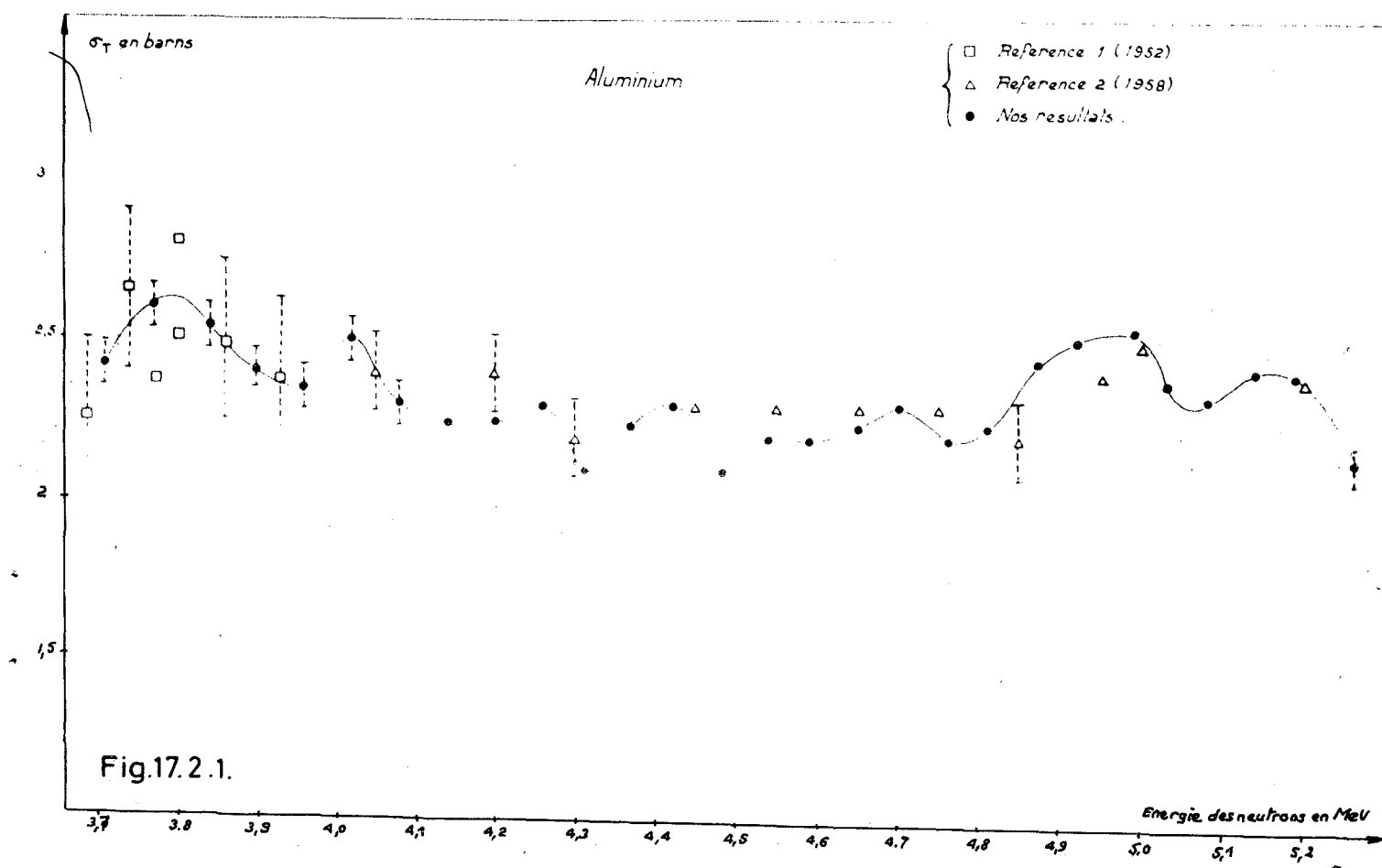


Fig.17.2.1.

SECTION DIFFÉRENTIELLE ÉLASTIQUE DES NEUTRONS DE 13.9 MeV

(Points expérimentaux non corrigés)

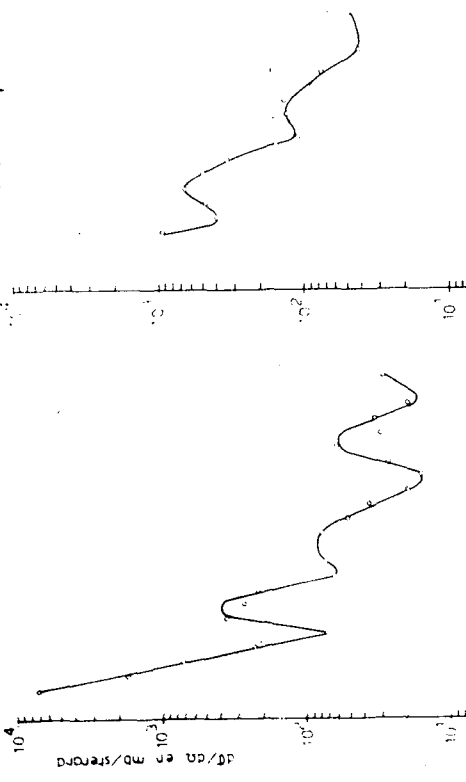


Fig.17.4.1.
Plutonium

Fig.17.4.2.
Uranium

SPECTRE DE TEMPS DE VOL $E_0 = 13.9$ MeV
(θ Labo = 83°)

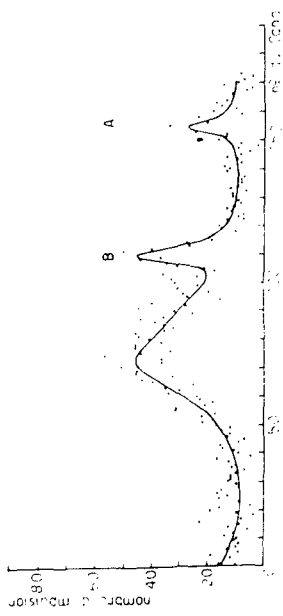


Fig.17.4.5.
Uranium

Fig.17.4.2.
Uranium

Fig.17.4.3.
Argent

Fig.17.4.4.
Nickel

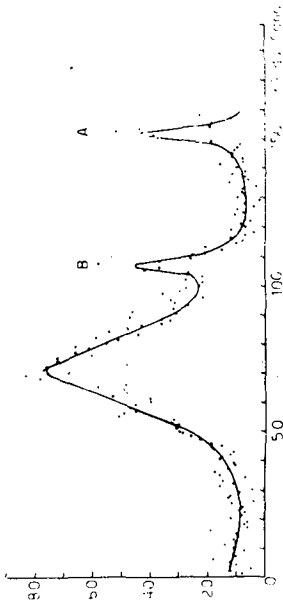


Fig.17.4.4.
Nickel

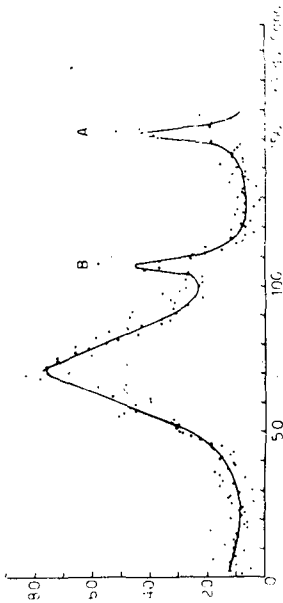


Fig.17.4.5.
Argent

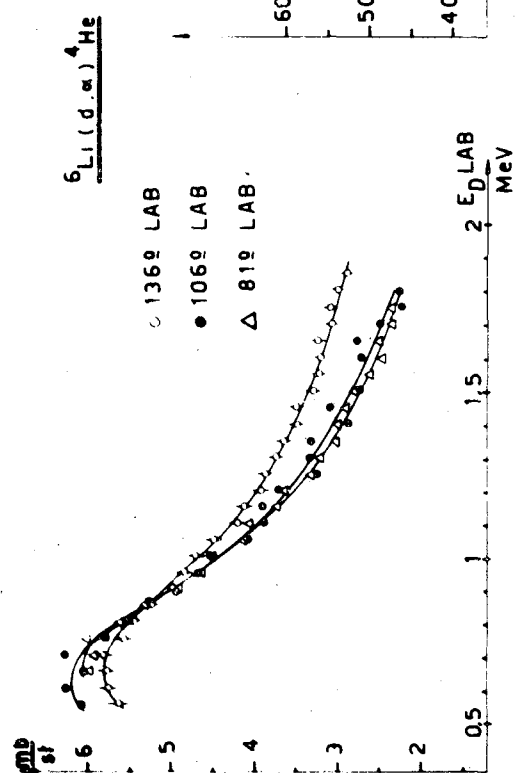


Fig.17.6.1.a.

$\frac{d\sigma}{d\Omega}(2\alpha)$

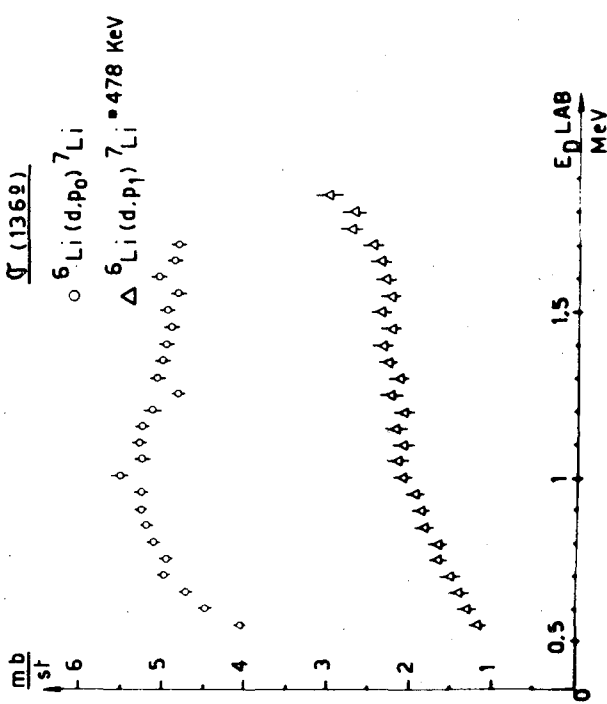


Fig.17.6.2.

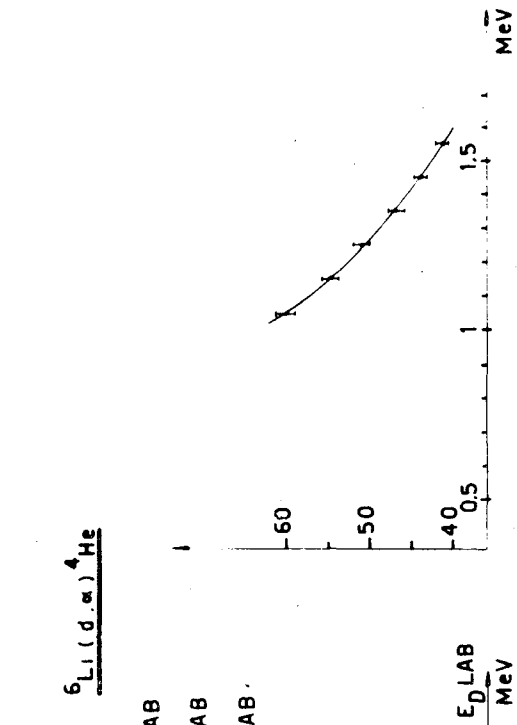


Fig.17.6.1.b.

$\frac{\Sigma_T(2\alpha)}{\Sigma_T(136^\circ)}$

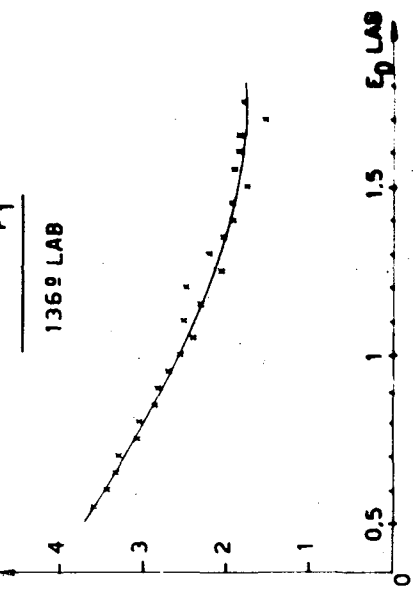


Fig.17.6.3.

DISTRIBUTION ANGULAIRE DE LA REACTION

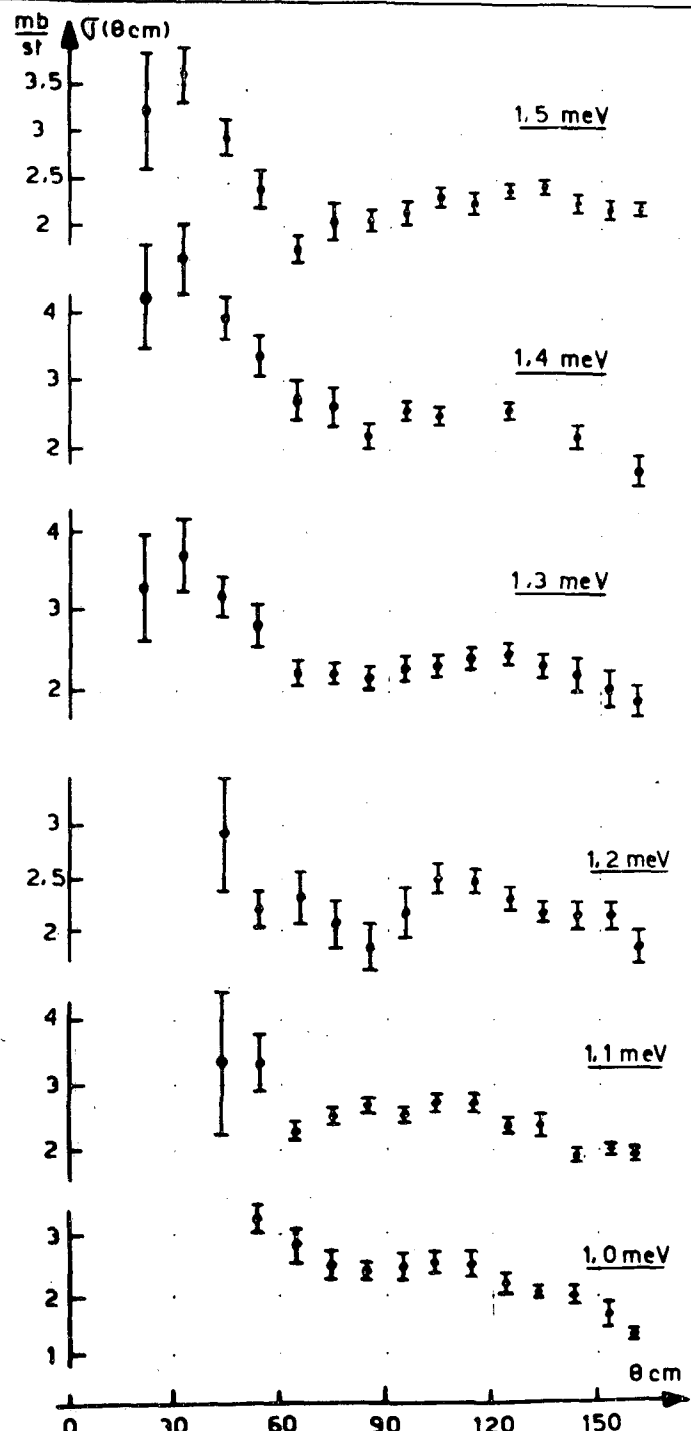
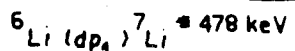


Fig.17.6.5.

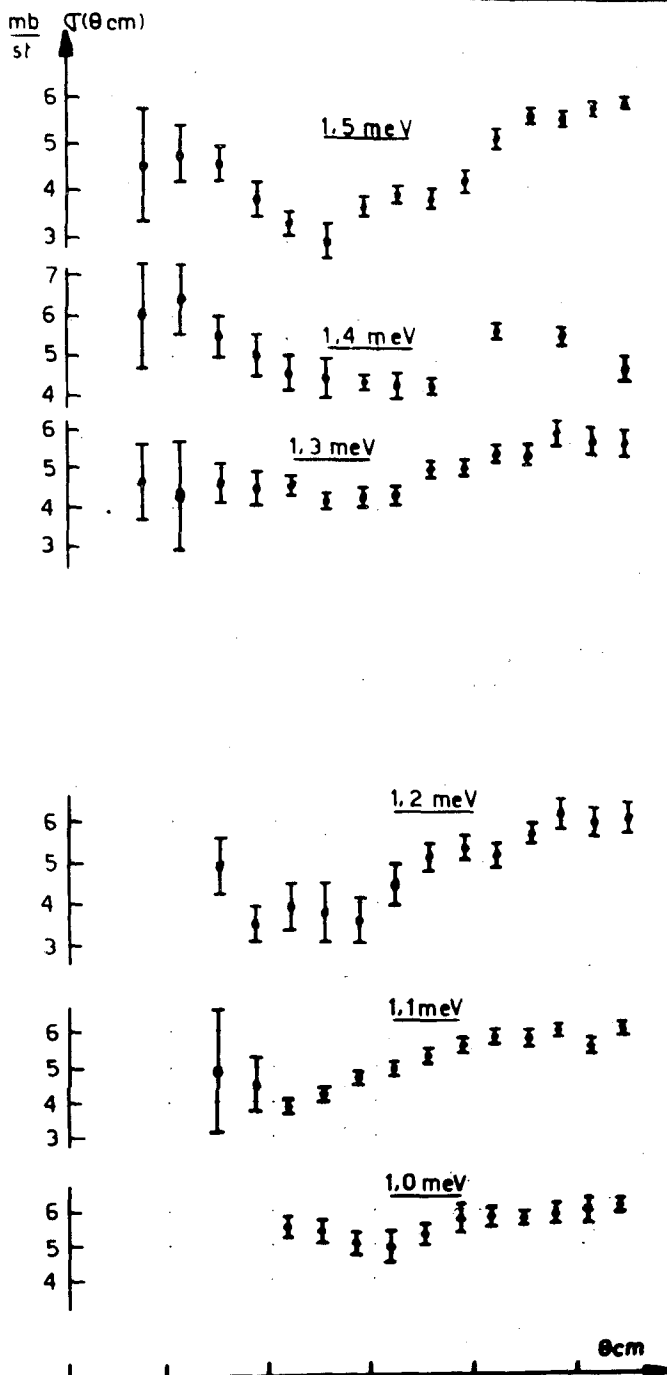
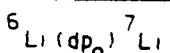


Fig.17.6.4.

18. INSTITUT NATIONAL DES SCIENCES ET TECHNIQUES NUCLEAIRES
DU C.E.A., SACIAY (France)

Des mesures de sections efficaces totales ont été effectuées pour les neutrons de la réaction $D(d,n)He^3$ produite à l'aide de l'Accélérateur SAME de 150 KV de l'I.N.S.T.N. Les neutrons sont caractérisés par les coïncidences avec les particules qui leur sont associées.

Les mesures, faites par transmission, portent sur l'Hydrogène, le Carbone, le Fluor, l'Aluminium et le Vanadium pour des neutrons d'énergie compris entre 2,600 et 2,850 MeV. Les neutrons sont détectés par un scintillateur plastique associé à un photomultiplicateur.

Une diode à jonction P N, solidaire du tube accélérateur, est disposée de façon à détecter les particules chargées émises sous un angle constant (actuellement 135°) par rapport à l'axe du faisceau de deutérons incidents.

La méthode utilisée permet d'obtenir une résolution de 50 KeV sur l'énergie des neutrons de la réaction (D,d).

Les résultats (1) sont consignés dans le tableau 18.1.

(1) Rapport C.E.A. 2399 (1964)

Tableau 18.1.

E neutrons MeV	barns Hydrogène	barns Carbone	barns Fluor	barns Aluminium	barns Vanadium
2,606		1,615 \pm 0,03	3,031 \pm 0,06		
2,623		1,646 \pm 0,01	2,860 \pm 0,01		3,938 \pm 0,06
2,671		1,657 \pm 0,02	2,838 \pm 0,03		3,896 \pm 0,08
2,717		1,694 \pm 0,02	2,789 \pm 0,02		3,683 \pm 0,03
2,749		1,720 \pm 0,02	2,705 \pm 0,02		3,612 \pm 0,05
2,770	2,37 \pm 0,02	1,810 \pm 0,04	2,600 \pm 0,02	2,935 \pm 0,015	
2,784		1,736 \pm 0,02	2,504 \pm 0,02		
2,794					3,766 \pm 0,05
2,817		1,885 \pm 0,02	2,504 \pm 0,05		3,868 \pm 0,06
2,833					3,775 \pm 0,07
2,850		1,880 \pm 0,04	2,330 \pm 0,04		

19. SERVICE DES EXPERIENCES CRITIQUES, CEA (France)

19.1. Physique expérimentale des réacteurs

19.1.1. Réseaux modérés à l'eau lourde - Programme de mesures sur AQUILON II
(Y.Girard - P.Lourme)

19.1.1.1. Etude systématique utilisant des barreaux cylindriques d'uranium naturel ou d'alliage U-Pu.

Ces études se sont poursuivies sur des barreaux métalliques de diamètre 2,92 cm en uranium naturel, légèrement appauvri (0,69%) ou légèrement enrichi (0,83 et 0,86%) ainsi que sur des alliages uranium-plutonium à environ 6% de 240 (uranium naturel plus 0,04% Pu 239 et uranium 0,2% 235 plus plutonium 239 0,3%).

Les expériences ont été effectuées à des pas carrés compris entre 110 et 210 mm, les mesures étant essentiellement des substitutions et des mesures d'indice de spectre (U-Pu, In/Mn, Lu/Mn) à température ambiante. Quelques mesures ont également été faites à 50°C et 80°C.

19.1.1.2. Etudes de détail sur des éléments combustibles EL4.

Dans un canal EL4 reconstitué (tube de force, tube de guidage, isolement) des mesures de distribution de flux (effet de bout, importance de l'acier) ont été faites sur des cartouches réelles EL4 à enrichissement 1,35% et naturel à gainage acier. Quelques mesures préliminaires ont porté sur des éléments à gainage beryllium.

19.1.1.3. Expériences préliminaires pour l'expérience critique EOLE.

Ces mesures utilisant une couronne nourricière de grappes d'oxyde enrichi (1,5 et 3,5%) ont permis de déterminer des tailles critiques, des valeurs d'antiréactivité d'absorbants, des indices de spectre dans une colonne thermique et des réseaux partiels.

19.1.1.4. Mesures sous contrat

Deux mois ont été consacrés à des mesures sur des réseaux à réfrigérant mélange eau-vapeur simulé par du polystyrène pour le compte de la Société italienne CISE. Le programme a comporté notamment 13 substitutions et plusieurs mesures de distribution de flux.

19.1.2. Réseaux modérés à l'eau légère (ALIZE II)

(Y.Girard - J.Bailly)

- a) Les études de base sur des réseaux eau légère - uranium très enrichi - aluminium ont été poursuivies et achevées. Les mesures de coefficient de température entre 20°C et 95°C ont été particulièrement nombreuses.
- b) Une série de mesures sur des réseaux d'oxyde enrichi à 3,5% a été effectuée pour le compte de la Société allemande AEG.

19.1.3. Réseaux modérés au graphite (CESAR)

(M.Sagot)

La construction de CESAR a été terminée en 1964. Les essais technologiques partiels, puis les essais d'ensemble se sont déroulés d'une manière satisfaisante. Les essais neutroniques en température ont commencé le 19 décembre 1964 par la première divergence et se poursuivront en janvier 1965.

La mise en exploitation normale de la pile est prévue en février 1965.

19.1.4. Etude de l'oxyde de beryllium et du graphite par la technique de la source pulsée de neutrons.

(M.Sagot)

Les mesures ont porté sur 14 gros empilements qui nous ont permis de déterminer le libre parcours de transport à la température de 21°C et pour une densité de 2,96.

$$\lambda_t = 1,59 \pm 0,02 \text{ cm.}$$

Le coefficient de refroidissement étant:

$$4,16 \cdot 10^5 \text{ cm}^{-4} \text{s}^{-1},$$

on a obtenu $V_{\Sigma} = 145 \text{ s}^{-1}$.

Le projet de travail sur l'oxyde de beryllium à haute température a été abandonné.

Un programme de mesures a commencé en 1964 sur le graphite. Les premiers résultats en seront publiés au colloque de KARLSRUHE en mai 1965. Ils porteront sur une nouvelle détermination des constantes du graphite et présenteront une étude systématique de la mise en équilibre du spectre des neutrons.

Le programme prévoit ensuite l'étude de l'anisotropie du graphite percé d'un réseau à canaux à diamètre variable.

19.2. Etudes de criticité
(C.Clouet d'Orval)

Au cours de l'année 1964, le groupe des Expériences Critiques Homogènes a achevé les études entreprises sur les trois matériaux fissiles ^{235}U , ^{239}Pu , et ^{233}U en solutions homogènes de sels nitriques dans l'eau légère. On rappelle que les géométries sont des cylindres nus ou réfléchis latéralement.

19.2.1. Uranium 235

Une série d'expériences sur la cuve de diamètre 300 mm, en réacteur nu, sur de fortes concentrations a donné des résultats intéressants. On a pu, en effet estimer le volume critique minimum en réacteur nu ($V_{c\min} \approx 16$ litres). En outre des études d'indices de spectre (rapport Pu/U5) ont permis de prolonger les résultats obtenus sur la cuve de diamètre 420 mm, l'année précédente, pour les H/U plus faibles et ceci avec une très bonne cohérence dans le domaine expérimental. Parallèlement des expériences de cinétique (neutrons pulsés) ont été effectuées, en vue de la détermination du B^2 neutre.

Une cuve de diamètre 250 mm, avec réflecteur latéral d'eau a été testée dans le cadre d'une comparaison, en géométrie identique, des deux sels fissiles d'uranium 235 et d'uranium 233. La masse critique minimum dans cette cuve, réfléchie, est $M_{c\min} = 1600$ g.

19.2.2. Uranium 233

La campagne sur l'uranium 233 a duré un peu moins de 6 mois compte tenu de la disponibilité du combustible et des temps morts dus aux traitements chimiques, rendus délicats par l'existence d'une activité γ importante. Du point de vue masses critiques nous avons étudié une cuve de 300 mm de diamètre,

nue ($M_{cmin} = 960 \text{ g}$), une cuve de diamètre 420 mm, nue ($M_{cmin} = 1310 \text{ g}$) et une cuve de diamètre 250 mm, réfléchie latéralement par de l'eau ($M_{cmin} = 960 \text{ g}$) et nue ($M_{cmin} = 1730 \text{ g}$).

Notons aussi que des expériences d'indices de spectre sur la cuve de diamètre 420 mm ont complété celles obtenues avec les sels de plutonium et d'uranium 235. Quelques expériences de cinétique (neutrons pulsés) ont été entreprises sur les cuves de diamètre 300 et 250 mm en réacteur nu. Les dé-pouilllements sont en cours actuellement.

19.2.3. Plutonium

Nous avons essayé de rendre critique une cuve de diamètre 206 mm, réfléchie par de l'eau latéralement. Compte tenu de la masse de plutonium utilisable (2,2 kg) nous n'avons pu approcher suffisamment le niveau critique, dans la gamme de concentrations étudiées, pour en tirer des résultats exploitables.

Un rapport, groupant les différents résultats obtenus sur les trois sels fissiles paraîtra bientôt. Mais d'ores et déjà nous pouvons signaler que le bon accord des résultats obtenus avec les expériences d'indices de spectre et ceux déduits, à partir d'un modèle de thermaliseur secondaire, permet de penser que les sections efficaces effectives (obtenues par ce modèle) sont les plus appropriées aux calculs intéressant ces milieux homogènes. Dans le cadre de cette étude comparative des trois corps fissiles on constate que pour une même géométrie de réacteur l'absorption du milieu est la plus faible pour les solutions d'uranium 233. Nous trouvons ensuite dans l'ordre d'absorption croissante les solutions d'uranium 235 et celles de plutonium 239. Notons aussi que, dans les gammes de concentrations étudiées, k_{∞} est une fonction croissante, sensiblement linéaire du laplacien géométrique critique B_1^2 . A même valeur de B_1^2 , $k_{\infty}(\text{Pu})$ et $k_{\infty}(\text{U233})$ sont sensiblement égaux. par contre $k_{\infty}(\text{U235})$ est plus petit, ce qui implique des fuites plus faibles dans les solutions d'uranium 235.

La station expérimentale du DIJON pense pouvoir entreprendre une étude des phénomènes d'interaction entre cylindres, avec l'uranium 235 et du plutonium en solution. Ces résultats viendront compléter ceux obtenus sur ALECTO II en 1963.

19.3. Mesure des sections efficaces par la méthode d'oscillation.

19.3.1. Mesures des sections efficaces effectives d'échantillons fissiles

(J.C. Carre - M.Robin - R.Vidal)

Ce travail est effectué dans le cadre des études du contrat EURATOM "Recyclage du Pu" n° 037.60-12.RdF. A l'aide d'une méthode d'oscillation, on détermine les sections efficaces effectives d'absorption et de fission d'un échantillon fissile inconnu par comparaison avec des échantillons étalons contenant de l'U 235 et du bore.

Cette méthode a fait l'objet du rapport CEA n° 2487 R.Vidal - O.Tretiakoff - J.C.Carre - M.Robin: "Mesure des sections effectives d'échantillons fissiles par une méthode d'oscillation dans les assemblages critiques".

19.3.1.1. Expériences sur les réseaux à l'eau lourde dans MINERVE

Les expériences sur MINERVE ont porté sur l'étude de la perturbation locale de flux mesurée au voisinage du barreau afin de définir les meilleures conditions de mesure et en particulier de déterminer les effets dus à l'hétérogénéité radiale des absorbeurs ou des matériaux fissiles ainsi que les effets en énergie.

Un nouvel appareillage d'enregistrement sur bande magnétique a été mis au point afin de développer les méthodes digitales pour l'analyse des signaux enregistrés.

19.3.1.2. Expériences sur les réseaux à graphite dans MARIUS

Les expériences sur MARIUS se caractérisent essentiellement par des mesures sur des alliages U-Pu sous forme de barreaux de Ø 29,2 mm et sur des éléments combustibles d'uranium naturel ayant subi des taux d'irradiation allant jusqu'à 2300 MWJ/T.

On a ainsi déterminé l'équivalence en U 235 et en bore d'échantillons d'alliage U-Pu constitués par des alliages d'uranium naturel ou légèrement appauvri (0,65%) contenant environ 0,05 et 0,075% de plutonium avec une teneur isotopique en Pu 240 variant entre 1 et 20% et quelques alliages d'uranium très appauvri (0,22%) contenant 0,30% et 0,35% de Pu à 8% de Pu240.

Les effets de la répartition en Pu ont été étudiés avec une série de billettes composées d'un noyau en U nat. et d'un tube en alliage U-Pu.

Des mesures sur la répartition des absorbeurs ont été aussi effectuées en utilisant des échantillons empoisonnés superficiellement ou de façon homogène avec du bore, du cuivre et du fer. A partir de ces résultats, on a mis aussi en évidence l'influence de la diffusion.

19.3.2. Mesure des intégrales de résonance sur MINVERVE (R.Vidal)

Les mesures d'intégrale de résonance d'absorption de matériaux en solution dans l'eau par méthode d'oscillation et leur comparaison aux valeurs calculées à partir des paramètres de résonance se sont poursuivies sur MINVERVE. Les valeurs mesurées pour l'intégrale de résonance au-dessus de la partie en $1/v$ correspondant à la dilution infinie ont été publiées dans le rapport CEA n° R 2486. - R.Vidal "Mesure des intégrales de résonance d'absorption".

Les résultats sont les suivants:

Indium	$I = 3200 \pm 70$ b	Cobalt	$I = 50 \pm 5$ b
Hafnium	$I = 2080 \pm 50$ b	Césium	$I = 450 \pm 15$ b
Argent	$I = 670 \pm 20$ b	Thorium	$I = 87 \pm 4$ b.

Une nouvelle série de mesures est en cours en utilisant un nouvel oscillateur imprimant aux échantillons des mouvements carrés, ce qui permet d'éliminer les effets de la diffusion. Avec ce nouvel appareillage, des corps peu capturants et très diffusants ont été mesurés sous forme métallique.

Les résultats provisoires, pour la dilution infinie et correspondant à l'intégrale au-dessus de la partie en $1/v$ sont les suivants:

Manganèse	I = 10,3 b	Cuivre	I = 2,2 b
Fer	I = 1 b	Zirconium	I = 1,06 b
Cobalt	I = 50,5 b	Molybdène	I = 22,5 b.
Nickel	I = 1 b		

19.3.3. Mesures des sections efficaces thermiques sur ZOE
(J.C.Carre)

Les sections efficaces de capture thermique de matériaux peu capturants ont été mesurées par rapport au bore par la méthode d'oscillation de phase sur ZOE. Les résultats pour des neutrons à 2200 m/s sont les suivants:

$$\begin{array}{ll} \text{Aluminium} & \sigma = 229 \pm 3 \text{ mb} \\ \text{Magnésium} & \sigma = 64,2 \pm 1,5 \text{ mb} \end{array} \quad \begin{array}{ll} \text{Fer} & \sigma = 2,53 \pm 0,03 \text{ b} \\ \text{Cuivre} & \sigma = 3,74 \pm 0,04 \text{ b.} \end{array}$$

Le principe et le détail des mesures sont donnés dans le rapport CEA n° R 2485: - J.C.Carre - R.Vidal: "Mesure des sections efficaces thermiques d'absorption de l'Al, du Mg, du Fe et du Cu par la méthode d'oscillation".

Les expériences en cours portent sur le cobalt et le zirconium.

On a obtenu les résultats provisoires suivants:

$$\begin{array}{ll} \text{Zirconium} & \sigma = 177 \text{ mb} \\ \text{Cobalt} & \sigma = 38,0 \text{ b.} \end{array}$$

20.

SERVICE DES PILES, CENTRE D'ETUDE NUCLEAIRE DE GRENOBLE (France)

Etallage de détecteurs à seuil (Titane, Fer, Cuivre)
par rapport au Nickel.

(R.Lloret)

On a mesuré dans différents emplacements du réflecteur et du cœur du réacteur SILOE, le rapport des sections efficaces des réactions $Ti^{46}(n,p)$; $Fe^{54}(n,p)$; $Cu^{63}(n,\alpha)$ à celle de la réaction $Ni^{58}(n,p)$. On donne la variation de ces rapports en fonction de l'indice de spectre.

$$\frac{A_{Ni}}{A_{Al}} / \frac{\sigma_{Ni}}{\sigma_{Al}}$$

Les extrapolations à $\gamma = 1$ conduisent, moyennant $\sigma_{Ni} = 90,6\text{mb}$ aux évaluations suivantes:

$\sigma_F = 8,7\text{ mb}$ pour la réaction $Ti^{46}(n,p) Sc^{46}$,

$\sigma_F = 0,44\text{mb}$ pour la réaction $Cu^{63}(n,\alpha) Co^{60}$,

On a mesuré au centre du cœur:

$\sigma_F = 79 \pm 8\text{ mb}$ pour $Fe^{54}(n,p) Mn^{54}$.

(Rapport INT/Pi (NT) 550 - 32/64 - CEN.G-27.10.1964)

21. ISTITUTO DI FISICA NUCLEARE - MOSTRA D'OLTREMARE - NAPOLI (Italy)

21.1. Experimental work on Nuclear Spectroscopy and Nuclear Reactions

21.1.1. Decay of the ^{150}Eu isomeric state and level structure of ^{150}Sm .

This investigation has been performed with γ - γ coincidence and summing coincidence-methods and with γ -scintillation technique. A decay scheme of the ^{150}Eu isomeric state ($T_{1/2} = 5\text{ }\mu\text{sec}$) is proposed and the level structure of the daughter ^{150}Eu is consistent with a vibrational description.

21.1.2. Properties of some lower excited states in ^{101}Ru from the decay of $5\text{ }\mu\text{sec}^{101}\text{Ru}$ (to be published in Nuclear Physics ⁽¹⁾)

Gamma-gamma angular correlations and half-life measurements with the delayed-coincidence method have been performed to study the properties of the lower excited states in ^{101}Ru , namely the 120 and 325 KeV levels. The results obtained are summarized in table 21.1.

Table 21.1.

Level (KeV)	$T_{1/2}$ (μsec)	Transition	Multipolarity	Spin and parity
0	-	-		$5/2^+$
128	0.55 ± 0.03	1 \rightarrow 0 (128 KeV)	M1(97%) + E2(3%)	$3/2^+$
		2 \rightarrow 1 (197 KeV)	M1 + E2	$3/2^+, 5/2^+$
325	± 0.3	2 \rightarrow 0 (325 KeV)	E2	$1/2^+$

21.1.3. Level structure of ^{134}Ba from the decay of ^{134}Ce and ^{134}Cs

This investigation has been performed with the aim of establishing a possible vibrational behaviour of ^{134}Ba . The β^- decay of ^{134}Cs has been investigated in details by performing γ - γ and summing coincidences. The existence of the following levels has been confirmed: 605 KeV (2+); 1170 KeV (2+); 1400 KeV (4+); 1640 KeV (3,4); 1770 KeV (2+?) and 1790 KeV (4+).

On the other hand the γ -ray spectrum, γ - γ coincidences and x - γ coincidences have been measured from the decay of ^{134}La ($T_{1/2} = 6\text{ m}$) in equilibrium with ^{134}Ce ($T_{1/2} = 76\text{ h}$) produced

by (p, xn) reactions at Orsay. These measurements are consistent with the presence of a new level at 1350 KeV which seems to have a 0^+ character. This enables us to establish the presence of a triplet of levels (2^+ at 1170 KeV, 0^+ at 1350 KeV and 4^+ at 1400 KeV) which can be interpreted as a 2-phonon triplet predicted by the vibrational model.

21.1.4. ($p, n\gamma$) reactions on ^{48}Ca

This work is performed at the 5 MeV Van de Graaff Laboratory of Legnaro (Padua) in collaboration with Padua and Trieste. The aim is to determine the properties of the levels of $^{48}_{21}\text{Sc}_{27}$ which can give some information on the proton-neutron residual interaction in the $f_{7/2}$ shell.

Preliminary measurements of neutron and gamma ray yields have been performed in the energy interval between 3 and 4 MeV.

Neutron-gamma coincidences have also been measured at certain neutron resonances. This work is under development.

21.1.5. α -particles from (n, α) reactions in Mo isotopes (published in Nuclear Physics) ⁽²⁾

Measurements with a solid state detector were taken of α -particles spectra from Mo $^{92, 94, 95, 96, 98, 100}$ isotopes irradiated with 15 MeV neutrons. The angular distribution of $\text{Mo}^{92}(n, \alpha)\text{Zr}^{89}$ reaction, was measured using the particular method of analysing the yield of the α -particles as a function of the distance between target and detector.

Results were analysed in terms of direct interactions theory. A fairly good agreement was found between theoretical calculations and experimental data either for spectroscopic factors of ground state transitions as well as for angular distributions of pick-up processes.

21.1.6. (n, p), (n, α) and ($n, 2n$) reactions on Mo isotopes

This work has been performed with the activation method.

The preliminary results on cross-sections have been reported at the annual meeting of S.I.F. (Catania 19-26 October 1964).

21.2. Theoretical work on Nuclear Spectroscopy

21.2.1. Level structure of Pt-isotopes

Calculations of the low energy spectrum and the electromagnetic transition probabilities have been undertaken on the basis of the shell model with appropriate residual interactions.

The energy-matrices have been diagonalized by means of a I.B.M. 7040 machine (Istituto Superiore di Sanità, Roma).

The main features of the experimental spectra are quite well fitted.

21.2.2. Neutron-proton pairing interaction in $f_{7/2}$ nuclei (2)

A generalized Bogoliubov transformation has been developed which takes into account the n-p pairing interaction in light nuclei, with particular attention to the $f_{7/2}$ region.

It is found, on the basis of the variational method, that the ground-state is given by the product of two Bogoliubov transformations respectively for neutrons and protons.

The comparison between the exact and the approximate solution for the ground-state energy in the case of an unique angular momentum j , shows the possibility of finding ground-state energies with an approximation similar to that used for single closed shell nuclei.

21.3. Research on nuclear fission

21.3.1. Heavy nuclei photofission

The photofission of ^{238}U and ^{232}Th induced by the Frascati electrosyncrotron γ -ray beam has been investigated in the energy range 300 ± 1000 MeV. For this experiment, which was started in '63, has been necessary an other exposure (Jan.'64) and the scanning of many loaded nuclear emulsions.

Several precautions have been taken in carrying out the experiment:

a) the loading of the emulsions has been checked quantitatively by measuring the radioactivity of the loading element.

- b) the scanning efficiency has been checked.
- c) the γ -ray dose has been checked by means of a Wilson quantameter compared with a pair spectrometer.
- d) the electron energy has been measured by determining the acceleration time.
- e) the low-energy γ -ray contribution (giant resonance) has been measured by means of the radioactivity induced in $\text{Cu} \xrightarrow{\gamma, n} \text{Cu}^{62}$.

Following this checking measurements some corrections have been applied to the final results, examined with a statistical procedure.

The values of σ_k , cross-section per equivalent quantum, and of the fissilities have been obtained. The σ_k , in the energy range 300 ± 1000 MeV, are constant within the experimental errors, the correct values being $\sigma_k(\text{U}) = (69 \pm 6)\text{mb}$ and $\sigma_k(\text{Th}) = (38 \pm 4)\text{mb}$.

The results of this experiment will be published.

21.3.2. Heavy nuclei fission induced by high energy protons

The data on U, Th, Bi, induced by the Saclay protosynchrotron 3.0 GeV proton beam, are being examined. These data will confirm, apart from other results, if the cross-sections decrease slowly between 0.8 and 20 GeV, and if the fissility (ratio between fission cross-section and total inelastic cross-section) is a decreasing function of the energy.

21.3.3. New techniques

The groups have started some research on fission physics by means of a detection technique similar, in some respects, to the nuclear emulsion one. Solid state nuclear detectors (mica, glass, etc.) are used. One of the advantages they have with respect to the emulsions is the possibility of exposures to high intensity beam ($10^{12} \pm 10^{14}$ protons/cm²).

These detectors, etched with particular acids, are observed with the optical microscope; the holes produced by fission fragments are similar to the fission tracks in nuclear emulsions.

With this new technique the group is studying, by means of the Frascati electrostatic synchrotron, the photofission between 300 + 1000 MeV of some nuclei (U 235 and Au) which cannot be studied with the nuclear emulsion technique.

In collaboration with a group of CERN-Geneva and a group from Warsaw, it has been planned to study fission cross-sections for many nuclei (from U to Ag) as a function of the energy for $E > 10$ GeV, using the CERN PS. Some preliminary research, to provide a technique by means of which the fission fragments are distinguished from nuclear disintegration ones, has been performed. The final experiment will be carried out in the next months.

References

- (1) G.Chilosi, G.Löbner, R.Moro, P.R.Speranza and G.B. Vingiani "Properties of some lower excited states in ^{101}Ru from the decay of $\beta\gamma$ ^{101}Ru " submitted to "Nuclear Physics".
- (2) P.Cuzzocrea, S.Notarrigo and A.Rubbino. " α -particles from (n,α) reactions in Mo isotopes at $E_n = 15$ MeV" Nuclear Physics 55, 364 (1964).

22. LABORATOIRE DE PHYSIQUE NUCLEAIRE, CENTRE D'ETUDES NUCLEAIRES
DE GRENOBLE, COMMISSARIAT A L'ENERGIE ATOMIQUE ET UNIVERSITE
DE GRENOBLE (France)

Diffusion de neutrons rapides de 14 MeV sur noyaux légers
(R. Bouchez)

22.1. $^6\text{Li}(n,n')$

Sections efficaces totales calculées :

$$Q = 0 ; \quad \sigma_e = 850 \text{ mb} \pm 90 ,$$

$$Q = -2,18 \text{ MeV}; \quad \sigma_{2,18} = 100 \text{ mb} \pm 25.$$

On a mis en évidence par diffusion $^6\text{Li}(n,n')$, outre le premier niveau de 2,18 MeV, les niveaux 1+ (3,56 MeV) et 2+ (4,52 MeV) à l'aide d'un spectromètre par temps-de-vol (résolution totale : 1,3 ns à 1m). Les sections efficaces différentielles élastiques et pour le premier niveau (2,18 MeV) ont été mesurées de 15° à 150° (L) et corrigées de la diffusion multiple.

Figure 22.1.: Sections efficaces différentielles de la diffusion élastique de 10° à 150° (centre de masse) corrigée de la diffusion multiple.

Figure 22.2.: Sections efficaces différentielles de la diffusion inélastique de 20° à 150° (centre de masse) également corrigée de la diffusion multiple.

Publications :

Note C.R. Acad. Sc., date probable de présentation à l'Académie des Sciences, début mars 1965.

22.2. ${}^7\text{Li}(\text{n},\text{n}')$

Section efficaces totales calculées :

$$\sigma_{(\text{n},\text{n}')\text{el}} + 0,48 \text{ MeV} = 1100 \pm 100 \text{ mb},$$

$$\sigma_{(\text{n},\text{n}')\text{el}} = 1020 \pm 100 \text{ mb}^*,$$

$$\sigma_{(\text{n},\text{n}')4,63 \text{ MeV}} = 150 \pm 20 \text{ mb}.$$

*En adoptant pour $\sigma_{(\text{n},\text{n}')0,48 \text{ MeV}}$ la valeur de $80 \pm 10 \text{ mb}$ ¹⁾.

La diffusion des neutrons rapides de 14 MeV sur le ${}^7\text{Li}$ a été étudiée par une méthode de temps-de-vol avec une résolution de 1,2 ns. Le niveau de 0,48 MeV n'a pas été séparé du pic de diffusion élastique ; des niveaux supérieurs, seul le 4,63 MeV apparaît excité.

Les distributions angulaires ont été faites de 15° à 130° pour ${}^7\text{Li}(\text{n},\text{n}') Q = 0$, $Q = -0,48 \text{ MeV}$ et pour ${}^7\text{Li}(\text{n},\text{n}') Q = -4,63 \text{ MeV}$. Les sections efficaces $\sigma_{(\text{n},\text{n}')\text{el}} + 0,48 \text{ MeV}$ et $\sigma_{(\text{n},\text{n}')4,63 \text{ MeV}}$ ont été calculées et sont en accord avec celles trouvées par Anderson et al²⁾ et Armstrong et al³⁾.

Les corrections de diffusion multiple sont en cours.

Figure 22.3.: Sections efficaces différentielles moyennes sur l'état fondamental $Q = 0$ et sur le premier niveau excité de 0,478 MeV (cette diffusion n'étant pas corrigée de la diffusion multiple).

Figure 22.4.: Sections efficaces différentielles de la diffusion inélastique sur le deuxième niveau de 4,63 MeV (cette diffusion n'étant pas corrigée de la diffusion multiple).

Publications

Article J. Phys. (en préparation, avril 1965)

-
- 1) BENVENISTE, MITCHELL, SCHRADER, ZENGER, Nucl. Phys. 38, 300 (1962).
 - 2) WONG, ANDERSON, McCLURE, Nucl. Phys. 33, 680 (1962).
 - 3) ARMSTRONG, GAMMEL, ROSEN, Nucl. Phys. 52, 505 (1964).

22.3. $^{12}\text{C}(n,n')$

Sections efficaces totales calculées :

$$\begin{aligned} Q = 0 &; \sigma_e = 800 \text{ mb}, \\ Q = -4,43 \text{ MeV} &; \sigma_{4,43} = 220 \text{ mb} \pm 30, \\ Q = -7,6 \text{ MeV} &; \sigma_{7,6} = 10 \text{ mb} \pm 10. \end{aligned}$$

On a mesuré, par diffusion de neutrons de 14 MeV sur ^{12}C , les sections efficaces différentielles élastiques de 10° à 160° et inélastiques sur les deux premiers niveaux (4,43 et 7,65 MeV) pour lesquelles on a effectué les corrections de diffusion multiple. La mesure de la distribution angulaire du niveau de 7,65 MeV a mis en évidence l'excitation $0+ \rightarrow 0+$.

Figure 22.5.: Sections efficaces différentielles de la diffusion élastique corrigée de la diffusion multiple.

Figure 22.6.: Sections efficaces différentielles de la diffusion inélastique sur le premier niveau excité de 4,43 MeV corrigée de la diffusion multiple.

Figure 22.7.: Sections efficaces différentielles de la diffusion inélastique sur le deuxième niveau excité de 7,65 MeV corrigée de la diffusion multiple. La courbe en traits pleins correspond à la courbe théorique de diffraction $J_0^2(kR)$ dans un rayon $R = 5f$.

Publications

Scattering of 14 MeV neutrons from ^{12}C and excitation of the 7.65 MeV level, BOUCHEZ R., DUCLOS J., PERRIN P., Nuclear Phys. 43, 628 (1963)

Etude de la diffusion multiple par la méthode de Monte-Carlo Application à la diffusion des neutrons rapides de 14 MeV par le carbone, NGUYEN VAN SEN, Thèse 3ème cycle, Grenoble, 1964, n° 389.

Mesure de la distribution angulaire à 14 MeV des neutrons de diffusion inélastique sur le niveau $0+$ de 7,65 MeV de ^{12}C , SZABO I., Thèse Docteur-Ingénieur, Grenoble, 1963, n° 383.

22.4. ${}^9\text{Be}(n,2n)$

Sections efficaces (d'après la littérature) :

$$\sigma_{(n,2n)} = 540 \text{ mb},$$

$$\sigma_t = 1,51 \text{ b}.$$

A l'aide d'un spectromètre à double temps-de-vol, on a observé que la réaction ${}^9\text{Be}(n,2n)$ se produit principalement avec formation d'états résonnants du ${}^9\text{Be}^\pi$ (6,76 MeV ;), 94 MeV ...) et a lieu faiblement par le processus direct ${}^8\text{Be}(0) + n_1 + n_2$, correspondant à l'éjection par un neutron incident de 14,5 MeV du neutron périphérique peu lié (1,66 MeV) dans le ${}^9\text{Be}$. (L'expérience se poursuit pour obtenir une meilleure statistique et à d'autres angles).

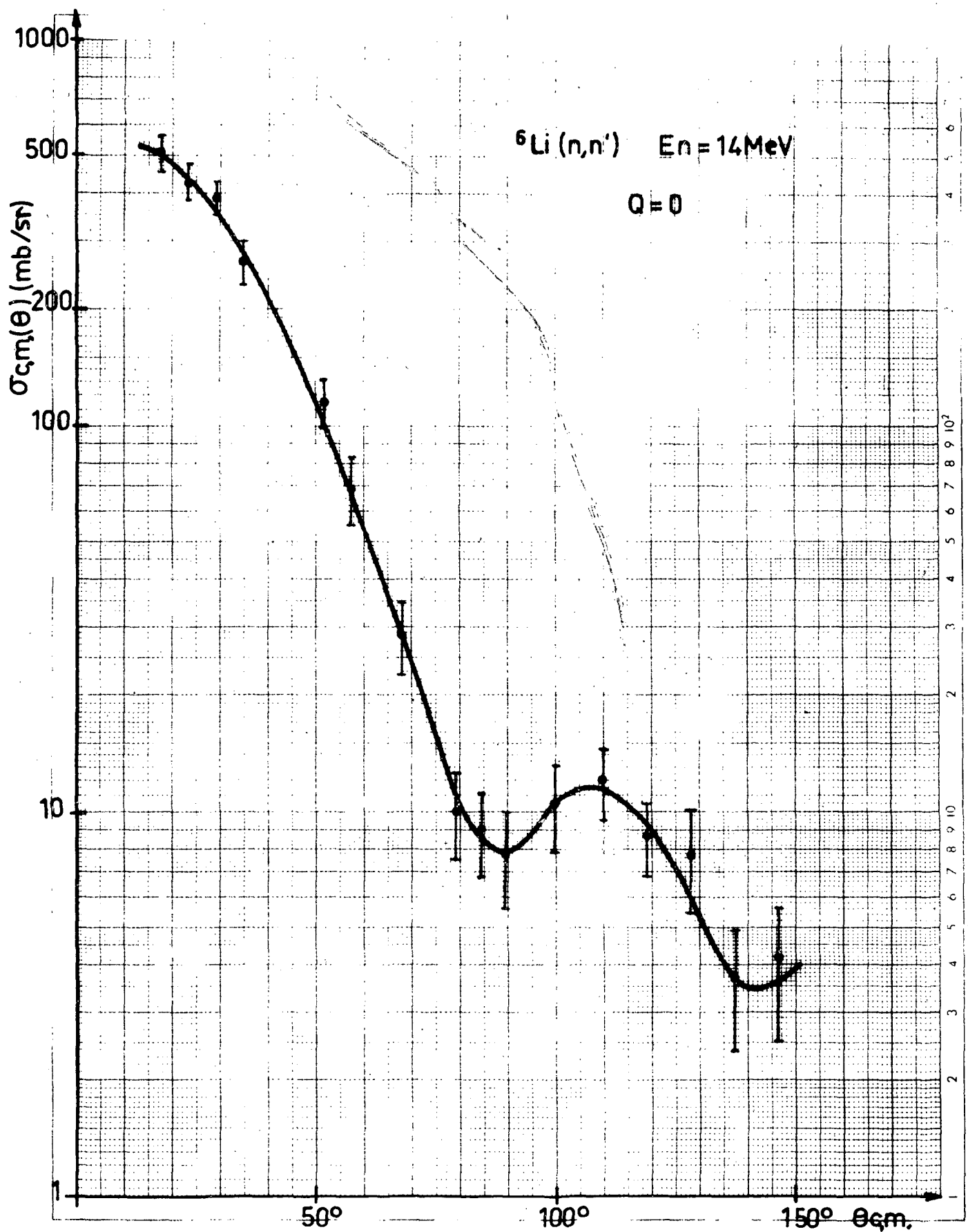
Figure 22.8.: Répartition des événements pour $E = (7,35 \pm 0,75)\text{MeV}$ correspondant à la désexcitation du niveau de 6,76 MeV du ${}^9\text{Be}$, montrant la formation d'états résonnants.

Figure 22.9.: Répartition des événements dans la bande ${}^8\text{Be}(0)$ corrigée du bruit-de-fond et de l'efficacité.

Publications

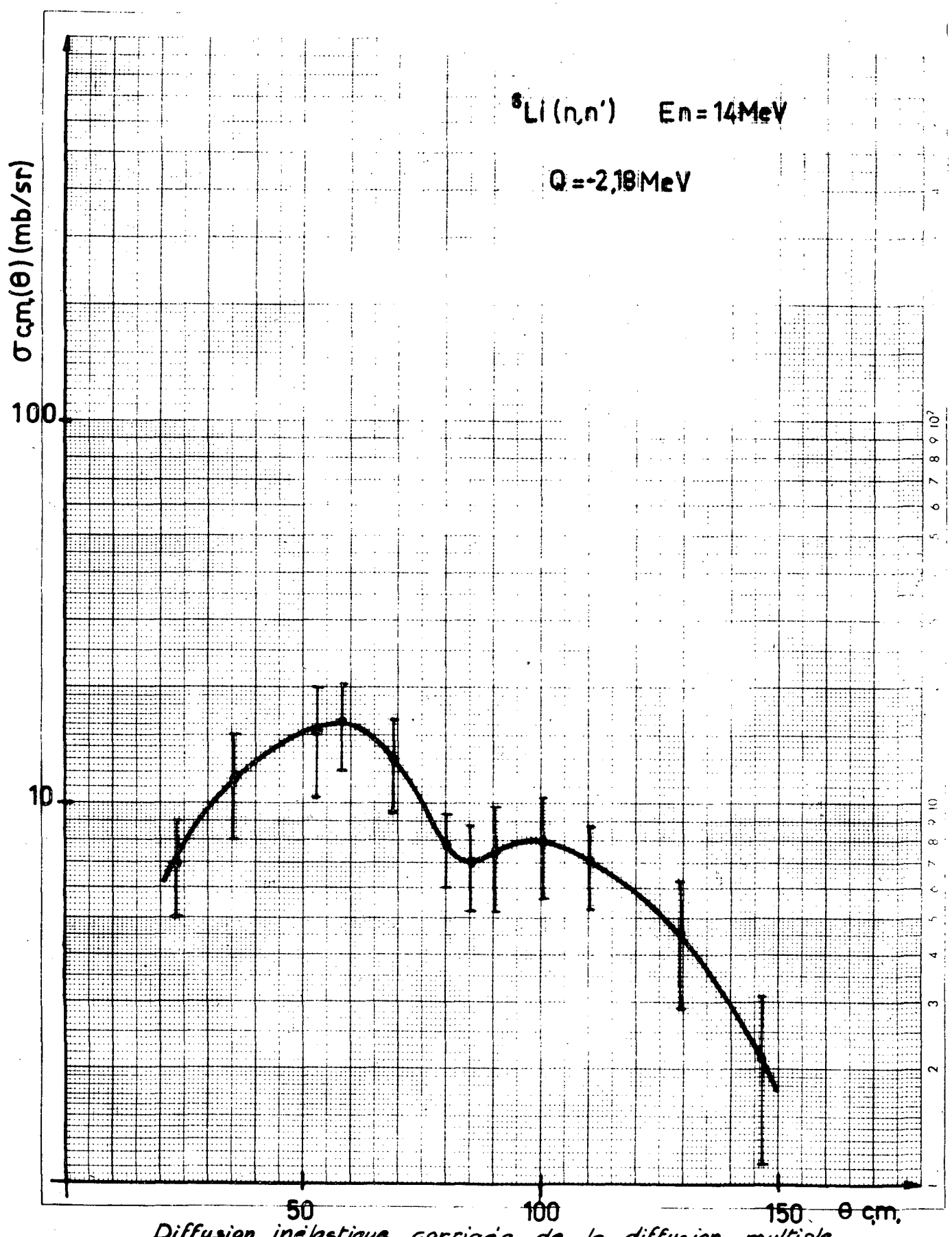
Mise en évidence d'états excités du ${}^9\text{Be}$ et du ${}^8\text{Be}$ dans la réaction ${}^9\text{Be}(n,2n)$ avec des neutrons de 14 MeV, BOUCHÉZ R., GONDRAND J-C., PERRIN P., PERRIN C., GIORNI A., QUIVY P., DUBUS M., C.R. Acad. Sc., (sous presse).

Spectromètre de neutrons rapides à double temps-de-vol et étude de la réaction ${}^9\text{Be}(n,2n)$, GONDRAND J-C., Thèse Docteur-Ingénieur, Grenoble, 1964, n° 449.



Diffusion élastique corrigée de la diffusion multiple

Fig. 22.1.



Diffusion inélastique corrigée de la diffusion multiple.

Fig. 22.2.

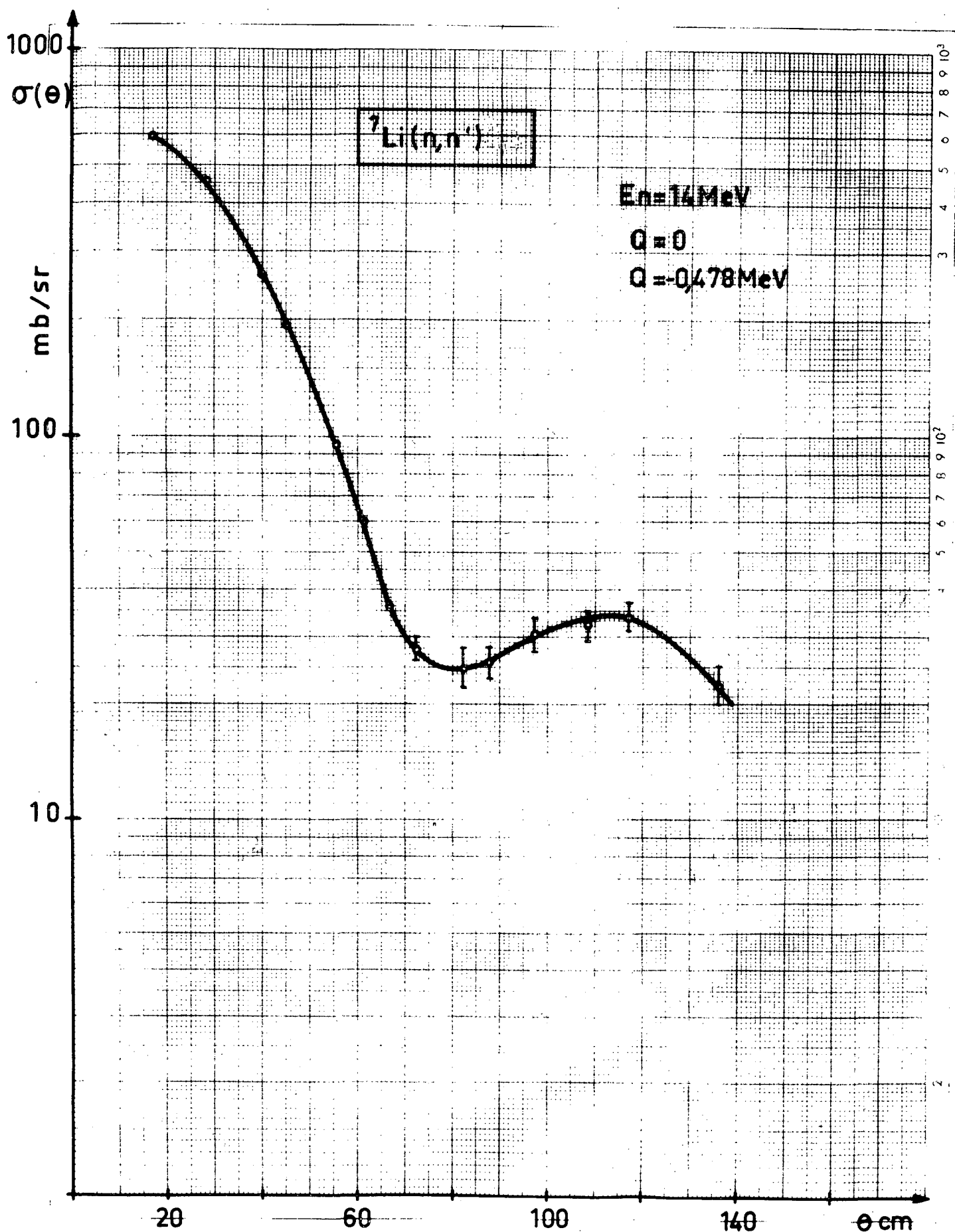


Fig. 22.3.

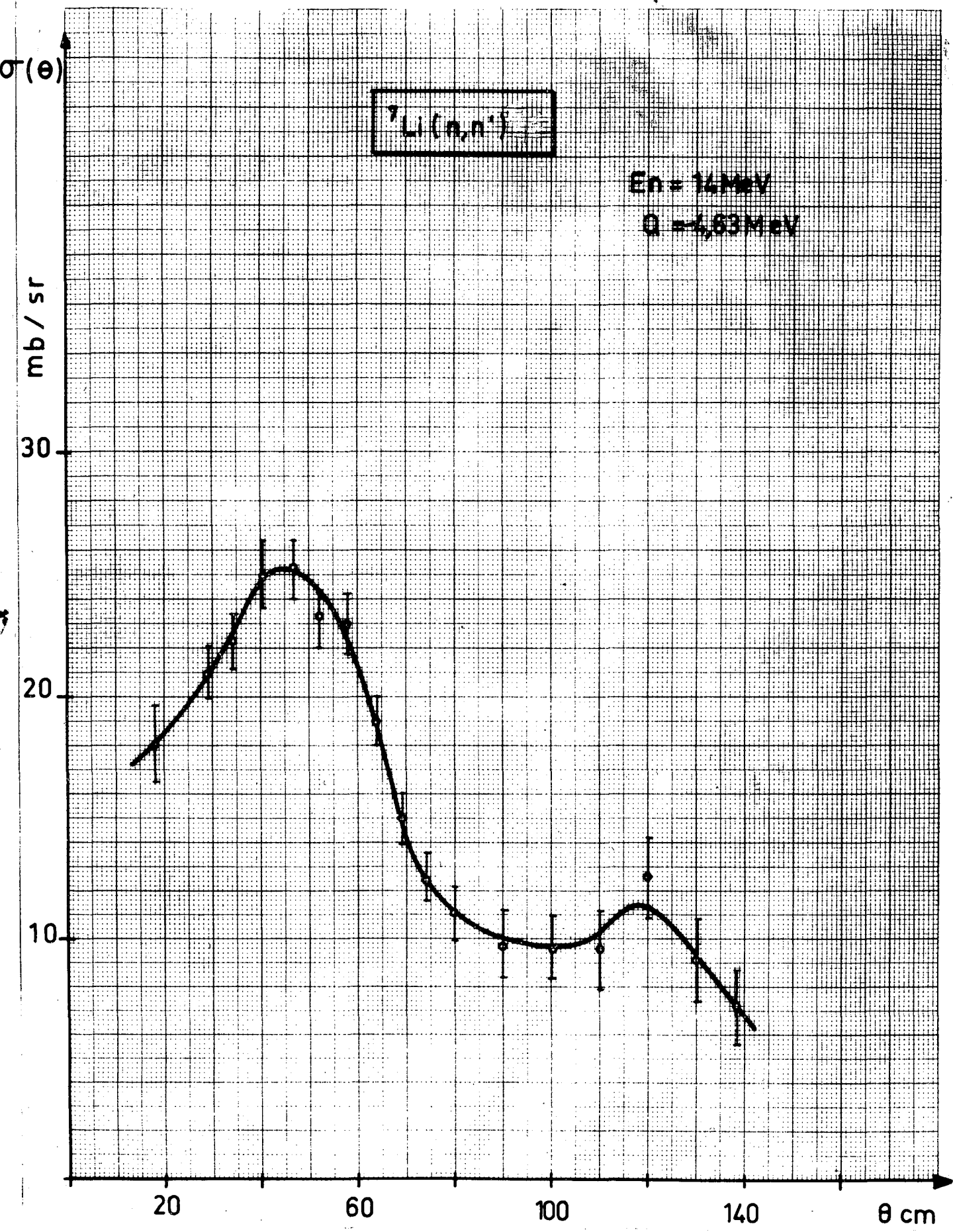


Fig. 22.4.

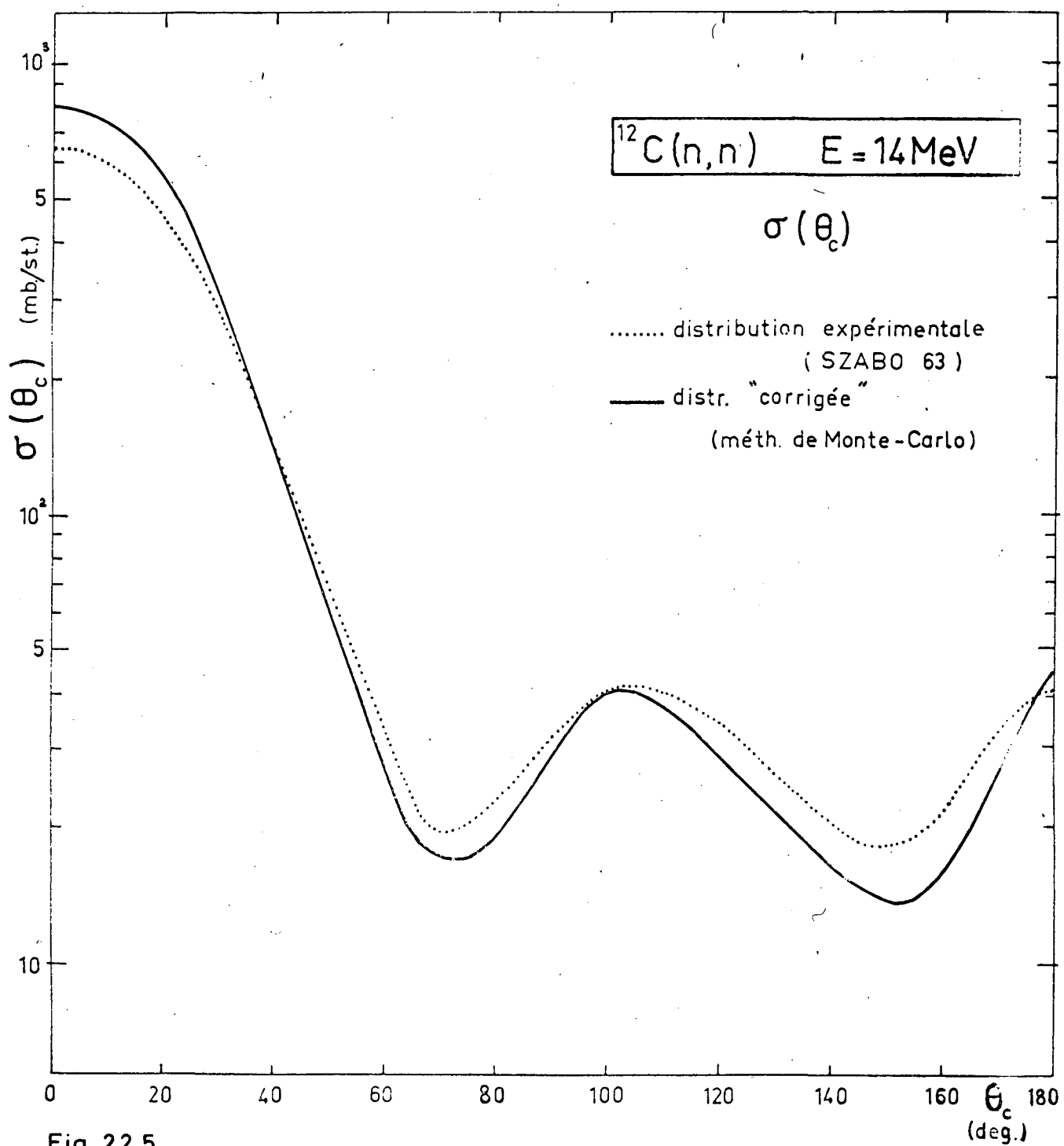


Fig. 22.5.

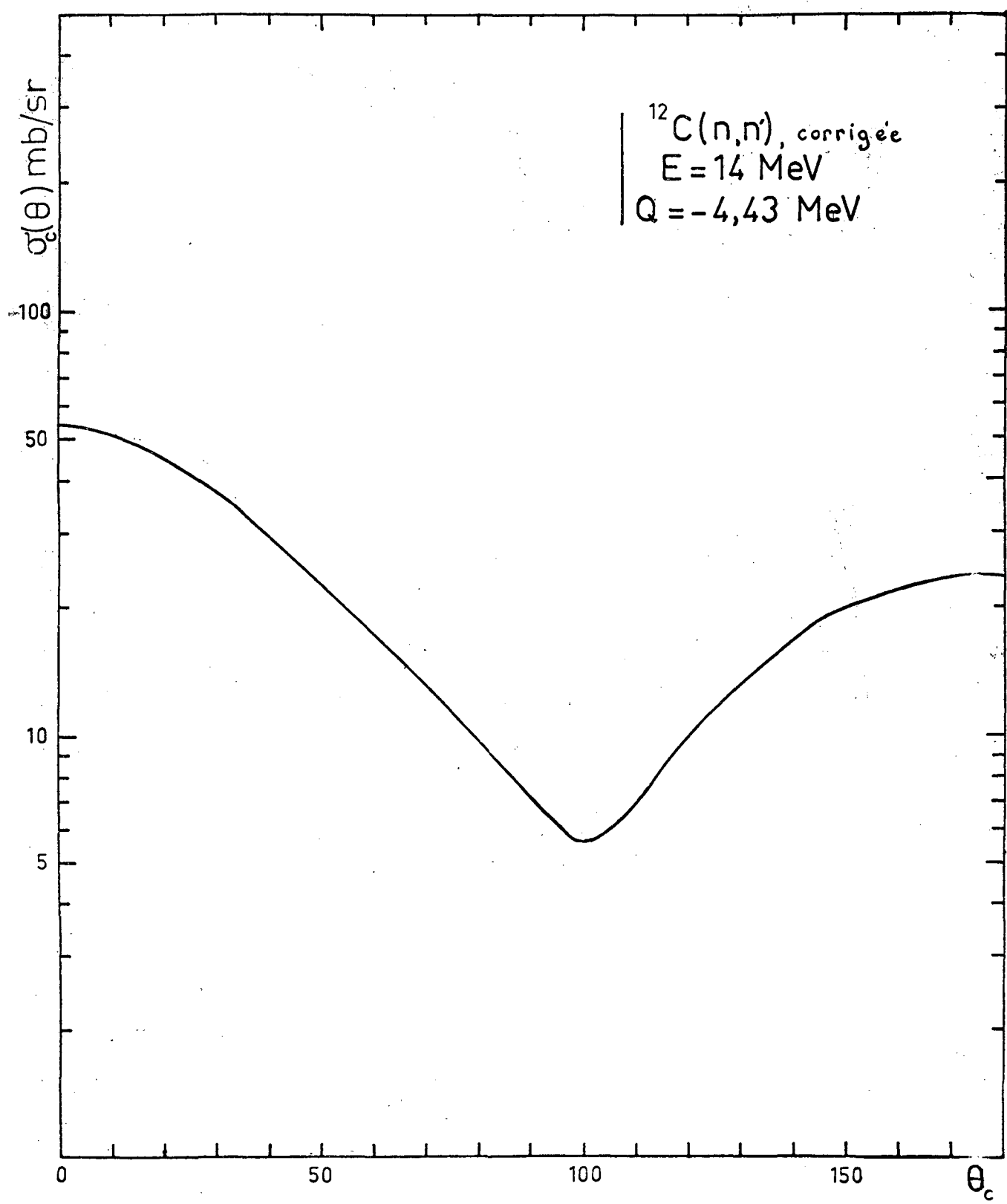


Fig. 22.6.

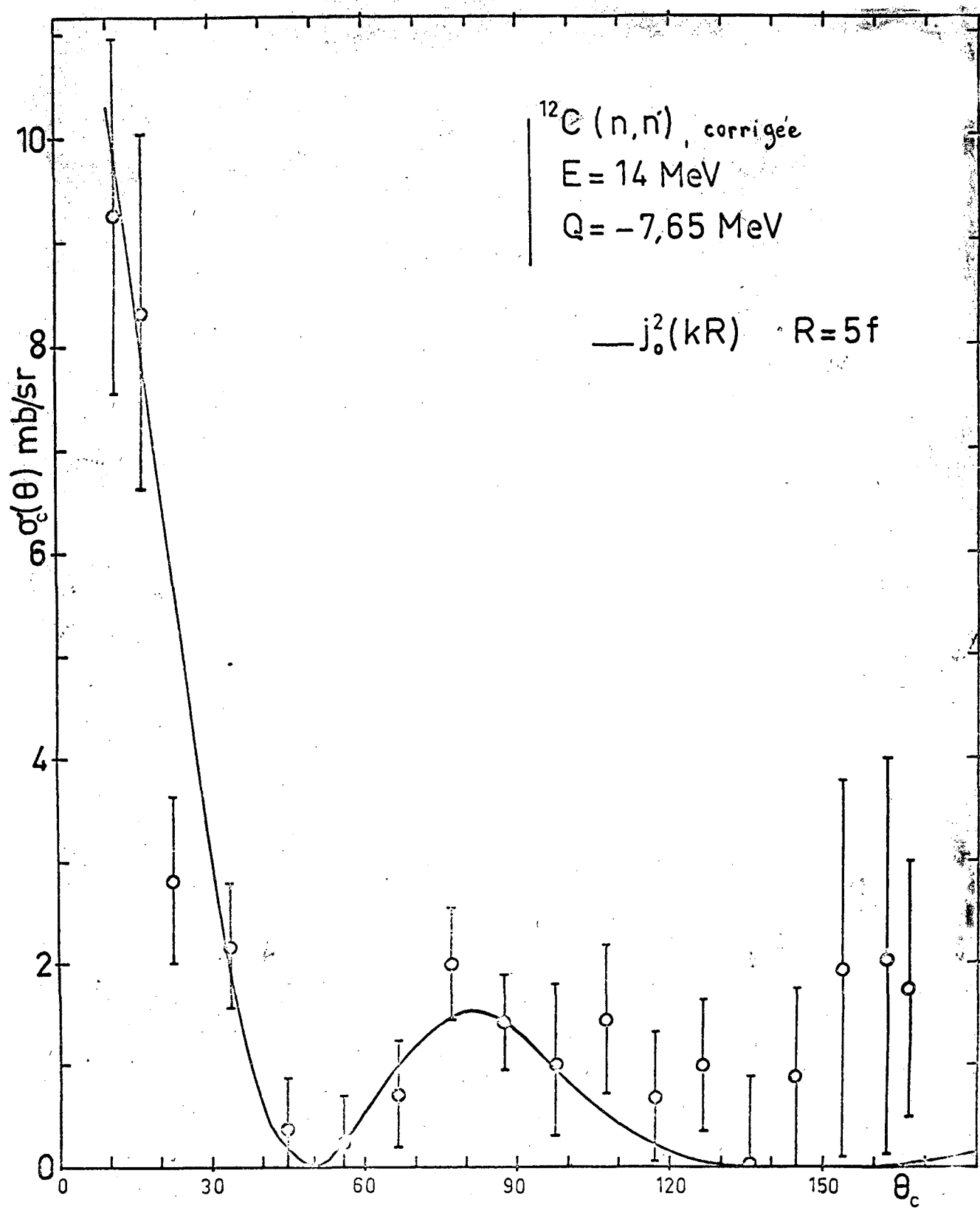
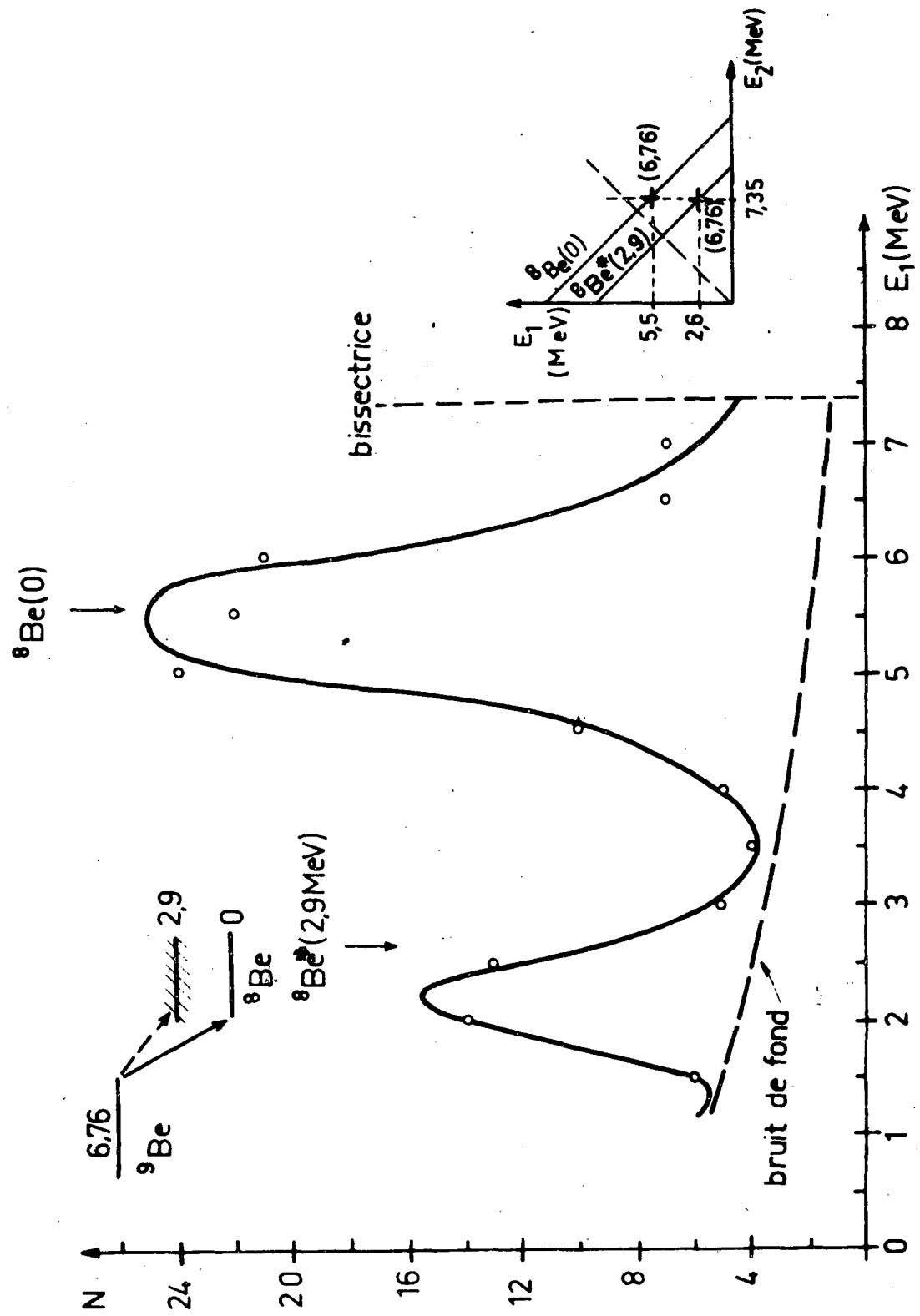
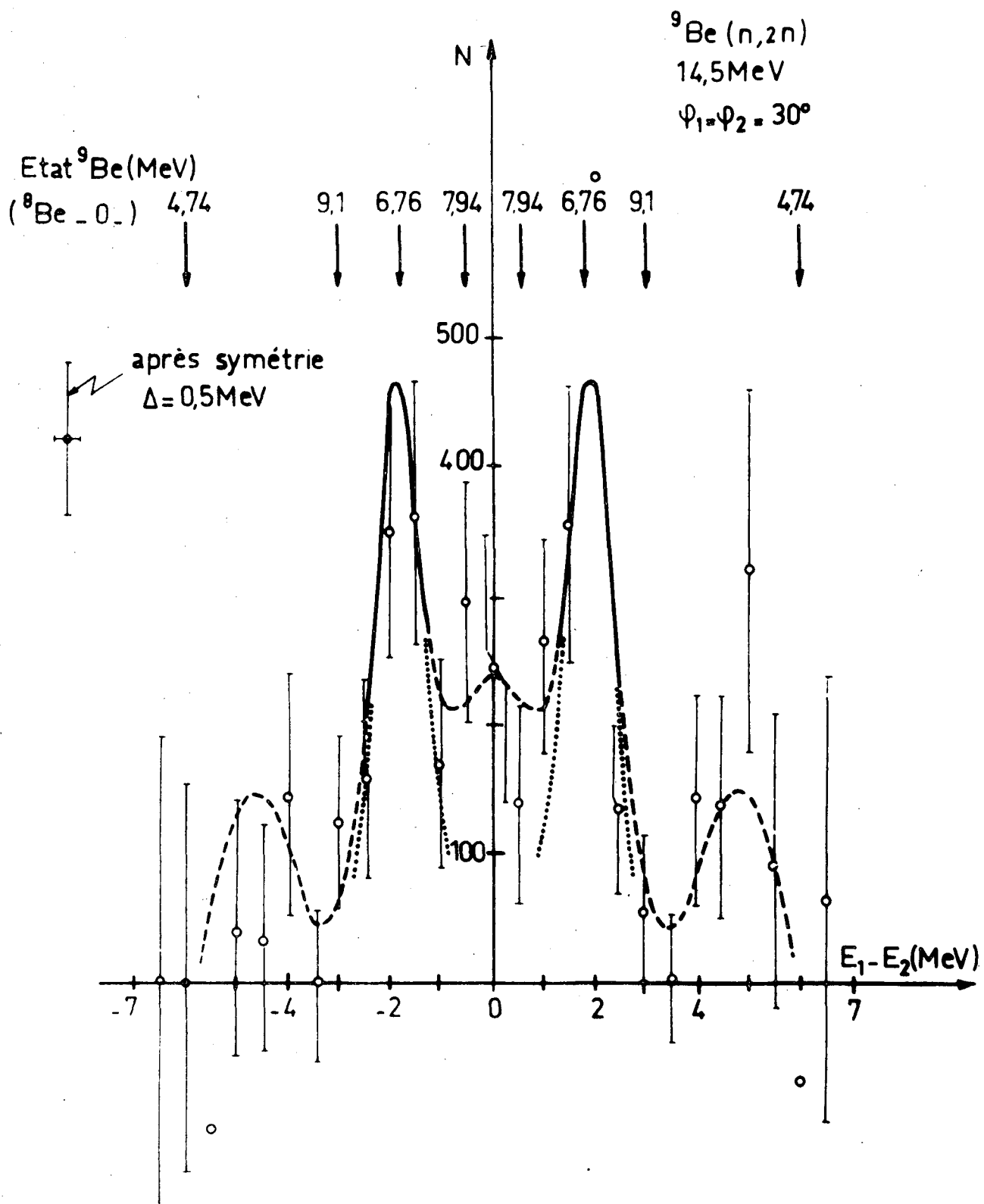


Fig. 22.7.



Répartition des événements pour $E = (7.35 \pm 0.75) \text{ MeV}$ correspondant à la désexcitation du niveau de 6.76 MeV du ${}^9\text{Be}$

Fig. 22.8.



Répartition des événements dans la bande ${}^8\text{Be}(0)$
 corrigée du bruit-de-fond et de l'efficacité

Fig. 22.9.